

Cross-talk between the primary tumour and brain metastases enhances the efficacy of immune checkpoint inhibition

David John Taggart

Submitted in accordance with the requirements for the degree of
Doctor of Philosophy

The University of Leeds
School of Medicine

October 2016

The candidate confirms that the work submitted is his/her own and that appropriate credit has been given where reference has been made to the work of others.

This copy has been supplied on the understanding that it is copyright material and that no quotation from the thesis may be published without proper acknowledgement.

Acknowledgements

Firstly, I would like to thank my main supervisor Dr Mihaela Lorgner for all the advice and help she gave throughout my PhD, especially for passing on all her vital *in vivo* expertise. Furthermore, I very much appreciate the time she took to help me attain my first post-doctoral position and her offer of continued future support. Many thanks also go to Professor Alan Melcher for his insightful immunological knowledge and input into my project. I also acknowledge Elizabeth Illet for her contribution.

I would also like to take this opportunity to express my extreme gratitude to Yorkshire Cancer Research for their funding of this PhD. Additionally, the support given by St. James's Biological Services staff was invaluable to my many *in vivo* studies and I am very grateful for all of their help throughout the past three years (during both day and night shifts!).

I will greatly miss (!) the (very) early starts and all-day implantation experiments with Tereza Andreou and appreciate all the help she, Jenny Williams and Nora Rippaus gave me with all the brains!

I would like to thank Karen J. ('Just-a-Technician') Scott for all the spleen-poppin'-related fun and for (relentlessly and loudly) reminding me that 'procrastination is the ruination of the working class'. I will miss the evenings of patient brain tumour dissection sessions and promise I will never, ever forget that if an antibody is 'gonnae bind, it's gonnae bind'!!!!!!

I struggle to comprehend how I will survive without Gemma Migneco's constant supply of Italian food (mainly sugar-based!) and hearing how every mouse, no matter how ugly, is 'soooooo cute'.

Big thanks also to Sam ('Sample') Turnbull for her crucial input into the selection of colour hues for all my graphs and kudos for her incredible talent to 'hedge-hog' when life gets too uncomfortable (as only she sees it).

Karen and Sam, Friday's will never be the same again without the weekly trips to McDonald's or Subway for food on 'Fun Time Fridays' – the arguments and muffin-tops were always worth it in the end! Julia (The Real-life Science Barbie) Cockle, your 'scientific ability' always made me smile and yes, I truly believe that one day you WILL save all the babies.

Lastly and most importantly, I would like to thank all of my family for their continued support throughout the past few years.

Abstract

Melanoma brain metastases (MBrM) are devastating, occurring in up to 60% of melanoma patients and are increasing in incidence as systemic treatments improve. MBrM are notoriously difficult to treat and patients suffer from extremely poor survival rates, resulting in these patients being excluded from clinical trials testing new treatments, thus highlighting a need for research in this field.

We developed a pre-clinical model where mice have simultaneous intracranial and extracranial B16 melanoma tumours to mimic the clinical setting. Notably, intracranial tumour growth was the survival-limiting factor, allowing the study of therapeutic effects specifically in the brain. Various combinations of anti-PD-1, anti-CTLA-4 and GM-CSF were investigated as potential therapies for MBrM. We found that the combination of anti-PD-1 and anti-CTLA-4 could prolong the survival of these mice; however, this was dependent on the presence of an extracranial tumour.

Functional studies revealed that natural killer cells and cytotoxic T-cells were essential mediators of this therapy. Moreover, examination of the infiltrating immune cell populations demonstrated an increase in CD45⁺ immune cells in the intracranial tumours of mice also bearing a flank tumour and receiving the anti-PD-1 and anti-CTLA-4 therapy. This increase was found to be a result of the increase in infiltrating T-cells and macrophages/microglia and was reliant on the presence of an extracranial tumour.

Analysis of cytotoxic T-cells revealed an increase in tumour antigen-specific cells in mice with an intracranial and extracranial tumour receiving treatment. Tumour antigen-specific T-cells within the blood showed an increased expression of homing receptors, which have been previously linked to an increase in T-cell infiltration into the brain.

In conclusion, we have demonstrated that the combination of anti-PD-1 and anti-CTLA-4 can be an effective therapy for the treatment MBrM, while also

identifying the main immune cell populations involved and a potential mechanism behind the therapeutic efficacy.

Table of Contents

Acknowledgements	iii
Abstract	iv
Table of Contents	vi
List of Tables	x
List of Figures	xi
Abbreviations	xvi
Chapter 1: Introduction	1
1.1 Brain metastases	2
1.2 Melanoma brain metastases	3
1.3 Treatment of melanoma brain metastases	6
1.4 A new direction in the treatment of melanoma brain metastases .	7
1.5 Understanding the tumour microenvironment	7
1.5.1 Cancer cells	8
1.5.2 Endothelial cells	8
1.5.3 Natural killer cells	9
1.5.4 Cytotoxic T-cells	11
1.5.5 T-helper cells.....	13
1.5.6 Regulatory T-cells	14
1.5.7 B-cells	15
1.5.8 Dendritic cells.....	16
1.5.9 Macrophages	18
1.5.10 Myeloid-derived suppressor cells.....	19
1.5.11 Neutrophils	20
1.6 Brain tumour microenvironment	22
1.6.1 Blood-brain barrier	24
1.6.2 Microglia	26
1.7 Immunotherapies	28
1.7.1 Immunotherapies in brain tumours	30
1.8 Immune checkpoint inhibition	31
1.8.1 Anti-CTLA-4	31
1.8.2 Anti-PD-1.....	36
1.8.3 Anti-PD-1 and anti-CTLA-4 combination therapy.....	41

1.9 Granulocyte-macrophage colony-stimulating factor	42
1.10 Project rationale.....	44
Chapter 2: Materials and methods.....	45
2.1 Cell lines and cell culture.....	46
2.2 Transduction of B16 F1 cells with firefly luciferase (Fluc)- expressing lentiviral vector	46
2.3 <i>In vivo</i> experiments	47
2.3.1 Implantation of cancer cells into the flank	47
2.3.2 Intracranial implantation of cancer cells	48
2.3.3 Measurement of flank tumour growth.....	49
2.3.4 Quantification of intracranial tumour growth.....	49
2.3.5 Administration of therapeutic antibodies and immune cell- depletion antibodies	50
2.3.6 Monitoring of symptoms related to intracranial growth.....	51
2.3.7 Isolation of blood	51
2.3.8 Terminal perfusion, tissue isolation and dissociation	51
2.4 Isolation of anti-F4/80 antibody produced by HP-198 cells	52
2.5 Quantification of IgG by ELISA.....	53
2.6 Flow cytometry	54
2.6.1 Extracellular staining	54
2.6.2 Intracellular staining	54
2.6.3 Flow cytometry analysis	54
2.7 <i>Ex vivo</i> stimulation of splenocytes	58
2.8 ELISpot	58
2.9 Statistical analysis.....	59
2.10 Buffers and reagents	60
Chapter 3: Developing a pre-clinical model for melanoma brain metastases and investigating the effects of various immunotherapy combinations	61
3.1 Introduction	62
3.2 Establishing a new preclinical melanoma metastasis model.....	63
3.3 A combination of immunotherapies is more effective in treating brain metastases	65
3.4 A flank tumour is essential for effective intracranial therapy	68
3.4.1 Treatment with anti-PD-1 plus anti-CTLA-4 with GM-CSF.....	69
3.4.2 Treatment with anti-PD-1 and anti-CTLA-4	74

3.5 A flank tumour is critical for prolonged survival of mice with melanoma brain metastases.....	78
3.6 Discussion.....	80

Chapter 4: Determining the functional roles of immune cells in the treatment of melanoma brain metastases with immune checkpoint therapy	87
4.1 Introduction	88
4.2 CD8⁺ T-cells and NK cells are essential for effective intracranial immune checkpoint inhibitor therapy.....	88
4.3 Antibody-mediated macrophage depletion within intracranial tumours.....	94
4.4 Discussion.....	99

Chapter 5: Investigating the role of the extracranial tumour and immune checkpoint therapy in the infiltration of immune cells into intracranial tumours.....	106
5.1 Introduction	107
5.2 A synergy between immune checkpoint therapy and extracranial tumour is required for increased infiltration of CD45⁺ immune cells into the intracranial tumour	107
5.3 A synergy between immune checkpoint therapy and extracranial tumour results in an increased CD3⁺ T-cell infiltration into intracranial tumours	111
5.4 Immune checkpoint therapy synergises with extracranial tumour to increase intracranial tumour-infiltrating CD8⁺ T-cells	111
5.5 Intracranial tumour-infiltrating CD4⁺ effector T-cells and T-Regs increase with immune checkpoint therapy	116
5.6 The ratio of CD8⁺ T-cells and CD4⁺ effector cells to T-Regs is unchanged in response to immune checkpoint therapy	120
5.7 NK cell infiltration is unaltered by immune checkpoint therapy or extracranial tumour	122
5.8 Immune checkpoint therapy and extracranial tumour synergise to increase microglia infiltration, while the therapy alone can increase macrophage infiltration into the intracranial tumour	125
5.9 Immune checkpoint therapy and extracranial tumours alter the infiltration of immune cells into intracranial tumours by different means	129

5.10 Discussion.....	130
Chapter 6: Investigating the effects of extracranial tumour and immune checkpoint therapy on peripheral immune cells	138
6.1 Introduction	139
6.2 Immune checkpoint therapy increases circulating T-Regs	139
6.3 CD8⁺ T-cells in the cervical lymph nodes have an increased expression of PD-1 in response to treatment	141
6.4 Immune checkpoint inhibition affects the immune cell populations within the spleen	143
6.5 Immune checkpoint therapy increases the activation potential of splenocytes	146
6.6 Immune checkpoint therapy increases IFN-γ production by splenocytes	153
6.7 Tumour-specific CD8⁺ T-cells can be detected in the B16-ova model	155
6.8 Tumour-specific CD8⁺ T-cells isolated from spleens have a different phenotype to their non-tumour-specific counterparts	157
6.9 Immune checkpoint therapy increases the expression of homing receptors on CD8⁺ T-cells in the circulation	169
6.10 Immune checkpoint therapy and extracranial tumour synergise to upregulate MHC I and ICAM-1 expression on endothelial cells in intracranial tumours	172
6.11 Discussion.....	177
Chapter 7: Conclusion	182
Appendix	187
8.1 List of suppliers	187
8.2 Statistical analyses tables	190
References	243

List of Tables

Table 1.1 Examples of pre-clinical studies involving anti-CTLA-4 therapy	34
Table 1.2 Examples of pre-clinical studies involving anti-PD-1 therapy	39
Table 2.1 List of extracellular flow cytometry antibodies.....	55
Table 2.2 List of extracellular flow cytometry antibodies and their corresponding isotypes.....	56
Table 2.3 List of intracellular flow cytometry antibodies	57
Table 2.4 List of intracellular flow cytometry antibodies and their corresponding isotypes.....	57
Table 3.1 Statistical analysis for the survival and tumour burden of mice with flank and intracranial B16 tumours treated with various combinations of anti-PD-1, anti-CTLA-4 and GM-CSF	69
Table 3.2 Statistical analysis for the effects of a flank tumour on the survival of mice treated with anti-PD-1 and anti-CTLA-4.....	79
Table 4.1 Statistical analysis for the survival and tumour burden of mice with flank and intracranial B16 tumours undergoing immune cell depletion and immune checkpoint therapy	95
Table 5.1 Immune cell types and phenotype markers used to identify each cell type	109
Table 5.2 Immune cell markers and their phenotypic description	115

List of Figures

Figure 1.1 The Clark's scale of melanoma progression	4
Figure 1.2 The stages of melanoma disease progression	5
Figure 1.3 Adaptive immune system-mediated cancer cell death	12
Figure 1.4 Drainage of antigens within the brain to the lymph nodes ..	23
Figure 1.5 The reversal of CTLA-4-mediated T-cell inhibition via anti- CTLA-4 therapy	32
Figure 1.6 The reversal of PD-1-mediated T-cell inhibition via anti-PD-1 therapy	37
Figure 2.1 Example of quantification of bioluminescence images	50
Figure 3.1 Establishing a timeline for subcutaneous tumour growth of B16 cells	64
Figure 3.2 Establishing a timeline for the intracranial growth of B16/Fluc cells	66
Figure 3.3 Experimental timeline of pre-clinical melanoma brain metastasis model	67
Figure 3.4 Flank and intracranial tumour measurements in mice with B16 tumours treated with various combinations of anti-PD-1, anti- CTLA-4 and GM-CSF	68
Figure 3.5 Survival of mice with flank and intracranial B16 tumours treated with various combinations of anti-PD-1, anti-CTLA-4 and GM- CSF	70
Figure 3.6 Individual survival curves of mice with flank and intracranial B16 tumours treated with various combinations of anti-PD-1, anti- CTLA-4 and GM-CSF	71
Figure 3.7 Experimental timeline for investigating the role of flank tumours in immune checkpoint therapy in MBrM	72
Figure 3.8 The effect of a flank tumour on the intracranial tumour growth in mice treated with the combination of anti-PD-1, anti-CTLA-4 and GM-CSF	73

Figure 3.9 Post-mortem brain images of mice treated with anti-PD-1, anti-CTLA-4 and GM-CSF or IgG control antibody with or without a flank tumour.....	75
Figure 3.10 The effects of a flank tumour on intracranial tumour growth in mice treated with anti-PD-1 and anti-CTLA-4	76
Figure 3.11 Post-mortem brain images of mice treated with anti-PD-1 and anti-CTLA-4 or IgG control antibody with or without a flank tumour	77
Figure 3.12 The effect of a flank tumour on the survival of mice treated with anti-PD-1 and anti-CTLA-4.....	79
Figure 4.1 Timeline for immune cell depletion experiments	90
Figure 4.2 Immune cell depletion was confirmed through blood analysis	91
Figure 4.3 Confirmation of immune cell depletion at experimental endpoint in intracranial tumours	92
Figure 4.4 Effects of immune cell depletion on the survival of mice bearing B16 flank and intracranial tumours undergoing immune checkpoint therapy	93
Figure 4.5 Quantification of the anti-F4/80 antibody produced by the HB-198 cell line.....	96
Figure 4.6 Depletion of macrophages with HB-198-derived anti-F4/80 antibody.....	97
Figure 4.7 Depletion of macrophages with a commercial anti-F4/80 antibody.....	98
Figure 5.1 Gating strategy for the main populations of infiltrating immune cells.....	108
Figure 5.2 Effects of immune checkpoint therapy and the extracranial tumour on the accumulation of CD45⁺ cells and CD3⁺ T-cells within the intracranial tumour.....	110
Figure 5.3 Gating strategy for CD3⁺ T-cell population subsets	112
Figure 5.4 Representative plots for the various markers expressed by CD8⁺ T-cells	113
Figure 5.5 The effects of immune checkpoint therapy and extracranial tumours on CD8⁺ T-cells and their activation markers.....	114

Figure 5.6 The effects of immune checkpoint therapy and extracranial tumours on different subsets of CD8⁺ T-cells	117
Figure 5.7 The effects of immune checkpoint therapy and extracranial tumours on inhibitory markers on CD8⁺ T-cells	118
Figure 5.8 The effects of immune checkpoint therapy on CD4⁺ T-cells and T-cell subsets	119
Figure 5.9 The effects of immune checkpoint therapy and extracranial tumours on CD25⁺ CD4⁺ T-cells and CD69⁺ CD4⁺ T-cells	121
Figure 5.10 The effects of immune checkpoint therapy and extracranial tumours on effector:regulatory T-cell ratios.....	122
Figure 5.11 The effects of immune checkpoint therapy and extracranial tumours on total number and activation status of NK cells.....	123
Figure 5.12 Representative plots for CD107a⁺ NK cells and CD11b⁺ CD27⁺ NK cells.....	124
Figure 5.13 The effects of immune checkpoint therapy and extracranial tumours on microglia and their expression of MHC II.....	126
Figure 5.14 Representative plots for MHC II⁺ microglia and MHC II⁺ macrophages	127
Figure 5.15 The effects of immune checkpoint therapy and extracranial tumours on macrophages and their expression of MHC II.....	128
Figure 5.16 Summary of the effects of immune checkpoint therapy and extracranial tumours on immune cells infiltrating into intracranial tumours	130
Figure 6.1 Effects of immune checkpoint therapy on immune cells in the blood of mice in the presence and absence of a flank tumour	140
Figure 6.2 Effects of immune checkpoint therapy on immune cells in the DCLNs in the presence and absence of a flank tumour.....	142
Figure 6.3 Effects of immune checkpoint therapy on CD8⁺ T-cells within the spleen of mice in the presence and absence of a flank tumour....	144
Figure 6.4 Effects of immune checkpoint therapy on CD4⁺ T-cells within the spleen of mice in the presence and absence of a flank tumour....	145
Figure 6.5 Effects of immune checkpoint therapy on NK cells within the spleen of mice in the presence and absence of a flank tumour	147

Figure 6.6 Representative flow cytometry plots for <i>ex vivo</i>-stimulated splenocytes.....	148
Figure 6.7 Potential of <i>ex vivo</i>-stimulated CD8⁺ T-cells to elicit an anti-tumour response	150
Figure 6.8 Potential of <i>ex vivo</i>-stimulated CD4⁺ T-cells to elicit an anti-tumour response	151
Figure 6.9 Potential of <i>ex vivo</i>-stimulated NK cells to elicit an anti-tumour response	152
Figure 6.10 Analysis of IFN-γ production by splenocytes in response to melanoma-specific peptides	154
Figure 6.11 The effect of a flank tumour on the intracranial tumour growth of B16-ova cells in mice treated with the combination of anti-PD-1 and anti-CTLA-4.....	156
Figure 6.12 Post-mortem images of mice with B16-ova/Fluc tumours treated with anti-PD-1 and anti-CTLA-4 in the presence and absence of a flank tumour.....	157
Figure 6.13 The effects of extracranial tumour and immune checkpoint therapy on the B16-ova tumour-specific CD8⁺ T-cell population in the brain, blood and spleen	158
Figure 6.14 The effects of extracranial tumour and immune checkpoint therapy on the phenotype of the CD8⁺ T-cell population in the spleens of mice with B16-ova tumours	159
Figure 6.15 The effects of extracranial tumour and immune checkpoint therapy on the phenotype of ova pentamer⁺ CD8⁺ T-cell population in the spleens of mice with B16-ova tumours	161
Figure 6.16 Comparison of ova-pentamer⁺ and ova-pentamer⁻ CD8⁺ T-cells for their expression of Ki67 and granzyme B in mice bearing an intracranial and flank tumour receiving treatment.....	162
Figure 6.17 The effects of extracranial tumour and immune checkpoint therapy on the inhibitory phenotype of the CD8⁺ T-cell population in the spleens of mice with B16-ova tumours	163
Figure 6.18 The effects of extracranial tumour and immune checkpoint therapy on the inhibitory phenotype of ova pentamer⁺ CD8⁺ T-cell population in the spleens of mice with B16-ova tumours	164

Figure 6.19 Comparison of ova-pentamer⁺ and ova-pentamer⁻ CD8⁺ T-cells for their expression of EOMES, TIM-3 and PD-1 in mice bearing an intracranial and flank tumour receiving treatment.....166

Figure 6.20 Potential of *ex vivo*-stimulated CD8⁺ T-cells to elicit an anti-tumour response from mice with B16-ova tumour167

Figure 6.21 Potential of *ex vivo*-stimulated CD4⁺ T-cells to elicit an anti-tumour response from mice with B16-ova tumour168

Figure 6.22 Representative flow cytometry plots for homing markers on CD8⁺ T-cells in the blood of mice with B16-ova tumours171

Figure 6.23 The effects of extracranial tumour and immune checkpoint therapy on the homing markers on the CD8⁺ T-cell population in the blood of mice with B16-ova tumours.....171

Figure 6.24 The effects of extracranial tumour and immune checkpoint therapy on the homing markers on ova-pentamer⁺ CD8⁺ T-cell population in the blood of mice with B16-ova tumours.....173

Figure 6.25 Comparison of ova-pentamer⁺ and ova-pentamer⁻ CD8⁺ T-cells for their expression of homing markers in mice bearing an intracranial and flank tumour receiving treatment.....174

Figure 6.26 Representative plots for ECs and their expression of homing markers175

Figure 6.27 The effects of extracranial tumour and immune checkpoint therapy on the homing marker expression on ECs within the intracranial tumours of mice with B16-ova tumours.....176

Abbreviations

~	Approximately
<	Less than
µg	Microgram
µl	Microlitre
ACK	Ammonium-chloride-potassium
ACT	Adoptive cell transfer
ANOVA	Analysis of variance
APCs	Antigen presenting cells
Arg-1	Arginase-1
ATCC	American Type Culture Collection
AWERC	Animal Welfare & Ethical Review Committee
B16/Fluc	Firefly luciferase-tagged B16 F1
BBB	Blood-brain barrier
bFGF	Basic fibroblast growth factor
BMDCs	Bone marrow-derived cells
B-Regs	Regulatory B-cells
BrM	Brain metastases
BSA	Bovine serum albumin
CAFs	Cancer-associated fibroblasts
CAR	Chimeric antigen receptor
CCL	C-C motif chemokine ligand
CCR	C-C motif chemokine receptor
CD	Cluster of differentiation
CD8 ⁺ T-cells	CD8 ⁺ Cytotoxic T-cells

CEA	Carcinoembryonic antigen
cm	Centimetre
CNS	Central nervous systemcontaining-molecule-3
CO ₂	Carbon dioxide
CSF	Cerebral spinal fluid
CSF-1	Colony-stimulating factor-1
CTLA-4	Cytotoxic T lymphocyte-associated antigen 4
CXCL	C-X-C motif chemokine ligand
DC	Dendritic cell
DCLNs	Deep cervical lymph nodes
DMEM	Dulbecco's modified eagle medium
DMSO	Dimethyl sulfoxide
EC	Endothelial cell
ECM	Extracellular matrix
EDTA	Ethylenediaminetetraacetic acid
EGF	Epidermal growth factor
EGFR	Epidermal growth factor receptor
ELISA	Enzyme-linked immunsorbent assay
ELISpot	Eznyme-linked immunospot
EMEM	Eagle's minimum essential medium
EOMES	Eomesodermin
EU	European union factor
FAS-L	FAS ligand
FBS	Foetal bovine serum
FDA	US Food and Drug Administration
Fluc	Firefly luciferase
Fox P3	Forkhead box P3

FSC	Forward scatter
g	Gram
<i>g</i>	Gravitational force
GBM	Glioblastoma multiforme
G-CSF	Granulocyte colony-stimulating factor
GM-CSF	Granulocyte-macrophage colony-stimulating
H&E	Haematoxylin and eosin
HBSS	Hank's balanced salt solution
HER2	Human epidermal growth factor receptor 2
HGF	Hepatocyte growth factor
HLA	Human leukocyte antigen
HPM	Harding-Passey melanoma
HSV	Herpes simplex virus
<i>i.p.</i>	Intraperitoneal
ICAM-1	Intracellular adhesion molecule-1
IDO	Indoleamine-2, 3-dioxygenase
IFN- γ	Interferon gamma
IFN- α	Interferon alpha
IL	Interleukin
ILC	Innate lymphoid cell
IMDM	Iscove's modified Dulbecco's medium
iNOS	Inducible nitric oxide synthase
irAE	Immune-related adverse events
<i>i.v.</i>	Intravenous
kg	Kilogram
KO	Knockout
LAG-3	Lymphocyte activation gene-3

LFA-1	Lymphocyte function-associated antigen-1
MBrM	Melanoma brain metastases
MCP	Macrophage chemoattractant protein
M-CSF	Macrophage colony-stimulating factor
mDCs	Myeloid dendritic cells
MDSCs	Myeloid-derived suppressor cells
MFI	Mean fluorescence intensity
mg	Milligram
MHC	Major histocompatibility complex
min	Minutes
ml	Millilitre
mm	Millimetre
MMP	Matrix metalloproteinase
MRI	Magnetic resonance imaging
MUC1	Mucin 1
NaOH	Sodium hydroxide
NCRs	Natural cytotoxicity receptors
NE	Neutrophil elastase
NF κ B	Nuclear factor-kappa B
ng	Nanogram
NICE	National Institute for Health Care and Excellence
NK cells	Natural killer cells
NO	Nitric oxide
NOD	Non-obese diabetic
NSCLC	Non-small-cell lung cancer
OS	Overall survival
OV	Oncolytic virus

ova	Ovalbumin
OX40L	OX40 ligand
PBMCs	Peripheral blood mononuclear cells
PBS	Phosphate-buffered saline
PBST	Phosphate buffered saline with tween
PD-1	Programmed cell death protein-1
pDCs	Plasmacytoid dendritic cells
PDGF	Platelet-derived growth factor
PD-L1	Programmed death ligand-1
Pen Strep	Penicillin streptomycin
PFS	Progression-free survival
PTPN11	Tyrosine-protein phosphatase non-receptor type 11
ROI	Region of interest
ROR	Retinoic acid related orphan receptor
ROS	Reactive oxygen species
RPMI	Roswell park memorial institute
RR	Response rate
SAS	Subarachnoid space
SCLC	Small-cell lung cancer
SEM	Standard error of the mean
SRS	Stereotactic radiosurgery
SSC	Side scatter
TAAAs	Tumour-associated antigens
TAMs	Tumour-associated macrophages
TANs	Tumour-associated neutrophils
T-Bet	T-box transcription factor TBX21

TCRs	T-cell receptors
T-DM1	Tratuzmab emtansine-1
TEC	Tumour endothelial cell
TGF- β	Transforming growth factor beta
TILs	Tumour-infiltrating lymphocytes
TIM-3	T-cell immunoglobulin- and mucin-domain-containing-molecule-3
TLRs	Toll-like receptors
TMB	Tetramethylbenzidine
TME	Tumour microenvironment
Tmem119	Transmembrane protein 119
TNF- α	Tumour necrosis factor alpha
T-Regs	Regulatory T-cells
TSAs	Tumour-specific antigens
TSLP	Thymic stromal lymphopoietin
T-VEC	Talimogene laherparepvec
UK	United Kingdom
USA	United States of America
VCAM-1	Vascular cell adhesion molecule-1
VEGF	Vascular endothelial growth factor
VLA-4	Very late antigen-4
WBRT	Whole-brain radiotherapy

Chapter 1:

Introduction

Chapter 1

1.1 Brain metastases

Due to the rise in more effective systemic treatments and diagnostic techniques, the occurrence of brain metastases (BrM) is becoming more prevalent¹⁻³. Of all the neurological complications associated with systemic cancer, BrM have been described as the “most common and devastating”³. BrM are thought to occur in approximately 10-20% of all cancer patients, although these statistics are based on population studies and are considered to greatly underestimate the true occurrence of BrM due to the age of the reports¹⁻⁷.

With the improvement of systemic therapies, the brain can act as a sanctuary to malignancies due to protection from the blood-brain barrier (BBB)³. In the case of human epidermal growth factor receptor 2⁺ (HER2⁺) breast cancer, trastuzumab, an effective therapeutic agent for HER2⁺ breast cancer, is unable to cross the BBB. This is becoming an ever-increasing issue, as one third of HER2⁺ breast cancer patients will develop BrM⁸⁻¹⁰.

The main site for BrM to occur is within the brain parenchyma; however, they can occur in the dura, leptomeninges, choroid plexus, pineal gland and the pituitary^{3,11}. While metastases can often occur simultaneously at different sites within the brain, they are not treated in a site-specific manner, even though site-specific phenotypes have been identified¹¹.

Tumour types differ in their propensity to metastasise to the brain; however, the most common primary tumour sources are lung cancer, breast cancer and melanoma, all of which account for 67-80% of BrM^{1,3,12-14}. It is also common for patients to have concurrent systemic metastases, with pulmonary metastases occurring most frequently^{15,16}. Nonetheless, there are cases where BrM have originated from an unidentified primary tumour

which, in some cases, may not be located following a post-mortem examination^{17,18}.

1.2 Melanoma brain metastases

Melanoma arises through the malignant proliferation of melanocytes in the skin¹⁹. The primary melanoma tumour can be classified using the Clark's model, which takes into account the surface area of the tumour and its vertical invasiveness (Figure 1.1)²⁰. The progression of the disease is characterised into various stages, from Stage 0 where the tumour is restricted to the surface of the skin, to Stage IV where the disease has become widespread and metastasised to other organs (Figure 1.2)²¹⁻²³. Melanoma will more commonly metastasise to the brain in the later stages (IV) of the disease. Nevertheless, it has been known to metastasise early on in the course of the disease, as evidenced by the recurrence of tumours at different sites to the primary tumour^{24,25}. Time to recurrence is usually four to five years in 40% of patients¹⁹. Common symptoms associated with melanoma brain metastases (MBrM) are progressive neurological deterioration and severe pain²⁶.

MBrM are thought to occur in up to 10% of all melanoma patients^{14,19,27}. This figure increases substantially when patients with metastatic melanoma are considered, as approximately 50% of these patients are diagnosed with MBrM and this number increases to 75% upon post-mortem examination^{3,14,19,25-29}. Once melanoma has metastasised to the brain, prognosis is extremely poor, with median overall survival (OS) ranging from four to six months from diagnosis without any intervention^{14,26,27,30,31}. With treatment, the median OS is six to nine months with the five-year survival rate reported as being as low as five percent^{14,19,26,28}.

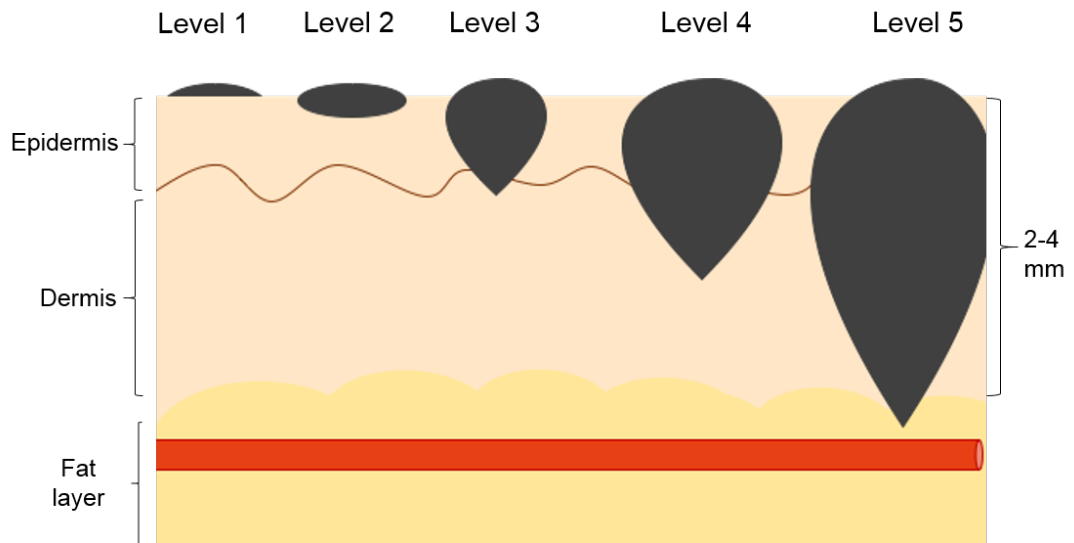


Figure 1.1 The Clark's scale of melanoma progression

The Clark's scale was devised by Clark *et al.* in 1969 as a measure of how deep the melanoma has spread within the skin and the scale is still in use. 'Level 1' melanoma is confined above the basement membrane and can be defined as being *in situ*. With 'Level 2', the cancer cells have breached the basement membrane and extended into the papillary dermis (epidermis) but have yet to reach the reticular dermis. 'Level 3' melanoma has passed the papillary dermis and begins to touch the reticular dermis. When the melanoma has spread into the reticular or deep dermis, this is defined as 'Level 4'. In cases of 'Level 5', the melanoma has grown into the subcutaneous fat underneath the skin.

Melanoma has been described as having the greatest preference to metastasise to the brain as compared to other primary tumours³².

Additionally, the location of the primary tumour can affect the likelihood of the tumour metastasising to the brain, as there is a higher incidence of MBrM arising from cutaneous tumours of the head and neck³³. MBrM are often found to be located in the cortex of the brain and are frequently found alongside leptomeningeal metastases (83% in one study)³⁴. In addition, to multiple lesions in the brain, 46-82% of MBrM patients will also have some form of extracranial disease^{31,35,36}.

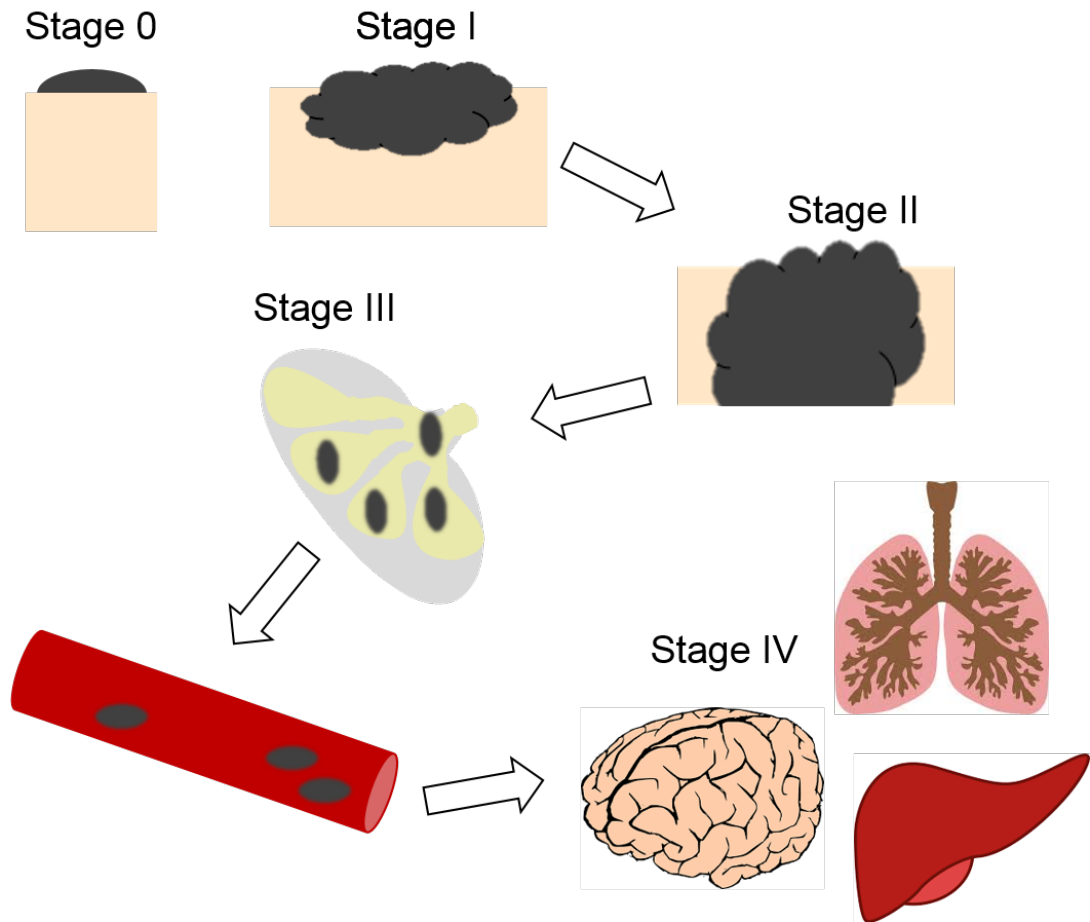


Figure 1.2 The stages of melanoma disease progression

The progression of melanoma is broken down into a number of stages, with each stage increasing in severity. **Stage 0** is where the melanoma is still on the surface of the skin (*in situ*) and is unlikely to spread to other organs at this stage. With **stage I** melanoma, the cancer cells are still within the skin and the tumour is still quite thin. Stage I can be broken into two further stages, Ia and Ib, depending on the tumour thickness, incidence of ulceration and mitotic rate. **Stage II** is when the tumour has grown through the epidermis and into the dermis; at this stage there is a higher chance of spread to other organs than the previous stage. Stage II can be broken down into three groups, A, B and C, depending on the tumour thickness and the incidence of ulceration. **Stage III** is characterised by the spread of cancer cells to the lymphatic system and the lymph nodes; this stage can be sub-divided into three groups, A, B and C, depending on the number and sizes of nodes involved. **Stage IV** is when disease has spread to the blood stream and the cancer has begun to metastasise to different organs. Melanoma commonly metastasises to the liver, lung and brain.

1.3 Treatment of melanoma brain metastases

Historically, metastatic melanoma has been a difficult disease to treat and MBrM is no different, with limited therapeutic options available until more recently³⁷. Even though there are some patients surviving long-term with MBrM, treatment is usually considered palliative²⁸.

A frequently used method is surgical resection of the tumour mass^{26,27,29,37}. This is normally used when there is a single large mass that is easily accessible²⁷. The performance status of the patient is also taken into account, especially in the cases where debulking the tumour will improve the quality of life for the patient by reducing BrM-related symptoms²⁷. The median OS following surgical resection is between eight and nine months^{27,38}.

As local relapse was found to occur after surgical resections in more than 50% of patients, whole-brain radiotherapy (WBRT) or stereotactic radiosurgery (SRS) was utilised instead or as an adjuvant therapy²⁶. WBRT has been mainly used following surgical resection of MBrM or in patients who were not suitable for surgery or SRS²⁶. SRS has more recently become the more favourable treatment option, due to its use of high-dose radiation in localised areas, sparing the rest of the brain tissue from unnecessary irradiation³⁷. SRS is normally used in patients with MBrM that are inaccessible via surgery or when the patient has one to three metastases which are up to three cm in size^{26,37}. SRS has been reported to have a local control rate of approximately 70-80% and there are ongoing studies investigating the use of SRS in patients with more than three metastases³⁹.

Systemic therapies have been trialled in patients with MBrM, although these results have been underwhelming^{28,40}. Temozolomide and fotemustine were both selected for MBrM trials due to their ability to cross the BBB and the pre-clinical evidence showing activity in extracranial melanoma^{28,40}. Temozolomide was tested in a phase II trial in patients with MBrM who had

received no previous radiotherapy and showed a response rate (RR) in six percent of patients²⁸. Fotemustine did not fare any better; in a randomised phase III trial, the RR was also six percent. These therapies were, however, more effective than dacarbazine, which showed no response at all⁴⁰.

1.4 A new direction in the treatment of melanoma brain metastases

Previously, Hanahan and Weinberg proposed six biological functions that cancer cells acquire to allow tumour formation: i) 'sustaining proliferative signalling'; ii) 'evading growth suppressors'; iii) 'activating invasion and metastasis'; iv) 'enabling replicative immortality'; v) 'inducing angiogenesis' and vi) 'resisting cell death'⁴¹. This concept was re-evaluated and updated with four new hallmarks in 2011, thus resulting in new avenues for treatment options⁴². 'Avoiding immune destruction' has now been accepted as a fundamental aspect in cancer development, along with the realisation that the immune system can be reinvigorated to eradicate cancer⁴². While there has been evidence that the immune system can eliminate cancer from as early as the 1890s, it has not been until more recently that the belief emerged that harnessing the immune system can be an effective treatment option^{43,44}.

1.5 Understanding the tumour microenvironment

Tumours are no longer thought of as masses of cancerous cells but as complex structures comprised of numerous types of cells⁴². Due to the complexity of the tumour microenvironment (TME) and the ability of cancer to alter the functions of its comprising cells, each cell type must be considered individually in terms of the role they can play to promote tumour growth and how this can be overturned.

1.5.1 Cancer cells

As the instigators of the disease, cancer cells are the source of a tumour and the driving force behind its progression. While they are immensely important in sustaining the tumour, they can make up as little as 30% of the tumour mass⁴⁵. Although cancer cells were originally viewed as a homogenous population, in reality, they are extremely heterogeneous as a result of hyper-proliferation and increasing numbers of mutations^{46,47}. This process results in distinct subpopulations that clonally expand to give rise to the tumour^{46,47}.

Even though cancer cells may not make up the bulk of the tumour mass, they contribute to the recruitment of various cells which compose the remainder of the tumour⁴⁵. This occurs through various mechanisms, as does the differentiation of immune cells to a more pro-tumourigenic phenotype⁴⁸. These mechanisms will be described in the following sections in more detail.

1.5.2 Endothelial cells

The stroma of the tumour, in some cases, can make up the bulk of a tumour, consisting of endothelial cells (ECs), fibroblasts and immune cells⁴⁹⁻⁵¹. The brain TME lacks fibroblasts and contains other brain-resident cells, for example, astrocytes. ECs are the cells that make up the vasculature of the blood and lymphatic vessels throughout the body, including tumours⁴⁹.

Tumour endothelial cells (TECs) form the vessels throughout the tumour, although these vessels are known to be morphologically abnormal⁵². Tumour blood vessels are characterised by chaotic branching and leakiness⁵². These vessels can be poorly perfused and others can have reversing blood flow, contributing to the hypoxic TME⁴⁹. The lymphatic vessels are comprised of cells similar to ECs; however, these vessels are normally non-functional and collapsed⁵³. There have been reports of functional lymphatic vessels at the periphery of the tumour and these have been associated with metastasis, as they provide a direct route to draining lymph nodes⁴².

1.5.3 Natural killer cells

Natural killer (NK) cells are innate lymphoid cells (ILCs) and form part of the innate immune system, the body's first line of defence⁵⁴. NK cells were the first ILCs discovered and have the ability to spontaneously lyse tumour cells without the need for activation by other immune cells and without major histocompatibility class (MHC) restriction⁵⁵. NK cells have an important role in the formation of cancer, as demonstrated by a Japanese longitudinal study where there was a substantial increase in cancer incidences in people with a lower NK cell cytotoxicity function over the 11-year period of the study⁵⁶. In addition, patients with a higher infiltration of NK cells in a number of solid tumours tend to have a better prognosis^{57,58}. NK cells are known to exert their cytotoxic effect through the release of perforin- and granzyme-mediated killing and through the activation of the caspase pathway⁵⁴.

NK cells detect their targets through a range of inhibitory, activating, adhesion and cytokine receptors, that allow them to distinguish the normal functioning cells from cells under stress⁵⁴. The cytolytic function of NK cells is highly controlled to prevent the unnecessary destruction of healthy cells, an example of this is through the expression of natural cytotoxicity receptors (NCRs)⁵⁹. When cells become 'stressed', they upregulate ligands that bind to NCRs, signalling to the NK cell that there is a problem⁵⁹. This can be illustrated by the binding of NKG2D ligands expressed by 'stressed' cells to the NK cell receptor, NKG2D⁵⁹. As cancer cells are not normally functioning cells, they respond to this 'stress' by expressing the cell-surface ligand B7-H6, a target for NCRs, more specifically, NKp30^{55,60}. B7-H6 has been found to be expressed on a number of malignancies, including lymphomas, leukaemias, carcinomas and melanomas⁵⁴.

Another mechanism that NK cells have adopted to locate their targets is through the expression of inhibitory receptors specific for MHC I molecules^{48,54}. As these receptors and ligands are highly polymorphic and encoded by numerous genes, NK cells must discriminate between self and non-self in an environment where self can vary between individuals⁵⁴. NK

cells become 'educated' through the engagement of their MHC I inhibitory receptors, which results in the maturation of a functional NK cell population that is adapted to their surrounding MHC I⁶¹⁻⁶³.

Tumours develop various mechanisms to avoid NK cell-mediated death as it is common for cancer cells to lose their MHC I molecule expression, making them a prime target for NK cell killing⁶⁴. It has been suggested that cancer cells can exploit 'gaps' in the NK cell's inhibitory repertoire by expressing non-classical MHC molecules, such as human leukocyte antigen (HLA)-G⁶⁴. Tumours such as melanoma take a different approach by upregulating MHC I expression to avoid NK cell-mediated death⁶⁵. Additionally, tumours can suppress NK cell function through the downregulation of NK cell-attracting chemokines, such as C-X-C motif chemokine ligand (CXCL)-2⁶⁶. Tumours can also affect the expression of NCRs as a result of the hypoxic TME by drastically decreasing the expression of NCRs. Moreover, cancer cells can also produce transforming growth factor beta (TGF- β) which has a negative effect on NK cell function by reducing their cytolytic activity⁶⁷. Furthermore, the constant exposure of NK cells to tumour antigens can result in antigen tolerance, characterised by the expression of T-cell immunoglobulin- and mucin-domain-containing-molecule-3 (TIM-3), which can end in NK cell exhaustion and loss of function⁶⁸.

There is also evidence of NK cells being repurposed by tumours via an alteration in NK cell phenotype from a cytotoxic function to a pro-angiogenic phenotype⁵⁵. This change in cell characteristic is believed to be induced by the hypoxic TME and the increase in production of TGF- β . This phenotypic modulation results in an increase in local production of vascular endothelial growth factor (VEGF), promoting tumour growth⁵⁵. There is evidence that these altered NK cells can also inhibit T-cell infiltration into the TME, further promoting a pro-tumourigenic environment⁴⁸.

1.5.4 Cytotoxic T-cells

T-cells play an essential role in immunoediting in response to therapy and are the cells that are associated with a long-term immune response⁴⁸. The T-cell family makes up a significant proportion of tumour-infiltrating lymphocytes (TILs) and are comprised of three distinct populations⁶⁹, each playing their own role. T-cells are distinct from other TILs based on their cluster of differentiation (CD) 3 expression and are further categorised by their expression of additional CD molecules⁶⁹. CD8⁺ cytotoxic T-cells (CD8⁺ T-cells) are one of the main effector populations that are responsible for an immune-based anti-tumour response^{70,71}.

CD8⁺ T-cells are believed to control local tumour growth through direct cytolytic killing of cancer cells via granzyme B- and perforin-mediated mechanisms or through the secretion of cytokines, such as interferon gamma (IFN- γ) or tumour necrosis factor alpha (TNF- α)^{72,73}. High numbers of tumour infiltrating CD8⁺ T-cells have been associated with a positive prognosis in a number of cancers, including melanoma, breast, ovarian and colorectal^{45,74-78}. Moreover, patients without metastases and a low level of CD8⁺ T-cell infiltration have been shown to have a poorer prognosis than patients with metastases and a high level of CD8⁺ T-cells⁷⁹.

Unlike NK cells, CD8⁺ T-cells are a part of the adaptive immune response and, therefore, must be 'educated' to recognise and respond to their targets⁵⁴. This 'education' occurs through the presentation of tumour-specific antigens (TSAs) or tumour-associated antigens (TAAs) by antigen presenting cells (APCs)^{48,80} (Figure 1.3). APCs present TSAs or TAAs to naïve T-cells at the lymph nodes, resulting in the activation of these cells against the specific antigens^{48,80}. It has been shown that CD8⁺ T-cells can recognise tumour-specific peptides with a single amino acid mutation⁴⁵. A

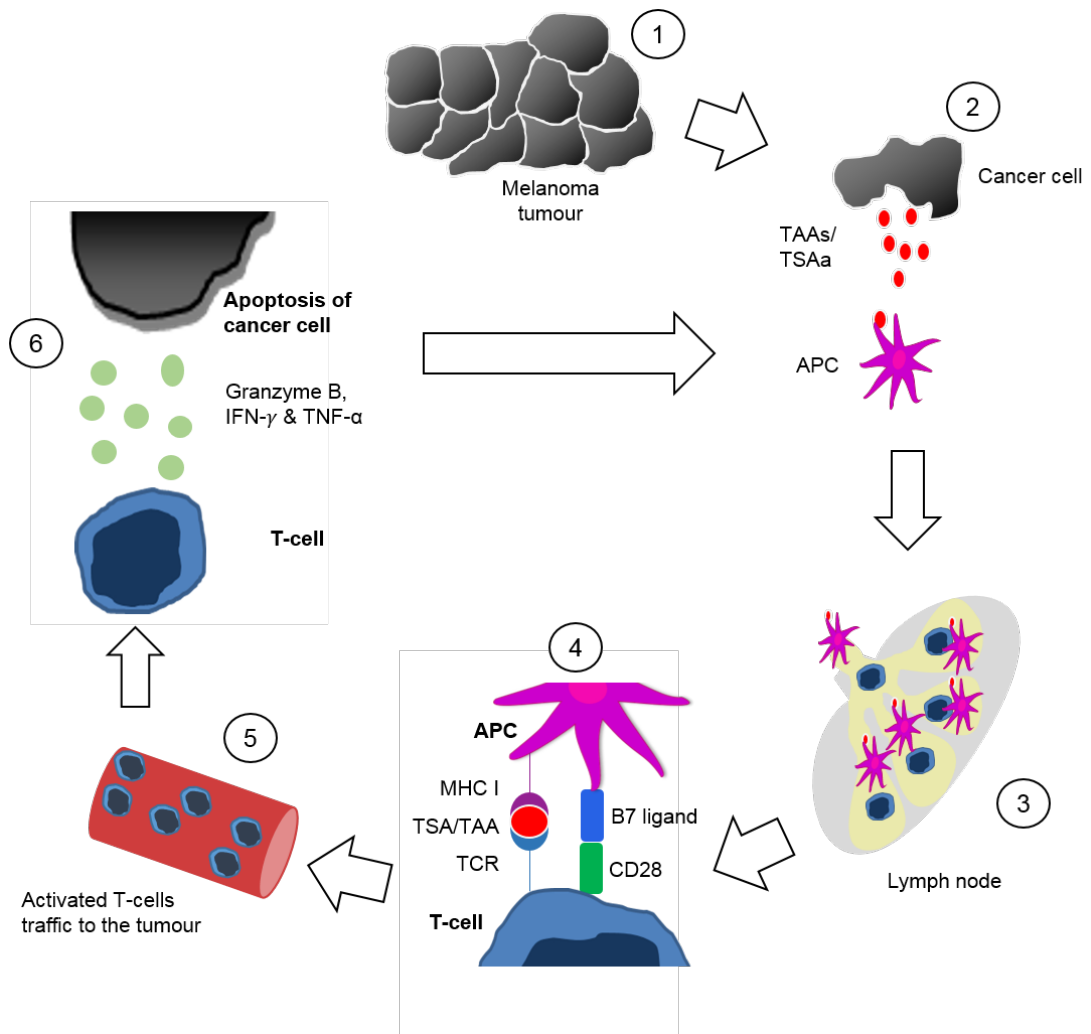


Figure 1.3 Adaptive immune system-mediated cancer cell death
(1) Upon death, cancers release a number of TAA and/or TSA. **(2)** These are internalised by APCs where they are subsequently processed into peptides and presented on MHC (I/II) molecules. APCs, such as DCs, will mature in response to this process, enabling their migration to the tissue draining lymph nodes **(3)**. Once at the lymph nodes **(4)**, DCs are able to activate naive T-cells through the co-stimulation receptors CD28 and TCR. **(5)** When activated T-cells become primed against the particular TSA/TAA that was responsible for their activation, they are able to enter the circulation where they will traffic to the tumour and elicit a cytotoxic response. **(6)** T-cells release a number of cytokines resulting in the activation of the caspase pathway and cancer cell apoptosis, followed by the release of additional TSAs and TAAs. There is evidence that a second antigen-presentation stage occurs at the disease site by tissue-resident APCs; this 'second touch hypothesis' is believed to be essential for CD4⁺ T-cell maturation.

number of studies have also demonstrated that responses to immunotherapies in melanoma, bladder and lung cancer may be specific to TSAs^{48,81}. This has been further supported by the evidence that patients with an increased mutational load have a prolonged survival⁸². In the case of TAAs, studies with melanoma patients have demonstrated that the recognition of the mutated form of p53 results in tumour-specific CD8⁺ T-cells⁸³. It has been suggested that this recognition is a result of excess levels of the antigen or the increased presentation as a result of cancer cell death⁸³.

An additional important feature of the CD8⁺ T-cell population is their ability to elicit a memory response that is characterised by their expression of CD45RO⁸⁴. An infiltration of memory CD8⁺ T-cells into tumours has been linked with a beneficial prognosis and there is evidence demonstrating that patients with an increased infiltration of memory CD8⁺ T-cells into the tumour core have a lower incidence of relapse^{79,85,86}.

Nonetheless, cancer cells have developed mechanisms in order to protect themselves from the cytotoxic effects of the CD8⁺ T-cells. Cancer cells can mount a direct defence, through the expression of inhibitory ligands, to suppress CD8⁺ T-cell activation (discussed further below)⁸⁷⁻⁸⁹. Cancer cells can also suppress CD8⁺ T-cell function through the secretion of interleukin (IL) -10 and TGF- β ⁹⁰⁻⁹². Furthermore, cancer cells recruit various immune cells and repurpose them to increase levels of immunosuppression within the TME^{42,48}.

1.5.5 T-helper cells

Aside from CD8⁺ T-cells, the remainder of the CD3⁺ T-cell family is comprised of CD4⁺ T-helper cells (CD4⁺ T-cells)^{69,93}. The CD4⁺ T-cell population is further divided based on the expression of Forkhead Box P3 (FoxP3), into the effector (FoxP3⁻) cells and the regulatory (FoxP3⁺) T-cells (T-Regs)^{69,93}. The CD4⁺ effector cells can then be further subdivided into

three main groups, each with a different function: T_{H1} , T_{H2} and T_{H17} . However, it is worth noting that $CD4^+$ T-cells are described as being 'plastic' as they can change their phenotype in response to the cytokines in the environment^{45,94}.

T_{H1} cells are able to facilitate the activation of $CD8^+$ T-cells and macrophages through the production of $IFN-\gamma$ and IL-2 to promote an anti-tumour response^{94,95}. T_{H2} cells, on the other hand, assist in the activation of B-cells through the production of IL-4, IL-5 and IL-6, resulting in B-cell proliferation and antibody production^{94,95}. T_{H17} cells can exert an anti- or pro-tumourigenic effect, depending on the cytokine milieu present in the environment⁹⁶. In the presence of IL-12, T_{H17} cells can differentiate into T_{H1} cells, gaining the ability to produce $IFN-\gamma$, allowing for an increase in $CD8^+$ T-cell stimulation. T_{H17} cells can also facilitate an improved immune response in cancer patients by producing granulocyte-macrophage colony-stimulating factor (GM-CSF), $TNF-\alpha$, IL-8 and IL-10⁹⁶. To defend against this, $TGF-\beta$, secreted by cancer cells results in T_{H17} cells adopting a regulatory phenotype and can stimulate the recruitment of T-Regs into the TME⁹⁷. In addition, T_{H17} cells can initiate FoxP3 and retinoic acid related orphan receptor (ROR) γ -t expression, resulting in $CD8^+$ T-cell inhibition, further promoting tumour growth⁹⁷.

1.5.6 Regulatory T-cells

T-Regs are the final subtype of $CD4^+$ T-cells and are a relatively rare population, making up less than five percent of the leukocyte population⁹⁸. Although T-Regs are a small population, they can have a significant effect on the immune system, an effect that is exploited by cancer cells^{45,71}. An increased infiltration of T-Regs into the TME has been associated with a poor outcome in patients, as has the ratio of $CD8^+$ T-cells or $CD4^+$ effector cells to T-Regs within the TME⁷⁸. A large infiltration of T-Regs into a tumour has also been linked to higher incidence of relapse⁷⁸. On the contrary, it should be noted that, in the case of colorectal cancer and a number of lymphomas, an increase in T-Regs has been associated with a better

prognosis⁷⁸. As highlighted by *in vivo* models lacking T-Regs, which demonstrated a robust anti-tumour immune response, T-Regs play a significant role in the initiation and growth of tumours^{99,100}.

It has been described that T-Regs have the ability to suppress the anti-tumour effect of a range of immune cells, including CD8⁺ T-cells, CD4⁺ T-cells, NK cells, B-cells and APCs^{101,102}. As previously discussed, T_H17 cells can promote the infiltration of T-Regs into the TME. This is thought to occur through cancer cell- and macrophage-derived C-C motif chemokine ligand (CCL) -22 binding to the C-C motif chemokine receptor (CCR) -4^{48,94}. It is believed that once T-Regs are recruited to the TME, they become activated through recognition of TAAs or self-antigens released by dying tumour cells¹⁰³. Upon activation, T-Regs expand and will selectively suppress the activation of TAA-specific T-cells (both CD8⁺ and CD4⁺ cells)¹⁰³. This suppression is achieved through the production of IL-10 and TGF-β, thus preventing cancer cell death and, in turn, further increasing the immunosuppression through the conversion of T_H17 cells into regulatory cells⁹⁷. There is also evidence of T-Regs eliminating effector CD4⁺ T-cells in a granzyme-B-dependent killing manner^{104,105}.

1.5.7 B-cells

B-cells are not commonly found within the TME; however, they can be found at the invasive margins of tumours¹⁰⁶. B-cells are more commonly found in adjacent lymphoid structures to the tumour or in the draining lymph nodes¹⁰⁶. While there is still much to be discovered about the exact role that B-cells play in the TME in humans, B-cell infiltration has been associated with a good prognostic outcome in some breast and ovarian cancers^{107,108}.

Conversely, in mouse models, B-cells have been shown to inhibit tumour-specific CD8⁺ T-cells. In a genetic model of skin cancer, B-cells and immunoglobulin deposits were found to promote tumour growth. Moreover, an immunosuppressive population of B-cells, known as regulatory B-cells (B-

Regs) has been described^{109,110}. B-Regs are challenging to distinguish from other B-cells due to the lack of specific cell surface markers; on the other hand, it is possible to distinguish them based on their production of IL-10^{106,111}. B-Regs have been implicated in an increase in tumour burden and immune inhibition in a model of inflammation-induced skin cancer and in a breast cancer lung metastases model^{112,113}. Nevertheless, it should be noted that these effects are not due to B-Reg infiltration into the TME; instead they are found in the draining lymph nodes where they appear to influence other immune cells^{112,113}.

1.5.8 Dendritic cells

Dendritic cells (DCs) are bone marrow-derived cells (BMDCs) and can be found in all tissues⁸⁰. DCs are essential in the adaptive immune response, playing the role of APCs. They are extremely efficient in this capacity as compared to other APCs and have been referred to as 'professional APCs'⁸⁰. There are two major types of DCs in humans and mice: myeloid DCs (mDCs; also referred to as conventional DCs) and plasmacytoid DCs (pDCs)^{80,114}. While DCs are mainly involved in the activation of T-cells, they have been shown to activate NK cells, resulting in a potent cytotoxic response to cancer cells¹¹⁵. There is also evidence showing DCs can adopt a cytotoxic phenotype¹¹⁶.

DCs are found in two forms: immature and mature^{80,114}. DCs in the peripheral tissue tend to be classed as immature cells and are proficient in capturing antigens, have a limited ability to secrete cytokines and express low levels of co-stimulatory molecules and unique chemokine receptors¹¹⁷. These include CCR7, a receptor essential for the trafficking of DCs to lymph nodes¹¹⁷. Whilst immature DCs can induce immune tolerance through T-cell deletion or the expansion of T-Regs¹¹⁴, DCs will rapidly mature in response to environmental signals through the activation of their CD40 receptor, which initiates the process of their differentiation¹¹⁴. Upon maturation, DCs downregulate their antigen-capture function, produce cytokines, increase expression of MHC II molecules and co-stimulatory receptors¹¹⁴.

DCs can capture antigens through a number of mechanisms and then migrate from the tissue to the draining lymph nodes¹¹⁷. Here, the DCs process antigens into peptides that are presented on cell-surface MHC I and MHC II molecules⁸⁰. Antigens can also reach lymph node-resident DCs via the lymph.¹¹⁸ Distinct T-cell responses are created depending on the location at which the antigens are captured by the DCs^{80,114}. Antigen-loaded DCs from the tissue then trigger the differentiation of antigen-specific T-cells to become effector T-cells with unique cytotoxic abilities and the capability to produce cytokines^{80,114}. In contrast, antigen-loaded DCs resident in the lymph nodes will primarily present antigens to CD4⁺ T-cells, resulting in IL-2 production and T-cell priming which leads to T-cell proliferation and clonal expansion¹¹⁸. These activated CD4⁺ T-cells can subsequently be differentiated into effector cells upon antigen presentation from tissue-resident DCs¹¹⁸.

Cancer cells have developed a number of mechanisms to interfere with the antigen-presentation process. The tumour-derived secretion of macrophage colony-stimulating factor (M-CSF; also known as colony-stimulating factor-1 (CSF-1)) and IL-6 skews the differentiation of monocytes to become macrophages rather than DCs¹¹⁹. In addition, tumour-derived glycoproteins, carcinoembryonic antigen (CEA) and mucin 1 (MUC1) are endocytosed by DCs; however, they become confined to early endosomes resulting in poor antigen presentation¹²⁰. Through the secretion of IL-10, cancer cells can cause antigen anergy, preventing DC maturation¹²¹. Likewise, tumour-derived factors can interfere with mDC maturation, resulting in a pro-tumourigenic phenotype. An example of this is thymic stromal lymphopoietin (TSLP), which stimulates DCs to secrete OX40 ligand (OX40L) to promote T_H2 cell differentiation⁸⁰. This, in turn, promotes the secretion of IL-4 and IL-13, stimulating macrophages to secrete epidermal growth factor (EGF), promoting cancer cell proliferation⁸⁰. Cancer cells can also inhibit interferon alpha (IFN- α) secretion through the stimulation of toll-like receptors (TLRs) on pDCs. As the cross-presentation of antigens is type I IFN-dependent, the reduction in IFN- α can prevent T-cell differentiation into effector cells¹¹⁴.

1.5.9 Macrophages

Tumour-associated macrophages (TAMs) are inflammatory immune cells present within the TME during all stages of tumour development and can make up 50% of a tumour's mass¹²². TAMs originate from monocytes in the circulation that are recruited to the tumour by tissue-resident macrophages or by tumour- or stroma-derived factors, such as CCL2¹²³. Additionally, the hypoxic TME, combined with VEGF, has been linked to macrophage recruitment¹²³.

Macrophages can be categorised based on their cytokine production. The 'classical' M1 macrophages produce T_H1 cytokines, resulting in anti-tumour immune responses¹²⁴. Macrophages become polarised towards the M1 phenotype in response to typical T_H1 cytokines, such as IFN- γ . M1 macrophages are classified by the high production of IL-12 and the low secretion of IL-10.¹²⁴ M1 macrophages produce effector molecules such as reactive oxygen and nitrogen intermediates, in addition to other inflammatory cytokines, including TNF- α and IL-1 β . They can also contribute to an anti-tumour response through the secretion of chemokines such as CXCL9 and CXCL10 which attract T_H1 lymphocytes¹²⁴.

On the other hand, the 'alternatively activated' M2 macrophages release T_H2 cytokines, including IL-6, IL-10 and TGF- β , promoting a pro-tumourigenic response¹²⁵. Within the TME, TAMs tend to present with the M2-like phenotype, due to the hypoxic surroundings and the factors secreted by T-Regs and DCs, such as IL-4¹²⁵. It has been shown that TAMs can first occur with an M1 phenotype and then switch to the M2 profile as a result of IL-4 secretion, in addition to cancer cell-derived M-CSF⁴⁸. Conversely to M1 macrophages, M2 TAMs produce very little IL-12 and produce high levels of IL-10¹²⁵. M2 TAMs are extremely poor at antigen presentation and they also express programmed death ligand-1 (PD-L1) and, as result, can directly inhibit CD8⁺ T-cells¹²⁶. *In vivo* models have demonstrated that TAMs with low levels of MHC II expression are associated with tumour growth and the

secretion of M2-related cytokines, whereas the MHC II^{high} population are linked to the M1 anti-tumourigenic response¹²⁷.

TAMs also play a significant role in the maintenance and growth of tumours. TAMs secrete growth factors such as EGF, VEGF and basic fibroblast growth factor (bFGF), promoting tumour growth¹²³. TAMs are heavily involved in the invasion and metastasis of cancer cells via the production of proteases, such as cathepsins, matrix metalloproteinases (MMP)-2 and MMP-9, which are responsible for the remodelling of the extracellular matrix (ECM)¹²⁸. Furthermore, TAMs promote angiogenesis and lymphangiogenesis through the secretion of VEGF, platelet-derived growth factor (PDGF), thymidine phosphorylase and CXCL8^{122,128}. TAMs also play a substantial role in the immunosuppression of the TME; they can suppress CD8⁺ T-cell activity through the production of arginase-1 (Arg-1), depleting the TME of arginine¹²⁴. Furthermore, the production of IL-10, inducible nitric oxide synthase (iNOS) and indoleamine-2, 3-dioxygenase (IDO) suppress the anti-tumour immune response alongside the expression of PD-L1, resulting in direct inhibition of CD8⁺ T-cells¹²⁴.

The prognostic significance of TAM infiltration into tumours is not as clear cut as other immune cells. A high infiltration of TAMs has been linked with a poor outcome in breast, cervical, bladder and gastric cancers¹²⁹. In contrast, a high infiltration of TAMs has been a positive prognostic marker in colorectal cancer and high-grade osteosarcoma¹²⁹.

1.5.10 Myeloid-derived suppressor cells

Myeloid-derived suppressor cells (MDSCs) are undifferentiated, immature myeloid cells and are commonly found in tumours^{130,131}. MDSCs are responsible for maintaining normal tissue homeostasis in response to infections and traumatic stress^{130,131}. Tumours recruit these cells early-on during tumour development and use their immunosuppressive abilities to promote tumour growth^{130,131}.

MDSCs suppress T-cell activity through a number of mechanisms. MDSCs produce nitric oxide (NO) and reactive oxygen species (ROS), resulting in T-cell apoptosis, inhibition of anti-tumour T-cell cytokine production, the blocking of T-cell receptors (TCRs) which leads to inhibition of T-cell migration and, thus, the apoptosis of cancer cells and the nitration of chemokines¹³¹. MDSCs express TGF- β 1 on their cell surface, leading to effector T-cell anergy. MDSCs can also influence a number of T-cell functions, such as the reduction of T-cell migration to lymph nodes through L-selectin downregulation¹³¹. There is also evidence to show that MDSCs downregulate the expression of TCR zeta-chain, resulting in the inability of T-cell membrane signal transmission¹³¹.

The production of NO by MDSCs can also induce chemoresistance in cancer cells, as NO can inactivate the caspase cascade, preventing cancer cell death¹³¹. Moreover, MDSCs can produce the same factors as TAMs, promoting angiogenesis, tumour growth and skewing of the immune system towards a T_H2 phenotype¹³¹. In general, a high infiltration of MDSCs is associated with a poor prognosis¹³².

1.5.11 Neutrophils

Neutrophils are one of the main components of blood; however, due to their limited life span and their fully differentiated phenotype, the role of neutrophils in cancer has previously been considered insignificant¹²⁴. In spite of this, tumour-associated neutrophils (TANs) have been confirmed to exert a pro- or anti-tumourigenic effect¹²⁴. Similarly to TAMs, *in vivo* evidence has suggested that neutrophils can be polarised toward these phenotypes in response to tumour-derived signals¹³³. In many ways, TANs act in a comparable way to TAMs in the TME, resulting in the naming of the 'N1' and 'N2' phenotypes¹³³.

In vivo models have revealed more about 'N1' TANs and how they can assume a cytotoxic phenotype. In the absence of TGF- β , TANs have the potential to eliminate cancer cells and inhibit tumour growth¹³³. Through the secretion of MMP-8, neutrophils have been shown to prevent tumourigenesis¹³³. There is also *in vitro* and *in vivo* evidence demonstrating the direct killing of cancers by neutrophils through superoxide anion generation, production of neutrophil elastase (NE) and phagocytosis¹²⁴. There does appear to be differences in the ability of neutrophils to lyse primary and metastatic tumours with the effects against the latter being less efficient¹²⁴.

'N2' TANs are recruited to the TME by cancer cells themselves, through the secretion of granulocyte stimulating-colony factor (G-CSF) and CXCL2¹³³. Tumour-derived GM-CSF has been observed to prevent TAN-mediated apoptosis and to have a priming effect, inducing neutrophilia. TANs have been shown to secrete oncostatin-M under the influence of cancer cells which, in turn, promotes the secretion of VEGF by cancer cells¹³³. Gene analysis of TANs have revealed that cytotoxic pathways used by neutrophils are severely downregulated in TANs and that TGF- β can prevent neutrophil degranulation, although the phagocytosis pathway appears to be unaltered in TANs¹³³. In addition, there is evidence that the tumours can prevent TAN-mediated apoptosis through the upregulation of nuclear factor-kappa B (NF κ B)¹²⁴. Like their TAM counterparts, TANs play a role in angiogenesis and tumour growth through the secretion of chemokines and MMPs¹²⁴. TANs have also been linked to the metastasis of melanoma to the lungs, as they have been shown to augment the ability of cancer cells to pass through the endothelium¹²⁴.

The infiltration of TANs has been associated with a poor clinical prognosis in colorectal, hepatocellular carcinoma and bronchioloalveolar carcinoma, to name just a few^{124,134}. TAN infiltration has also been linked to more aggressive gliomas and pancreatic tumours¹²⁴. Nevertheless, as with most immune cells, the prognostic significance of this tends to vary depending on

tumour type, as a high TAN infiltration has been associated with a better prognosis in gastric cancer^{124,134}.

1.6 Brain tumour microenvironment

The central nervous system (CNS) has always been described as being an immune-privileged site¹³⁵. This has been demonstrated by the injection of immunogenic material, such as cancer cells with non-self-antigens, into the brain parenchyma. These cells did not elicit an adaptive immune response as they would have if injected outside of the CNS¹³⁵; however, it should be noted that immune privilege does not mean that an immune response will never occur¹³⁵.

Immune cells are found within the brain and CNS^{135–137}; it has been proposed that the interstitial fluid of the CNS drains into the cerebral spinal fluid (CSF) within the subarachnoid space (SAS). It is believed that antigens within the CSF are detected by APCs in the SAS¹³⁸. Additionally, antigens within the CSF are thought to travel to the nasal mucosa where they can accumulate in the deep cervical lymph nodes (DCLNs)¹³⁹. In this case, the CSF is thought to act as lymph. Nevertheless, more recently it has been revealed that the mouse brain does in fact have lymphatic vessels that line the dural sinus and these vessels are connected to DCLNs¹⁴⁰ (Figure 1.4). These two processes, in combination, are likely to contribute to the immune surveillance of the brain and CNS.

TILs were first reported to be found within human glioma samples in 1960¹⁴¹. Another study investigated TILs in glioma using human post-mortem tissue and found significant infiltration of TILs in about one third of the samples; another third demonstrated a slight infiltration and in the remaining samples there was no evidence suggesting TIL infiltration¹⁴². It was also noted that TIL infiltration was associated with higher grades of disease¹⁴². This finding

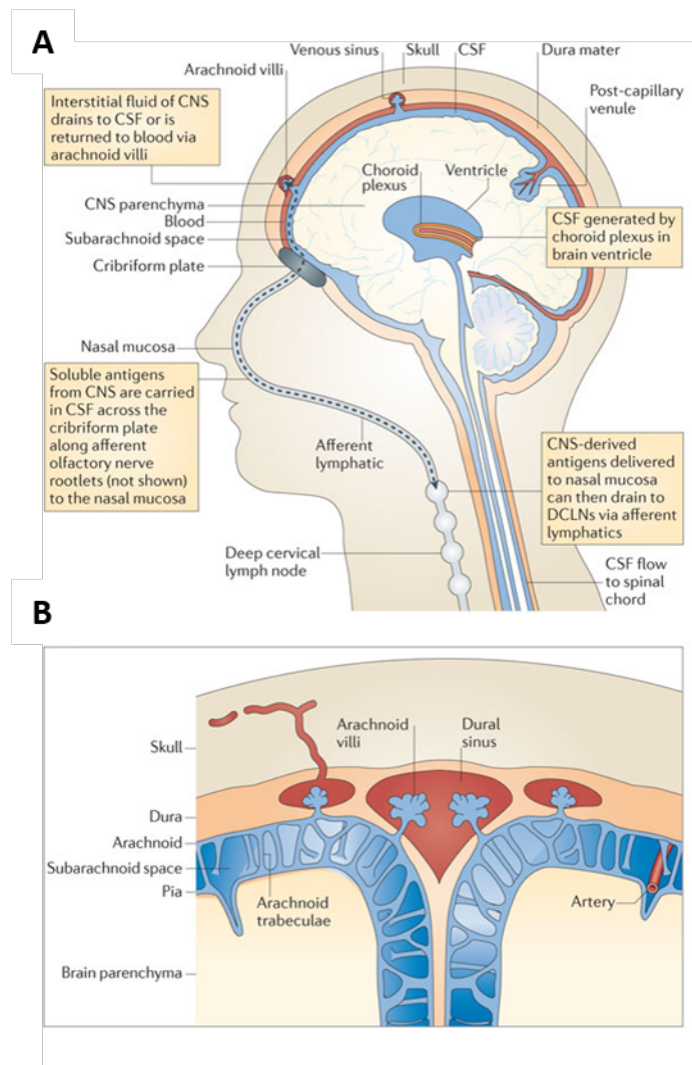


Figure 1.4 Drainage of antigens within the brain to the lymph nodes

(A) Interstitial fluid within the CNS can contain soluble antigens, **(B)** this fluid can subsequently return to the blood through the arachnoid villi or drain into the CSF. The CSF is continuously produced by the choroid plexus and it is believed to be reabsorbed into the lymphatics where it drains to the DCLNs via the nasal mucosa¹³⁵. Reprinted by permission from Macmillan Publishers Ltd: The anatomical and cellular basis of immune surveillance in the central nervous system. *Nat Rev Immunol.* 2012;12(9):623-635.

Doi:10.1038/nri3265, copyright 2012

was supported by other studies which additionally observed a variation in the expression CD8⁺ and CD4⁺ T-cells between tumour samples¹⁴¹. Moreover, the infiltration of TILs into gliomas has yet to be associated with either a beneficial or poor outcome¹⁴³.

T-cells are not the only immune cells found within the CNS; DCs have been isolated from the CSF of patients suffering from neurological diseases¹⁴⁴. DCs can be found within the brain parenchyma and are localised close to the myeloid cells rather than neurons¹⁴⁴. It is thought that DCs are involved in immune surveillance and have been investigated in the context of an autoimmune encephalomyelitis model, where it was demonstrated that they could prime an inflammatory response from T-cells at the onset of the disease. However, DCs appear to become less efficient as the disease progresses¹⁴⁴. There is evidence showing that these DCs are unable to reactivate the disease-affected T-cells and that, for this process, DCs from the periphery are required¹⁴⁴.

Due to the previous lack of focus on the treatment of brain tumours as a whole, relatively little is known about the infiltration of immune cells into BrM. Nevertheless, the information that is available reveals that immune cells are able to reach tumours within the brain parenchyma, mostly in models of multiple sclerosis, giving hope that an immunotherapy could have a therapeutic effect^{145,146}. There are, however, other obstacles that must be taken into consideration first, such as the BBB and immune cells that are exclusive to the brain.

1.6.1 Blood-brain barrier

The BBB is a unique, selectively permeable tissue that surrounds the blood vessels to separate the extracellular fluid of the brain from the blood in circulation^{137,147}. The BBB limits the brain to the exposure of antigens and molecules in the circulation that could potentially alter the delicate brain environment¹⁴⁸. The BBB hinders the detection of early stage malignancies,

as the contrast agents used for magnetic resonance imaging (MRI) are unable to cross the BBB unless it has been compromised¹⁴⁹. This occurs as tumours grow; however, this is linked to a poor prognosis¹⁴⁸⁻¹⁵⁰.

The BBB is comprised of ECs connected by tight junctions, which prevent the free movement of small molecules and metabolites from the blood, with the exception of glucose and a number of immunoglobulins^{148,151}. This process is controlled by the astrocytes and pericytes that are resident in the perivascular space and are responsible for the maintenance of the BBB and the regulation of capillary blood flow¹⁵². Pericytes control the permeability of the BBB through signalling pathways, with ECs using PDGF- β and TGF- β , resulting in a decrease in the permeability of the BBB¹⁵².

As previously described, the BBB remains intact during the early stages of tumour growth; conversely, as some tumours begin to increase in size, the blood vessels within the brain can become leaky¹⁴⁹. This feature has been linked to the dissociation of pericytes and astrocytes (that also play a role in the BBB tightness)¹⁵². An investigation into this process revealed that the blood vessels are more permeable than normal brain blood vessels in the vast majority of brain tumours^{148,150}. Further to this, a study revealed that in spite of this increase in BBB permeability, the uptake of paclitaxel and doxorubicin in the brain was lower than 15% of the uptake observed in extracranial metastatic lesions¹⁵³. This indicates, that even when compromised, the permeability of the BBB is still significantly lower than the permeability of the extracranial blood vessels.

Research into other diseases of the CNS has revealed more about the ability of T-cells to cross the BBB. This occurs through the interaction of the BBB ECs, which express intracellular adhesion molecule-1 (ICAM-1) and vascular cell adhesion protein-1 (VCAM-1), with activated T-cells expressing lymphocyte function-associated antigen-1 (LFA-1) and very-late antigen-4

(VLA-4)¹⁴⁶. Resting T-cells have also been shown to possess the ability to cross the BBB, although this is limited in comparison to activated T-cells¹⁴⁶. Additionally, *in vitro* studies have revealed that the process of migration of leukocytes across the BBB can, in itself, increase the permeability of the BBB, allowing for further transmigration¹⁴⁶. Likewise, TNF- α and IFN- γ have been revealed to increase the permeability of the BBB by upregulating the secretion of various chemokines that promote leukocyte adhesion and aid their migration across the BBB^{146,154,155}. TNF- α can also increase the expression of ICAM-1 and VCAM-1 to further increase the transmigration of T-cells.

1.6.2 Microglia

The brain contains a unique population of macrophages called the microglia that take up residency in the brain during embryonic development^{156,157}. It was found that microglia originate from primitive myeloid progenitor cells derived from the yolk sac¹⁵⁷. Microglia are long-lived cells and are believed to proliferate *in situ*¹⁵⁶. However, monocytes are able to infiltrate into the brain and differentiate into microglia-like cells¹⁵⁸. These cells are believed to make up a minority of the microglia due to the slow proliferative rate of monocytes in the brain parenchyma¹³⁷. In humans, microglia were previously unable to be distinguished from other macrophages in the brain; however, more recently, a cell-surface protein, transmembrane protein 119 (Tmem119), has been reported to be highly expressed specifically on microglia in humans and mice¹⁵⁹. On the other hand, in mice, microglia and macrophages can easily be distinguished from each other by their expression of CD45, with microglia being CD45^{low} and macrophages being CD45^{high}¹¹.

Microglia are the main effector cells of the CNS and are capable of stimulating an immune response^{160,161}. Once activated, microglia exist in two forms: in the first, microglia have hyper-dilated stellate morphology and express MHC I; these are referred to as 'activated' microglia^{160,161}. The

second type is known as the 'reactive' or 'amoeboid' microglia; these cells, as suggested by the name, have an amoeboid morphology and express MHC I and MHC II. Along with their increased antigen presentation capability, these cells also have an increased phagocytic activity^{160,161}. Microglia are responsible for maintaining the delicate homeostatic environment of the brain by controlling inflammation to prevent irreversible neurone damage¹⁶². Microglia have the ability to phagocytose apoptotic neurons and cellular debris, in addition to secreting cytokines in a manner to minimise inflammation¹⁶²

Once cancer cells begin to enter the brain, microglia respond immediately and have even been found to surround single cancer cells¹⁶³. Gliomas have been found to secrete a number of factors, such as macrophage chemoattractant protein (MCP)-1 and -3, G-CSF and hepatocyte growth factor (HGF), which could be responsible for the attraction of these cells¹⁶⁴⁻¹⁶⁶. It has been reported, however, that microglia and macrophages respond to different chemotactic stimuli¹⁶⁵. The number of macrophages and microglia within the TME is correlated to a higher vascular density. Macrophages and microglia are more common in higher-grade gliomas, such as glioblastoma multiforme (GBM)¹⁶⁷. Both cell types have been found to make up to 78% of cells in human gliomas and up to 70% of cells in BrM¹³⁷.

Similarly to macrophages in extracranial tumours, microglia can contribute to the suppressive intracranial TME^{168,169}. First of all, microglia have been found to express FAS ligand (FAS-L). FAS-L can induce apoptosis in Fas⁺ T-cells, thus reducing T-cell infiltration¹⁷⁰. Tumours can also suppress microglia function through the secretion of TGF- β and IL-10¹⁷¹. This suppresses the anti-tumourigenic functions of microglia by downregulating TNF- α and MHC II expression¹⁷².

1.7 Immunotherapies

As previously described, most immune cells have the potential to provoke some form of an anti-tumour response. Immunotherapies aim to take advantage of this to invoke cancer cell death¹⁷³. These can affect a single immune cell population or affect a number of populations at the same time¹⁷³. The main goal of immunotherapy is to provoke a durable and long-lasting immune response to prevent cancer growth and eventually eliminate the cancer and prevent any regrowth¹⁷³.

Cancer vaccines have been one type of immunotherapy that has been investigated to break the immune tolerance acquired by cancer cells. As a result, cancer vaccines focus on expansion and activation of the DC population^{48,80}. A drawback of this particular therapeutic approach is difficulty with the selection of the most appropriate antigen¹⁷⁴. Early trials used short peptides; however, these trials lacked an effective DC-activating adjuvant leading to disappointing outcomes. It was later shown that the effectiveness of the short peptide vaccines can be enhanced when administered with IL-2¹⁷⁵. Other approaches include the GVAX vaccine; this involved injecting an irradiated (to prevent replication) prostate cancer line that had been genetically-modified to produce GM-CSF. While early trials were promising, the vaccine failed in phase III as a result of a lack of clinical efficacy¹⁷⁶. The most promising approach has involved the isolation of DCs from the patient's peripheral blood mononuclear cells (PBMCs), stimulating them *ex vivo* and reinjecting them into the patient¹⁷⁷. This approach has also been applied to prostate cancer with sipuleucel-T, which involved the stimulation of DCs with GM-CSF and a fusion protein consisting of prostatic acid that has been linked to DC growth¹⁷⁷. The treatment resulted in a four-month increase in survival and, in 2010, was approved for use in the United States of America (USA) by the US Food and Drug Administration (FDA)¹⁷⁷.

Another emerging immunotherapy is the use of oncolytic viruses (OVs). OVs are naturally occurring or genetically-altered viruses that will selectively replicate within cancer cells¹⁷⁸. The aim of OV therapy is for the virus to

replicate within cancer cells, resulting in their death and the release of TSAs, provoking an immune response¹⁷⁹. A number of OV's are undergoing clinical trials including reovirus, Newcastle Disease Virus and herpes simplex virus (HSV)¹⁸⁰⁻¹⁸². In 2015, a modified HSV was FDA-approved under the name Talimogene laherparepvec (T-VEC) for the treatment of advanced melanoma. T-VEC demonstrated a 26% RR and was the first OV to be approved worldwide due to both this and its mild side-effects¹⁸⁰.

Adoptive cell transfer (ACT) is another promising immunotherapy and involves the isolation of lymphocytes from PBMCs, tumour draining lymph nodes or tumour tissue¹⁸³. These are expanded *ex vivo* and subsequently reinfused into the patient¹⁸³. ACT using TILs involves the reinfusion of TILs that have been expanded *ex vivo* with a cocktail of cytokines from resected tumour tissue¹⁸³. When combined with lymphodepletion, ACT of TILs has resulted in the complete regression of melanoma; the lymphodepletion is believed to enhance the therapy by eliminating immunosuppressive cells such as T-Regs and MDSCs and by increasing levels of IL-7 and IL-15¹⁸³.

One of the most successful immunotherapies to date uses chimeric antigen receptor (CAR) T-cell therapy. This therapy involves genetically altering patients T-cells to express receptors known as CARs, which allow T-cells to recognise TSA. These T-cells are then cultured, expanded and subsequently reinfused into the patient¹⁸⁴. This therapy has been extremely successful in the treatment of refractory B-cell leukaemia, where in a clinical trial of the 30 adults and children treated, 27 had a complete response, with 22 of these patients showing minimal or no residual disease. While seven of these patients relapsed, 19 were still in remission at the time the study was reported¹⁸⁵. There are risks with this type of therapy, as a fatality occurred in a trial studying HER2⁺ CAR T-cell therapy for GBMs, suggesting that CAR T-cells that target antigens ubiquitously expressed on normal tissue must be used carefully and in as low a dose as possible¹⁸⁶⁻¹⁸⁸.

1.7.1 Immunotherapies in brain tumours

Despite the presence of the BBB and the 'immune-privileged' status of the brain, there has been a focus on treating brain tumours with immunotherapies. Monoclonal antibodies have been developed to target antigens specifically expressed on glioma or antigens that are overexpressed on brain tumour cells¹⁸⁶. Bevacizumab is a humanised monoclonal antibody that targets VEGF and was the first monoclonal antibody approved for use for the treatment of GBM. Bevacizumab can be used as a monotherapy or in conjunction with radiotherapy where it has been shown to improve six-month progression-free survival (PFS) by 25-65%, due its ability to radiosensitise the tumour^{186,189}.

The epidermal growth factor receptor (EGFR) has also been targeted in this manner. Cetuximab was one of these agents; although its effectiveness was not to the level of bevacizumab, it is currently used to treat a number of extracranial cancers¹⁸⁶. Nimotuzumab proved to be more promising, with efficacy seen in both adults and paediatric tumours when combined with radiation¹⁹⁰. For adults, the median OS was 15 months and with the paediatric cohort, the median OS increased from four months to 10 months¹⁹⁰.

CAR T-cell therapy has also been a focus in the treatment of brain tumours. IL-13R α 2 is preferentially expressed on GBM cells, thus leading to the development of an IL-13 zetakine CAR. Intratumoural injections of zetakine CAR-expressing T-cells were seen to eliminate an orthotopic tumour established from patient cells expressing IL-13R α 2¹⁹¹. This work has translated into the clinic, where, in 2015, it was reported that three patients had received this treatment following surgical resection of their tumours. Two out of the three had no signs of tumour recurrence at the resection border (something that is commonly seen following surgical resection) as seen by MRI¹⁹².

1.8 Immune checkpoint inhibition

The immune system has a number of built-in mechanisms that prevent it from activating out of turn. Unfortunately, when this goes awry it can result in autoimmunity, where the immune system begins to attack healthy tissue¹⁹³. These mechanisms are commonly known as the immune checkpoints and are essential for maintenance of self-tolerance¹⁹³. Cancer cells have developed a number of mechanisms to hijack these inhibitory pathways for self-perseverance. This can result in the inhibition of the innate and adaptive immune systems, leading to a more immunosuppressed TME¹⁹³. To combat this new treatment, options are currently being investigated with the hope to overcome this inhibition. To achieve this, monoclonal antibodies have been developed to target specific cell-surface receptors that are known to negatively-regulate immune cell activation (mainly T-cells). The main targets of these new therapies are cytotoxic T-lymphocyte-associated protein-4 (CTLA-4) and programmed death protein-1 (PD-1)¹⁹³. Additional therapies are also being developed against other targets, such as lymphocyte activation gene-3 (LAG-3) and TIM-3^{194,195}.

1.8.1 Anti-CTLA-4

CTLA-4 (also known as CD152) was the first immune checkpoint to be investigated as a therapeutic target¹⁹⁶. CTLA-4 is exclusively expressed on T-cells and its main function is to regulate the early stages of T-cell activation¹⁹³. CTLA-4 acts as an inhibitory receptor to the co-stimulatory receptor CD28, which itself requires a co-stimulus from the TCR interacting with a MHC-bound antigen to elicit an activation response (Figure 1.5)^{197,198}. CD28 shares the same ligands as CTLA-4: B7.1 and B7.2 (also known as CD80 and CD86, respectively)¹⁹⁸. Both B7 ligands have a much higher affinity for CTLA-4 as compared to CD28, thus, a relatively low expression level of CTLA-4 can prevent T-cell activation¹⁹⁸.

While the exact mechanisms of action for CTLA-4 are not clearly understood, it is believed that due to the higher affinity for the B7 ligands, CTLA-4 outcompetes CD28 as well as producing an inhibitory response¹⁹³.

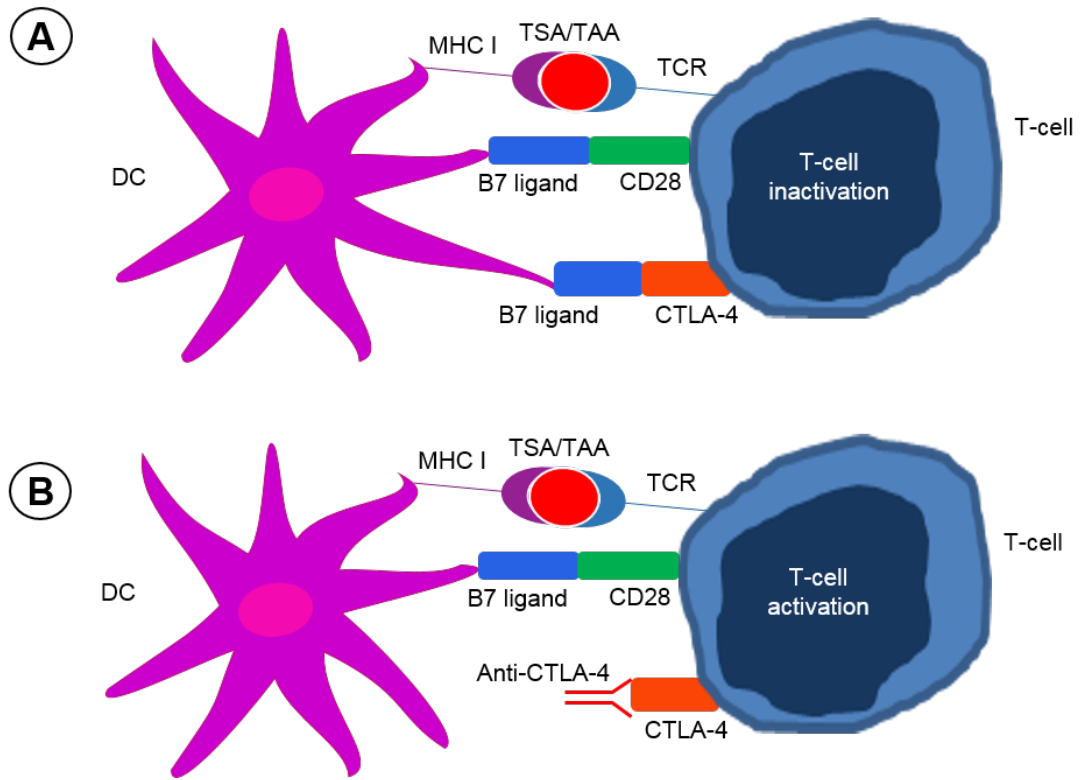


Figure 1.5 The reversal of CTLA-4-mediated T-cell inhibition via anti-CTLA-4 therapy

(A) T-cell activation requires the co-stimulation of the TCR along with CD28. The TCR is activated through the stimulation of MHC-bound peptides, while CD28 has two potential ligands. Collectively known as the B7 ligand family, B7.1 (CD80) and B7.2 (CD86) are expressed by a number of APCs (e.g. DCs). Nevertheless, B7 ligands will also bind to the inhibitory ligand CTLA-4 (CD152). The B7 ligands have a much higher affinity for CTLA-4 and will preferentially bind to this receptor resulting in T-cell inactivation. **(B)** In the presence of an anti-CTLA-4 antibody, the ligation of B7.1 and B7.2 to CTLA-4 becomes physically impeded. Therefore, CD28 can become activated, resulting in T-cell activation.

CTLA-4 is expressed on activated CD8⁺ T-cells and CD4⁺ T-cells, yet it appears to play a larger physiological role in the CD4⁺ T-cell population. CTLA-4 has been shown to inhibit the activation of CD4⁺ effector cells, while enhancing the immunosuppressive activity of T-Regs¹⁹³. Some studies have identified tyrosine-protein phosphatase non-receptor type 11 (PTPN11; also known as SHP2) as crucial for the inhibition of the kinase signals that are induced by CD28 and TCR activation¹⁹⁹. CTLA-4 has also been implicated in the removal of B7 ligands from the surface of APCs. Finally, CTLA-4 has been demonstrated as an essential part of the immune system's regulation²⁰⁰. The knockout (KO) of CTLA-4 is lethal in mice, due to the hyper-activation of the immune system²⁰¹.

The initial idea of blocking the CTLA-4 receptor to treat cancer was met with scepticism due to the lethality of CTLA-4 KO mouse model, as well as the lack of evidence of the expression of the B7 ligands by tumour. In spite of this, in 1996, anti-CTLA-4 was first demonstrated to inhibit tumour growth of a colon carcinoma cell line that had been transfected to express B7.1²⁰². This model used an immunogenic cell line due to the expression of the B7 ligand. As such, the therapeutic effect was not replicated in mouse systems, where poor immunogenic tumours such as the B16 melanoma model were used²⁰³. Although anti-CTLA-4 was ineffective as a monotherapy, efficacy was seen in the B16 model when CTLA-4 blockade was combined with the GVAX vaccine (irradiated B16 cells expressing GM-CSF)²⁰⁴. It was believed that the vaccine was needed to induce a strong enough anti-tumour immune response for the anti-CTLA-4 to have a therapeutic effect²⁰⁴. This approach led to the use of anti-CTLA-4 in a number of other tumour models, to varied success (Table 1.1).

Following the successful pre-clinical studies, the production of fully humanised anti-CTLA-4 antibodies began. This led to two antibodies, ipilimumab and tremelimumab, beginning clinical treatment in 2000²⁰⁵. Like most anti-cancer agents, early trials involved patients with advanced disease who failed to respond to conventional therapies. Both antibodies showed

Tumour type	Cell line	Outcome	Reference
Brain	GL261	OS = 50% with monotherapy, 100% in combination with anti-CD25	206
	SMA-560	OS = 80% with monotherapy	207
Bladder	MB49	Tumour rejection	208
Melanoma	B16	73% long-term survivors in combination with Gvax	93
	B16	Tumour rejection = 10% in combination with Fvax, 50% in combination with Fvax and anti-PD-1	209
	B16F10	Monotherapy ineffective, 40% long-term survival in combination with anti-CD40 and ad-li-GP vaccine	210
Breast	4T1	Tumour-free mice = 1/9 with monotherapy, 6/9 with irradiation	211
	4T1	Monotherapy ineffective, tumour rejection in combination with irradiation	212

Table 1.1 Examples of pre-clinical studies involving anti-CTLA-4 therapy

promising results to begin with, as they showed an objective clinical response (no further growth of metastatic tumours and a 50% reduction in tumour size) in approximately (~) 10% of patients. Immune-related adverse events (irAEs) were observed in ~25% of patients, with colitis being a common event²¹³. Tremelimumab was the first agent to reach a phase III trial; this randomised trial compared the effects of tremelimumab to dacarbazine in the treatment of metastatic melanoma. The trial showed no differences between the two therapeutic agents²¹⁴. The phase III trial for ipilimumab was a randomised three-arm trial in patients with advanced melanoma. Patients received either ipilimumab, the gp100 vaccine (a melanoma-specific peptide) or both agents as a combination therapy²¹⁵. Patients receiving ipilimumab benefited from a three and half-month increase in survival, as compared to the gp100 vaccine cohort. The combination therapy had no beneficial effect over the ipilimumab therapy alone²¹⁵. In 2010, ipilimumab was approved by the FDA for the treatment of metastatic melanoma, due to it being the first therapy to show efficacy in this disease group¹⁹³. Ipilimumab was approved for use in the United Kingdom (UK) and European Union (EU) in 2012 and is also undergoing trials in small-cell lung cancer (SCLC) and non-small-cell lung cancer (NSCLC), bladder cancer and prostate cancer^{216,217}.

While the majority of clinical information regarding ipilimumab focuses on the treatment of the extracranial disease, its effects on BrM are now being investigated. An example of this is in a study where the outcome of melanoma patients with BrM, who were treated with SRS and ipilimumab, were compared to patients who only received SRS. The median survival of the patients receiving ipilimumab was 21.3 months, compared to nearly five months in the SRS only cohort²¹⁸; the two-year survival rates were 47.2%, compared to 19.7%²¹⁸. Another study compared a similar cohort of patients with BrM receiving SRS and ipilimumab to patients with no BrM receiving ipilimumab only²¹⁹. The median OS of these cohorts were 29.3 and 33.1 months, respectively, indicating that patients with MBrM could benefit from ipilimumab treatment, as they have a similar outcome to patients without BrM²¹⁹. Another retrospective study, examined the effects of receiving

ipilimumab in 38 patients with MBrM. In this study, three patients had a partial response and five had stable disease, while 15 patients had disease progression and the remaining 15 died²²⁰. The median OS was 101 days; however, it should be taken into account that some of the patients received a range of treatments, including WBRT, SRS and surgical resection²²⁰. In addition, there has been a reported case where a patient with an untreated MBrM had a complete response with ipilimumab²²¹. Margolin *et al.* compared the outcome of MBrM patients receiving ipilimumab who were either asymptomatic and not receiving corticosteroids or symptomatic and receiving corticosteroids²²². They reported that nine out of 51 patients who were asymptomatic achieved disease control, while only one of the 21 patients with symptomatic disease achieved disease control²²². Likewise, one individual with symptomatic intracranial disease had extracranial disease control, compared to 14 patients in the other cohort²²². Therefore, even though it is thought that ipilimumab is unable to cross the BBB, it can still be beneficial for MBrM patients²²³.

1.8.2 Anti-PD-1

PD-1 (also known as CD279) is another emerging target for use in immunotherapy and has produced promising results^{48,176,193}. The main function of PD-1 is to limit the activation of T-cells during an inflammatory response to limit autoimmunity²²⁴. PD-1 has two ligands: PD-L1 (also known as B7-H1 and CD274) and PD-L2 (also known as B7-DC and CD273) (Figure 1.6)²²⁴. Unlike CTLA-4, PD-1 has been found to be expressed by a number of immune cell populations, including T-cells, NK cells and B-cells^{225,226}. PD-L1 and PD-L2, on the other hand, have been found to be expressed by a number of cells including cancer cells, TAMs and DCs²²⁶. Additionally, there is now evidence that PD-L1 can interact with the CD80 molecule expressed on T-cells and can behave as an inhibitory receptor²²⁷. However, the relevance of this interaction has not been investigated in the context of cancer.

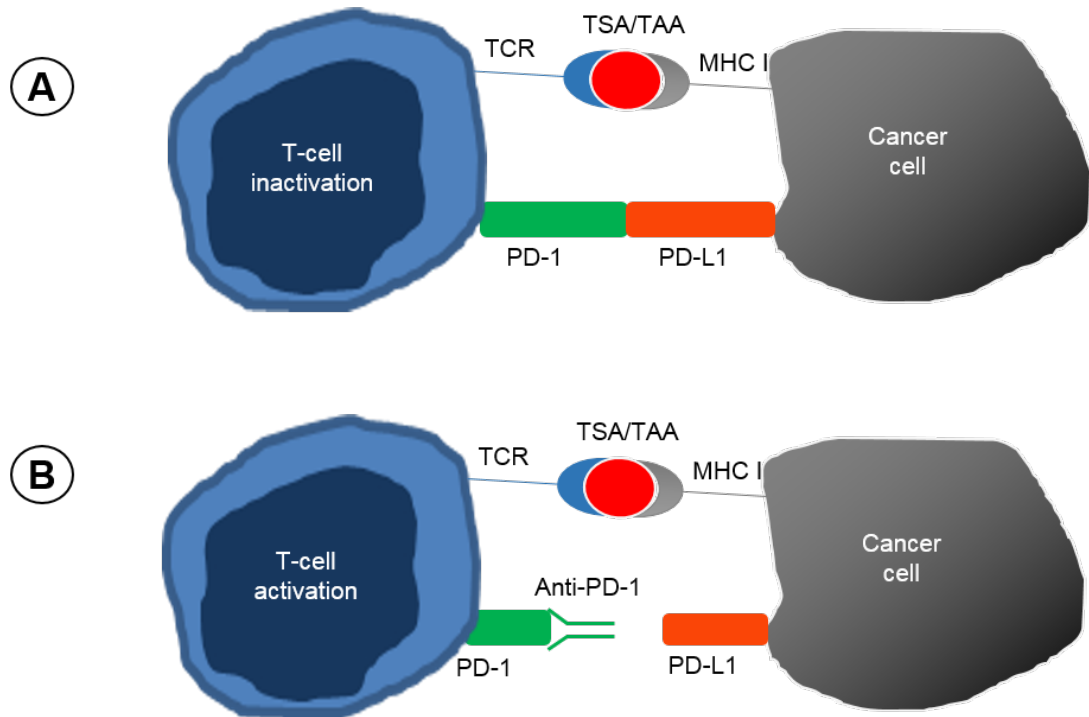


Figure 1.6 The reversal of PD-1-mediated T-cell inhibition via anti-PD-1 therapy

(A) Upon activation, T-cells will upregulate the inhibitory receptor, PD-1 (CD279) as a measure to prevent the unnecessary 'switching on' of the immune system. Cancer cells are able to hijack this mechanism through the over-expression of PD-L1 (CD274 or B7-H1) and PD-L2 (CD273 or B7-H2). Likewise, through various mechanisms, cancer cells can upregulate the expression of these inhibitory molecules on immune cells such as TAMs, TANs and DCs. The ligation of PD-1 to either of these inhibitory molecules will activate a cascade pathway leading to T-cell deactivation. **(B)** In the presence of an anti-PD-1 antibody, the PD-1 receptor becomes physically impeded, thus preventing its ligation and the subsequent inactivation of the T-cell, resulting in a more potent anti-tumour response.

Upon activation, T-cells will upregulate the expression of PD-1 and when this receptor becomes activated by one of its ligands, inhibitory signals are initiated^{193,228,229}. As with CTLA-4, PD-1 is believed to exert its effect through the inhibition of kinases that play a role in T-cell activation through PTPN11, although other pathways are likely to play a role as well¹⁹⁹. PD-1 can also affect the interaction time between T-cells and DCs through the TCR stop signal pathway. In addition, PD-1 is highly expressed on T-Regs and is thought to enhance their activation and proliferation²³⁰. This is another mechanism that cancer cells can exploit, by upregulating PD-L1 and further suppressing the immune system.

PD-1 became attractive as a new therapeutic target due to the large number of TILs that express PD-1 in a variety of tumours^{224,225}. In addition, PD-1⁺ CD8⁺ T-cells have been linked to an anergic or exhausted state and it is believed the blockade of PD-1 could reverse this state in humans, as has been demonstrated in mice^{195,228,231}. *In vivo* experiments have revealed that the forced expression of PD-L1 on mouse cancer cells inhibited T-cell responses within the TME¹⁹³. Melanoma, ovarian and lung cancer were the first to be reported to have a high level of PD-L1 expression, although a number of other human malignancies have been revealed to upregulate PD-L1²³²⁻²³⁴. As with CTLA-4, the evidence behind the potential efficacy of PD-1 blockade and the fact that PD-1 KO models were not lethal like CTLA-4 KO models led to a number of pre-clinical studies blocking PD-1 and its ligands (Table 1.2)²³⁵.

The first anti-PD-1 clinical trial was reported in 2010, where an anti-PD-1 antibody, nivolumab, was administered at various doses to patients with tumours of diverse origins²³⁶. The trial reported a number of cases of tumour regression including mixed responses, partial responses and one complete response²³⁶. Another trial described 16 out of 39 patients with advanced melanoma having an objective response, with an additional 14 patients demonstrating a mixed response or disease stabilisation²³⁷. Similar results were seen in renal and lung cancer^{193,238}. As predicted by the pre-clinical

Tumour type	Cell line	Outcome	Reference
Brain	GL261	OS = 30% with monotherapy, 100% when combined with SRS and anti-TIM-3	239
	GL261	OS = 56% with monotherapy, 75% when combined with anti-CTLA-4	240
Ovarian	ID8	OS= 0% with monotherapy, 50% in combination with trabectedin	241
Melanoma	B16F10	Tumour free mice = 0/10 with monotherapy, 7/10 when combined with anti-4-1BB	242
	B16-tk	OS = 0% with monotherapy, 45% in combination with reovirus	243
	B16	OS = 0% with monotherapy, 20% in combination with radiotherapy, 80% in combination of radiotherapy and anti-CTLA-4	231
Breast	4T1	Significant reduction in tumour volume when used in combination with SRS	244
Colon	CT26	OS = 20% with monotherapy, 100% in combination with anti-CTLA-4	245

Table 1.2 Examples of pre-clinical studies involving anti-PD-1 therapy

models, the number of irAEs was less than with anti-CTLA-4 therapy, with only one patient presenting with severe irAEs^{236–238}. A phase III trial comparing the efficacy of nivolumab compared to dacarbazine or carboplatin in patients with advanced melanoma reported its findings in 2014. The trial demonstrated that patients administered with nivolumab had an objective response rate of 31.7%²⁴⁶. Nivolumab was approved by the FDA for the treatment of malignant melanoma in 2014 and for NSCLC and renal cell carcinoma in 2015. Nivolumab was also approved for use in the EU in 2015.

Pembrolizumab is another anti-PD-1 antibody that has shown similar effects to nivolumab. Pembrolizumab was first investigated in a large phase I trial that included a total of 411 patients with melanoma. After 18 months, the RR was 34% and the response was maintained in 81% of these patients with an OS of 25.1 months²⁴⁷. The subsequent phase II study compared the effects of pembrolizumab to chemotherapy in melanoma patients who had disease progression following ipilimumab treatment²⁴⁸. This study showed that 38% of patients receiving pembrolizumab had a six-month PFS compared to the patients receiving chemotherapy, where 16% had six-month PFS²⁴⁸. The phase III trial moved on to compare the benefits of pembrolizumab over ipilimumab²⁴⁹. The RR was improved from 11.9% in the ipilimumab arm to ~33% when pembrolizumab was given (administered every two to three weeks). The RRs were maintained in ~90% of the patients, irrespective of treatment²⁴⁹. Due to the promising early stage results, pembrolizumab was given accelerated approval by the FDA in 2014 and was approved for use in Europe in 2015.

More recently, there is evidence emerging that pembrolizumab can have efficacy in the brain²⁵⁰. This study involved 18 patients with melanoma and 18 with NSCLC who had at least one untreated or progressive BrM, which was up to 20 millimetres (mm) in diameter²⁵⁰. With the melanoma cohort, 22% showed a partial response to the treatment, while the NSCLC cohort observed a response in 33%, including four (22%) complete responses²⁵⁰.

1.8.3 Anti-PD-1 and anti-CTLA-4 combination therapy

After promising results were seen when anti-PD-1 and anti-CTLA-4 were used as monotherapies, the idea to use both agents as a combination therapy quickly followed. There is evidence showing that the signalling pathways which CTLA-4 and PD-1 activate result in the inhibition of the protein kinase B (Akt) pathway¹⁹⁹. There is still a lot of work needed to fully understand the mechanism through which CTLA-4 and PD-1 inhibit T-cell activation, yet it is known that PTTN11 is involved in both pathways¹⁹⁹. While both of these cascades converge on the Akt pathway, they inhibit this process through distinct mechanisms, meaning that a combination therapy would have the potential to have an additive or synergistic effect on preventing the inhibition of the Akt pathway¹⁹⁹.

The first clinical study using both agents was to determine the safety of the combination therapy and was a dose escalation study^{251,252}. The study reported a RR in 65% of patients across all doses, with 31% of patients showing a reduction in tumour size by 80% or more²⁵². A major concern with the combination treatment was the potential for an increase in irAEs; however, there was no increase in the incidences or severity of irAEs when compared to those observed when either of the monotherapies were administered^{229,252}. The phase III trial for the combination therapy recruited 945 patients who had previously been untreated and, again, showed that combination treatment was more effective than either monotherapy²⁵³. The trial reported PFS of 11.9 months with the combination therapy, compared to three months with ipilimumab and seven months with nivolumab²⁵³. Interestingly, the trial showed that patients with PD-L1⁺ tumours had a prolonged PFS of 14.0 months and that PD-L1⁻ patients also had an increased PFS with the combination therapy when compared to both of the monotherapies²⁵³. The OS of these patients has yet to be reported as the study is still ongoing at this time (September, 2016). The combination therapy was FDA-approved for the treatment of advanced melanoma in September 2016 after receiving fast-track approval²⁵⁴ and was accepted for

use in the UK for treatment of the same patient group by the National Institute for Health and Care Excellence (NICE) in July 2016²⁵⁵.

1.9 Granulocyte-macrophage colony-stimulating factor

GM-CSF has been used as adjuvant therapy for a number of different immunotherapies, with the belief that it can enhance the immune response through the maturation of DCs²⁵⁶. There is already evidence that GM-CSF can be a beneficial adjuvant, as with OV's such as reovirus. Studies have shown that GM-CSF was essential for reovirus therapy to inhibit B16 tumour growth^{257,258}. GM-CSF has also been used as an adjuvant therapy in a number of clinical trials to variable success¹⁷⁹.

There is evidence that GM-CSF can enhance immune checkpoint therapy. In pre-clinical models, the GM-CSF-secreting GVAX vaccine was necessary for the effective therapy of B16 tumours treated in combination with anti-CTLA-4 antibody²⁵⁹. A clinical trial using GM-CSF in combination with ipilimumab also reported an increase in survival in patients with melanoma receiving the combination therapy²⁶⁰. This trial reported the combination therapy had a one-year survival rate of 68.9%, compared to 52.9% with ipilimumab monotherapy²⁶⁰.

Pre-clinical studies have also been completed using GM-CSF and anti-PD-1. The combination of anti-PD-1 and GM-CSF-secreting cells prolonged the survival of mice with B16 tumours and CT26 colon carcinoma tumours²⁶¹. At this time, there are no reported clinical trials using this combination; however, there is an ongoing trial investigating the effects of the combination of nivolumab and ipilimumab with and without GM-CSF²⁶².

As expected, there is no clinical evidence as to the effects of combination therapy using GM-CSF and checkpoint inhibitors in the brain. Nevertheless, there is sufficient pre-clinical and clinical evidence in other sites to suggest

that the combination of these three agents may provide an effective therapy for the treatment of MBrM and other BrMs.

1.10 Project rationale

The treatment of MBrM and BrM in general is an area of research that receives little attention, despite the clear clinical need for more effective treatment options. The purpose of this project was to demonstrate that patients with MBrM can benefit from immunotherapy treatment. This project aimed to:

1) Develop a new *in vivo* model for the study of MBrM

A new model of MBrM was developed to give a better representation of the human disease as in the majority of cases there is some form of extracranial disease.

2) Develop a combination immunotherapy for the treatment of MBrM

The various combinations of anti-PD-1, anti-CTLA-4 and GM-CSF were investigated to determine which combination provided the best outcome in mice with MBrM.

3) Determine which immune cells are the mediators of the therapeutic efficacy in the brain

Once the optimal therapy had been determined, the immune cells responsible for therapeutic effect were investigated through *in vivo* depletion studies and phenotypic analysis of tumour-infiltrating immune cells.

4) Investigate possible mechanisms with a focus on functionally-implicated immune cell populations

Once the critical immune cells had been identified, their functionality was examined through *ex vivo* analysis.

Chapter 2:

Materials and methods

Chapter 2

2.1 Cell lines and cell culture

B16 F1 melanoma cells were obtained from the American Type Culture Collection (ATCC) and were cultured in Dulbecco's modified eagle medium (DMEM) (Sigma-Aldrich) supplemented with 10% foetal bovine serum (FBS) (Gibco), 1x L-glutamine (Gibco) and 1x penicillin streptomycin (Pen strep) (Gibco). The anti-F4/80 producing HB-198 cell line was also obtained from the ATCC and cultured in Roswell park memorial institute medium (RPMI) (Sigma-Aldrich) supplemented with 20% FBS and 1x Pen strep.

Cells were cultured in a Sanyo carbon dioxide (CO₂) incubator in a humidified environment supplemented with five percent CO₂. Both cell lines were cultured in 25-, 75- and 150 cm² plastic tissue culture flasks (Corning). B16 F1 were cultured to near confluency and propagated by removing the culture medium and washing cells with phosphate-buffered saline (PBS) (Sigma-Aldrich) and subsequently treating with 1x trypsin (Hyclone). Once cells had detached from the surface of the flask the trypsin was quenched by the addition of fresh cell culture medium containing serum. Cells were pelleted by centrifugation at 350 g for 5 minutes. Cells were diluted to an appropriate ratio depending on intended use. As a non-adherent cell line, HB-198 cells were cultured until they reached a density of 1 x 10⁶ cells per ml. The cells were pelleted and diluted for further propagation. Stocks of both cell lines were frozen in 10% dimethyl sulfoxide (DMSO) (Sigma-Aldrich) in culture medium and stored at -196 °C in liquid nitrogen.

2.2 Transduction of B16 F1 cells with firefly luciferase (Fluc)-expressing lentiviral vector

B16 F1 cells were seeded into a six-well plate (Corning) at a density of 1 x 10⁵ cells in 2 ml of medium. Once the cells had adhered to the plate 1 ml of medium was removed and replaced with 1 ml of pFUW-Fluc lentiviral

stock¹⁵⁰ mixed with polybrene (Sigma-Aldrich; 8 ng/ml). Cells were incubated overnight and the following morning the cells were washed with PBS and received fresh medium. Upon reaching confluency the cells were further propagated and tested for their strength of firefly luciferase expression. Successful transduction was confirmed by adding 1 µl of luciferin (15 mg/ml) (Regis) to a serial dilution of cells and measuring the light emission as photons per second using the IVIS Spectrum (Perkin Elmer).

2.3 *In vivo* experiments

All procedures were approved by the University of Leeds Animal Welfare & Ethical Review Committee (AWERC) and performed under the approved UK Home Office project license in line with the Animal (Scientific Procedures) Act 1986 and in accordance with the UK National Cancer Research Institute Guidelines for the welfare of animals²⁶³.

Mouse strains used for *in vivo* experiments were C57BL6 (Charles River) and albino C57BL6 (B6N-Tyr^{c-Brd}; Charles River) as specified for individual experiments. All mice were female and aged between 6 and 8 weeks at the beginning of each experiment. Mice were housed in individually ventilated cages with a maximum of eight mice per cage at the St James's Biological Services Facility.

2.3.1 Implantation of cancer cells into the flank

The firefly luciferase-tagged B16 F1 (B16/Fluc) cells were propagated to sub-confluency to ensure the cells were in their exponential growth phase. Once detached from the flask, cells were washed twice in 10 ml of PBS and counted in a 1:1 ratio with trypan blue (Sigma-Aldrich) to distinguish live from dead cells using a Neubauer haemocytometer (Weber Scientific). Cells were re-suspended in PBS at 4×10^6 cells/ml for implantation of 2×10^5 cells in 50 µl per mouse.

Prior to implantation the left flank of each mouse was shaven with an Aesculap Isis rodent shaver (AgnTho's). C57BL6 mice were anaesthetised with isoflurane (Zoetis) and injected using 0.5 ml insulin syringes (Terumo). Forceps (Fine Science Tools) were used to raise the skin to inject the cells and to prevent the injection of cells into the muscle.

2.3.2 Intracranial implantation of cancer cells

B16/Fluc cells were prepared as previously described with the exception that cells were washed with DMEM without supplements. Cells were subsequently re-suspended at 5×10^7 cells/ml in DMEM without supplements for the injection of 1×10^5 cells in 2 μ l. Cells were kept on ice during the procedure for a maximum time of 3 hours before fresh cells were prepared.

Prior to surgery, the heads of the mice were shaven to remove as much fur as possible. Mice were anaesthetised with isoflurane and placed onto the digital Just For Mice stereotaxic instrument (Harvard Apparatus) for surgery. Mice were secured by placing their teeth into the teeth-bar and inserting ear-bars into both ears to prevent any movement. Lubrithal eye gel (Dechra) was applied to prevent eyes drying-out during the procedure. The surgical area on the head was sterilised with Hibiscrub (Mölnlycke Health Care) and subsequently with 70% ethanol. A vertical incision was made across the head with surgical scissors (Fine Science Tools) to gain access to the skull. The underlying membrane was dried with a sterile cotton-tip applicator to allow the skull to dry out to visualise the anatomy. A surgical micro-drill (Roboz) was used to drill a small hole in the skull, the drill site was located in the upper right hemisphere of the brain, ~2 mm to the right of the midline and ~2 mm anterior from the bregma. A customised needle (Hamilton) was inserted 4 mm into the brain parenchyma and retracted by 1 mm. Once there was no evidence of bleeding, 1 μ l of the suspension was injected followed by an additional 1 μ l after a 30 second interval. The needle was retracted mm by mm in 30 second intervals and the hole was sealed with bone wax (Harvard Apparatus). The skin incision was closed with tissue adhesive

(Vetbond; Santa Cruz Animal Health) and mice were placed in a warming chamber to recover. During the procedure mice were also given an intramuscular injection of Baytril (antibiotic; Bayer) and a subcutaneous injection of Metacam (analgesic; Boehringer Ingelheim).

2.3.3 Measurement of flank tumour growth

Flank tumour diameters were measured using digital calipers (Mahr) with measurements being taken in 2 dimensions. Tumour volume was calculated from these diameters using the following equation²⁶⁴:

$$Tumour\ volume = \left(\frac{1}{2} tumour\ length\right) \times (tumour\ width^2)$$

Tumour length was defined as the larger of the 2 diameters and tumour width was defined as the smaller diameter.

2.3.4 Quantification of intracranial tumour growth

Intracranial tumour growth was quantified via non-invasive bioluminescence imaging using the IVIS Spectrum. Mice were anaesthetised and given a subcutaneous injection of 80 µl of luciferin (15 mg/ml). After a predetermined time of 15 minutes for optimal luciferin circulation, mice were placed in the IVIS Spectrum. Images were subsequently analysed with the Living Image software (Perkin Elmer). Quantification was carried out by selecting a region of interest (ROI) as demonstrated in Figure 2.1.

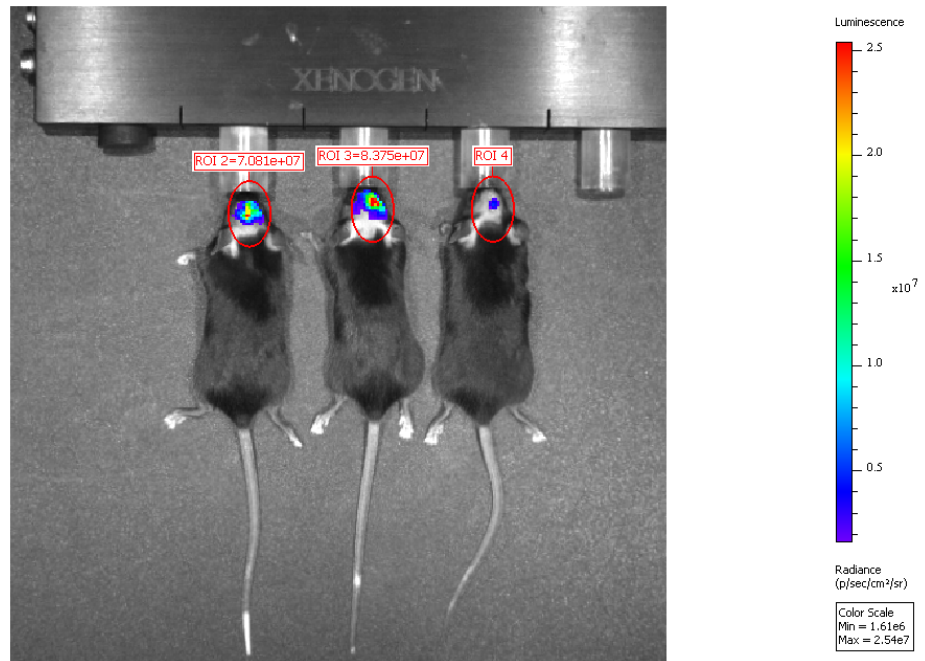


Figure 2.1 Example of quantification of bioluminescence images
A ROI was drawn around the head of each mice ensuring the entire signal was encompassed. The same size of ROI was used for the analysis of all mice.

2.3.5 Administration of therapeutic antibodies and immune cell-depletion antibodies

Prior to treatment, mice were randomised into experimental groups based on the intracranial bioluminescence signals ensuring equal distribution of tumour burden between groups. All treatments were administered by an intraperitoneal (*i.p.*) injection. Anti-PD-1 (clone RMP1-14; Bio X Cell), anti-CTLA-4 (clone 9D9; Bio X Cell) and IgG isotype (clone MPC11; Bio X Cell) were administered at 200 μg per dose (10 mg/kg based on the average weight of a mouse being 20 g). GM-CSF (Peprotech) was administered at 300 ng. All treatments were diluted in sterile PBS to give a final volume of 100 μl per dose. Mice received 4 doses of therapeutic antibodies and/or GM-CSF, as outlined in Figure 3.3.

Immune cell-depletion antibodies were administered by an *i.p.* injection of either anti-CD8 α (clone YTS.4; Bio X Cell), anti-CD4 (clone GK1.5; Bio X

Cell), anti-asialo-GM1 (polyclonal rabbit IgG; Cedarlane) or anti-F4/80 (clone CL:A3-1; Bio-Rad or produced from HB-198 cell line). All depletion antibodies were administered at 100 µg and were diluted in sterile PBS for a final volume of 100 µl per dose. Antibodies were administered every 4 days for the duration of the experiment with the exception of the commercially produced anti-F4/80, which was administered every 2 days as outlined in Figure 4.1.

2.3.6 Monitoring of symptoms related to intracranial growth

For survival studies mice were carefully monitored for the presentation of symptoms relating to intracranial tumour growth. Due to the sudden on-set of these symptoms the mice in survival studies were monitored every 2 hours from day 9-post intracranial implantation onwards. Common symptoms observed were piloerection, closing of eyes, isolation, loss of balance, hunching and a general lack of movement. When symptoms became apparent, mice were closely monitored for any increases in symptom severity and were euthanized when this occurred. Rarer symptoms observed included aggression towards other mice, continuous jumping within the cage and diarrhoea.

2.3.7 Isolation of blood

Blood samples of mice were collected by puncturing the tail vein with a needle (BD Biosciences) and collecting the blood (5-8 drops) directly into ammonium-chloride-potassium (ACK; see sub-chapter 2.10) buffer to lyse the red blood cells. After a few minutes the ACK buffer was diluted with cold incubation buffer (see sub-chapter 2.10) and the cells were stored on ice until the remaining samples were collected. Once all samples were collected, the cells were prepared as stated previously.

2.3.8 Terminal perfusion, tissue isolation and dissociation

Mice were injected with a lethal dose of Lethobarb (pentobarbital; 0.3 ml; Merial) and terminally perfused with 15 ml PBS with heparin sodium (5000

units/ml; Fannin). The brain was removed and the tumour was dissected from the brain parenchyma. Tumours were chopped finely with scalpels, incubated in a collagenase solution (see sub-chapter 2.10) and dissociated by pipetting until the cells were in a single-cell suspension. The cells were washed in cold incubation buffer and centrifuged at 400 *g* at 4 °C. The cells were inspected under the microscope for evidence of myelin; if present myelin was removed using myelin-removal beads (Miltenyi) according to the manufacturer's instructions.

The DCLNs were isolated from the mice under the dissection microscope (Omano). Upon removal the DCLNs were incubated in collagenase solution for 15 minutes at 37 °C. The DCLNs were punctured with a needle and the suspension was pipetted up and down a number of times to ensure the maximum release of cells from the nodes. The suspension was subsequently washed, counted and the cells were prepared for flow cytometry analysis.

Spleens were isolated from mice after terminal perfusion and spleens were crushed through a 70 µm filter (Greiner Bio-one) using the plunger of a 5 ml syringe. The filter was washed with Hank's balanced salt solution (HBSS) (Sigma-Aldrich) and the cells were subsequently pelleted by centrifugation at 350 *g* for 5 minutes. Following this, the red blood cells within the splenocytes were lysed with ACK buffer and washed with fresh HBSS. The cells were counted and used for flow cytometry analysis.

2.4 Isolation of anti-F4/80 antibody produced by HP-198 cells

HP-198 cells were expanded in culture and seeded at a density of 1×10^6 cells/ml. Cells were cultured for 5 days until the majority of cells had died. The media was collected, centrifuged and the supernatant filtered through a 0.22 µm filter (Millipore) to remove any cell debris.

Supernatants were concentrated using a Centricon® Plus-70 filter device (Millipore) by centrifuging the samples at 3500 g for 40 minutes. The filter prevented anything the size of an IgG or larger to pass through, resulting in a concentrated solution containing the depletion antibody. This process was repeated after the concentrate was washed with PBS to remove unwanted components of the supernatant.

2.5 Quantification of IgG by ELISA

A rat IgG Enzyme-Linked Immunosorbent Assay (ELISA) kit (Rat IgG total Ready-SET-Go! kit; eBioscience) was used to quantify the amount of anti-F4/80 antibody produced by the HB-198 cells. The capture antibody (Rat IgG total Ready-SET-Go! kit; eBioscience) was diluted in coating buffer and 100 µl of this solution was added to a 96-well plate (Corning) overnight. The plate was washed twice with 400 µl of PBS with Tween-20 (PBS-T; Sigma-Aldrich) and 250 µl of blocking buffer (Rat IgG total Ready-SET-Go! kit; eBioscience) was added for 2 hours at room temperature. This buffer was removed and standards were prepared as instructed, in triplicate. The remaining wells were filled with serial dilutions of the concentrated IgG solution and incubated for 2 hours at room temperature. The plate was then washed with 200 µl of PBS-T 3 times and 100 µl of the detection antibody (Rat IgG total Ready-SET-Go! kit; eBioscience) diluted in assay buffer (Rat IgG total Ready-SET-Go! kit; eBioscience) for 1 hour at room temperature. The plate was washed a further 4 times and 100 µl of substrate solution (Rat IgG total Ready-SET-Go! kit; eBioscience) was added for 15 minutes at room temperature before 50 µl of sulphuric acid (Sigma-Aldrich) was added to stop the reaction. The plate was subsequently read at 450nm using a colorimetric microplate reader (Thermo Fisher Scientific).

2.6 Flow cytometry

2.6.1 Extracellular staining

Once in a single-cell suspension, tumour cells were counted and $2-5 \times 10^5$ cells were used per multi-colour flow cytometry panel. Cells were blocked with 10% rat serum (Bio Rad) in incubation buffer for 10 minutes at 4 °C. A master mix of antibodies was made and added to the cells for a minimum time of 30 minutes in the dark at 4 °C (see Table 2.1 and 2.2 for information). After this incubation period, the cells were washed with cold incubation buffer, centrifuged at 350 g for 5 minutes at 4 °C and aspirated. Depending on the staining panel cells were either re-suspended in 200 µl of incubation buffer for analysis or proceeded for intracellular staining.

2.6.2 Intracellular staining

Following extracellular staining, cells were re-suspended in freshly prepared cold fixation/permeabilisation buffer (Miltenyi), vortexed and incubated for 30 minutes at 4 °C in the dark. Cells were then washed with cold incubation buffer, centrifuged at 350 g for five minutes at 4 °C and aspirated. This step was repeated with cold freshly prepared permeabilisation buffer (Miltenyi), following this cells were re-suspended in 50 µl of permeabilisation buffer and antibodies were added (see table 2.3 and 2.4 for further details). Cells were incubated with the antibodies at 4 °C for 30 minutes in the dark. Following this, the cells were washed twice in permeabilisation buffer and re-suspended in 200 µl for analysis.

2.6.3 Flow cytometry analysis

Samples were analysed on the BD LSR II Flow Cytometry Analyser (BD Bioscience). Flow cytometry data was analysed using the FACS Diva 7 software (BD Bioscience). Population gates were set based on the shift past the isotype control (see Table 2.2 and 2.4 for list of antibodies).

Cell marker	Fluorophore	Clone	Company
CD3e	APC-Vio770	17A2	Miltenyi
CD3e	PE-Vio770	17A2	Miltenyi
CD3	Vioblue	17A2	Miltenyi
CD4	PerCP Vio 700	GK1.5	Miltenyi
CD4	PE-Vio770	GK1.5	Miltenyi
CD8	Viogreen	53-6.7	Miltenyi
CD11b	BV605	M1/70	Biolegend
CD25	PE-Vio770	7D4	Miltenyi
CD27	PerCP eFluor710	LG.7F9	eBioscience
CD31	PE	390	eBioscience
CD69	PE	H1.2F3	Miltenyi
CD107a	PE	1D48	Miltenyi
CCR7	Alexa Fluor 700	4B12	eBioscience
DX5	APC	DX5	Miltenyi
F4/80	Alexa Fluor 700	CL:A3-1	Bio Rad
ICAM-1	FITC	YN1/1.7.4	eBioscience
LFA-1	PerCP Cy5.5	H155-78	Biolegend
MHC I	PE-Cy7	AF6-88.5.5.3	eBioscience
MHC II	Vioblue	M5/114.15.2	Miltenyi
NKp46	BV605	29A1.4.9	Biolegend
NKp46	FITC	29A1.4.9	Miltenyi
Ova pentamer	APC	N/A	Proimmune
PD-1	eFluor 450	J43	eBioscience
TIM-3	PE-Cy7	RMT3-23	eBioscience
VLA-4	Vioblue	R1-2	Miltenyi

Table 2.1 List of extracellular flow cytometry antibodies

Cell marker	Isotype	Company
CD3e	Rat IgG2b	Miltenyi
CD3e	Rat IgG2b	Miltenyi
CD3	Rat IgG2b	Miltenyi
CD4	Rat IgG2b	Miltenyi
CD4	Rat IgG2b	Miltenyi
CD8	Rat IgG2a	Miltenyi
CD11b	Rat IgG2b	Biolegend
CD25	Rat IgM	Miltenyi
CD27	Hamster IgG	eBioscience
CD31	Rat IgG2a	eBioscience
CD69	Hamster IgG	eBioscience
CD107a	Rat IgG2a	Miltenyi
CCR7	Rat IgG2a	eBioscience
DX5	IgM	Miltenyi
F4/80	Rat IgG2b	Bio Rad
ICAM-1	Rat IgG2a	eBioscience
LFA-1	Rat IgG1	Biolegend
MHC I	Mouse IgG2a	eBioscience
MHC II	Rat IgG2b	Miltenyi
NKp46	Rat IgG2a	Biolegend
NKp46	Rat IgG2a	Miltenyi
Ova pentamer	Control pentamer	Proimmune
PD-1	Rat IgG2b	eBioscience
TIM-3	Rat IgG2a	eBioscience
VLA-4	Rat IgG2b	Miltenyi

Table 2.2 List of extracellular flow cytometry antibodies and their corresponding isotypes

Cell marker	Fluorophore	Clone	Company
EOMES	APC	REA116	Miltenyi
EOMES	PE	REA116	Miltenyi
FOX P3	APC	3G3	Miltenyi
Granzyme B	PerCP eFluor710	NGZB	eBioscience
IFN- γ	FITC	XMG1.2	eBioscience
Ki67	FITC	SolA15	eBioscience
TNF- α	PE	MP6-XT22	eBioscience

Table 2.3 List of intracellular flow cytometry antibodies

Cell marker	Isotype	Company
EOMES	REA	Miltenyi
EOMES	REA	Miltenyi
FOX P3	Mouse IgG1	Miltenyi
Granzyme B	Rat IgG2a	eBioscience
IFN- γ	Rat IgG1	eBioscience
Ki67	Rat IgG2a	eBioscience
TNF- α	Rat IgG1	eBioscience

Table 2.4 List of intracellular flow cytometry antibodies and their corresponding isotypes

2.7 *Ex vivo* stimulation of splenocytes

Splenocytes isolated from mice were cultured overnight in Iscove's modified Dulbecco's medium (IMDM) (Sigma-Aldrich) supplemented with 5% FBS, 1x L-glutamine, 50 units/ml IL-2 (Proleukin; Prometheus) and 1x Pen Strep. Cells were cultured at a density of 5×10^5 cells in 500 μ l of medium, 1x cell stimulation cocktail (eBioscience) and protein export inhibitor (eBioscience). The following day cells were washed in incubation buffer and prepared for flow cytometry analysis as previously described for the staining of extracellular makers.

Following extracellular staining, the cells were fixed with intracellular fixation buffer (eBioscience) for 30 minutes at room temperature. The cells were subsequently washed twice with freshly prepared permeabilisation buffer (eBioscience) and re-suspended in 50 μ l of the same buffer. The intracellular staining antibodies (see Table 2.1 and 2.2) were added to the cells for 30 minutes in the dark at room temperature. After this incubation cells were washed with permeabilisation buffer and re-suspended in 200 μ l of the same buffer for flow cytometry analysis.

2.8 ELISpot

Splenocytes were isolated from mice and processed for the detection of IFN- γ using an enzyme-linked immunospot (ELISpot) assay (Mouse IFN gamma ELISpot Ready-SET-Go! kit; eBioscience). The day prior to splenocyte isolation, 96-well PVDF membrane ELISpot plates (Millipore) were moistened with 70% ethanol, then coated with the IFN- γ capture antibody (Mouse IFN gamma ELISpot Ready-SET-Go! kit; eBioscience) diluted in ELISpot coating buffer (Mouse IFN gamma ELISpot Ready-SET-Go! kit; eBioscience) overnight. The following day the plate was washed twice with 200 μ l of sterile ELISpot coating buffer and the wells were blocked with 200 μ l of the splenocyte culture medium (with supplements) for 2 hours at room temperature. Isolated splenocytes were added to the wells at the density of 5×10^5 cells in 100 μ l of splenocyte culture medium. Cells were cultured

overnight with either no stimulation, stimulation cocktail (1x), gp100 peptide (5 ng/ml; Sigma-Aldrich), Trp2 peptide (5 ng/ml; Sigma-Aldrich) or B16 cell lysate. B16 lysate was produced when 1×10^7 B16/Fluc cells per ml of PBS were lysed by 3 repeated cycles of freeze-thaw.

The following days the cells were removed and the plate was washed 3 times with PBS-T. The detection antibody (Mouse IFN gamma ELISpot Ready-SET-Go! kit; eBioscience) was diluted in ELISpot assay diluent (Mouse IFN gamma ELISpot Ready-SET-Go! kit; eBioscience) and 100 μ l was added to each well for 1 hour at room temperature. The plate was washed four times with PBS-T. The Avidin-HRP solution (Mouse IFN gamma ELISpot Ready-SET-Go! kit; eBioscience) was diluted in ELISpot assay diluent and 100 μ l was added to each well and incubated for 1 hour at room temperature. The plate was once again washed 3 times with PBS-T and twice with PBS. Tetramethylbenzidine (TMB; Mabtech) was added to each well (100 μ l) and was removed after ~10 minutes when spots became visible. The plate was thoroughly washed with water and left to dry in the dark. The plate was read using SD32G2 AID ELISpot Reader System (AID Diagnostika) and quantified by ELISpot Software Version 4.0 (AID Diagnostika).

2.9 Statistical analysis

Statistical analysis was carried out using Graph Pad Prism v7 (Graph Pad Software). All error bars on graphs represent standard error of the mean (SEM). Statistical tests used were analysis of variance (ANOVA) with a post hoc test for multiple comparisons, Mann-Whitney test and paired T-test. All tests were 2-tailed statistical tests.

2.10 Buffers and reagents

Unless stated otherwise all components are manufactured by Sigma-Aldrich.

ACK Buffer

In 500 ml water: 0.15 M ammonium chloride
10 mM Potassium bicarbonate
0.1 mM Ethylenediaminetetraacetic acid (EDTA)
pH 7.2-7.4

Collagenase solution (5X)

In 6.6 ml EMEM: 3 mg/mL collagenase (Roche)
250 U/mL hyaluronidase

Incubation buffer

In 500 ml PBS: 5% Bovine serum albumin (BSA)
2 mM EDTA

PBST

In 1 liter of water: 9.6 g PBS
0.5 ml Tween-20

Chapter 3:

**Developing a pre-clinical model
for melanoma brain metastases
and investigating the effects of
various immunotherapy
combinations**

Chapter 3

3.1 Introduction

MBrM has long been associated with a poor clinical outcome. Although treatment regimens have significantly improved, the median survival rate remains below one year^{14,26,27,31}. With chemotherapies proving to be mostly ineffective against MBrM, standard care of treatment usually consists of surgical resection or a radiotherapy using either WBRT or SRS on well-defined lesions^{26,37}. With an increase in the incidence of MBrM, the development of an effective, novel therapy has never been more necessary.

In recent years, immunotherapies have been introduced into the clinic, most notably in the treatment of metastatic melanoma. With these new treatments, such as immune checkpoint inhibitors, the prognosis for metastatic melanoma has significantly improved^{26,37}. However, as with many new treatments, patients with active metastasis have been left out of these clinical trials due to their poor prognosis, combined with the belief that patients with brain tumours are unlikely to benefit from immunotherapies^{26,37}.

This chapter will describe the establishment of a new *in vivo* model that is a more accurate representation of the human disease than the models currently employed, by also taking into account the presence of extracranial disease. This model will be used to test whether different immunotherapies (e.g. anti-PD-1, anti-CTLA-4, GM-CSF and their combinations) have a therapeutic effect on mice with MBrM. The effect of extracranial disease on intracranial tumours will also be explored, as well as how this can impact on treatment outcome.

3.2 Establishing a new preclinical melanoma metastasis model

In this study, the B16 F1 cell line²⁶⁵ was selected over other murine melanoma cell lines, such as K1735²⁶⁶ or Harding-Passey Melanoma²⁶⁷ (HPM), due to its spontaneous origin, in addition to its metastatic nature. Moreover, the B16 cell line is commonly used in melanoma studies due to its lack of a BRaf mutation²⁶⁵; a common form of mutation seen in the human disease. While widely considered to be poorly immunogenic²⁶⁸, B16 has been used extensively in a range of immunotherapy research, most notably anti-PD-1 and anti-CTLA-4³⁷, hence, making the B16 model a good candidate for studying the effects of immune checkpoint inhibitors on MBrM. There are also a number of transgenic mouse models that spontaneously develop melanoma with a number of these developing metastases^{269,270}, the secondary disease is mostly limited to the visceral organs²⁷⁰. More recently, a new model of spontaneous brain metastases, where mice are given a subdermal injection of Ret-melanoma cells was described²⁷¹. In this model, the primary tumours are surgically removed, allowing for metastatic growth, with a number of these mice ultimately developing macrometastases in the brain. The disadvantages of this model is, however, the high wastage of animals (only ~25% of all mice will develop brain macrometastases), high costs and long duration.

In order to mimic the clinical situation where the majority of patients with MBrM have concurrent extracranial disease, we sought to establish a model with simultaneous intracranial and extracranial tumours^{31,35,36}. To create a timeline for the extracranial tumour growth, B16/Fluc cells (2×10^5 and 5×10^5) were subcutaneously implanted into the flank of C57BL6 mice. While a palpable tumour took approximately the same time (seven days) to become established for both cell concentrations, the growth following this varied (Figure 3.1A). Tumour volumes in mice implanted with 5×10^5 cells tended to have more variability within the group, whereas mice implanted with 2×10^5 cells developed tumours of a more comparable size. The group implanted with 5×10^5 cells reached their maximum allowable tumour diameter (15 mm) between days 14-18, while in the group implanted with $2 \times$

10^5 cells, tumours reached their maximum size between days 16-18 (Figure 3.1B). As a result, the concentration of 2×10^5 cells was selected going forward, due to the lower intragroup variance.

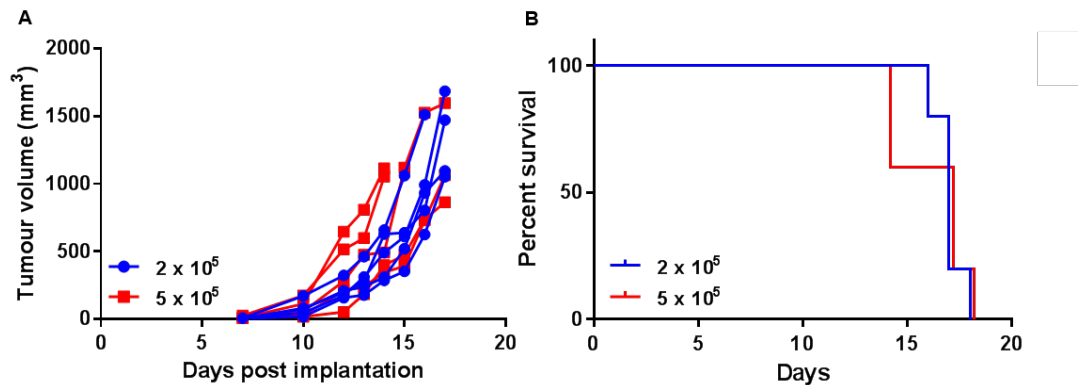


Figure 3.1 Establishing a timeline for subcutaneous tumour growth of B16 cells

(A) B16 cells (2×10^5 or 5×10^5) were subcutaneously injected into C57BL6 mice. Tumours were measured with calipers regularly until tumour dimensions reached their maximum allowable size of 15 mm, with the tumour volumes subsequently calculated. **(B)** Curves showing the time taken for the tumours of each group of mice to reach their maximum allowable size. (n = five mice per group; statistical test used was Log-rank).

To establish a timeline for intracranial tumour growth in mice with a flank tumour, 1×10^5 B16/Fluc cells were intracranially implanted into mice that previously had a subcutaneous injection of 2×10^5 B16/Fluc cells. The intracranial growth in these mice was directly compared to intracranial growth in mice without a flank tumour to determine the role of extracranial disease in intracranial tumour growth. Intracranial tumour growth between the two groups was compared by non-invasive bioluminescence imaging (Figure 3.2). The data were presented as fold change between the bioluminescence signal on a respective day and the initial signal (day two-post intracranial implantation) (Figure 3.2B). Upon comparison of the growth curves it was apparent that the flank tumour did not impact the growth of the intracranial tumour. This was further confirmed as there was no significant difference ($P = 0.94$) in the survival of the mice between the two groups (Figure 3.2C). The majority of the mice in both groups showed terminal

symptoms 10 days-post intracranial implantation with bioluminescence imaging also showing there was no significant difference in tumour burden at this time point ($P = 0.82$).

3.3 A combination of immunotherapies is more effective in treating brain metastases

Since the immune checkpoint inhibitors anti-PD-1 and anti-CTLA-4 are known to be an effective combination treatment for metastatic melanoma²⁶, this principle was applied to our MBrM model. In addition, GM-CSF, having been previously demonstrated to enhance the effects of other immunotherapies, was also included^{179,259}.

The MBrM model was used to test the effectiveness of anti-PD-1, anti-CTLA-4 and GM-CSF as individual therapies, in addition to all possible combinations (see Figure 3.3 for experimental timeline). The majority of the mice were sacrificed once they presented with terminal symptoms that were associated with brain tumour growth. In two cases out of 32, mice had to be sacrificed as their flank tumour reached its maximum allowable dimensions.

Flank tumour measurements taken the day following the final dose of treatment (day nine) showed that GM-CSF as a single agent was ineffective at reducing extracranial tumour growth. In contrast, anti-PD-1 and anti-CTLA-4, as monotherapies, displayed a tendency towards reduced flank tumour growth, although this was only statistically significant with the anti-PD-1 monotherapy ($P = 0.0379$) at this timepoint. When combined as dual therapies, all combinations resulted in a significantly decreased tumour burden ($P = 0.003$ (anti-PD-1 & GM-CSF); 0.0011 (anti-CTLA-4 & GM-CSF); 0.0006 (anti-PD-1 & anti-CTLA-4) and 0.0003 (anti-PD-1, anti-CTLA-4 & GM-CSF)). This was also the case when all three agents were used in combination (Figure 3.4A and Table 3.1).

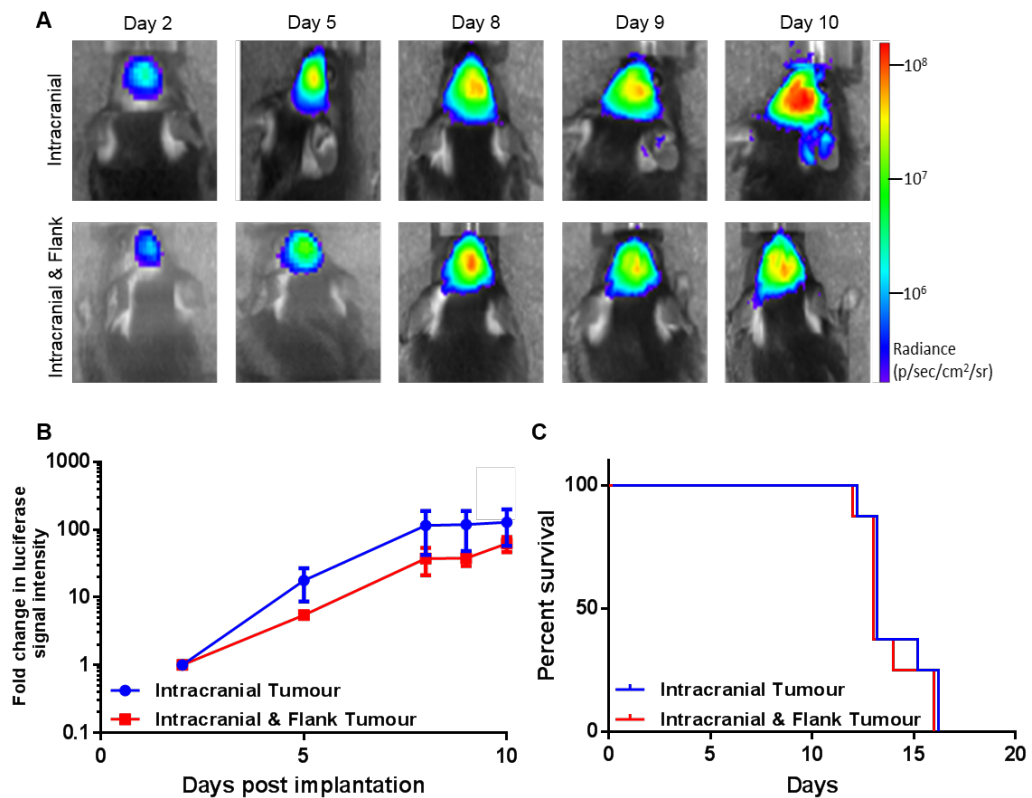


Figure 3.2 Establishing a timeline for the intracranial growth of B16/Fluc cells

(A) C57BL6 mice were subcutaneously implanted with 2×10^5 B16/Fluc cells three days prior to being intracranially implanted with 1×10^5 B16/Fluc cells (Intracranial & Flank). Intracranial tumour growth was monitored with non-invasive bioluminescence imaging and compared to the growth of mice that only received an intracranial tumour (Intracranial). Mice were imaged regularly until they presented with terminal symptoms related to intracranial tumour growth. **(B)** Bioluminescence images were quantified and the fold change in luciferase signal intensity between the respective day and day two-post tumour implantation was calculated as a measure of tumour growth. **(C)** Survival curves of C57BL6 mice with B16/Fluc intracranial tumours and mice with B16/Fluc subcutaneous (flank) and intracranial tumours. Mice were sacrificed once they presented with terminal symptoms related to intracranial growth. (n= five mice per group; error bars represent SEM; statistical tests used were Students T-test and Log-rank).

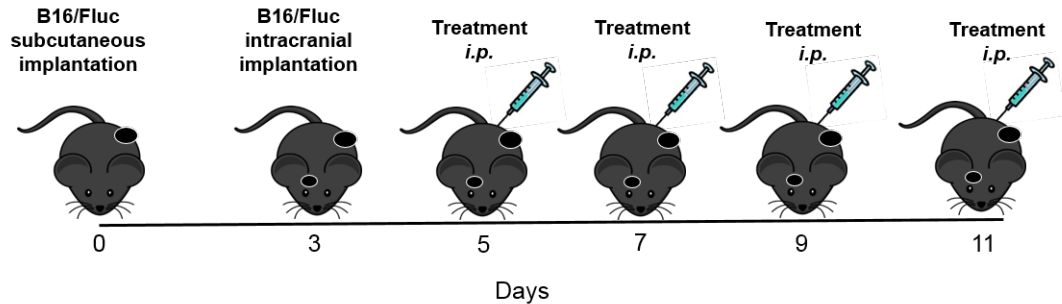


Figure 3.3 Experimental timeline of pre-clinical melanoma brain metastasis model

B16/Fluc cells (2×10^5) were subcutaneously implanted into C57BL6 mice three days prior to the intracranial injection of B16/Fluc cells (1×10^5). Mice were grouped based on their intracranial bioluminescence signal prior to the administration of therapy, ensuring an equal distribution of intracranial tumour sizes between the groups. Treatment was administered *i.p.* on days five, seven, nine and 11. Flank tumours were measured with calipers and intracranial tumour growth was quantified by non-invasive bioluminescence imaging.

Bioluminescence imaging was used concurrently as an indication of brain tumour growth, with the fold change in luciferase signal intensity between day two and day nine being calculated as a measure of tumour growth (Figure 3.4). Analysis showed that GM-CSF, anti-PD-1 and anti-CTLA-4 as monotherapies did not have a significant effect on brain tumour growth. Moreover, when anti-PD-1 or anti-CTLA-4, respectively, were administered as a combination therapy with GM-CSF, there was no significant change in intracranial tumour growth as compared to the isotype control group. This was in contrast to observations with the extracranial tumour growth. Nonetheless, a significant reduction in brain tumour growth was observed in mice that received anti-PD-1 plus anti-CTLA-4 ($P = 0.0145$) or anti-PD-1 plus anti-CTLA-4 with GM-CSF ($P = 0.027$) (Figure 3.4B and Table 3.1).

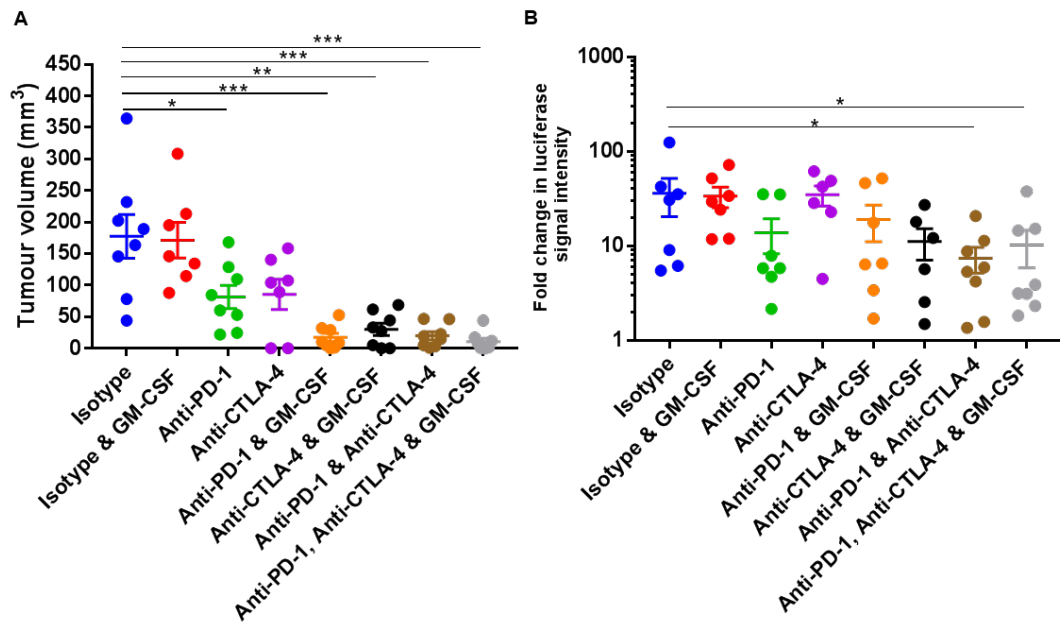


Figure 3.4 Flank and intracranial tumour measurements in mice with B16 tumours treated with various combinations of anti-PD-1, anti-CTLA-4 and GM-CSF

Tumour measurements were taken from mice treated with various combinations of anti-PD-1, anti-CTLA-4 and GM-CSF the day after they received the final dose of treatment. **(A)** Flank tumour sizes were quantified using calipers, with tumour measurements being taken from two dimensions and the tumour volume subsequently calculated. **(B)** Intracranial tumour burden was measured using non-invasive bioluminescence imaging; the fold change in luciferase signal between the final day and the day treatment began is presented. (n = seven for anti-CTLA-4 groups and n = eight for all other groups; error bars represent SEM; see Table 3.1 for statistics).

The survival of mice correlated to intracranial, rather than extracranial tumour burden and significantly improved survival was observed only in mice that received anti-PD-1 plus anti-CTLA-4 and anti-PD-1 plus anti-CTLA-4 with GM-CSF (P = 0.034 and 0.0019, respectively) (Figure 3.5, 3.6 and Table 3.1).

3.4 A flank tumour is essential for effective intracranial therapy

Having established two effective therapies, we next asked: ‘Is a flank tumour necessary for intracranial efficacy of immune checkpoint inhibition?’. This question was addressed by comparing intracranial tumour growth upon treatment between mice with an intracranial tumour only and mice with an

intracranial and flank tumour. We focused on two treatment combinations that resulted in intracranial efficacy, namely anti-PD-1 plus anti-CTLA-4 and anti-PD-1 plus anti-CTLA-4 with GM-CSF.

Compared to isotype (n)	Survival (P)	Tumour volume	Fold change in luciferase activity
Isotype and GM-CSF (n=8)	0.9342	0.9551	0.3552
Anti-PD-1 (n=8)	0.2905	0.0379	0.0772
Anti-CTLA-4 (n=8)	0.1353	0.0522	0.4178
Anti-PD-1 & GM-CSF (n=8)	0.4782	0.0003	0.2675
Anti-CTLA-4 & GM-CSF (n=7)	0.0872	0.0011	0.0688
Anti-PD-1 & Anti-CTLA-4 (n=8)	0.0034	0.0006	0.0145
Anti-PD-1, Anti-CTLA-4 & GM-CSF (n=8)	0.0019	0.0003	0.0270

Table 3.1 Statistical analysis for the survival and tumour burden of mice with flank and intracranial B16 tumours treated with various combinations of anti-PD-1, anti-CTLA-4 and GM-CSF

For the survival study, statistical significance was calculated by the Log-rank test. The significance threshold was adjusted to 0.00714 to compensate for multiple comparisons. For the tumour volume and fold change in luciferase activity, pairwise Mann-Whitney tests were used.

3.4.1 Treatment with anti-PD-1 plus anti-CTLA-4 with GM-CSF

A group of mice first received a subcutaneous injection of B16/Fluc cells. These mice were intracranially injected with B16/Fluc cells three days after the subcutaneous injection, along with a second group of mice without a flank tumour. Mice were imaged two days after intracranial implantation and grouped based on the signal intensity from their intracranial tumours. Treatment with anti-PD-1 plus anti-CTLA-4 with GM-CSF began on the same day (Figure 3.7). Mice began to show symptoms 10 days-post intracranial implantation and, as a result, all mice were sacrificed after final tumour measurements were taken.

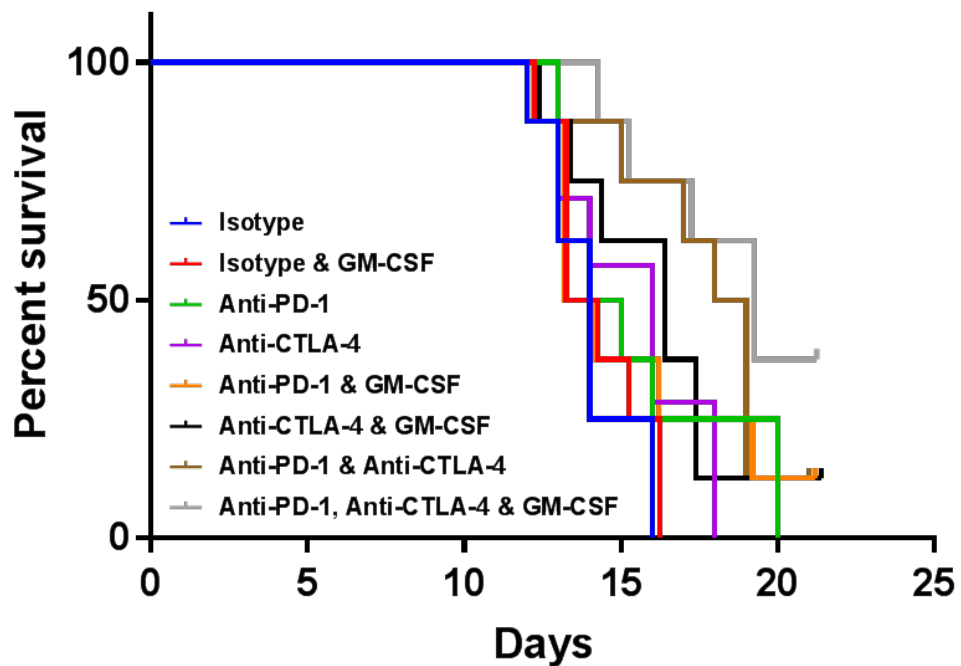


Figure 3.5 Survival of mice with flank and intracranial B16 tumours treated with various combinations of anti-PD-1, anti-CTLA-4 and GM-CSF

C57BL6 mice were subcutaneously implanted with B16/Fluc cells and three days later intracranially implanted with B16/Fluc cells. Mice were imaged using non-invasive bioluminescence imaging two days after intracranial implantation and were grouped based on initial intracranial signals. Mice were then given either an IgG isotype or various combinations of anti-PD-1, anti-CTLA-4 and GM-CSF. Treatments were given four times over six days and mice were sacrificed when they presented with terminal symptoms. (See Table 3.1 for statistics).

As previously observed, there was a significant difference in flank tumour volume between treated and non-treated mice (Figure 3.8A). The fold change in luciferase signal intensity between days two and 10 was calculated. This revealed that treatment had no effect on intracranial tumour growth in the absence of a flank tumour (Figure 3.8B). Intracranial luciferase signal intensities were also similar in mice receiving IgG isotype control antibody in the absence or presence of a flank tumour. However, there was a significant reduction in luciferase signal intensities in mice with a flank and intracranial tumour that received treatment, as compared to the other three groups, suggesting a reduction in tumour burden (Figure 3.8C).

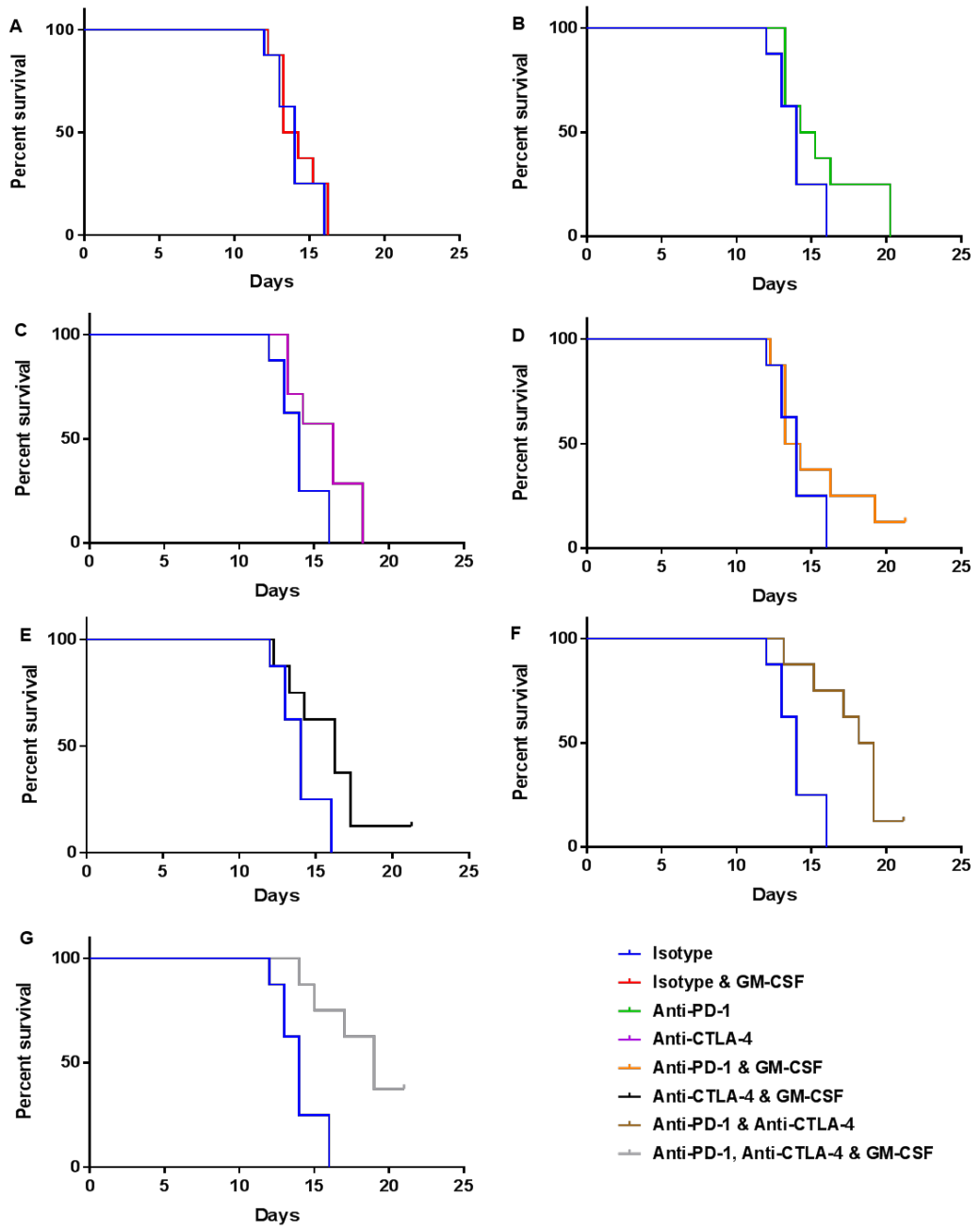


Figure 3.6 Individual survival curves of mice with flank and intracranial B16 tumours treated with various combinations of anti-PD-1, anti-CTLA-4 and GM-CSF
See Figure 3.5 for details.

Finally, post-mortem examination of tumour burden was performed visually, as the tumours were easily distinguished from normal brain tissue due to the dark pigment of B16 cells. In line with our quantification, mice from the two control groups and the treatment group with an intracranial tumour only grew larger tumours, as compared to the treatment group with an intracranial plus a flank tumour (Figure 3.9).

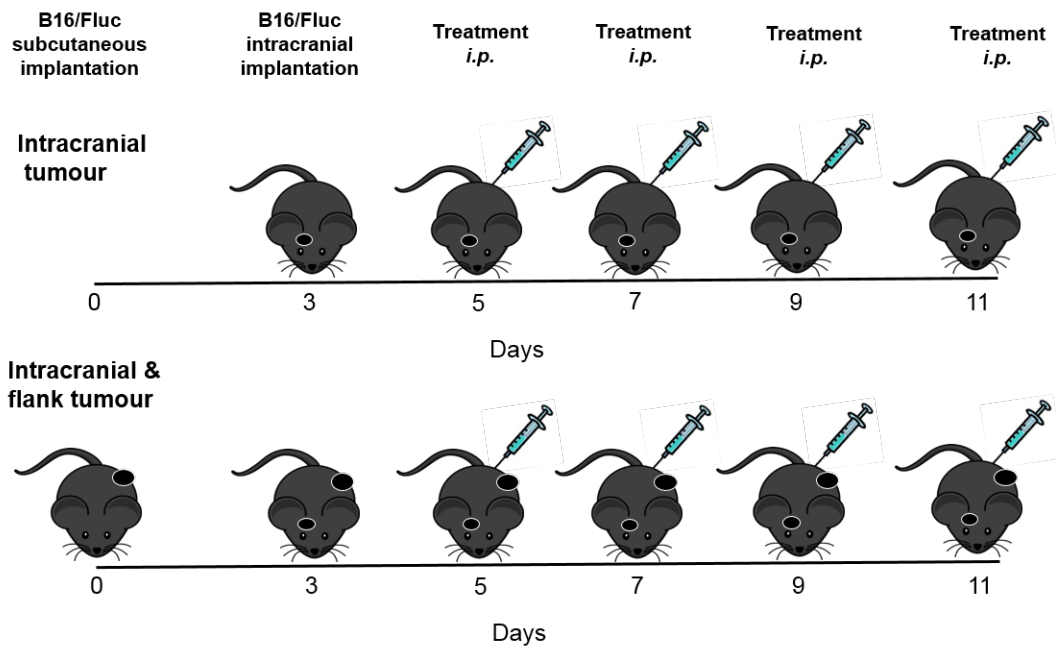


Figure 3.7 Experimental timeline for investigating the role of flank tumours in immune checkpoint therapy in MBrM

C57BL6 mice were intracranially implanted with 1×10^5 B16/Fluc cells while one group of mice had also been subcutaneously implanted with 1×10^5 B16/Fluc cells in the flank three days prior. Mice were non-invasively imaged with bioluminescence imaging two days-post intracranial implantation and grouped based on the quantification of the intracranial tumour burden. The two groups of mice were further subdivided into an IgG control group and a treatment group. Treatment was administered on days five, seven, nine and 11. Flank tumours were measured with calipers and intracranial tumour growth was monitored by non-invasive bioluminescence imaging.

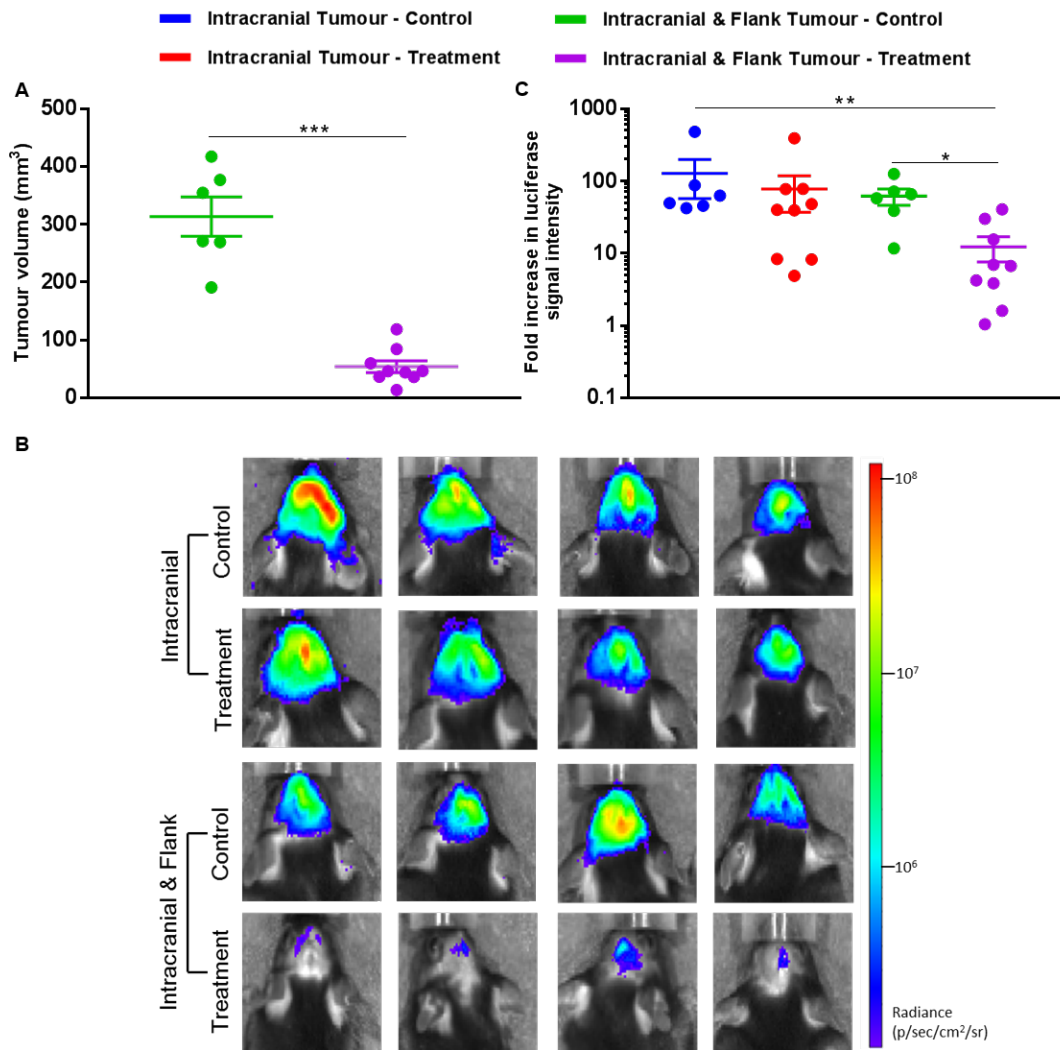


Figure 3.8 The effect of a flank tumour on the intracranial tumour growth in mice treated with the combination of anti-PD-1, anti-CTLA-4 and GM-CSF

C57BL6 mice were intracranially implanted with B16/Fluc cells with an additional group also subcutaneously implanted with B16/Fluc cells. These two groups of mice were each sub-divided into two further groups, one of which received the IgG isotype (Control) antibody while the other received the combination of anti-PD1, anti-CTLA-4 and GM-CSF (Treatment). Treatment was administered four times over six days. **(A)** Flank tumour measurements were taken using calipers two days after the final dose of treatment was administered. Measurements were taken from two dimensions and the tumour volume was subsequently calculated. **(B)** Representative bioluminescence images of mice taken 10 days-post intracranial implantation of cancer cells. **(C)** The fold change in luciferase signal intensity was calculated between day two and the day after the final dose of treatment was administered. (n = six, six, six, eight; error bars represent SEM; statistical significance was determined by pairwise Mann-Whitney tests).

3.4.2 Treatment with anti-PD-1 and anti-CTLA-4

After the treatment with anti-PD-1, anti-CTLA-4 and GM-CSF proved to inhibit intracranial tumour growth in the presence of a flank tumour, GM-CSF was removed from the treatment regime to determine if checkpoint inhibitors alone could replicate this response, as they have previously been shown to increase survival when used in combination.

As in the previous experiment, the effects of anti-PD-1 plus anti-CTLA-4 on tumour growth were monitored in mice with only an intracranial tumour and in mice with an intracranial and flank tumour. Unlike the previous experiment, mice began to show terminal symptoms nine days-post intracranial implantation of cancer cells. Therefore, the tumour measurements were taken on this day before the mice were euthanized. There was a significant decrease in flank tumour size in mice that received the treatment (Figure 3.10A). Moreover, the same trend in intracranial tumour growth was observed as was seen when two immune checkpoint inhibitors plus GM-CSF were used. Mice in the two control groups and mice with an intracranial tumour only that received treatment all had similar luciferase signal intensities. In contrast, the mice with a flank and intracranial tumour that received treatment displayed a significantly lower fold change in luciferase signal intensity pre- / post-treatment, once again suggesting a reduction in intracranial tumour burden (Figure 3.10B and C).

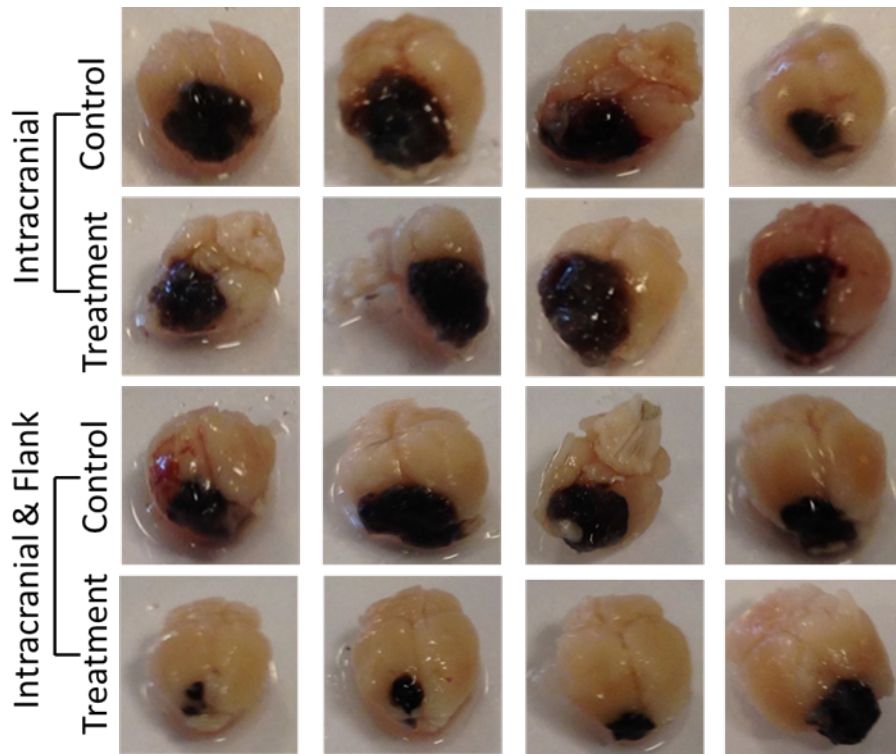


Figure 3.9 Post-mortem brain images of mice treated with anti-PD-1, anti-CTLA-4 and GM-CSF or IgG control antibody with or without a flank tumour

See Figure 3.8 for experimental details. Mice were terminally perfused with PBS two days after the final dose of treatment was administered and the brains were removed for post-mortem examination. Tumours are black due to the melanin secreted by the B16 melanoma cells.

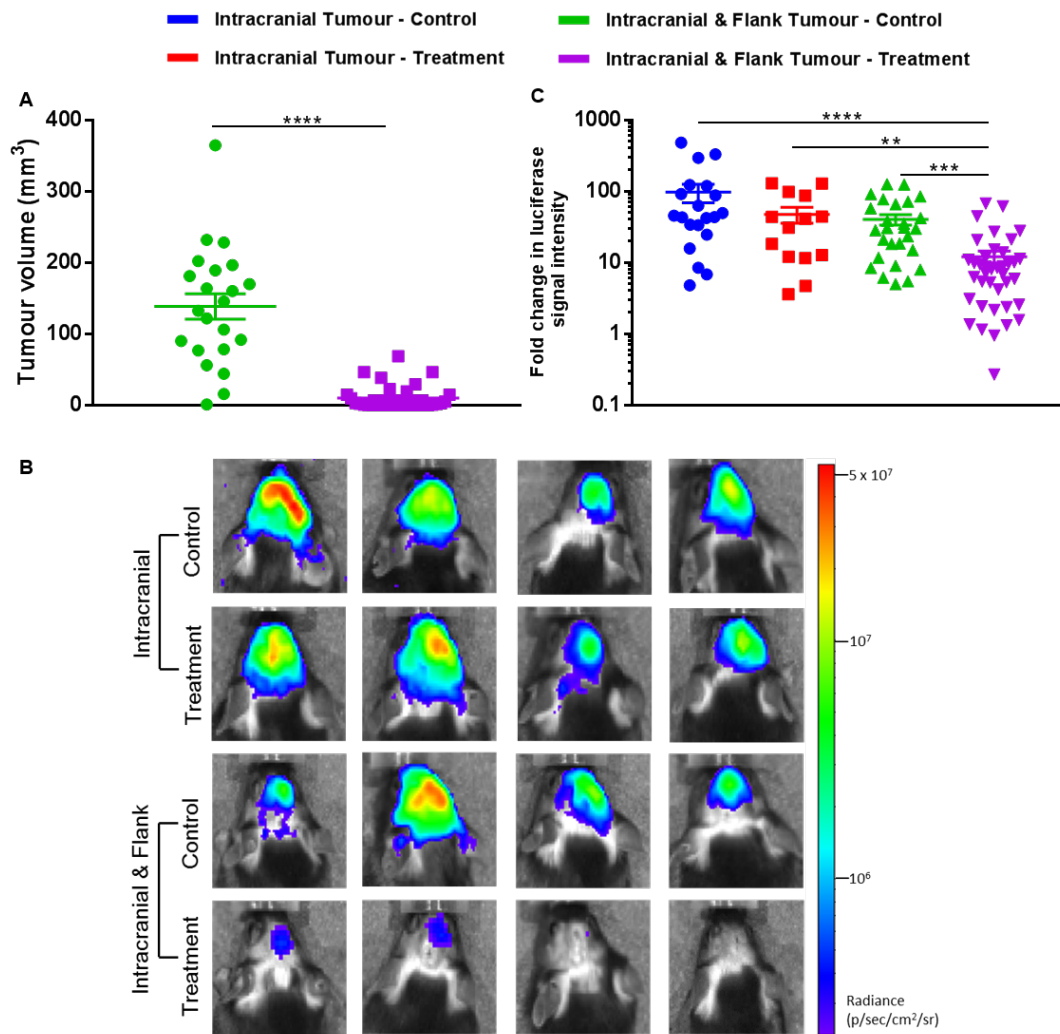


Figure 3.10 The effects of a flank tumour on intracranial tumour growth in mice treated with anti-PD-1 and anti-CTLA-4

B16/Fluc cells were intracranially implanted into mice with an additional group also subcutaneously implanted with B16/Fluc cells. These two groups of mice were subdivided into two further groups, one of which received the IgG isotype (Control) antibody while the other received the combination of anti-PD1 and anti-CTLA-4 (Treatment). Treatment was administered four times over six days. **(A)** Flank tumour measurements were taken the day after the final dose of treatment was administered using calipers. Measurements were taken from two dimensions and the tumour volume was subsequently calculated. **(B)** Representative bioluminescence images of mice taken nine days-post intracranial implantation. **(C)** The fold change in luciferase signal intensity was calculated as previously described. (n = 20, 14, 25, 42; data is from four independent experiments; error bars represent SEM; statistical significance was determined by pairwise Mann-Whitney tests).

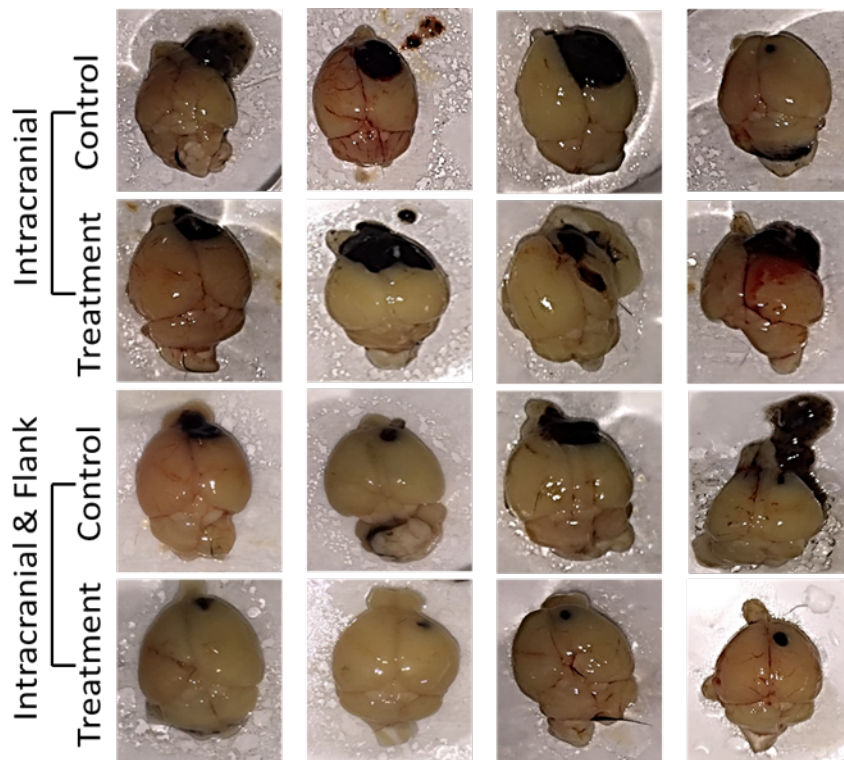


Figure 3.11 Post-mortem brain images of mice treated with anti-PD-1 and anti-CTLA-4 or IgG control antibody with or without a flank tumour
See Figure 3.10 for experimental details. Mice were terminally perfused with PBS the day following the final dose of treatment and the brains were removed for post-mortem examination. Tumours are black due to the melanin secreted by the B16 melanoma cells.

These observations were again confirmed with post-mortem examination of the brains, where the mice with an intracranial and flank tumour receiving anti-PD-1 plus anti-CTLA-4 had smaller tumours than the other three groups. (Figure 3.11).

3.5 A flank tumour is critical for prolonged survival of mice with melanoma brain metastases

Since giving GM-CSF alongside checkpoint inhibitors had little to no additional advantage over immune checkpoint therapy alone ($P = 0.857$), GM-CSF was omitted from the treatment for future experiments. As it was confirmed that a flank tumour was essential for reducing intracranial tumour growth, the next step was to see how the flank tumour would affect OS in the context of the combined anti-PD-1 and anti-CTLA-4 therapy. Mice were implanted with tumours and treatment was administered as outlined in Figure 3.7. The survival curves of mice in both control groups and in the treatment group with only an intracranial tumour followed near identical trends with the last of these mice only living to day 16 before succumbing to their intracranial disease (Figure 3.12). Nevertheless, mice with an intracranial and flank tumour who received the treatment had a significantly prolonged survival compared to the other groups ($P = 0.0027$ (intracranial tumour – control); 0.004 (intracranial – treatment); 0.0023 (intracranial and flank - control)) (Table 3.2). A number of these mice eventually had to be sacrificed due to symptoms from their intracranial tumour; however, approximately 40% of these mice survived until the endpoint of the experiment (day 21) and presented with little to no visible tumour burden upon post-mortem examination.

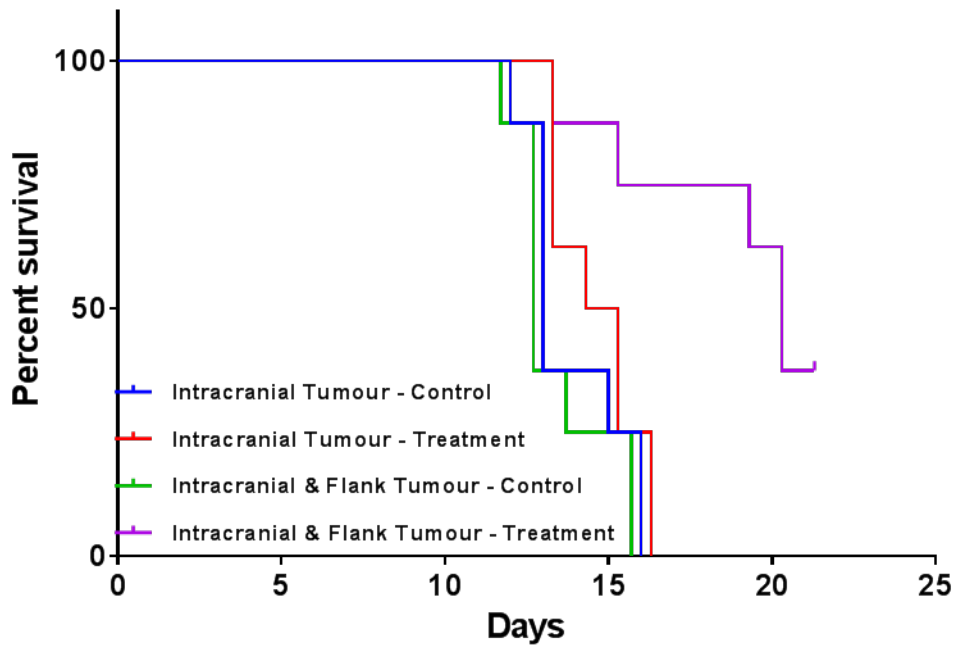


Figure 3.12 The effect of a flank tumour on the survival of mice treated with anti-PD-1 and anti-CTLA-4

B16/Fluc cells were intracranially implanted into mice with an additional group also subcutaneously implanted with B16/Fluc cells. These two groups of mice were subdivided into two further groups, one of which received the IgG isotype (Control) antibody while the other received the combination of anti-PD1 and anti-CTLA-4 (Treatment). Treatment was administered four times over six days. Mice were sacrificed once they presented with terminal symptoms.

Compared to treatment group with intracranial & flank tumour	P
Intracranial Tumour – Control	0.0027
Intracranial Tumour – Treatment	0.004
Intracranial & Flank Tumour – Control	0.0023
Overall	0.003

Table 3.2 Statistical analysis for the effects of a flank tumour on the survival of mice treated with anti-PD-1 and anti-CTLA-4

For the survival study, statistical significance was calculated by the Log-rank test. Significance threshold was adjusted to 0.0167 to compensate for multiple comparisons.

3.6 Discussion

In this chapter we have established a novel model of MBrM that allows for quantification of intracranial therapeutic efficacy in the presence of extracranial disease. In this study, the B16 F1 melanoma cell line was used to model MBrM. While, in essence, the B16 model is a suitable model for studying MBrM, there are a few drawbacks. On rare occasions, mice were found dead with no signs of flank tumour ulceration and post-mortem examination revealed them to have died from a brain haemorrhage caused as a result of intracranial tumour growth.

The rapid growth of B16 cells may be an important factor in the unexpected and sudden death of the mice. The short timeline from tumour initiation to the experimental endpoint (nine to 10 days) is also a poor representation of the human disease. This model also presented other issues; for instance, the onset of terminal symptoms that would normally develop over time in other intracranial models would be sudden and difficult to intercept in an appropriate amount of time. As a result, for survival studies, mice had to be monitored regularly from the point that terminal symptoms would begin to present. The Ret-melanoma model of spontaneous brain metastases may prove to be a more translatable model due the three- to six-month time from initiation to development of brain metastases²⁷¹. Moreover, the slower time for tumour progression to occur may increase the therapeutic effect of checkpoint inhibitor therapy.

For the purpose of this study, the intracranial implantation of cancer cells¹⁶³ was selected for the initiation of intracranial tumours. This method has a number of advantages over others used to induce brain tumour growth, such as the procedure itself being simpler than other methods, allowing higher throughput and, therefore, larger experimental groups. Moreover, this technique results in the growth of a large single tumour in the brain parenchyma, which is advantageous for analysis of the TME by flow cytometry. However, it should be noted there were instances where cancer cells would disseminate through the brain, mainly the midline, forming small,

lethal tumours in the brain stem. Other procedures, such as carotid artery injection¹⁵⁰, tend to result in the formation of multiple microlesions. While this is clinically relevant, it would make further analyses of the tumours more challenging. Additionally, this procedure is more surgically demanding, resulting in a lower throughput and additional complications related to the surgery (risk of stroke and death). Conversely, both of these methods are better suited to the purpose of this study than the tail vein²⁷² and the intracardiac injection methods. While the tail vein injection intravenous (*i.v.*) technique will produce brain metastases in a low proportion of mice, the cells will primarily disseminate to the lungs²⁷³. The intracardiac procedure has a higher occurrence of intracranial tumour development, although this does appear to be reliant on the initial number of cells injected²⁷³. This method has also been shown to give rise to metastases in most visceral organs, making this more suitable for the study of metastases in general, rather than metastatic disease in a specific location²⁷³. This technique has, however, been reported to be highly variable, with its outcome being susceptible to a number of variables, such as the number of sites that tumours can simultaneously metastasise to. More importantly, when studying brain metastases with these methods, the mice have a higher likelihood of developing terminal symptoms from metastatic disease in other organs before an intracranial tumour has time to establish^{272,273}. This issue can arise in the Ret-melanoma model that spontaneously develop metastases in the brain; as a result, a larger number of mice are required to obtain efficient numbers of mice bearing intracranial metastases²⁷¹. The important characteristic of our model is that it allows the study of survival in dependence of the intracranial tumour growth and in the presence of extracranial disease.

Whilst subcutaneous tumour growth can easily be monitored, observing intracranial tumour growth represents more of a challenge. Traditional techniques such as MRI can be used; however, this can be expensive and time-consuming²⁷⁴. Firefly luciferase reporter tags have become extremely useful for monitoring tumour growth, especially for intracranial tumours, allowing for high-throughput and relatively accurate imaging^{274,275}.

Nonetheless, bioluminescence imaging does have some shortcomings. For example, the IVIS used for this imaging is unable to image C57BL6 mice in three dimensions due to the pigment in their skin. As a result, bioluminescence imaging cannot take into account the depth of the tumour within the tissue. Thus, a tumour on the surface of the brain will have a larger signal intensity than a tumour of equal size growing within the brain parenchyma²⁷⁵. With this in mind, the fold change in luciferase signal intensity was calculated as a measure of tumour growth to account for this variance. Additionally, the strain of mouse must also be considered when using bioluminescence imaging, as the skin pigment and dark fur of C57BL6 mice can be a hindrance if not controlled for correctly²⁷⁶. This may not always be possible, as mice can occasionally have a thicker coat of fur and removing this can be difficult, while nothing can be done to change their skin pigmentation. Nevertheless, as previously discussed, these issues can be partially controlled by focusing on the fold change in luciferase intensity rather than the final signal intensity. A major advantage bioluminescence imaging has over an MRI is its ability to detect tumours at much earlier stages in their development²⁷⁵. Studies have shown that there is a strong correlation in tumour growth, in a therapeutic response context, between these two methods^{277,278}. As such, while bioluminescence imaging is an extremely useful tool for monitoring intracranial growth, it must be used in conjunction with other methods for precise conclusions to be made. In our study, we were able to confirm reduced tumour growth as quantified by bioluminescence imaging and by visual examination of the brains post-mortem.

Although there has been a substantial amount of research focusing on the use of immune checkpoint inhibitors to treat cancer, there has been a severe lack of research on brain tumours. This work, however, has proved useful as a basis for this study. As such, the dose of 10 mg/kg of anti-PD-1 and anti-CTLA-4 were selected after being reported to be effective in multiple sources^{93,209,231,259,279–281}. Likewise, the treatment regime of four doses over six days has also previously been reported to be effective in other studies²⁴⁵

and, when considering the timeline of the MBrM model, this regimen seemed the most appropriate.

There has been evidence to show that the addition of GM-CSF can be beneficial for immunotherapies^{179,259}. This effect was not observed in the case of intracranial tumours in our model. The combinations of anti-PD-1 or anti-CTLA-4, respectively, with GM-CSF, had a significant effect on the flank tumour growth in our study, as previously reported^{204,259,261}. Moreover, the triple therapy combination did not have any survival advantage over the combination of anti-PD-1 plus anti-CTLA-4 alone. As a result, it was decided to omit GM-CSF from the therapy in future experiments. Additionally, as the effects of GM-CSF on T-cells are not fully understood^{179,282} and these are the main population known to be involved in immune checkpoint therapy, it was decided to focus on the mechanism behind effective immune checkpoint therapy within the brain first, before adding an additional layer of complexity.

While this is the first reported study showing the effective treatment of brain metastases with immune checkpoint inhibitors, it is not the first to show efficacy in the brain. A study has recently reported that anti-PD-1 and anti-CTLA-4 can lead to the long-term survival of mice with intracranial GL261 tumours, a mouse model of glioma²⁴⁰. Nevertheless, there are a number of significant differences between the GL261 model and the MBrM model. Firstly, the GL261 model is a less aggressive model with terminal symptoms presenting after approximately 21 days²⁴⁰, compared to nine days for the B16 MBrM model. This slower model allows for multiple treatment cycles each consisting of multiple doses, in addition to allowing more time for the treatment to take effect. Another point that must be taken into consideration is that in the GL261 study, the treatment began with an initial dose of 20 mg/kg before continuing with subsequent doses of 10 mg/kg. While there is no reported evidence that a larger initial dose makes a significant difference to overall outcome, this has interesting implications for future studies as a larger initial dose may have significant effect on the overall outcome of the efficacy of treatment. From the translational aspect, this lower dose may be

more advantageous due to more prominent occurrences of irAEs in humans treated with checkpoint inhibitors that are rarely observed in mice²⁸³; especially as in the clinic anti-PD-1 doses tend to range from 2-10mg/kg²⁸⁴⁻²⁸⁶, while anti-CTLA-4 doses tend to be 10 mg/kg^{246,287}.

This study demonstrated that immune checkpoint therapy can increase the survival of mice with an intracranial and flank tumour. This increase in survival can be directly related to inhibition of the intracranial tumour growth. As previously observed, mice bearing a flank tumour alone did not present with any symptoms indicating metastases elsewhere in the body. In addition, the flank tumour took an average of 17 days to reach its maximum allowed dimension, whereas the mice with intracranial tumours began showing symptoms from day nine. As such, it can be concluded that the terminal symptoms that the mice presented with were a consequence of intracranial tumour growth and not a consequence of the extracranial disease.

Although the combination of anti-PD-1 and anti-CTLA-4 failed to inhibit intracranial tumour growth in some mice with an intracranial and flank tumour, this was not unexpected. It has widely been reported that there are responders and non-responders both in the clinic and in pre-clinical studies^{231,288}. While there has been a substantial amount of research into why this occurs and whether it is possible to predict who will benefit the most from this treatment, there has been little progress. Differences in TIL phenotype have been observed after treatment; however, there are no predictive biomarkers²⁸⁹⁻²⁹¹. Other studies have suggested that mutational load within the tumour could be a prognostic marker for immune checkpoint therapy response, as a higher mutational load has been correlated with an increase in survival²⁹². Nevertheless, this study would suggest that the patients with brain metastases that would fall into the responder category could benefit from this treatment. In addition, the discovery of a reliable predictive biomarker could ensure that brain metastasis patients are no longer overlooked for immune checkpoint therapy.

The lack of a complete response to the treatment in all mice may be due to the aggressive nature of the B16 tumours and the short progression time for the intracranial tumours. While this may be problematic in the rapid MBrM model, this may not apply to other cell lines as the previously discussed GL261 model²⁴⁰ showed slower tumour progression and a higher response rate to the therapy. Fortunately, this may not pose to be a problem in the clinic as even the patients with the worst prognosis tend to have a few months of survival from the diagnosis of their brain metastases^{26,27,29}. This may allow for the extra time needed to elicit an effective anti-tumour immune response, although other factors, as previously discussed, will also play a role in the outcome.

The difference in complete responses between the MBrM model and the commonly used subcutaneous or intracranial models are most likely due to the tumour site. Historically, the brain has been described as an immune-privileged site due to the presence of the BBB²⁹³. This opinion is starting to change with the more recent discovery of a lymphatics system within a mouse brain^{140,294}. As this is still an emerging field of research, the differences and similarities between the CNS lymphatics and the lymphatics in the rest of the body are unknown. Further investigation may give rise to explanation for the observed differences between intracranial and extracranial tumours.

As discussed in this chapter, effective immune checkpoint therapy for intracranial tumours requires extracranial disease. This should not, however, exclude patients without extracranial disease at the time of diagnosis from this treatment; the vast majority of patients would have previously experienced some form of extracranial disease and this may be sufficient to have the desired effect. Addressing this would require additional research involving mice that had been cured from their extracranial disease and subsequently challenged with an intracranial tumour. While this has been shown in subcutaneous models^{204,295-297}, it would be interesting to revisit this

in the context of intracranial tumours to investigate if this protection is, indeed, truly systemic.

In summary, this study demonstrates that the combination of anti-PD-1 and anti-CTLA-4 can effectively treat melanoma brain metastases with and without the addition of GM-CSF. However, this effect is reliant on the presence of a flank tumour, as the therapy is ineffective in mice with only an intracranial tumour. We developed this model with a translational aspect in mind, to provide evidence that patients with melanoma brain metastases may benefit from this therapy in spite of their poorly viewed prognosis.

Chapter 4:

Determining the functional roles of immune cells in the treatment of melanoma brain metastases with immune checkpoint therapy

Chapter 4

4.1 Introduction

With a substantial amount of research focusing on the use of immune checkpoint inhibitors into the treatment of cancer, there has been a considerable effort put into the mechanisms behind this. Since immune checkpoint inhibitors alter the immune system and the activation state of immune cells, there has been an emphasis on discovering which immune cell populations are crucial to the therapeutic effect and which can be detrimental.

While previous research has identified a number of essential immune cell populations for effective immune checkpoint inhibitor therapy, the research has mainly been based on flank tumour models. As such, this must be revisited in the context of intracranial tumours, as the role of the BBB and the uniqueness of the brain microenvironment cannot be ignored.

This chapter will focus on determining which immune cell populations are the 'major players' in the therapeutic effect seen when mice with B16 intracranial and flank tumours are treated with the combination of anti-PD-1 plus anti-CTLA-4. This was achieved through the *in vivo* depletion of various immune cell populations in mice receiving anti-PD-1 plus anti-CTLA-4 and the subsequent quantification of the survival.

4.2 CD8⁺ T-cells and NK cells are essential for effective intracranial immune checkpoint inhibitor therapy

A literature search into the main immune cell populations involved in immune checkpoint inhibitor therapy clearly revealed CD4⁺ T-cells, CD8⁺ T-cells and NK cells as the crucial cells involved^{195,231,242,243,280,285}, thus becoming the first three candidates for *in vivo* depletion. As outlined in the previous chapter, the presence of an extracranial tumour was fundamental for the

combination of anti-PD-1 and anti-CTLA-4 to have a therapeutic effect. As a result, this model was used for the following immune cell depletion experiments.

The experimental timeline closely followed that outlined in the previous chapter (Figure 3.7), with all mice receiving four doses of anti-PD-1 plus anti-CTLA-4 (Figure 4.1). In addition, mice were given *i.p.* injections of either an anti-CD8 α antibody (CD8⁺ T-cell depletion), anti-CD4 antibody (CD4⁺ T-cell depletion) or anti-Asialo GM1 antibody (NK cell depletion) every four days for the duration of the experiment. Initial injections of cell-depleting antibodies were administered three days prior to the subcutaneous implantation of B16/Fluc cells (day -three) to allow for the population of interest to be fully depleted before tumour initiation. Blood samples were collected prior to treatment administration and two days-post intracranial implantation (day five) to confirm that the immune populations of interest were depleted. Samples were analysed by flow cytometry in comparison to the blood of mice bearing flank and intracranial tumours that had not undergone immune cell depletion. This analysis confirmed that each of the intended cell populations had been successfully depleted (Figure 4.2). In the blood, CD8⁺ T-cells were depleted to 0.3% \pm 0.09%; NK cells were depleted to 0.45% \pm 0.18%; CD4⁺ T-cells were depleted to 0.86% \pm 0.13%. ($P = <0.0001$; 0.02; <0.0001 , respectively).

The mice were closely monitored following the final treatment dose for terminal symptoms caused by the intracranial tumour and euthanized once the symptoms became apparent. The intracranial tumours were then isolated and the infiltrating immune cells were examined by flow cytometry to confirm that the intended immune cell populations were depleted within the tumour. In the intracranial tumour, CD8⁺ T-cells were depleted to 0.16% \pm 0.03%; NK cells were depleted to 0.63% \pm 0.24%; CD4⁺ T-cells were depleted to 0.76% \pm 0.46%. ($P = <0.0001$; 0.0017; 0.0026, respectively)

(Figure 4.3). NK cell-depleted mice presented with terminal symptoms earlier than the other groups, with the entire group having to be sacrificed by day 16 (Figure 4.4A). This decrease in survival compared to the non-immune cell-depleted mice was statistically significant ($P < 0.0001$), highlighting the importance of NK cells.

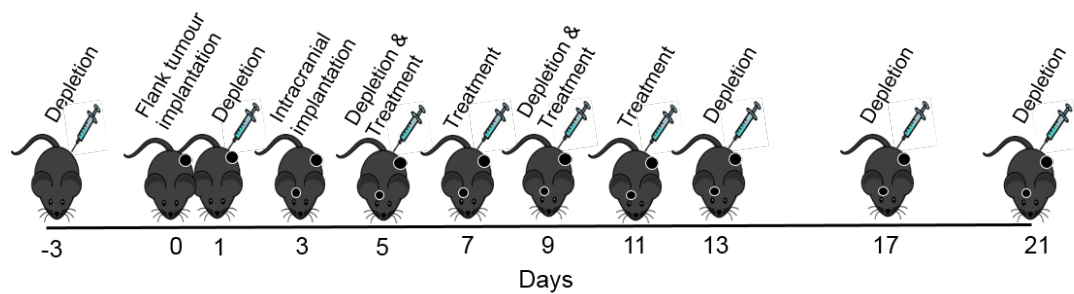


Figure 4.1 Timeline for immune cell depletion experiments

C57Bl6 mice were randomised into groups and given an *i.p.* injection of either anti-CD8 α (CD8 depletion), anti-CD4 (CD4 depletion), anti-Asialo GM1 (NK depletion) or anti-F4/80 (macrophage depletion). All mice received a subcutaneous injection of 2×10^5 B16/Fluc cells, three days following the initial injection of the depleting antibody (day 0), along with a group of mice that had received no immune cell depletion. Following this, three days later, all mice received an intracranial injection of 1×10^5 B16/Fluc cells (day three). Two days-post intracranial implantation (day five), all mice were treated with anti-PD-1 plus anti-CTLA-4 and were given three subsequent doses two days apart (days seven, nine and 11). The immune cell-depleted mice all received top-up injections of their depletion antibodies every four days until the end of the experiment (days one, five, nine, 13 and 17) or until the mouse had to be euthanized. Mice were sacrificed once they presented with terminal symptoms resulting from their intracranial tumour growth.

In the case of the CD8⁺ T-cell-depleted mice, a number also displayed symptoms due to intracranial growth from as early as day 10. Nevertheless, the presentation of terminal symptoms was staggered compared to the NK cell-depleted mice. There was ultimately a significant decrease in survival of the CD8⁺ T-cell-depleted mice as compared to the non-immune cell-depleted mice ($P = 0.002$) and one mouse survived until the end of the experiment (day 21).

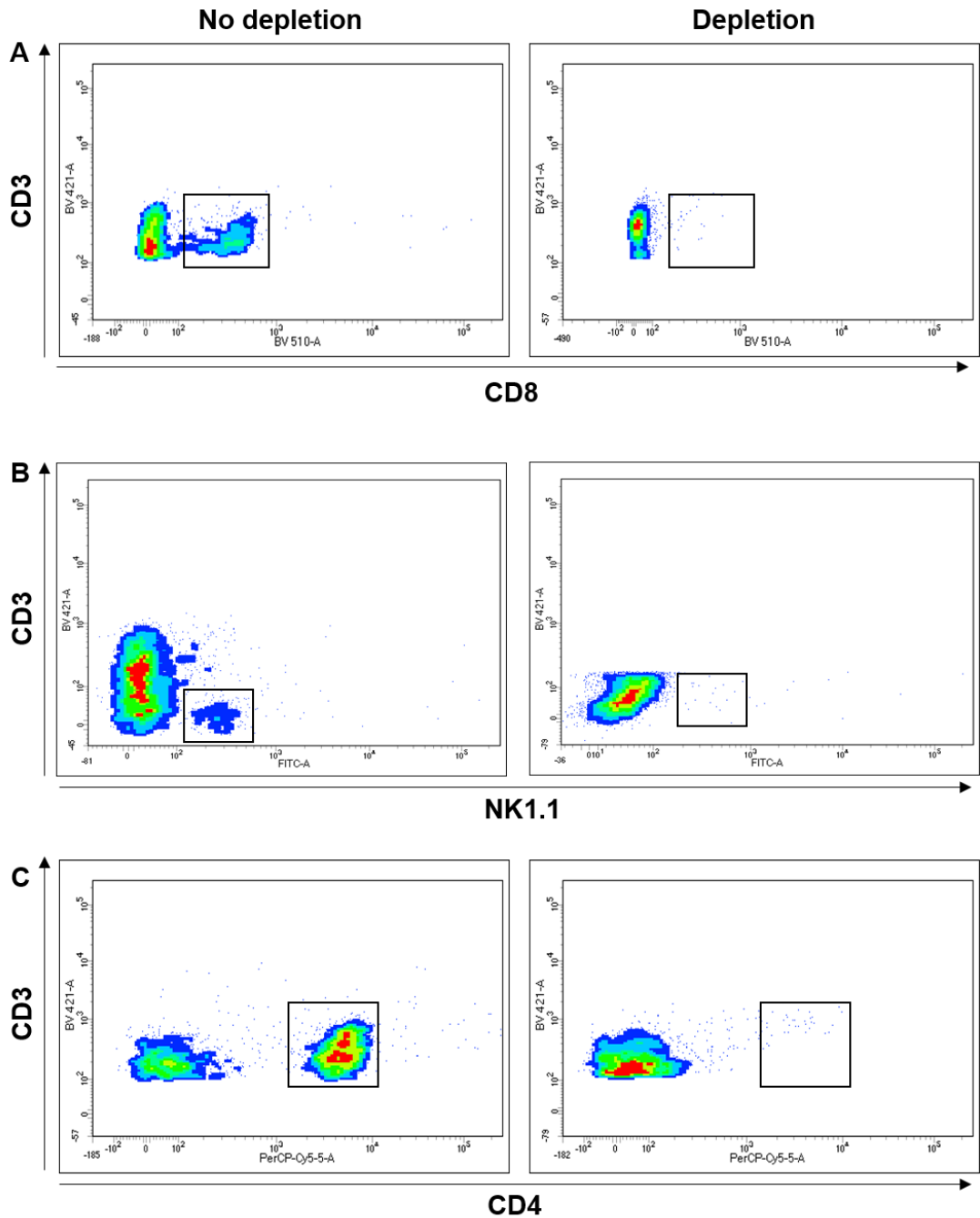


Figure 4.2 Immune cell depletion was confirmed through blood analysis

Immune cell-depleting antibodies were administered as outlined in Figure 4.1. On day five, blood samples were taken from mice in each immune cell depletion group and compared to blood taken from non-immune cell-depleted mice by flow cytometry. **(A)** Anti-CD8, **(B)** anti-Asialo GM1 and **(C)** anti-CD4 .

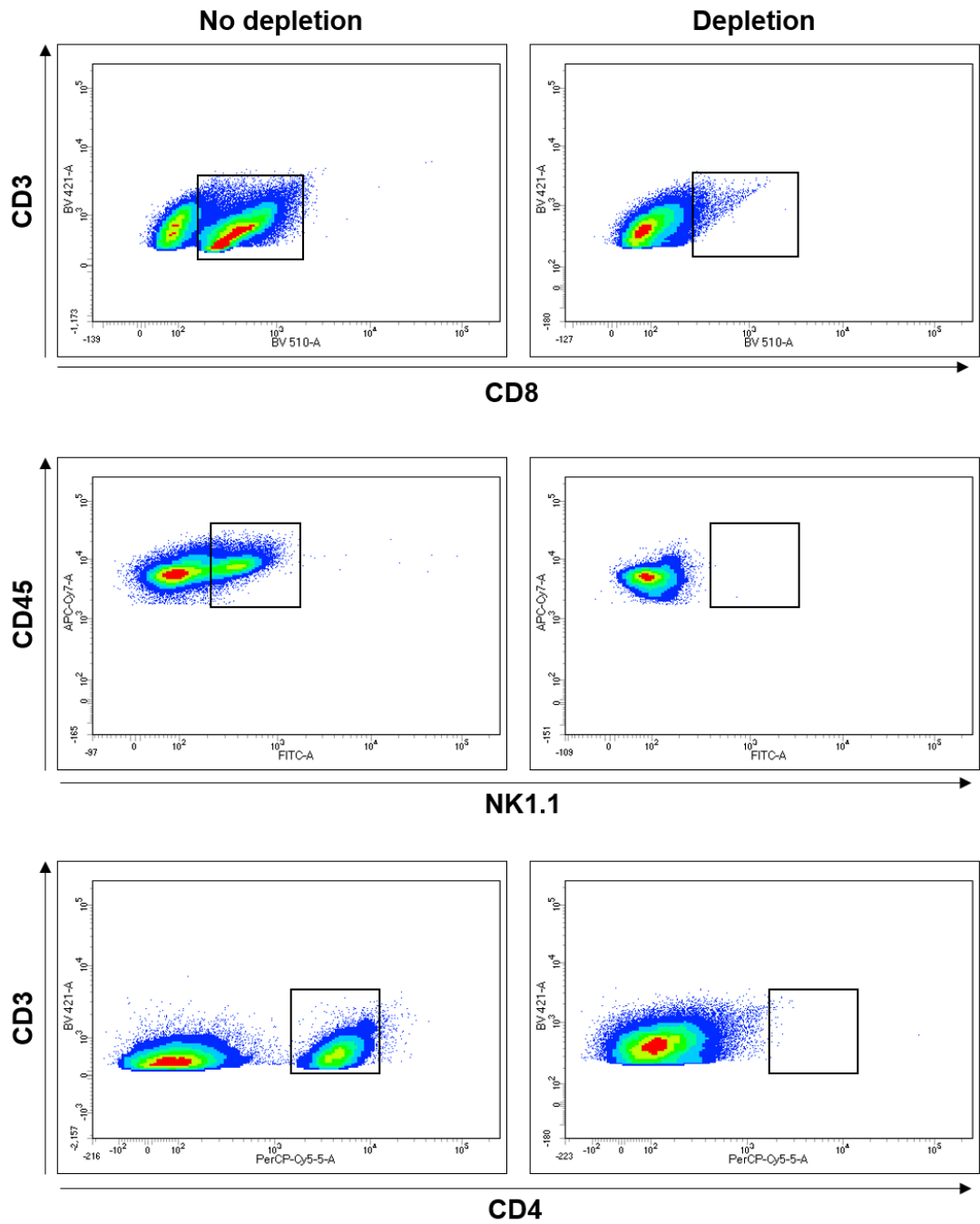


Figure 4.3 Confirmation of immune cell depletion at experimental endpoint in intracranial tumours

Tumours were enzymatically dissociated into a single-cell suspension and stained for flow cytometry to ensure that the intended immune cell populations had been depleted within the intracranial tumour.

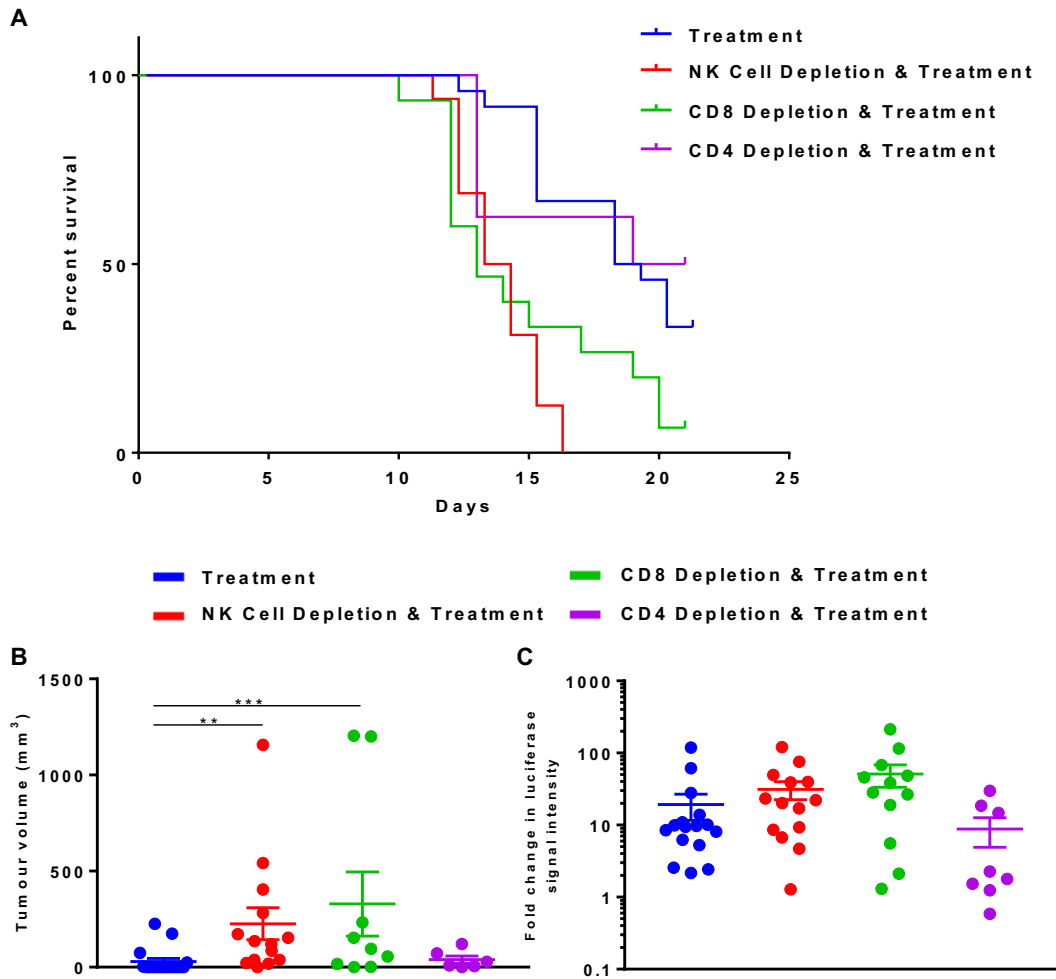


Figure 4.4 Effects of immune cell depletion on the survival of mice bearing B16 flank and intracranial tumours undergoing immune checkpoint therapy

(A) The survival of mice with B16 intracranial and flank tumours treated with anti-PD-1 plus anti-CTLA-4 plus respective immune cell-depleting antibodies were compared to the survival of non-immune cell-depleted mice receiving the same treatment. (B) Flank tumour measurements were taken and tumour volume was calculated at the terminal time point. (C) Bioluminescence imaging was used to measure intracranial tumour burden nine days-post intracranial implantation (day 12) and the fold change in luciferase signal intensity between day five and day 12 was calculated. (See Table 4.1 for statistics).

Prolonged survival was not, however, observed in the CD4⁺ T-cell-depleted mice, with 50% of the mice surviving until the end of the experiment (P = 0.96 in comparison to the non-immune cell-depleted mice). There were some noticeable differences between the mice that survived until day 21 compared to those that had to be sacrificed earlier: while also presenting with symptoms associated with intracranial tumour growth, the mice that were sacrificed earlier additionally exhibited eczema-like symptoms, indicative of an autoimmune response²⁸⁰.

The terminal flank tumour dimensions were also recorded, with the tumour volumes subsequently calculated. This analysis revealed that flank tumours were significantly larger in mice that were depleted of their NK cells and those who received the CD8 depletion antibody as compared to the non-immune cell-depleted mice (P = 0.0004 and 0.0011, respectively) (Figure 4.4B). There was, however, no noticeable difference between the CD4⁺ T-cell-depleted mice and the non-immune cell-depleted mice.

In addition, bioluminescence imaging was performed on day 12 to assess whether there was any indication of differences in intracranial tumour size between the groups. While there was no statistically significant difference between any of the groups, there was a tendency for mice in the CD8- and NK cell-depleted groups to have an increased fold change in luciferase signal intensity when compared to the non-immune cell-depleted group (Figure 4.4C and Table 4.1).

4.3 Antibody-mediated macrophage depletion within intracranial tumours

One of the major immune cell populations that has received relatively little attention in the context of immune checkpoint inhibition are macrophages. While they are not as renowned for their cancer-killing ability as CD8⁺ T-cells and NK cells, under specific conditions they can directly eliminate cancer cells^{298 299}. Macrophages do, however, play a crucial role in tumour

development, whether that be pro- or anti-tumourigenic. Macrophages have long been known to act as APCs, aiding the adaptive immune system³⁰⁰. Tumours can also recruit TAMs to support their development by inducing an anti-inflammatory environment favouring tumour growth³⁰⁰. Likewise, macrophages and cells of a similar lineage have been shown to express PD-L1, suggesting they may have a role in anti-PD-1 therapy and, thus, warrant further study³⁰⁰.

Compared to treatment	Survival (P)	Tumour volume	Fold change in luciferase activity
NK cell depletion & treatment	<0.0001	0.0004	0.1536
CD8 depletion & treatment	0.002	0.0011	0.0999
CD4 depletion & treatment	0.96	0.0828	0.1719
Macrophage depletion (HP-198) & treatment	0.0003	-	-
Macrophage depletion (commercial) & treatment	0.24	-	-

Table 4.1 Statistical analysis for the survival and tumour burden of mice with flank and intracranial B16 tumours undergoing immune cell depletion and immune checkpoint therapy

For the survival study, statistical significance was calculated by the Log-Rank test. The significance threshold was adjusted to 0.0125 to compensate for multiple comparisons. For the tumour volume and Fold change in luciferase activity statistical analyses, pairwise Mann-Whitney tests were used.

To address their role, an anti-F4/80 antibody was used to deplete macrophages in the mice. The anti-F4/80 antibody was collected from the cell culture medium of the HP-198 cell line³⁰¹, concentrated and quantified using a rat IgG ELISA (Figure 4.5). The antibody was then utilised in the same schedule as previously described (Figure 4.1), every four days. The depletion efficacy was tested through flow cytometry analysis of blood samples. The results of this analysis proved to be inconclusive, as a distinct macrophage population was not detected, even in the non-immune cell-depleted mice (Figure 4.6A). The mice receiving the anti-F4/80 antibody began to show symptoms earlier than mice in the other depletion groups,

with the entire group having to be euthanized by day 14 (Figure 4.6B). While this turned out to be statistically significant when compared to the non-immune cell-depleted mice ($P = 0.0003$), there was no conclusive evidence this was due to the depletion of macrophages. The mice presented with symptoms following the anti-F4/80 antibody injection, suggesting there may have been some toxicity caused by the antibody itself.

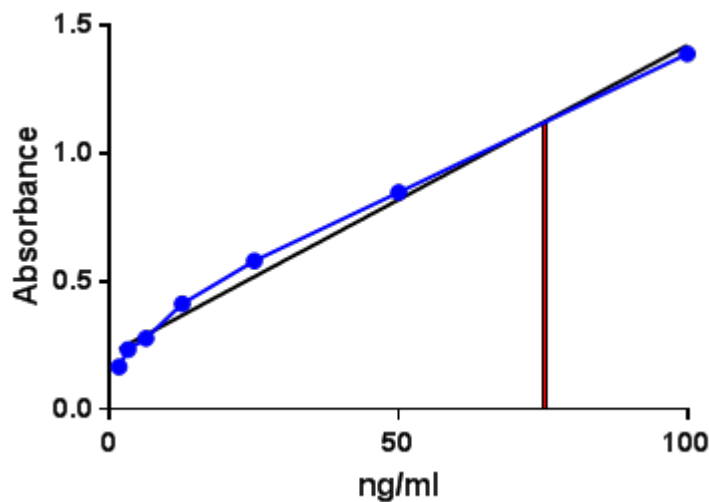


Figure 4.5 Quantification of the anti-F4/80 antibody produced by the HB-198 cell line

The supernatants from HP-198 cultures were collected, filtered and concentrated. The concentration of antibody was determined using an IgG ELISA. Serial dilutions of the supernatants were analysed and the dilution that gave an optical density that fell in the exponential region of the standard curve was used to extrapolate the total stock concentration of antibody within the supernatants.

As the results from the macrophage depletion experiment were unreliable, it was decided to repeat the experiment with a commercially available antibody which has a macrophage-depleting function³⁰². The same schedule as used previously (Figure 4.1) was repeated, with the exception of the depletion antibody being administered every two days (as this was previously reported to result in successful depletion³⁰²). Since checking the blood of mice proved to be an ineffective method for confirming macrophage depletion, we decided to analyse the intracranial tumours instead (Figure 4.7A). The anti-F4/80 antibody was well-tolerated by the mice, with no signs of toxicity. The

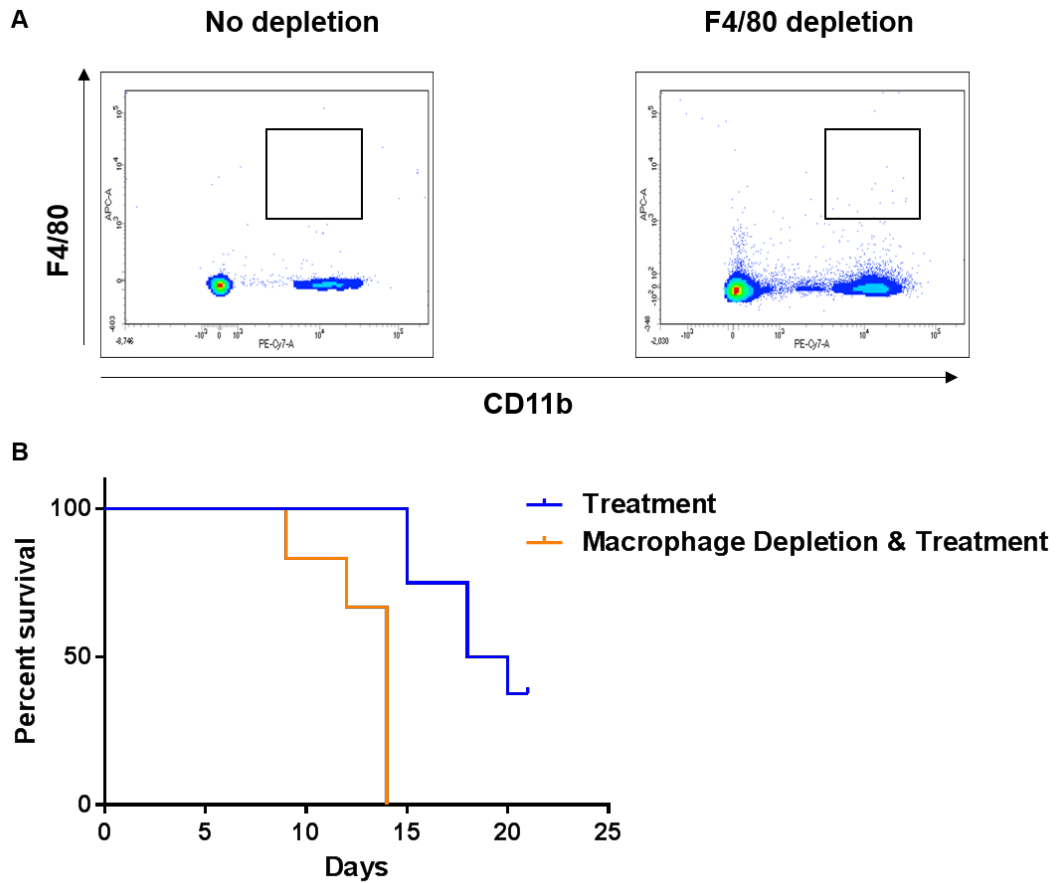


Figure 4.6 Depletion of macrophages with HB-198-derived anti-F4/80 antibody

(A) Mice were injected with anti-F4/80 antibody as outlined in Figure 4.1; on day five blood samples were collected and compared to those taken from mice that did not undergo immune cell depletion. **(B)** The survival of these mice was subsequently compared to the survival of mice that had not undergone immune cell depletion. (See Table 4.1 for statistics).

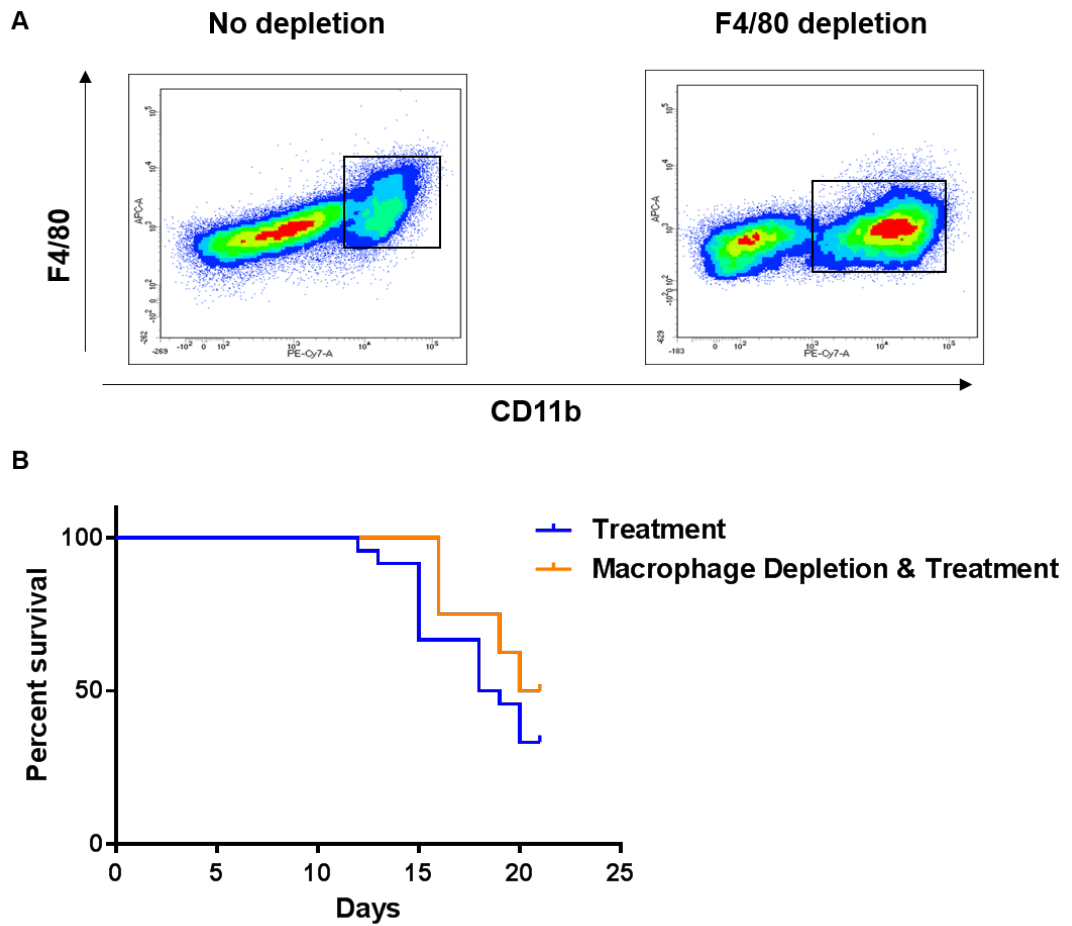


Figure 4.7 Depletion of macrophages with a commercial anti-F4/80 antibody

(A) Mice were injected with an anti-F4/80 antibody as outlined in Figure 4.1; on day five blood samples were collected and compared to those taken from mice that did not undergo immune cell depletion. **(B)** The survival of these mice was subsequently compared to the survival of mice that had not undergone immune cell depletion. (See Table 4.1 for statistics).

mice that received the anti-F4/80 antibody took longer to show terminal symptoms than the non-immune cell-depleted mice. The first macrophage-depleted mouse began showing symptoms at day 16, compared to non-immune cell-depleted mice showing symptoms at day 13. By the end of the experiment (day 21), 50% of macrophage-depleted mice were still alive; nevertheless, this was not significant ($P = 0.34$) when compared to the survival of non-immune cell-depleted mice (Figure 4.7B). Once again, however, a definitive conclusion could not be made, as the flow cytometry analysis of the tumours showed there was still macrophages present within the intracranial tumour of the macrophage-depleted mice ($17.95\% \pm 3.38\%$; $P = 0.54$, as compared to the non-immune cell-depleted mice).

4.4 Discussion

This chapter validated the role of three distinct immune cell populations in immune checkpoint inhibitor therapy. We demonstrated that $CD8^+$ T-cells are crucial for effective anti-PD-1 plus anti-CTLA-4 therapy within the brain. The importance of $CD8^+$ T-cells was in-line with their implication in effective anti-PD-1 treatment, as well as anti-CTLA-4 treatment and the combination treatment with additional therapeutic agents in extracranial tumours^{195,231,242,243,280,284,285}. The successful treatment of B16 tumours with anti-PD-1 or anti-CTLA-4 plus different oncolytic viruses has been shown by others to be dependent on $CD8^+$ T-cells^{243,303}. While Reardon *et al.* did not analyse the functional importance of $CD8^+$ T-cells in the orthotopic GL261 glioma model, they did show an increase in $CD8^+$ T-cell infiltration²⁴⁰.

It should be noted that the antibody used in this study does not exclusively deplete $CD8^+$ T-cells, as subsets of DCs, NK cells and thymocytes also express $CD8\alpha$ ^{304,305}. There have also been reports of a small subset of regulatory T-cells that express the $CD8\alpha$ glycoprotein³⁰⁶. Any depletion of $CD8\alpha^+$ DCs could have had a significant effect in the model used in this study, as these cells are known to be more efficient at the cross-presentation of exogenous cell-bound and soluble antigens on MHC I, as compared to

CD8 α ⁻ DCs³⁰⁴. Additionally, CD8 α ⁺ DCs are more competent in the phagocytic uptake of dead cells and the presentation of dead-cell-associated antigens³⁰⁴. While the exact role of these cells is currently unknown in the context of immune checkpoint therapy, we cannot exclude their involvement in the model used here. That being said, it has been suggested that the additional effects caused by the depletion of CD8 α ⁺ DCs in addition to CD8⁺ T-cells would be minimal due to their close association with the CD8⁺ T-cells³⁰⁴. There are other methods available to deplete CD8⁺ T-cells, such as CD8 α KO mice³⁰⁷. The KO model cannot, however, discriminate between these cell types and still lacks all CD8⁺ populations³⁰⁸.

Another population of immune cells that proved to be essential for immune checkpoint therapy in the brain were the NK cells. As demonstrated here, upon NK cell depletion, immune checkpoint therapy was ineffective in mice with B16 flank and intracranial tumours. This supports evidence presented by others who have looked at the functional importance of NK cells in the context of immune checkpoint inhibitor therapy in extracranial tumours. In particular, in the B16 flank model, there is evidence showing the importance of NK cells when anti-PD-1 is used in combination with reovirus²⁴³. A similar study using Newcastle Disease Virus plus anti-CTLA-4 also showed the functional importance of NK cells in the treatment of B16 flank tumours³⁰³. Another group demonstrated that the rejection of B16 flank tumours was dependent on NK cells when treating with anti-CTLA-4 plus a GM-CSF-producing vaccine²⁰⁴. Similar effects were seen when anti-PD-1 was used in combination with an Adenosine A2A receptor inhibitor to treat orthotopic 4T1 tumours³⁰⁹. Notably, one study examining the efficacy of immune checkpoint inhibitors in the GL261 glioma model reported an increase in intratumoural infiltration of NK cells, without evaluating their functional contribution²⁴⁰. Interestingly, when mice with subcutaneous 4T1 tumours were treated with radiotherapy plus anti-PD-L1, the therapeutic effectiveness was unaffected by the absence of NK cells²⁸¹. Even though anti-PD-1 and anti-PD-L1 are thought to work through similar mechanisms, there clearly are some differences in their mechanism of action³¹⁰. An example being an anti-PD-1

can, in theory, block the interaction with PD-L1 and PD-L2, whereas an anti-PD-L1 antibody will still allow the interaction between PD-L2 and PD-1³¹⁰.

Even though the anti-Asialo GM1 used here is a commonly utilised antibody for the *in vivo* depletion of NK cells, it does not exclusively deplete this cell population. The expression of Asialo GM1 has been reported on subpopulations of NK T-cells, CD8⁺ T-cells and gamma/delta T-cells³¹¹. There has also been reports of Asialo GM1 expression on activated CD4⁺ T-cells, macrophages and eosinophils³¹¹; one study has also shown that the anti-Asialo GM1 antibody functionally depletes basophils³¹¹. Perhaps, for these reasons, there are alternative methods to specifically deplete NK cells *in vivo*, such as using NK cell KO mice³¹² or an anti-NK1.1 depletion antibody³¹³. Notably, however, some strains of mice will not express the NK 1.1 allotype³¹¹ and, for this reason, the anti-Asialo GM1 antibody is more commonly used for the depletion of NK cells *in vivo*.

While the functional roles of CD8⁺ T-cells and NK cells in immune checkpoint therapy in our model could be demonstrated within the restraints discussed above, the depletion of CD4⁺ T-cells had no significant impact on the treatment efficacy. In fact, the major effect of the CD4⁺ T-cell depletion was an increase in autoimmune inflammatory symptoms (e.g. eczema-like skin lesions), which have previously been described as a consequence of CD4⁺ T-cell depletion²⁸⁰. There are a number of different reports on the importance of CD4⁺ T-cells in immune checkpoint therapy. Some studies reported that the depletion of these cells has little to no effect on the overall survival of mice with extracranial B16 tumours when treated with either anti-PD-1²⁴³ or anti-CTLA-4^{303,204} in combination with other agents. Conversely, Davilla *et al.* used anti-CTLA-4 as one of the components of their combination therapy and found that the treatment was ineffective when B16 cells were implanted into CD4⁺ T-cell KO mice³¹⁴. Furthermore, CD4⁺ T-cell depletion did not affect the growth of d42ml-T3 sarcoma tumours treated with anti-CTLA-4³¹⁵. On the contrary, CD4 T-cell depletion partly affected the long-term survival of mice with Fo5 (breast) tumours when they were treated

with anti-PD-1, anti-CTLA-4 and trastuzumab emtansine (T-DM1)²⁸⁰. It should be noted that this may be in part a result of the autoimmunity caused by the depletion, as the authors did note that more than half of the mice presented with severe autoimmune inflammatory symptoms²⁸⁰. In conclusion, the role of CD4⁺ T-cells may be dependent on a number of factors, such as tumour type, tumour location and/or type of combination treatment used.

As with the other depletion antibodies, the anti-CD4 antibody used in this study does not exclusively deplete CD4⁺ T-cells. While not a prominent population in mice, one study found that there is a population of DCs which express CD4³¹⁶, in addition to CD4⁺ macrophages in mice and humans³¹⁷. That being said, there is no evidence to suggest they would play a prominent role in immune checkpoint inhibitor therapy. Another point that must be taken into consideration is that the CD4⁺ T-cell population is made up of a number of different populations with distinct functions³¹⁸. The CD4⁺ T-cell population can be divided into effector and regulatory cells, with each population having been implicated in anti-CTLA-4 therapy⁹³. It has been suggested that one of the mechanisms of effective anti-CTLA-4 therapy is through the depletion of T-Regs within the tumour^{93, 319}. While there is no reported method of selectively depleting the effector CD4⁺ T-cells, it is possible to deplete the T-Reg population. While some studies used an anti-CD25 antibody³²⁰, this will also deplete effector CD4⁺ T-cells³²¹ in addition to activated CD8⁺ T-cells³²². Taking this into account, a more appropriate model would be the inducible T-Reg KO model³²³. In this case, the effector CD4⁺ T-cells would be fully functional and, if used alongside an antibody-mediated CD4 depletion model, this may provide extra information about the roles of the effector and regulatory T-cell populations.

In our model, it was observed that the CD8- and NK cell-depleted mice had an increased flank tumour burden at the terminal timepoint as compared to the non-immune cell-depleted mice. This indicated that these immune cell populations were essential for the extracranial therapy as well, although

there were some cases in each of these depletion groups where there appeared to be some inhibition of tumour growth. This could suggest that, in some individuals, the role of the NK cells or CD8⁺ T-cells may have a more prominent role in the therapeutic effect than in others, and one immune cell population may be able to compensate for the missing population in the case of the depletion studies.

Along with the increased flank tumour burden in the CD8- and NK cell-depleted mice, there was a strong indication of an increased intracranial tumour burden in these groups. Although the latter did not reach statistical significance, it should be taken into account that, in both of these groups, some mice had to be sacrificed before the day of imaging due to their intracranial tumour burden, which removed mice with the highest intracranial tumour burden from the endpoint analysis. The drawbacks of bioluminescence imaging^{275–277}, as discussed in the previous chapter, must also be considered, as these may have contributed to the lack of significant differences.

While this study was unable to provide evidence that macrophages have a functional role in intracranial immune checkpoint inhibitor therapy, this should not rule them out from future studies. Other methods are available for the depletion of macrophages, such as the CD11b-DTR transgenic model³²⁴. However, these mice are generated from the non-obese diabetic (NOD) background and have also been shown to lack the brain-resident macrophages (microglia) after induction³²⁵, making this particular model inappropriate for the nature of this study. The most widely used method for the *in vivo* depletion of macrophages is by using clodronate-containing liposomes^{326, 28, 29}. While this form of depletion has been reported to mainly localise to the injection site³²⁶, there has been a report of clodronate-containing liposomes being used to deplete intracranial macrophages³²⁹. While the CD11b-DTR transgenic model and the clodronate-containing liposomes are useful, they do have their drawbacks, with the most important, in the context of this study, being the lack of specificity. Both have been

shown to also deplete monocytes, neutrophils and MDSCs, although this has been reported to a higher degree in the CD11b-DTR transgenic model³³⁰.

In this study, we were unable to successfully deplete macrophages using the anti-F4/80 antibody produced by the HB-198 cell line. This may be due to the method used to isolate the antibody from the cell culture medium. In theory, the centricons used in this study should have removed everything larger than an IgG from the cell culture medium; however, this may have not been the case, as toxicity was observed in the mice and may have been caused by IgGs within the FBS that was used as a medium supplement. IgGs denature at higher temperatures than those used to heat-inactivate FBS³³¹, meaning it is possible that these intact IgGs were also injected into the mice. This may have been solved by culturing the HB-198 cells in a lower concentration of FBS or by using FBS with a low concentration of IgG. Another option would be to use a previously successful method to isolate the antibody from this cell line: Tidball and Wehling-Henricks used ammonium sulphate precipitation to isolate the anti-F4/80 antibody and were successful in depleting macrophages in the muscle³⁰¹. Although, it should be noted, that complete depletion was not achieved and the mice were given a dose of the antibody every 24 hours for seven days.

When the commercially purchased anti-F4/80 antibody was used in our study, the protocol may have required optimisation as there was a tendency for the mice receiving the anti-F4/80 antibody to present with terminal symptoms at a later timepoint, suggesting that administration of higher doses of anti-F4/80 antibody may have resulted in significantly prolonged survival. In addition, it should also be taken into account that a number of cell types express F4/80, such as monocytes³³². This, in turn, could result in the unwanted depletion or partial depletion of the microglia population. There is, however, an inducible macrophage KO model on a C57BL6 background³³³, a potential option that would eliminate the need for a

depletion antibody, although it has been shown that this would also lead to the depletion of neutrophils³³³.

This section of the study focused on the depletion of major immune cell populations that have previously been linked to immune checkpoint inhibitor therapy, although there are a number of other cell types that could warrant further examination; one such population is MDSCs. These have been shown to have a pro-tumourigenic role in B16²⁹⁵ and 4T1 tumour models²⁴⁵. Although, as with all of the discussed immune populations, there is no functional data on their role within intracranial tumours in the context of immune checkpoint inhibitor therapy. Another major immune cell population within the brain that should be investigated are the microglia. Like macrophages, microglia have been associated with affecting intracranial tumour growth^{168,169,334}, making this an interesting population to investigate in the context of immune checkpoint therapy.

Chapter 5:

**Investigating the role of the
extracranial tumour and immune
checkpoint therapy in the
infiltration of immune cells into
intracranial tumours**

Chapter 5

5.1 Introduction

As described in the introduction (Chapter 1), immune checkpoint inhibitors are able to effectively treat cancer by altering the immune system. While the functional aspects of this can be explored through immune cell depletion *in vivo* models, this is obviously not possible in the human setting. However, comparisons can be made between humans and *in vivo* models by examining changes in tumour-infiltrating immune cells in response to immune checkpoint therapy.

Previous studies have reported a number of changes that occur within the TME in response to immune checkpoint therapy^{208,231,259}. These changes can be particular cell populations increasing or decreasing in overall numbers, in addition to the phenotypical changes occurring within the cell populations. As most of the research in this field is focused on extracranial disease, intracranial disease must be considered separately.

This chapter will focus on examining the effects of the combination of anti-PD-1 plus anti-CTLA-4 on the TME within the intracranial tumour.

Furthermore, the role of the flank tumour will be investigated to understand how extracranial disease can influence the susceptibility of intracranial tumours to immune checkpoint therapy.

5.2 A synergy between immune checkpoint therapy and extracranial tumour is required for increased infiltration of CD45⁺ immune cells into the intracranial tumour

B16/Fluc cells were implanted into mice and treatment was administered as previously outlined in Figure 3.7; intracranial tumours were isolated on day 12 and analysed by flow cytometry. Live cells were first separated from dead

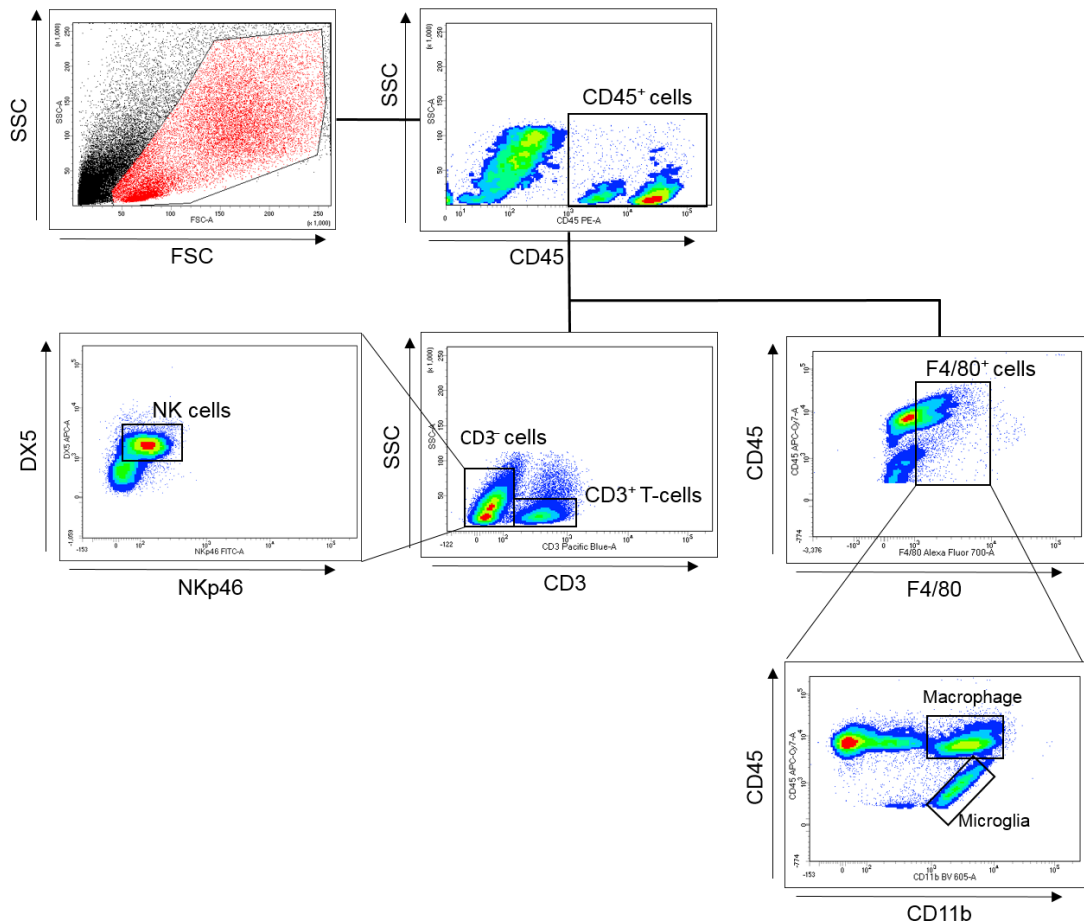


Figure 5.1 Gating strategy for the main populations of infiltrating immune cells

Intracranial tumours were dissociated into a single-cell suspension, stained for various markers and analyzed by flow cytometry. Live cells were gated based on their forward scatter (FSC) and side scatter (SSC). NK cells were defined as the CD3⁻ DX5⁺ and NKp46⁺ population within the CD45⁺ gate; T-cells were defined as the CD3⁺ population within the CD45⁺ gate; macrophages and microglia were separated from other cells by gating on the CD45⁺ F4/80⁺ population, followed by gating on CD45⁺ and CD11b⁺ cells. Microglia and macrophages could be clearly distinguished based on their CD45 expression levels (macrophages: CD45^{high}, microglia: CD45^{low}).

cells and cellular debris based on forward and sideward scatter as demonstrated in Figure 5.1. Immune cells were identified with the pan-hematopoietic marker, CD45 (Figure 5.1), that is expressed on all differentiated hematopoietic cells apart from plasma cells and erythrocytes³³⁵. CD45⁺ cells were further categorised into the main subsets of immune cells (see Table 5.1 for markers for each cell type), namely: NK cells, T-cells, macrophages and microglia (Figure 5.1).

Cell type	Cell identification markers
CD45 ⁺ cells	CD45 ⁺
T-cells	CD45 ⁺ , CD3 ⁺
CD8 ⁺ T-cells	CD45 ⁺ , CD3 ⁺ , CD8 α ⁺
CD4 ⁺ T-cells	CD45 ⁺ , CD3 ⁺ , CD4 ⁺
CD4 ⁺ effector cells	CD45 ⁺ , CD3 ⁺ , CD4 ⁺ , Fox P3 ⁻
T-Regs	CD45 ⁺ , CD3 ⁺ , CD4 ⁺ , Fox P3 ⁺
NK cells	CD45 ⁺ , CD3 ⁻ , NKp46 ⁺ , DX5 ⁺
Microglia	CD45 ^{low} , CD11b ⁺ , F4/80 ⁺
Macrophages	CD45 ^{high} , CD11b ⁺ , F4/80 ⁺

Table 5.1 Immune cell types and phenotype markers used to identify each cell type

In comparison to the other three groups, mice with a flank and intracranial tumour that received treatment had a substantially increased percentage (~two-fold) of CD45⁺ cells within the intracranial tumour (Figure 5.2A). Notably, there was no difference between the two control groups, demonstrating that a flank tumour by itself cannot increase immune cell

infiltration into the intracranial tumour. In the absence of flank tumour, treatment resulted in only a non-significant tendency towards an increased intracranial infiltration of CD45⁺ cells. Consequently, only synergy between immune checkpoint therapy and extracranial tumour resulted in an increase of CD45⁺ cell infiltration into intracranial tumours.

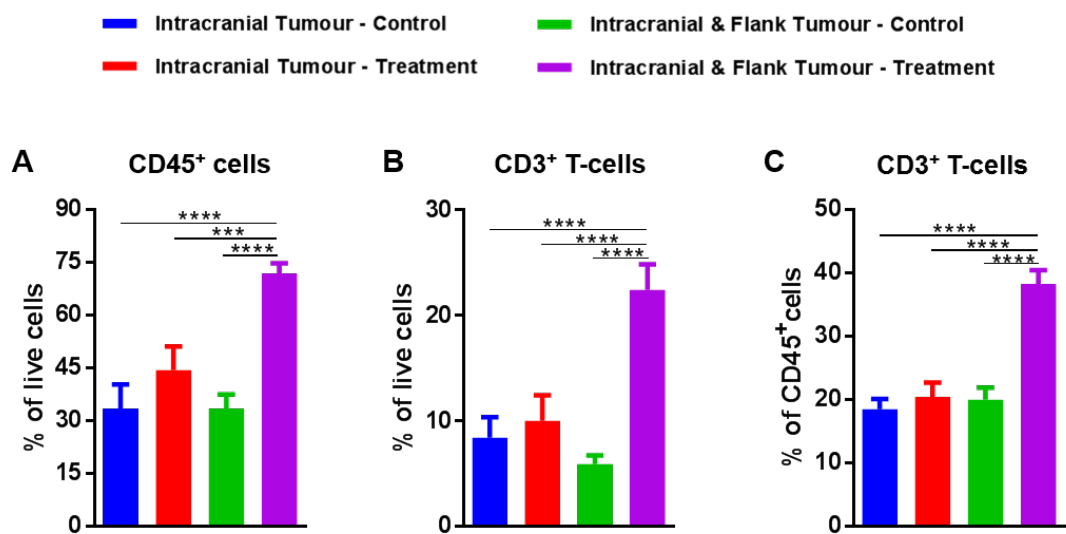


Figure 5.2 Effects of immune checkpoint therapy and the extracranial tumour on the accumulation of CD45⁺ cells and CD3⁺ T-cells within the intracranial tumour

(A) The percentage of CD45⁺ cells infiltrating into B16 intracranial tumours within the live cell population. (B) The percentage of CD3⁺ cells infiltrating into B16 intracranial tumours within the live cell population. (C) The percentage of CD3⁺ cells infiltrating into B16 intracranial tumours within the CD45⁺ population. (See appendix (page 189) for n numbers, number of independent experiments, statistical tests utilised and P values; error bars represent SEM).

5.3 A synergy between immune checkpoint therapy and extracranial tumour results in an increased CD3⁺ T-cell infiltration into intracranial tumours

The same trends seen with the CD45⁺ cells were also observed when the CD3⁺ T-cell population was analysed. The percentage of CD3⁺ T-cells within the intracranial tumour in treated mice with an intracranial and flank tumour was significantly increased (~two-fold), compared to the other groups (Figure 5.2B). These trends closely followed those of the CD3⁺ T-cells within the CD45⁺ population, with the same experimental group showing an approximate two-fold increase in infiltrating CD3⁺ T-cells over the other groups (Figure 5.2C).

5.4 Immune checkpoint therapy synergises with extracranial tumour to increase intracranial tumour-infiltrating CD8⁺ T-cells

The CD3⁺ T-cell population was further sub-divided into two distinct sub-populations: CD8⁺ T-cells and CD4⁺ T-cells (Figure 5.3). The percentage of intracranial CD8⁺ T-cells increased in treated mice that had intracranial and flank tumours, in comparison to the other three groups (Figure 5.5A). While the increase was quite striking (~three-fold) and highly significant within the total live cell population, it was less dramatic when the CD8⁺ T-cells were analysed within the CD3⁺ T-cell population (~15%) and reached significance in comparison to the two control groups but not to the mice bearing only an intracranial tumour receiving treatment (Figure 5.5B).

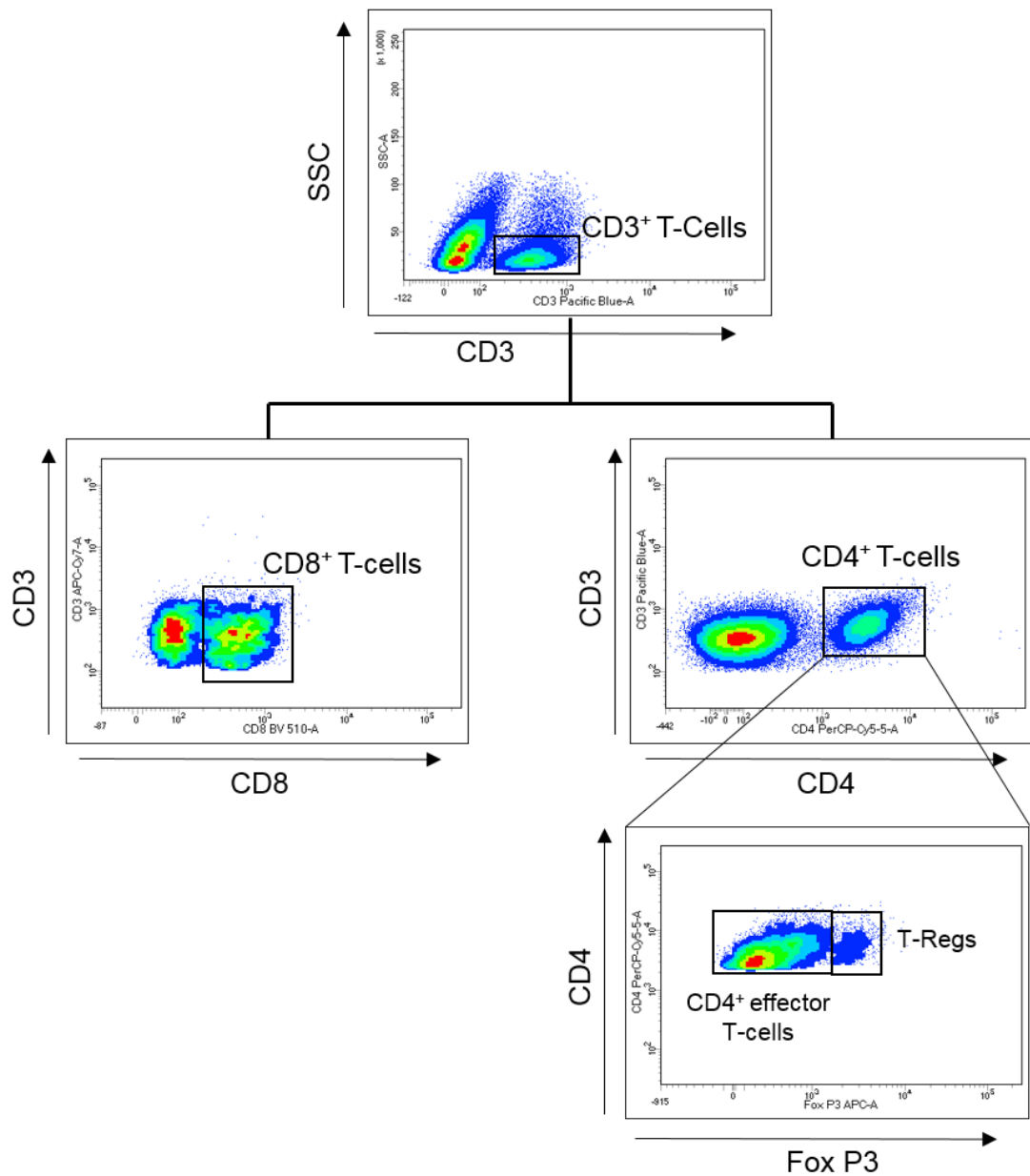


Figure 5.3 Gating strategy for CD3⁺ T-cell population subsets

The CD3⁺ T-cell population was divided into two subsets based on CD8 α (CD8⁺ T-cells) and CD4 (CD4⁺ T-cell) expression. The CD4⁺ T-cell population was further divided into CD4⁺ effector T-cells (Fox P3⁻) and T-Regs (Fox P3⁺).

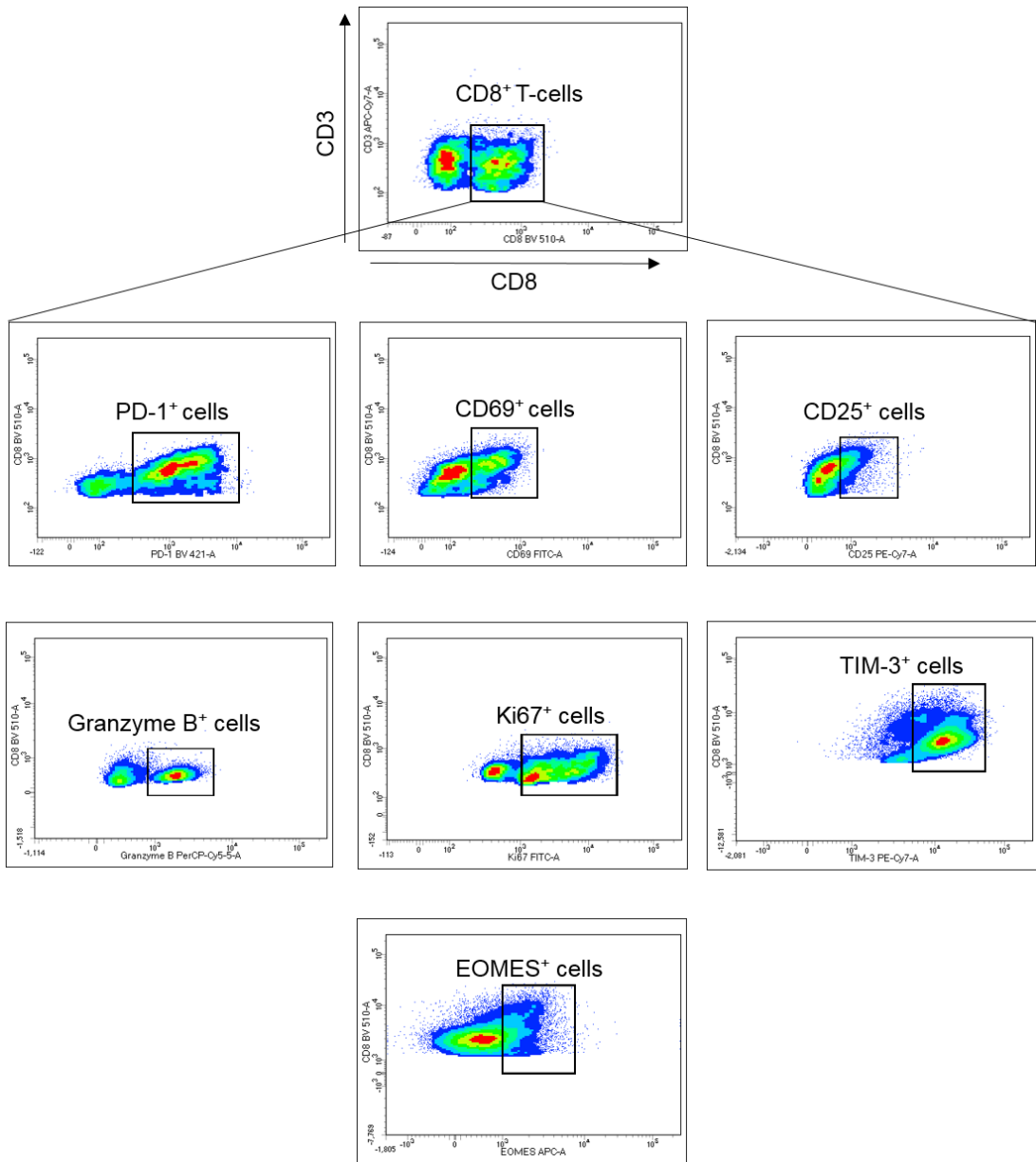


Figure 5.4 Representative plots for the various markers expressed by CD8⁺ T-cells

Plots for mice with an intracranial and flank tumours that were treated with anti-PD-1 and anti-CTLA-4 are shown.

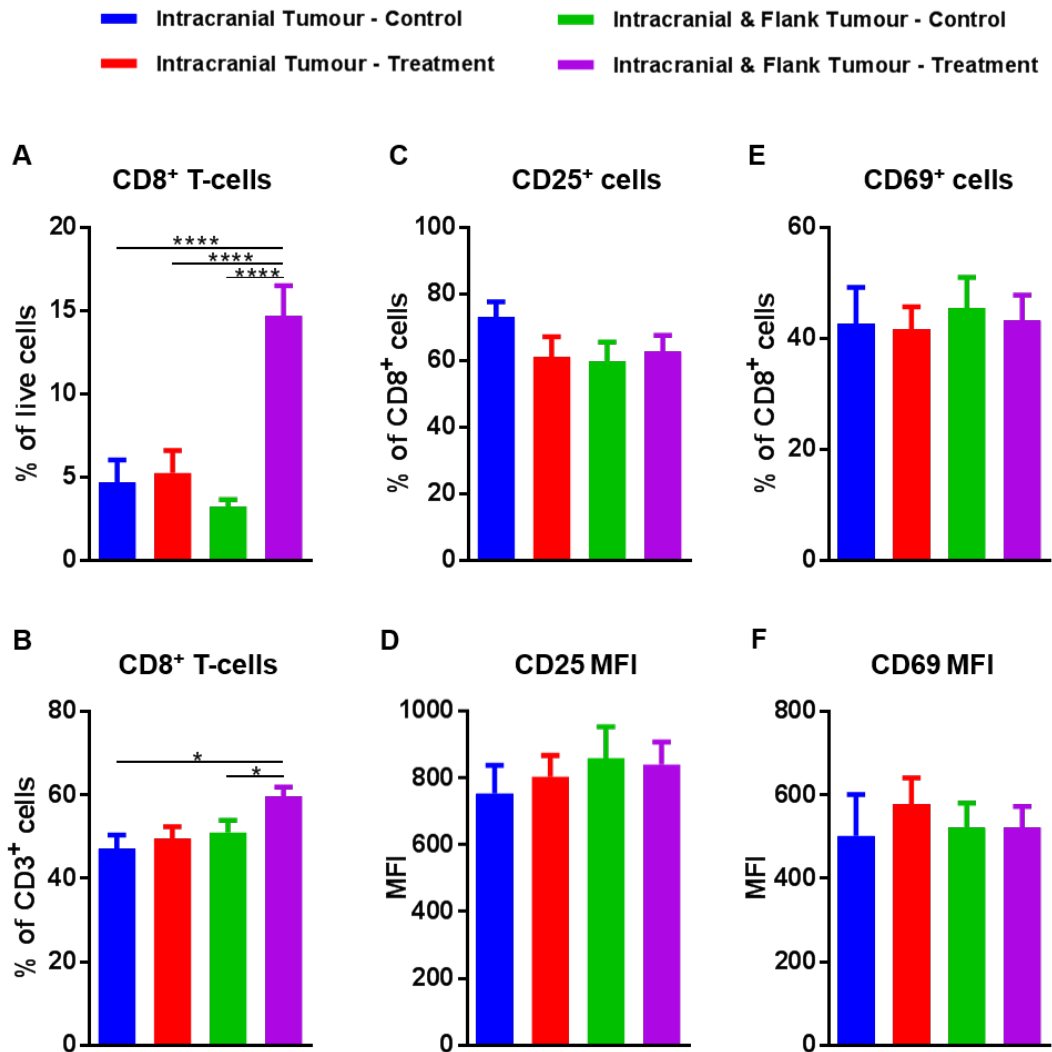


Figure 5.5 The effects of immune checkpoint therapy and extracranial tumours on CD8⁺ T-cells and their activation markers

(A) The percentage of infiltrating CD8⁺ T-cells into B16 intracranial tumours within the live cell population and (B) within the CD3⁺ T-cell population. (C) The percentage of CD25⁺ cells within the CD8⁺ T-cell population. (D) The expression level of CD25 on CD8⁺ T-cells shown as MFI. (E) The percentage of CD69⁺ cells within the CD8⁺ T-cell population. (F) The expression level of CD69 on CD8⁺ T-cells shown as MFI. (See appendix (pages 190-191) for n numbers, number of independent experiments, statistical tests utilised and P values; error bars represent SEM).

The phenotype of the CD8⁺ T-cell population was then investigated through the expression of extracellular and intracellular markers relating to the activation/inhibitory status of these cells (Figure 5.4; see Table 5.2 for description of specific phenotype markers). CD25 was selected as one of these, with its expression indicating a cell in a mid-late activation state³³⁶. In addition to CD25, CD69 is an activation marker expressed by CD8⁺ T-cells and is described as an early-stage activation marker³³⁷. An increase in CD8⁺ T-cell proliferation has been associated with successful immune checkpoint therapy; Ki67 has become a standard marker for detecting cell proliferation due to its ubiquitous expression through the entire proliferation cycle and absence in resting cells³³⁸. Granzyme B production by CD8⁺ T-cells has also been used as a measure of activation due to its role in the induction of apoptosis, along with being used as a T-cell reinvigoration marker in the context of immune checkpoint inhibition²³¹.

Cell marker	Description
CD25	Mid-late-stage activation marker
CD69	Early-stage activation marker
PD-1	Activation marker/exhaustion marker
Granzyme B	Protease produced by cytotoxic effector cells
Ki67	Proliferation marker
TIM-3	Exhaustion marker
EOMES	Transcription factor associated with T-cell exhaustion
CD107a	Functional marker of NK cell activity
CD27	Marker of mature effector NK cells
MHC II	Marker of antigen presentation phenotype

Table 5.2 Immune cell markers and their phenotypic description

Activation markers can be revealing when investigating an immunotherapy mechanism; however, inhibitory markers can be just as telling. TIM-3 is a marker reported to be associated with the most inhibited and dysfunctional CD8⁺ T-cells^{195,339,340}. The PD-1 receptor is widely viewed as an inhibitory receptor due to its function^{89,341}; on the other hand, it can also be considered as an activation receptor^{228,342}. To study the expression of the PD-1 receptor, we used the anti-PD-1 antibody clone J43 that binds to a different epitope than the RMP1-14 clone used for the anti-PD-1 treatment^{242,343}. Finally, whereas the exact role of eomesodermin (EOMES) seems to be ambiguous, it is clear that this transcription factor has an important role in tumour immunology and is normally associated with an exhausted phenotype of CD8⁺ T-cells^{231,344-346}.

Consistently, neither the extracranial tumour nor the immune checkpoint therapy significantly altered the percentage of CD8⁺ cells expressing any one of the markers studied (Figures 5.5, 5.6 and 5.7). Similarly, the expression levels of these markers, as represented by the mean fluorescence intensity (MFI) also remained unchanged across the groups. Nevertheless, there was one exception to these observations. In the case of PD-1, there was found to be a significant increase (~20%) in the percentage of PD-1⁺ cells within the CD8⁺ T-cell population when the control group of mice with an intracranial tumour only was compared to the control group of mice with an intracranial and flank tumour (Figure 5.7C). While there was an indication of the same trend for PD-1 expression levels between the two control groups, this ultimately proved to be a non-significant change (Figure 5.7D).

5.5 Intracranial tumour-infiltrating CD4⁺ effector T-cells and T-Regs increase with immune checkpoint therapy

Flow cytometry analysis revealed that the percentage of CD4⁺ T-cells within the total live cell population in intracranial tumours increased in both treatment groups when compared to the two control groups (Figure 5.8A).

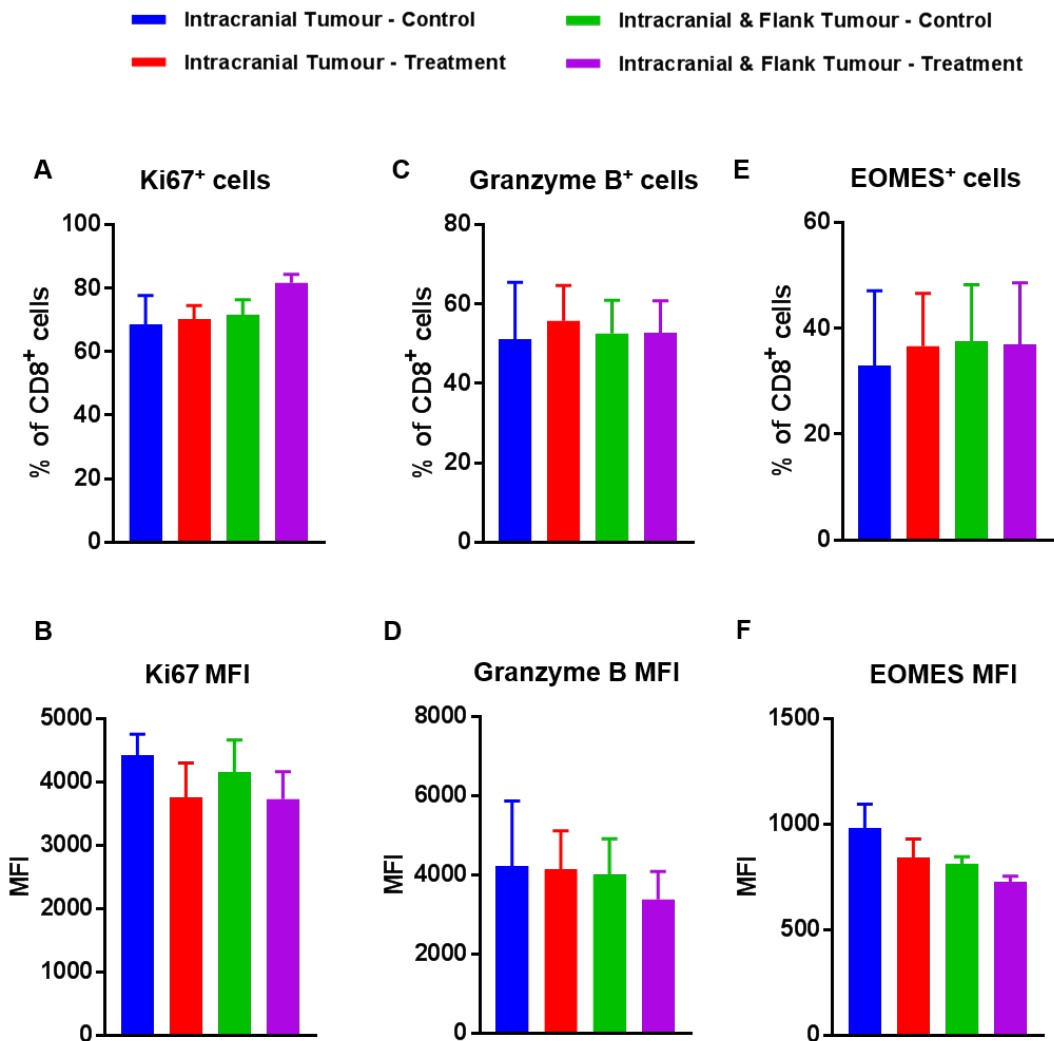


Figure 5.6 The effects of immune checkpoint therapy and extracranial tumours on different subsets of CD8⁺ T-cells

(A) The percentage of Ki67⁺ cells within the CD8⁺ T-cell population infiltrating into B16 intracranial tumours. (B) The expression level of Ki67 in CD8⁺ T-cells shown as MFI. (C) The percentage of Granzyme B⁺ cells within the CD8⁺ T-cell population infiltrating into B16 intracranial tumours. (D) The expression level of Granzyme B in CD8⁺ T-cells shown as MFI. (E) The percentage of EOMES⁺ cells within the CD8⁺ T-cell population infiltrating into B16 intracranial tumours. (F) The expression level of EOMES in CD8⁺ T-cells shown as MFI. (See appendix (pages 192-193) for n numbers, number of independent experiments, statistical tests utilised and P values; error bars represent SEM).

■ Intracranial Tumour - Control ■ Intracranial & Flank Tumour - Control
■ Intracranial Tumour - Treatment ■ Intracranial & Flank Tumour - Treatment

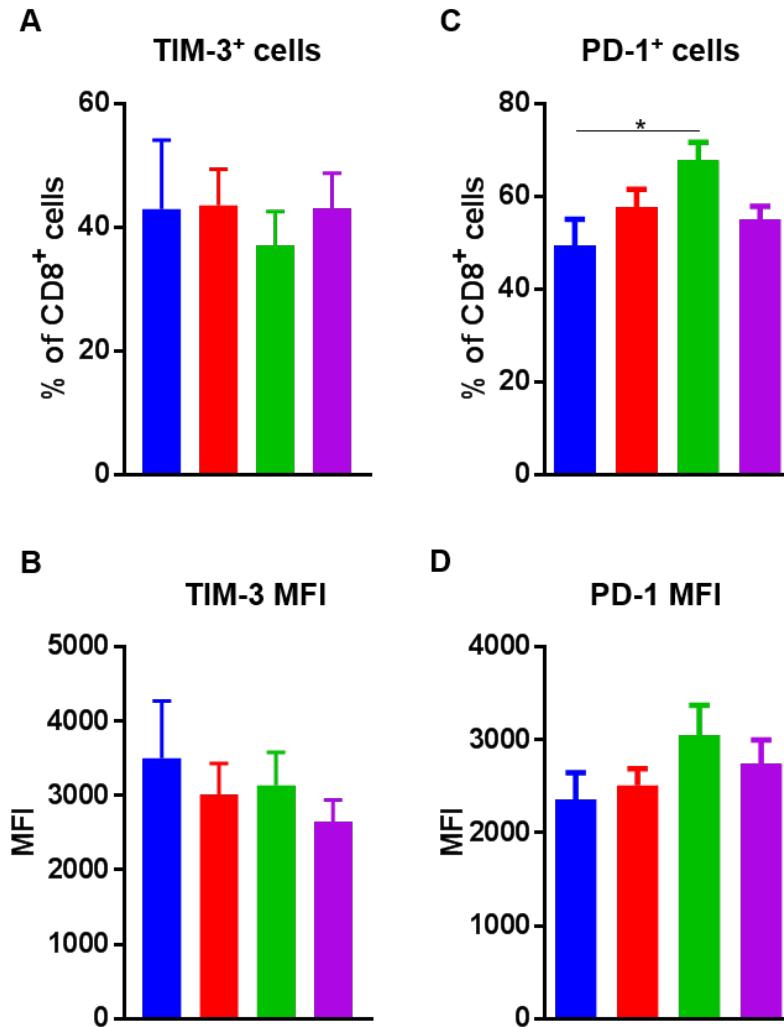


Figure 5.7 The effects of immune checkpoint therapy and extracranial tumours on inhibitory markers on CD8⁺ T-cells

(A) The percentage of TIM-3⁺ cells within the CD8⁺ T-cell population infiltrating into B16 intracranial tumours and their (B) expression level of TIM-3 in CD8⁺ T-cells shown as MFI. (C) The percentage of PD-1⁺ cells within the CD8⁺ T-cell population infiltrating into B16 intracranial tumours and their (D) expression level of PD-1 in CD8⁺ T-cells expressed as MFI. (See appendix (pages 194-195) for n numbers, number of independent experiments, statistical tests utilised and P values; error bars represent SEM).

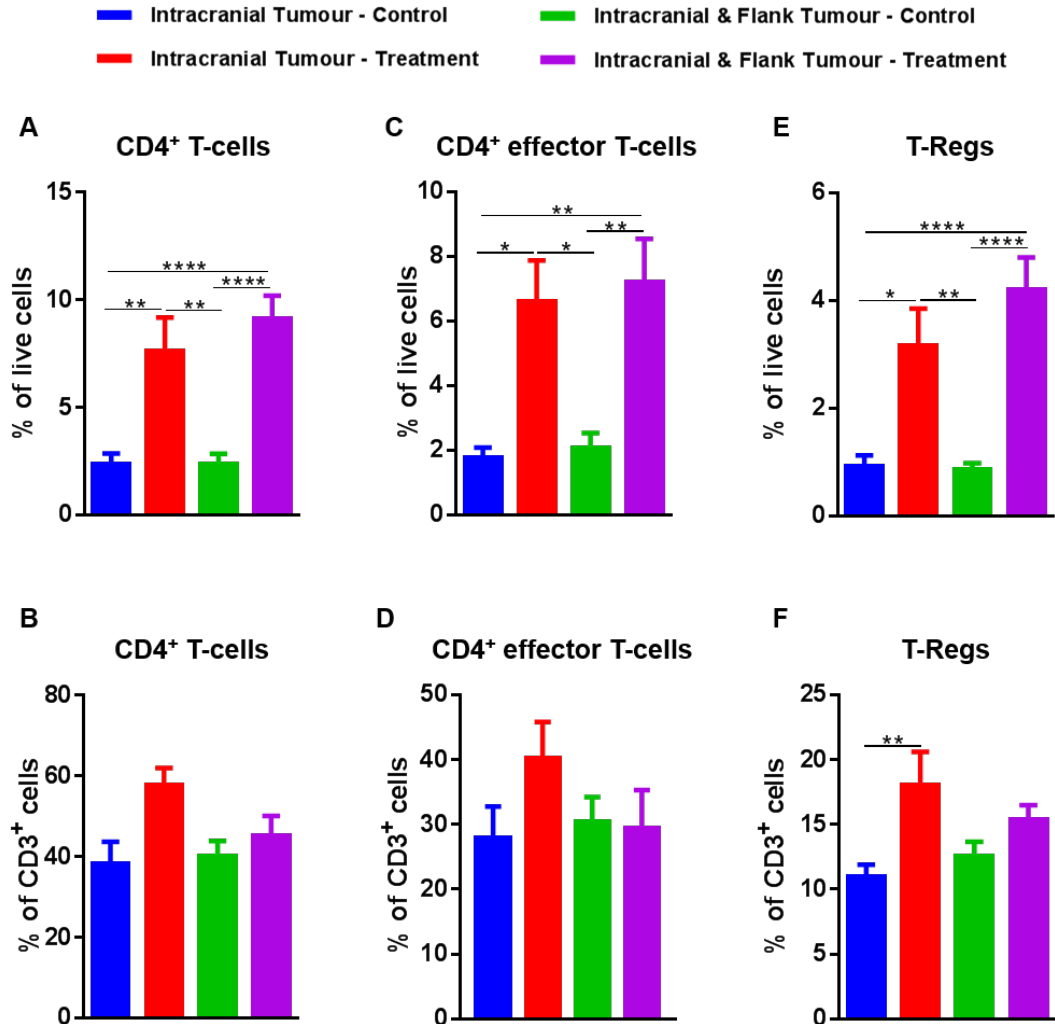


Figure 5.8 The effects of immune checkpoint therapy on CD4⁺ T-cells and T-cell subsets

(A) The percentage of CD4⁺ T-cells infiltrating into B16 intracranial tumours within the live cell population and (B) within the CD3⁺ T-cell population. (C) The percentage of effector CD4⁺ T-cells infiltrating into B16 intracranial tumours within the live cell population and (D) within the CD3⁺ T-cell population. (E) The percentage of T-Regs infiltrating into B16 intracranial tumours within the live cell population and (F) within the CD3⁺ T-cell population. (See appendix (pages 195-197) for n numbers, number of independent experiments, statistical tests utilised and P values; error bars represent SEM).

The CD4⁺ T-cell population was further sub-divided into CD4⁺ effector T-cells (CD4⁺ FoxP3⁻) and T-Regs (CD4⁺ FoxP3⁺) (Figure 5.3; Table 5.1). Percentages of both CD4⁺ effector T-cells and T-Regs within the total cell population increased significantly in both treatment groups in comparison to the control groups (Figure 5.8C and E). When analysed as a proportion of CD3⁺ T-cells, T-Regs were significantly increased in intracranial tumours upon therapy, only in the absence of extracranial tumour. There was a tendency towards an increased proportion of the total CD4⁺ T-cell population as a whole and CD4⁺ effector T-cells in the same experimental groups (Figure 5.8B, D and F). When the activation state of these CD4⁺ T-cell populations was examined, we found no alterations in the expression of the activation markers CD25 and CD69 across different groups (Figure 5.9).

5.6 The ratio of CD8⁺ T-cells and CD4⁺ effector cells to T-Regs is unchanged in response to immune checkpoint therapy

The ratio of CD8⁺ T-cells to T-Regs was calculated by dividing the percentage of CD8⁺ cells within the CD3⁺ population by the percentage of T-Regs within the CD3⁺ population for each individual mouse. There were no statistically significant differences between any of the groups. Nevertheless, there was a tendency towards a decrease in the CD8⁺ T-cell:T-Reg ratio between control and treatment groups (Figure 5.10A).

The ratio of CD4⁺ effector cells to T-Regs was calculated by the same method. While there were no significant changes in the CD4⁺ effector T-cell:T-Reg ratio between the groups, there did seem to be a slight tendency towards a decrease in the treatment group with intracranial and flank tumours compared to the other three groups (Figure 5.10B).

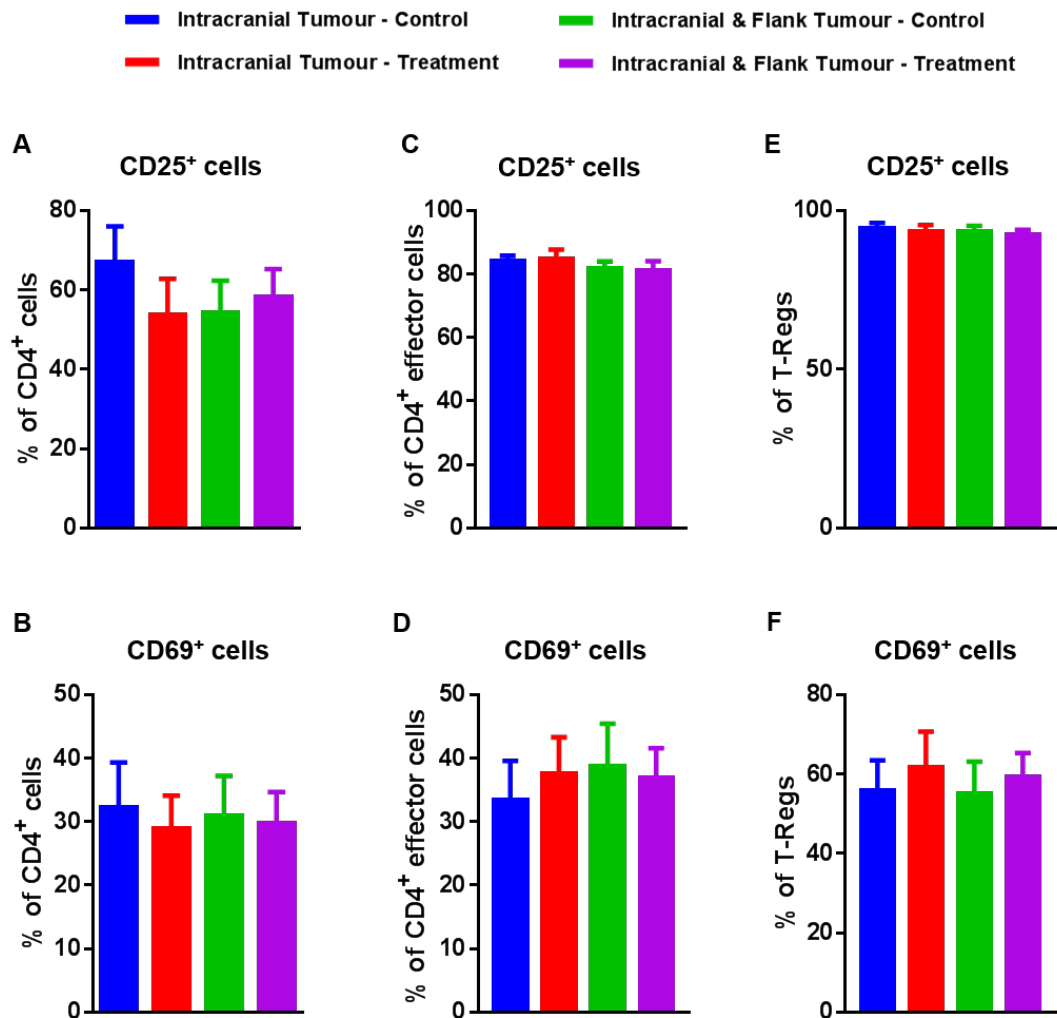


Figure 5.9 The effects of immune checkpoint therapy and extracranial tumours on CD25⁺ CD4⁺ T-cells and CD69⁺ CD4⁺ T-cells

(A) The percentage of CD25⁺ CD4⁺ T-cells infiltrating into B16 intracranial tumours within the CD4⁺ population. (B) The percentage of CD25⁺ CD4⁺ effector T-cells infiltrating into B16 intracranial tumours within the CD4⁺ effector T-cell population. (C) The percentage of CD25⁺ T-Regs infiltrating into B16 intracranial tumours within the T-Reg population. (D) The percentage of CD69⁺ CD4⁺ T-cells infiltrating into B16 intracranial tumours within the CD4⁺ population. (E) The percentage of CD69⁺ CD4⁺ effector T-cells infiltrating into B16 intracranial tumours within the CD4⁺ effector T-cell population. (F) The percentage of CD69⁺ T-Regs infiltrating into B16 intracranial tumours within the T-Reg population. (See appendix (pages 197-199) for n numbers, number of independent experiments, statistical tests utilised and P values; error bars represent SEM).

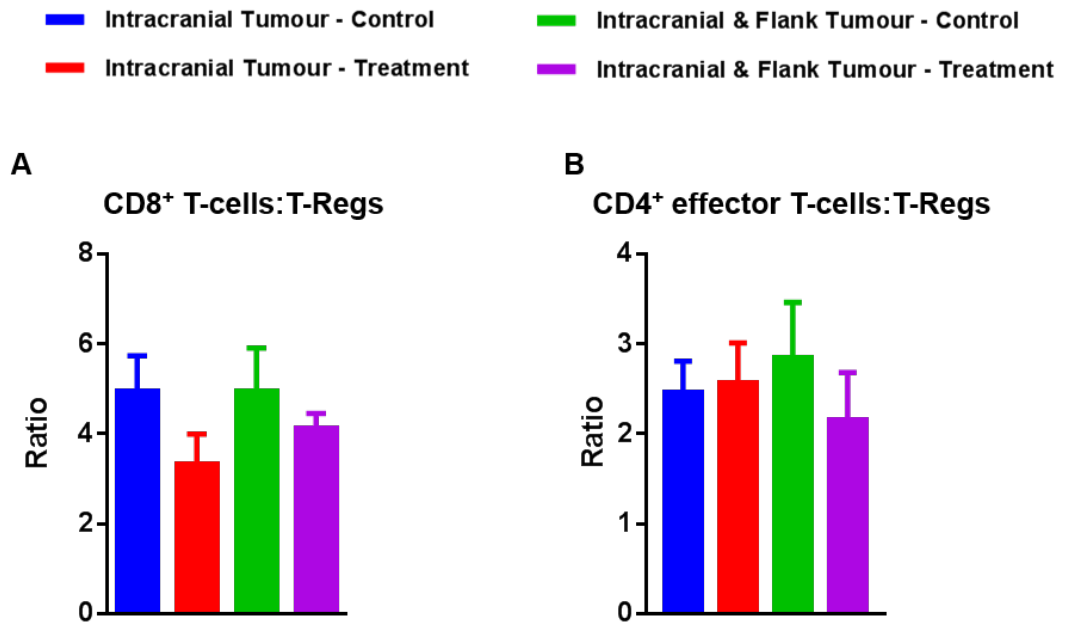


Figure 5.10 The effects of immune checkpoint therapy and extracranial tumours on effector:regulatory T-cell ratios

(A) The effects of anti-PD-1 and anti-CTLA-4 on the intracranial tumour ratio of CD8⁺ T-cells:T-Regs. (B) The effects of anti-PD-1 and anti-CTLA-4 on the intracranial tumour ratio of CD4⁺ effector T-cells:T-Regs. (See appendix (page 199) for n numbers, number of independent experiments, statistical tests utilised and P values; error bars represent SEM).

5.7 NK cell infiltration is unaltered by immune checkpoint therapy or extracranial tumour

One of the other main components of the CD45⁺ population that was investigated due to its importance in the earlier depletion studies (Chapter 4) was the NK cell population (Figure 5.1). When the intracranial tumours were analysed by flow cytometry there were no discernible differences in the percentage of NK cells detected between any of the groups (Figure 5.11A). Conversely, a significant decrease in NK cells was seen within the CD45⁺ population in mice with an intracranial and flank tumour receiving treatment, as compared to the two control groups (Figure 5.11B). Moreover, the percentage of NK cells within the CD45⁺ population appeared to be slightly, although non-significantly, decreased upon therapy in the absence of an extracranial tumour.

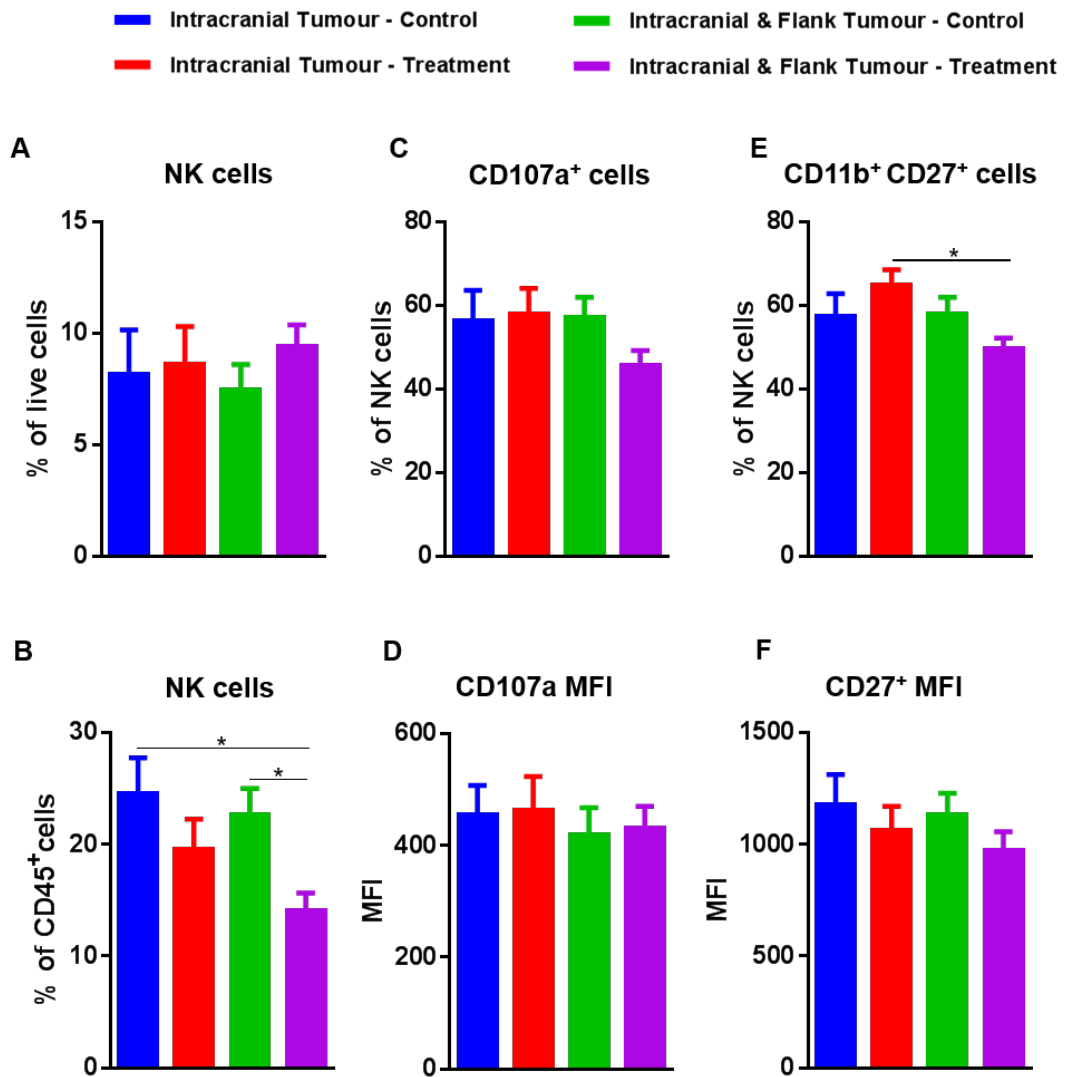


Figure 5.11 The effects of immune checkpoint therapy and extracranial tumours on total number and activation status of NK cells

(A) The percentage of NK cells infiltrating into B16 intracranial tumours within the live cell population and (B) in the CD45⁺ population. (C) The percentage of CD107a⁺ NK cells infiltrating into B16 intracranial tumours within the NK cell population. (D) The expression of CD107a on NK cells shown as MFI. (E) The percentage of CD11b⁺ CD27⁺ NK cells infiltrating into B16 intracranial tumours within the NK cell population. (F) The expression of CD27 on NK cells shown as MFI. (See appendix (pages 200-201) for n numbers, number of independent experiments, statistical tests utilised and P values; error bars represent SEM).

The activation state of the NK cells was first investigated by looking at the surface expression of CD107a (Figure 5.12) as this has been shown to be a functional marker on activated NK cells³⁴⁷. Cell-surface expression of CD107a indicates cytotoxic activity, as this protein relocates to the cell surface after degranulation has taken place. There were, however, no significant differences in CD107a expression between the groups when the percentage of CD107a⁺ NK cells was examined (Figure 5.11C). There did appear to be a tendency towards a decrease in the percentage of CD107a⁺ cells within the NK cell population in mice with intracranial and flank tumours receiving treatment, as compared to the remaining groups. Additionally, there were no changes to the MFI levels of CD107a between the groups (Figure 5.11D).

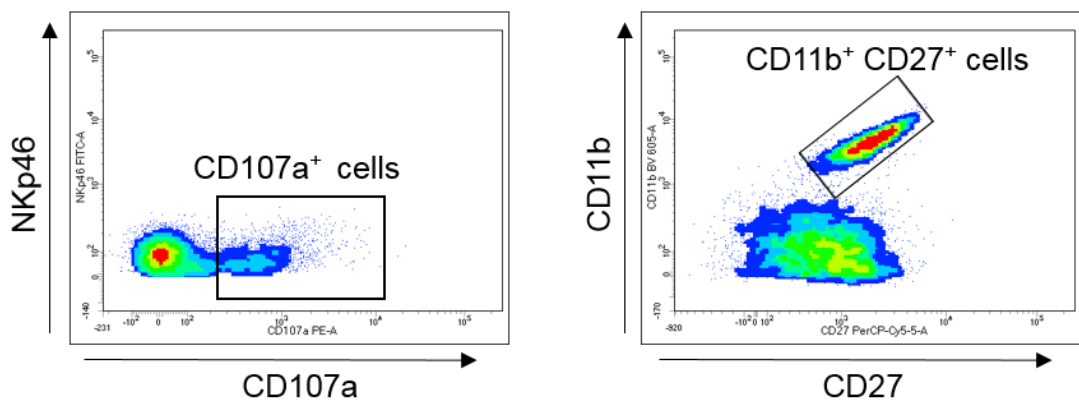


Figure 5.12 Representative plots for CD107a⁺ NK cells and CD11b⁺ CD27⁺ NK cells

The NK population was defined by gating on the CD3⁻, NKp46⁺ and DX5⁺ population. The NK cell population was divided into two subsets based on the expression of CD107a and the co-expression of CD11b and CD27.

NK cells that are double positive for CD11b and CD27 have been shown to have a greater effector function³⁴⁸. In the present study, the majority of NK cells found within the intracranial tumour were of the CD11b^{high} CD27^{high} phenotype, which is associated with an increased effector function³⁴⁸ (Figure

5.12). When these populations were examined as a proportion of the total NK cell population, there was a significant decrease (~10%) in CD11b⁺ CD27⁺ NK cells in mice with an intracranial and flank tumour receiving treatment when compared to mice with an intracranial tumour only receiving treatment (Figure 5.11E). There were, on the other hand, no changes to the CD27 expression levels on the NK cells across the groups (Figure 5.11F).

5.8 Immune checkpoint therapy and extracranial tumour synergise to increase microglia infiltration, while the therapy alone can increase macrophage infiltration into the intracranial tumour

The final main populations that made up the CD45⁺ population within the intracranial tumours were the macrophages and the microglia (brain-resident macrophages³⁴⁹). As demonstrated in Figure 5.1, macrophages and microglia were distinguished based on their surface marker expression. Both cell types express CD45, CD11b and F4/80; however, macrophages are CD45^{high}, whereas microglia are CD45^{low}¹¹.

It was found that the percentage of microglia within intracranial tumours significantly increased (~two-fold) in mice with an intracranial and flank tumour receiving treatment, in comparison to the other groups (Figure 5.13A). On the contrary, when examined as a percentage of the CD45⁺ population there appeared to be a non-significant tendency towards a decrease in microglia in this group as compared to other groups (Figure 5.13B).

MHC II expression on microglia was investigated to indicate the antigen-presenting capabilities of these cells (Figure 5.14). The total percentage of MHC II⁺ microglia increased significantly (~two-fold) within the live cell

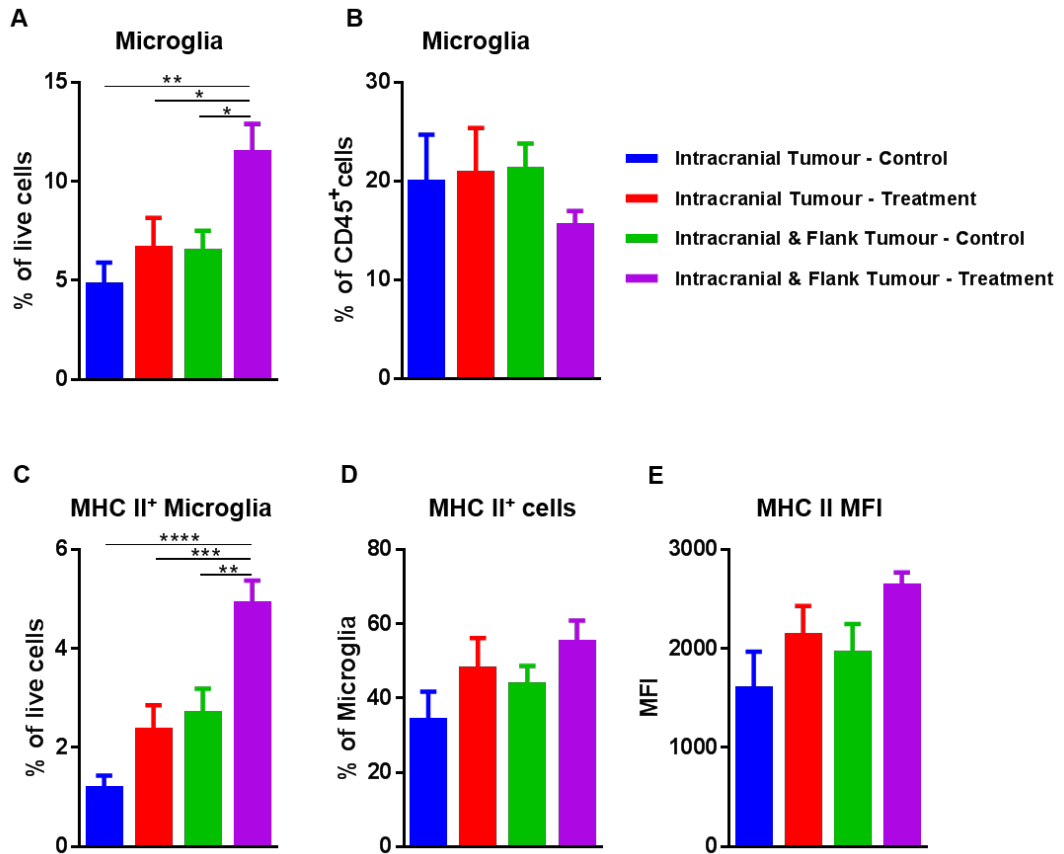


Figure 5.13 The effects of immune checkpoint therapy and extracranial tumours on microglia and their expression of MHC II

(A) The percentage of microglia infiltrating into B16 intracranial tumours within the live cell population and (B) within the CD45⁺ population. (C) The percentage of MHC II⁺ microglia infiltrating into B16 intracranial tumours within the live cell population and (D) within the microglia population. (E) The expression of MHC II on microglia shown as MFI. (See appendix (pages 202-203) for n numbers, number of independent experiments, statistical tests utilised and P values; error bars represent SEM).

population in mice bearing an intracranial and flank tumour receiving treatment (Figure 5.13C). However, the percentage of MHC II⁺ cells within the microglia population remained unchanged, as did the expression level for MHC II as represented by MFI (Figure 5.13D and E). Yet, there was a non-significant trend for the MFI to be higher in the treatment group of mice with an intracranial and flank tumour.

In the case of macrophages, there was a significant increase (~two-fold) in the percentage of macrophages within the intracranial tumours of treated mice bearing intracranial and flank tumours, as compared to mice in the two control groups (Figure 5.15A). While not statistically significant, there was a tendency in the treatment group of mice bearing only an intracranial tumour to have a higher percentage of macrophages than the two control groups. When the macrophages were analysed as a percentage of the CD45⁺ population, there were no significant changes observed between the groups (Figure 5.15B). Conversely, there was a trend towards increased percentages of macrophages in the two control groups.

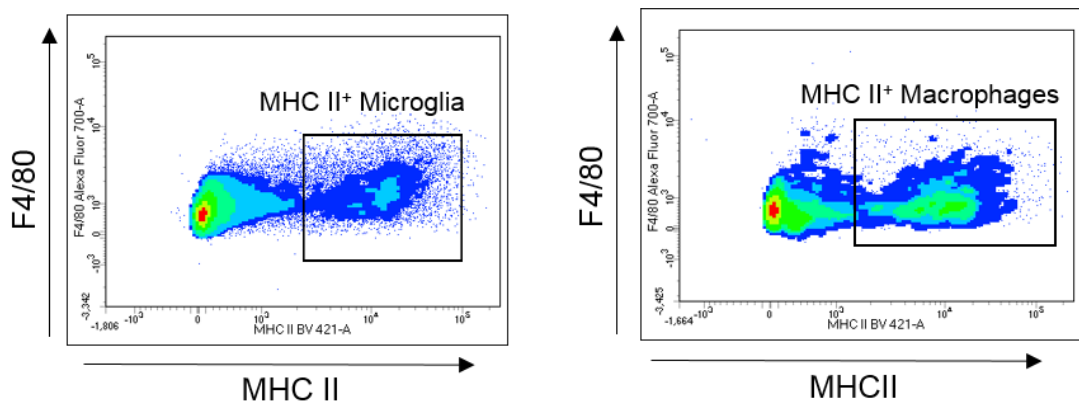


Figure 5.14 Representative plots for MHC II⁺ microglia and MHC II⁺ macrophages

The MHC II⁺ population was gated on within the macrophage and microglia populations.

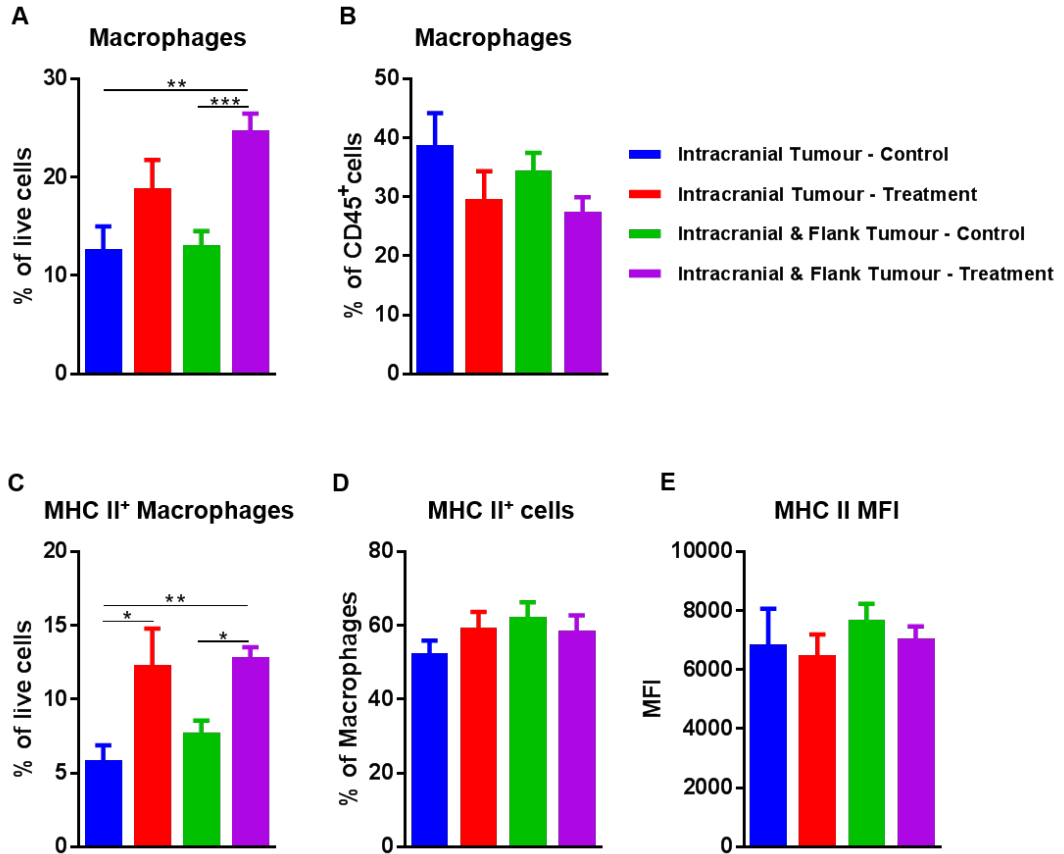


Figure 5.15 The effects of immune checkpoint therapy and extracranial tumours on macrophages and their expression of MHC II

(A) The percentage of macrophages infiltrating into B16 intracranial tumours within the live cell population and (B) within the CD45⁺ population. (C) The percentage of MHC II⁺ macrophages infiltrating into B16 intracranial tumours within the live cell population and (D) within the macrophage population. (E) The expression of MHC II on macrophages shown as MFI. (See appendix (pages 203-205) for n numbers, number of independent experiments, statistical tests utilised and P values; error bars represent SEM).

The MHC II expression on macrophages was also examined, in the same manner as the microglia (Figure 5.14). It was found that the mice in the treatment groups had an increased percentage (~two-fold) of MHC II⁺ macrophages within the live cell populations as compared to control groups (Figure 5.15C). These alterations were statistically significant between treated mice bearing an intracranial and flank tumour and the two control groups. In addition, the increase in treated mice with an intracranial and flank tumour was significant in comparison to the two control groups was. When the MHC II⁺ population was examined within the macrophage population the analysis revealed no significant changes amongst the groups (Figure 5.15D). Likewise, while there were no significant changes in the levels of MHC II expression on macrophages (Figure 5.15E); however, there were clear differences in the MHC II expression levels between macrophages and microglia. Macrophages tended to have an increased MHC II expression over the microglia and these differences were independent of treatment and flank tumour status.

5.9 Immune checkpoint therapy and extracranial tumours alter the infiltration of immune cells into intracranial tumours by different means

As summarised in Figure 5.16, extracranial tumours themselves have no influence over the infiltration of immune cells into intracranial tumours. This is not the case for immune checkpoint therapy, as macrophages, T-Regs and CD4⁺ effector T-cells were increased within intracranial tumours upon therapy in the absence of extracranial tumours. Nevertheless, it is evident that there are some underlying synergistic mechanisms involving the checkpoint therapy and extracranial tumours that resulted in the increased infiltration of CD8⁺ T-cells and microglia into the tumour.

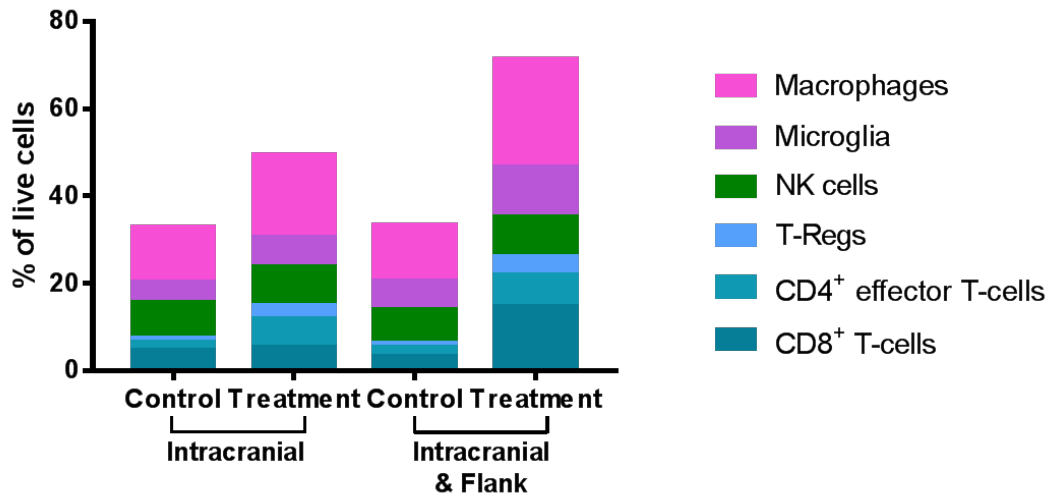


Figure 5.16 Summary of the effects of immune checkpoint therapy and extracranial tumours on immune cells infiltrating into intracranial tumours

Average percentages of each of the immune cell populations examined within the live cell population that infiltrated into B16 intracranial tumours.

5.10 Discussion

One of the first observations made was the general increase in CD45⁺ cells in intracranial tumours of mice with intracranial and flank tumours that received the combination of anti-PD-1 and anti-CTLA-4. This was in-line with previous reported increases in immune cells as a requirement for effective immune checkpoint therapy^{199,350}. In the present study, an interesting finding was the role of the extracranial tumour with regards to the therapeutic efficacy in the brain. While extracranial tumours alone had no effect on immune cell infiltration into intracranial tumours, they were clearly essential for effective immune checkpoint therapy. Likewise, when a flank tumour was absent there was only a fairly modest increase in CD45⁺ cells in the intracranial tumour when treatment was administered. This would suggest that extracranial tumours have a systemic function that is necessary for CD8⁺ T-cells and microglia to infiltrate into the brain in the context of immune checkpoint therapy. This hypothesis would disagree with the findings by Reardon *et al.* who showed an increase in tumour-infiltrating immune cells in an orthotopic glioma model in response to anti-PD-1 plus anti-CTLA-4²⁴⁰.

This difference may be due to the noted responses being tumour type-dependent. It is also known that variations in cytokine milieu are responsible for differences in immune cell infiltration³⁵¹.

Taking into account the functional data from the cell depletion studies (Chapter 4) and the data from this chapter, increased intracranial infiltration of CD8⁺ T-cells upon therapy in mice with extracranial and intracranial tumours was most likely one of the major factors responsible for the therapeutic efficacy. This would be in line with a number of the other studies which showed the essential role of CD8⁺ T-cells in immune checkpoint therapy in their respective models^{176,193,209,231,288}.

When the CD8⁺ T-cell population was explored in more detail, there were no changes to the percentage of CD25⁺ or CD69⁺ cells within the CD8⁺ T-cell population. This indicates that this T-cell population as a whole is not becoming more activated but simply increasing in number. When the inhibitory markers PD-1 and TIM-3 were examined, the same observations were made. A combination of these markers have been associated with the most inhibited and exhausted CD8⁺ T-cells^{195,231,340}. When the proportion of the PD-1⁺ and TIM-3⁺ cells within the CD8⁺ T-cell population was scrutinised, there were no variations between the groups. This would, again, insinuate that the overall phenotype of the CD8⁺ T-cell population remains unaffected. There was, on the other hand, a significant increase in PD-1⁺ CD8⁺ T-cells in the control group of mice with intracranial and flank tumours when compared to the control group of mice with only an intracranial tumour. This would suggest that extracranial tumours may be systemically increasing the expression of PD-1 on CD8⁺ T-cells. Cytokine and gene expression analysis may be able to give a clearer picture on how much influence the extracranial disease has over the intracranial tumour in this regard.

Another marker that has been strongly associated with the exhausted T-cell phenotype is EOMES^{231,345,352}. EOMES⁺ cells are described as expressing a number of inhibitory markers and have an extremely limited ability to

proliferate³⁵². It has, however, been suggested that this can be reversed through immune checkpoint therapy²³¹. While there was no change in the percentage of EOMES⁺ cells within the CD8⁺ populations studied, there was a small decrease, although non-significant, in EOMES expression, which could indicate these cells are being, in some way, released from their inhibition. Conversely, it should also be taken into consideration that EOMES is not solely associated with T-cell inhibition. It has been demonstrated through KO models that EOMES, along with T-box transcription factor TBX21 (T-Bet), is essential for CD8⁺ T-cells to successfully infiltrate into tumours³⁴⁶. As a result, it is difficult to make a solid conclusion over whether the expression of EOMES is beneficial or a hindrance in the context of our therapy.

Ki67 and granzyme B have been associated with effective immune checkpoint therapy due to the increased proliferation and effector phenotype²³¹ that their expression results in. It has been suggested that CD8⁺ T-cells which express PD-1 and EOMES, while co-expressing Ki67 and granzyme B, represent a reinvigorated CD8⁺ T-cell population that has overcome the suppressive tumour microenvironment²³¹. This subset of cells was not found in this study, suggesting other mechanisms may be involved within the brain. In addition, there was no change in the overall expression of these markers between the groups. This would suggest the phenotype of the intracranial infiltrating CD8⁺ T-cell population is unaffected by immune checkpoint therapy and that the therapeutic effect seen is a result of the increase in CD8⁺ T-cell infiltration.

As demonstrated in the previous chapter, CD4⁺ T-cells were not a crucial population required for effective immune checkpoint therapy within the brain. Interestingly, the treatment caused an increase in CD4⁺ T-cell infiltration that was independent of the presence of the flank tumour. This increase was seen in both the CD4⁺ effector T-cell population and that of the T-Regs. The increase in the CD4⁺ effector T-cells has been documented by Curran *et al.* in an intradermal B16 model using the combination of anti-CTLA-4, anti-PD-

1 and anti-PD-L1²⁰⁹. Their findings, in relation to T-Regs, conversely differ from the finding of the present study as it is claimed that this particular anti-CTLA-4 clone has a T-Reg-depleting function, which has also been replicated in other studies^{209,353,354}. In spite of this, there has been another study using a human HER2-expressing orthotopic breast cancer cell line model that also found an increase in T-Regs when using the combination of T-DM1, anti-PD-1 and anti-CTLA-4²⁸⁰. This occurrence may be due to a number of reasons, such as tumour type, tumour location, tumour burden and mouse strain. The tumour location may be an important factor in this study as the BBB may have restricted access of antibodies to the tumour, thereby hindering intratumoural T-Reg depletion. It should also be taken into consideration that the T-Reg-depletion claims stem from analysis of the percentage of T-cells within the TIL population rather than within the total cell population. This could be misleading, as changes within the TIL population may not be a true reflection of changes within the TME as a whole. The reported decrease in T-Reg numbers may have been a result of the increase in CD8⁺ T-cells within the TIL population and taking into account total cell population, may have resulted in a different conclusion. The one thing that is clear in our model is that the increase in CD4⁺ T-cells is a result of the combination treatment and independent of the extracranial disease.

When the cell-surface expression of CD69 was examined within each specific CD4⁺ T-cell type, there were no changes between the groups. This would, again, suggest that the overall phenotype of the cells remains unchanged after checkpoint therapy.

It has been proposed that the intratumoural effector T-cell (CD4⁺ and CD8⁺): regulatory T-cell ratio can be an indication of effective immune checkpoint therapy^{93,209}. This was not the case in this study as the ratios remained unaltered between different groups, including that in which intracranial therapeutic efficacy was observed. Similarly, no changes in CD4⁺ effector T-cell:T-Reg ratios were observed in the study using the human HER2-

expressing orthotopic breast cancer cell line that saw a therapeutic effect when treating with T-DM1, anti-PD-1 plus anti-CTLA-4²⁸⁰. This would suggest that while these ratios may be a potential gauge for a successful treatment, they are not an absolute indicator; however, this analysis in our study was performed at the terminal timepoint for the majority of the mice and analysis at earlier timepoints may have revealed changes between the groups.

One surprising finding from analysis of the tumour-infiltrating immune cells was the resulting data from the NK cells. Surprisingly, there was no fluctuations in the percentage of intracranial NK cells between any of the groups, despite their obvious importance for the efficacy of treatment, as demonstrated in the cell depletion studies detailed in the previous chapter. It should be noted that while there was a significant decrease in NK cells as a percentage of CD45⁺ cells in the intracranial and flank treatment group, this is simply a consequence of the increase in other cell populations. Even though the only other report to date showing effective immune checkpoint therapy in the brain described an increase in the infiltration of NK cells²⁴⁰, this may not always be beneficial. One study has shown that the cytokine milieu within the TME is able to convert NK cells into MDSCs as a mechanism of immune evasion³⁵⁵. Since the study used the pancreatic TC-1 cell line, it is unclear whether this phenomenon is cell line-specific or would translate into our MBrM model. Gene expression analysis could help make this clearer, as tumour-derived GM-CSF has been to be an instigator of this process³⁵⁵. Further NK cell and MDSC phenotyping would also help shed some light on whether this process was taking place.

In our study, in addition to the number of NK cells remaining unchanged, there were no variations in their expression of the activation markers, CD107a and CD27. This was, again, unexpected, due to the important role that NK cells had in this therapy, as demonstrated in the cell depletion studies. This lack of change observed for NK cells is most likely due to the limited choice of activation markers analysed. On the other hand, while the

expression of particular markers can be a useful indicator of a cell's activation state, *ex vivo* functional studies may prove to be more informative.

Despite the exact role of bone marrow-derived macrophages remaining unclear from the depletion studies, the flow cytometry data did provide some interesting results concerning macrophages and their brain-resident counterparts, the microglia. Both of these populations substantially increased in the mice with an intracranial and flank tumour receiving treatment compared to the other groups. Additionally, there were no changes to the MHC II expression levels between the groups, suggesting treatment did not increase their antigen-presentation ability but simply increased the total numbers of these cells.

Due to the lack of immunotherapy-based research carried out on brain tumours, it is difficult to make conclusions about the role of microglia and macrophages, especially as the only published work in this field neglects these populations²⁴⁰. There has been some research into the role of microglia as APCs; however, it has been reported elsewhere that while microglia are able to be functional APCs they are not as well-equipped for this purpose as macrophages^{11,293}. Conversely, one cell marker is not sufficient to make a definitive conclusion on the phenotype of these cells. It is known that macrophages can express various markers suggesting, suggesting these cells have pro- and anti-tumourigenic properties¹¹. Therefore, a more detailed screening would be needed to shed some light on the role that they play in immune checkpoint therapy.

One aspect of immune checkpoint therapy that has been widely discussed is the issue of why some patients and mice respond to the therapy and others do not^{231,288,290}. It has been suggested that the expression of certain markers can separate responders from non-responders^{231,288}. This was not possible in this study, as the phenotype of the intracranial infiltrating cells remained unaltered in mice receiving treatment. It should be noted that these tumours are within an organ that has been described as immune-privileged²⁹³ and it

is known there are substantial differences between tumour sites. As previously mentioned, gene expression data may help to isolate possible predictive markers.

As described beforehand in Chapter 3, our treatment prevented the majority of flank tumours from developing and growing. While this was beneficial from a therapeutic aspect, it did prevent the analysis of these tumours, making comparison between the two tumour sites impossible. As mentioned previously, there were always some mice that did not respond to the treatment so it would not be appropriate to compare their flank tumour to their intracranial tumour where a therapeutic difference was seen. Correlation or differences between the sites may still be possible if the tumours were to be examined at the gene expression level, as significantly less tissue would be required in comparison to flow cytometry.

Even though a considerable number of cell markers were investigated in this study, there are still a number of others that would be beneficial for future analysis. For example, DCs, MDSCs, neutrophils and B-cells were not included in this analysis and DCs, B-cells and neutrophils have been shown to express PD-1^{199,356,357}; it would, therefore, be possible for them to be affected in some manner by an anti-PD-1 antibody. It has been suggested by one clinical study that tumours with a high infiltration of MDSCs may not respond to immunotherapies. Further analysis of the tumour-infiltrating cells would be needed to determine if this applies to the intracranial tumours in our model¹³⁰. Additionally, studies have demonstrated a decrease in the MDSC population in response to immune checkpoint therapy²⁹⁵; something that could be examined in the context of the MBrM model in the future.

Although it is now universally accepted that PD-L1 expression can only poorly predict the response to immune checkpoint therapy^{289,290}, it could still provide useful information. PD-L1 expression is not limited to tumour cells, it has been found to be expressed on T-cells, B-cells, DCs and macrophages^{357,358} in humans and mice. PD-L1 expression levels may

reveal more information on such populations as macrophages, which could have a positive or negative effect on tumour growth and immune checkpoint therapy. It would also be interesting to investigate whether extracranial disease has any influence over the expression of PD-L1 on intracranial cells, possibly resulting in positive or negative changes to levels of immunosuppression.

As an aside, anti-TIM-3 treatment has been shown to be effective in preclinical models and is currently being used in clinical trials^{195,340,359}. Furthermore, there has been a population of T-Regs described which express TIM-3 that have been associated with a highly suppressive function and are only found in tumour³⁶⁰. This could further strengthen the case of using an anti-TIM-3 therapeutic and provide a rationale to include anti-TIM-3 into our treatment regime, in spite of TIM-3 expression remaining unaltered in our hands.

In summary, this chapter demonstrates that whilst there seemed to be an increase in the infiltration of CD8⁺ T-cells into the intracranial tumours of mice with an intracranial and flank tumour receiving treatment, there were no changes to their phenotype, in terms of their expression of such markers as: CD69, CD25, Granzyme B, PD-1, EOMES, TIM-3 and Ki67. While CD4⁺ T-cell infiltration increased with treatment independent of flank tumour status, NK cell infiltration remained unaltered across all groups. Additionally, there was an increase in the infiltration of microglia and macrophages into the intracranial tumours of mice also bearing a flank tumour and receiving treatment, although there were no changes to their MHC II expression levels.

Chapter 6:

Investigating the effects of extracranial tumour and immune checkpoint therapy on peripheral immune cells

Chapter 6

6.1 Introduction

As described in the previous chapters, a number of immune cell populations were identified as essential facilitators for effective immune checkpoint therapy within the brain.

The systemic effects of the treatment are also of interest, due to the nature of the therapy. The system-wide effects of immunotherapies are of particular importance when it comes to tolerability, due to the increase in irAEs. Likewise, examining the systemic changes in response to immune checkpoint therapy may reveal markers that could act as biomarkers and possibly predict the overall outcome. Moreover, peripheral changes in immune cells may be indicative of overall mechanisms responsible for therapeutic efficacy.

This chapter will focus on the systemic effects of immune checkpoint therapy by investigating the immune cell populations within the blood, lymph nodes and spleen. The functional capacity of some of these cells will also be explored in the search for a potential mechanism behind the therapy. Lastly preliminary investigations into potential alterations of the vasculature of the brain metastases upon anti-PD-1 and anti-CTLA-4 therapy will be performed, as this may affect the trafficking of T-cells into the brain.

6.2 Immune checkpoint therapy increases circulating T-Regs

Blood samples were taken from mice on day 11 (Figure 3.7), before the final dose of treatment was administered. Flow cytometry analysis revealed that there were no changes, upon therapy or due to the presence of the extracranial tumour, to the percentage of NK cells and CD3⁺ T-cells within the CD45⁺ population (Figure 6.1A and B). When the CD3⁺ T-cell population was further examined, there were no changes to the percentage of CD8⁺ T-

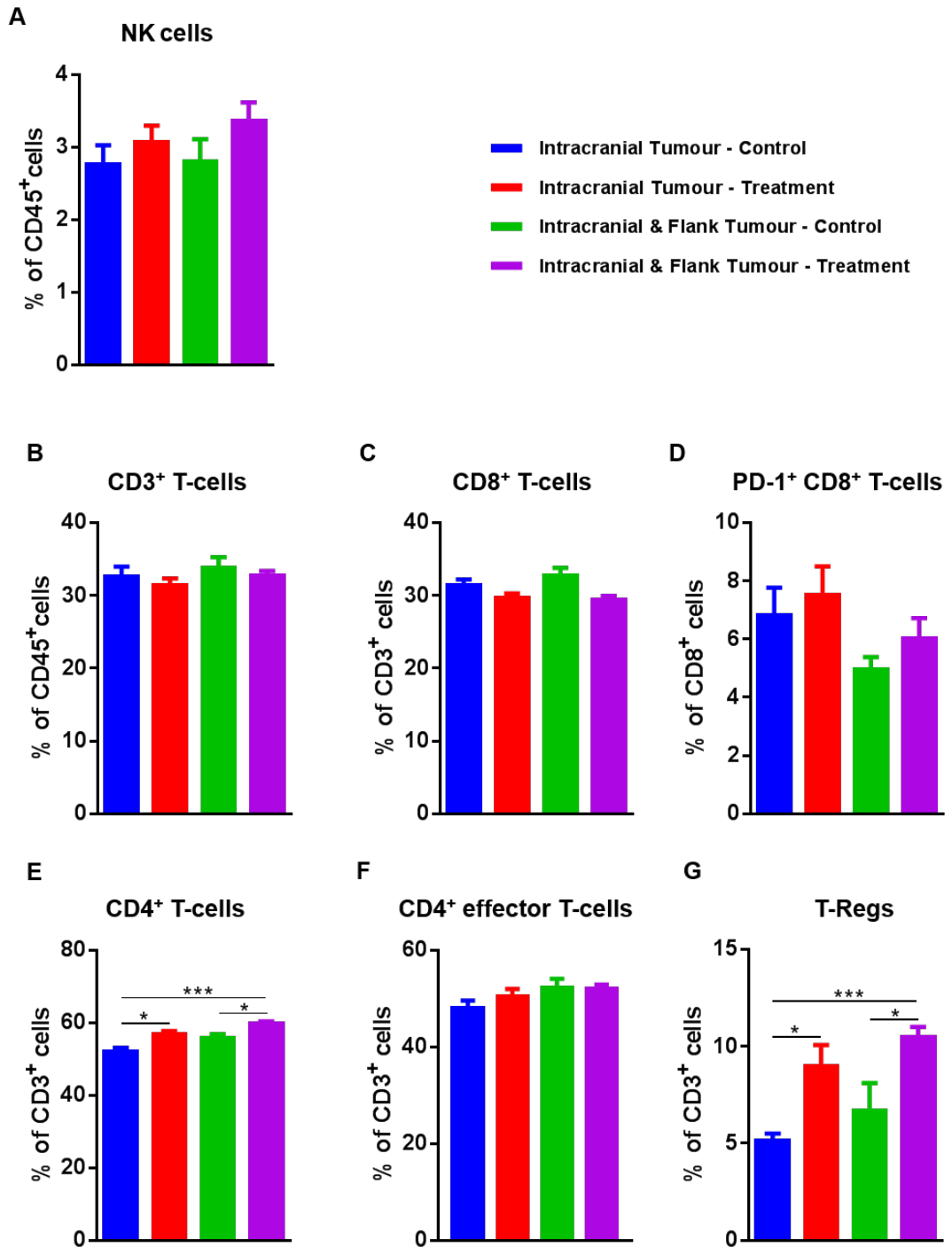


Figure 6.1 Effects of immune checkpoint therapy on immune cells in the blood of mice in the presence and absence of a flank tumour
Blood samples taken from mice were processed and analysed by flow cytometry for: **(A)** NK cells, **(B)** CD3⁺ T-cells, **(C)** CD8⁺ T-cells, **(D)** PD-1⁺ CD8⁺ T-cells, **(E)** CD4⁺ T-cells, **(F)** CD4⁺ effector T-cells and **(G)** T-Regs. (See appendix (pages 205-207) for n numbers, number of independent experiments, statistical tests utilised and P values; error bars represent SEM).

cells and the percentage of PD-1⁺ CD8⁺ T-cells (Figure 6.1C and D). Conversely, as seen in the intracranial tumours, there was a significant increase in CD4⁺ T-cells in both treatment groups (Figure 6.1E). Looking within the CD4⁺ T-cell population, this increase did not come from the CD4⁺ effector cells but from the T-Regs (Figure 6.1F and G).

6.3 CD8⁺ T-cells in the cervical lymph nodes have an increased expression of PD-1 in response to treatment

Although it was previously believed the brain was devoid of a lymphatic system, there is now evidence of lymphatic vessels in the brain^{140,294}; likewise, it is known that these vessels drain to the DCLNs^{140,361}. For this reason, it was decided to analyse these lymph nodes in the mice used in our model.

There were no discernible differences between the number of cells collected from the lymph nodes between the groups in response to treatment or the presence of the flank tumour (Figure 6.2A). Flow cytometry was used to further analyse the T-cell population within the lymph nodes. There were no significant changes to the CD3⁺ T-cell population as a whole between the groups (Figure 6.2B); similarly, within the CD3⁺ T-cell population there were no changes to the percentage of CD8⁺ T-cells (Figure 6.2C). Nonetheless, there was an increase in the PD-1⁺ CD8⁺ T-cell population in the mice within the two treatment groups in comparison to the control groups (Figure 6.2D). This difference, however, was only significant between the mice with intracranial and flank tumours in the control group and the two treatment groups, although, there was a trend for the mice in the control group with intracranial tumours only to have fewer PD-1⁺ CD8⁺ T-cells.

In the case of the CD4⁺ T-cells, there were no significant differences between the groups, even though there was a trend for the mice in the control group with intracranial tumours only to have fewer CD4⁺ T-cells (Figure 6.2E). This was again seen when the CD4⁺ effector T-cells were

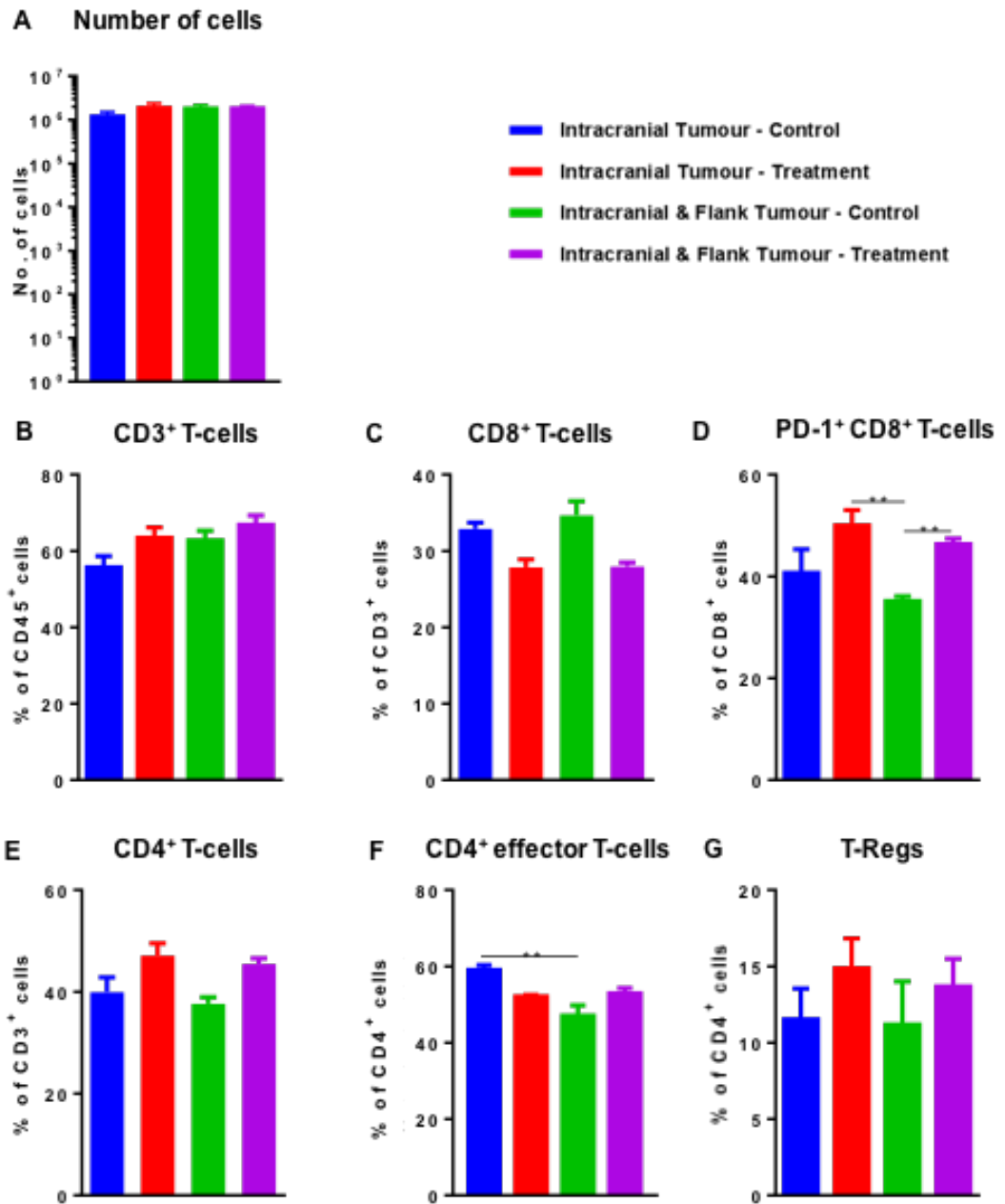


Figure 6.2 Effects of immune checkpoint therapy on immune cells in the DCLNs in the presence and absence of a flank tumour

DCLNs were harvested from mice and analysed for: **(A)** Total number of cells, **(B)** CD3⁺ T-cells, **(C)** CD8⁺ T-cells, **(D)** PD-1⁺ CD8⁺ T-cells, **(E)** CD4⁺ T-cells, **(F)** CD4⁺ effector T-cells and **(G)** T-Regs. (See appendix (pages 207-209) for n numbers, number of independent experiments, statistical tests utilised and P values; error bars represent SEM).

examined. Nonetheless, on this occasion there was a significant decrease in CD4⁺ effector T-cells between the control group with intracranial tumours only and the control group with flank and intracranial tumours. Following the tendency seen in the blood and tumour analyses, there was an increase in the percentage of T-Regs within the CD3⁺ T-cell population in the treatment groups as compared to the control groups. The difference in this instance was not statistically significant.

6.4 Immune checkpoint inhibition affects the immune cell populations within the spleen

As a lymphatic organ that has roles in both innate and adaptive immune responses, the spleen is often used to examine the systemic functions of the immune system *in vivo*³⁶². There was an increase in the number of cells within the spleen upon immune checkpoint inhibition in comparison to the non-treated mice (Figure 6.3A) that was only significant between the treatment group of mice with an intracranial tumour only and the two control groups.

There appeared to be a small, yet non-significant, decrease in the percentage of CD3⁺ T-cells upon treatment in comparison to the control groups (Figure 6.3B). The same trend was observed for the CD8⁺ T-cells, with a statistically significant increase observed in the control group of mice with intracranial and flank tumours compared to the two treatment groups (Figure 6.3C). Phenotypic analysis of the CD8⁺ T-cells did not reveal any changes between the groups in terms of the percentage of CD25⁺, CD69⁺ and PD-1⁺ CD8⁺ T-cells (Figure 6.3D, E and F).

When the percentage of CD4⁺ T-cells were examined, there was found to be a significant increase in both treatment groups as compared to the two control groups (Figure 6.4A). Phenotypic analysis showed no difference between the groups in the percentage of CD25⁺ cells (Figure 6.4B). On the other hand, there was an increase, albeit a non-significant one, in CD69⁺

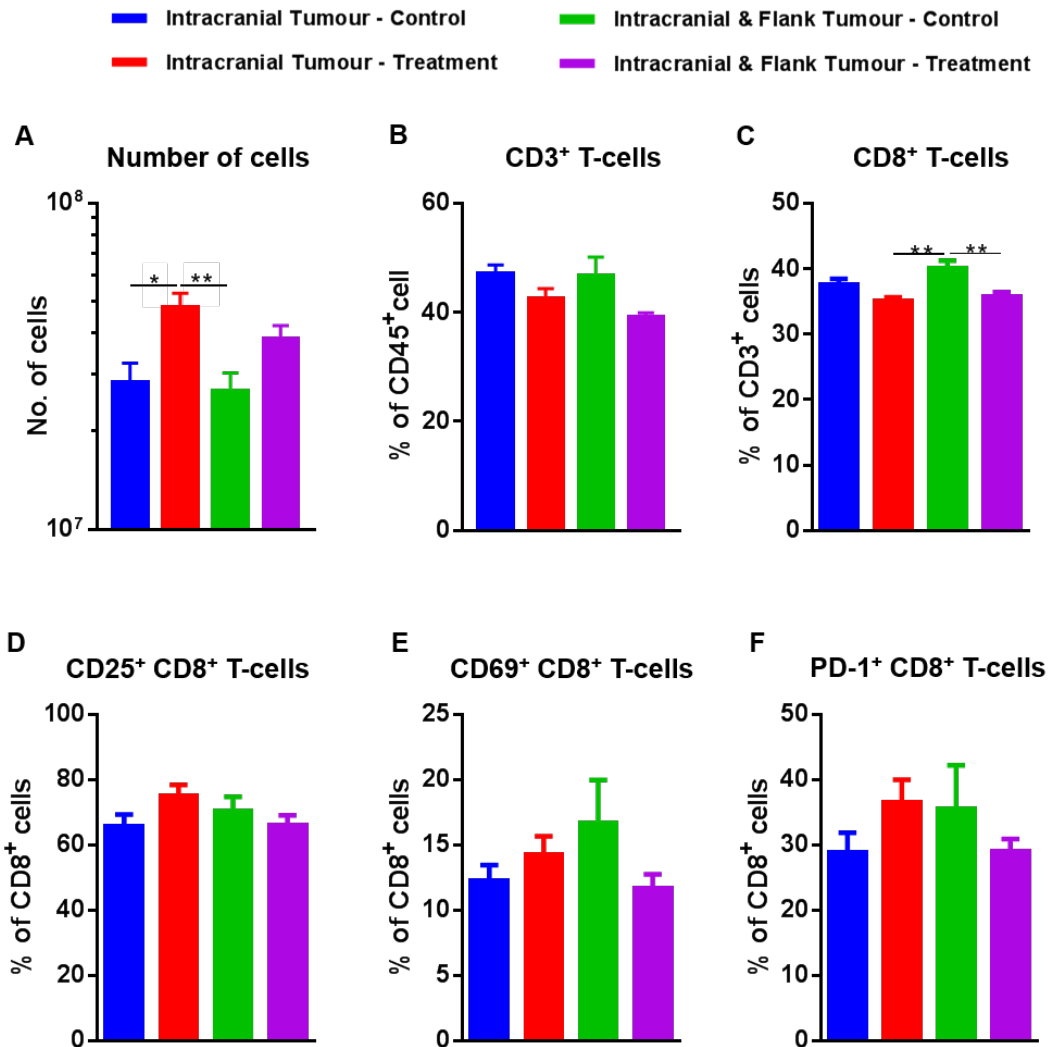


Figure 6.3 Effects of immune checkpoint therapy on CD8⁺ T-cells within the spleen of mice in the presence and absence of a flank tumour

Splenocytes from mice were harvested and analysed for: **(A)** Total number of splenocytes, **(B)** CD3⁺ T-cells, **(C)** CD8⁺ T-cells, **(D)** CD25⁺ CD8⁺ T-cells, **(E)** CD69⁺ T-cells, and **(F)** PD-1⁺ CD8⁺ T-cells. (See appendix (pages 210-211) for n numbers, number of independent experiments, statistical tests utilised and P values; error bars represent SEM).

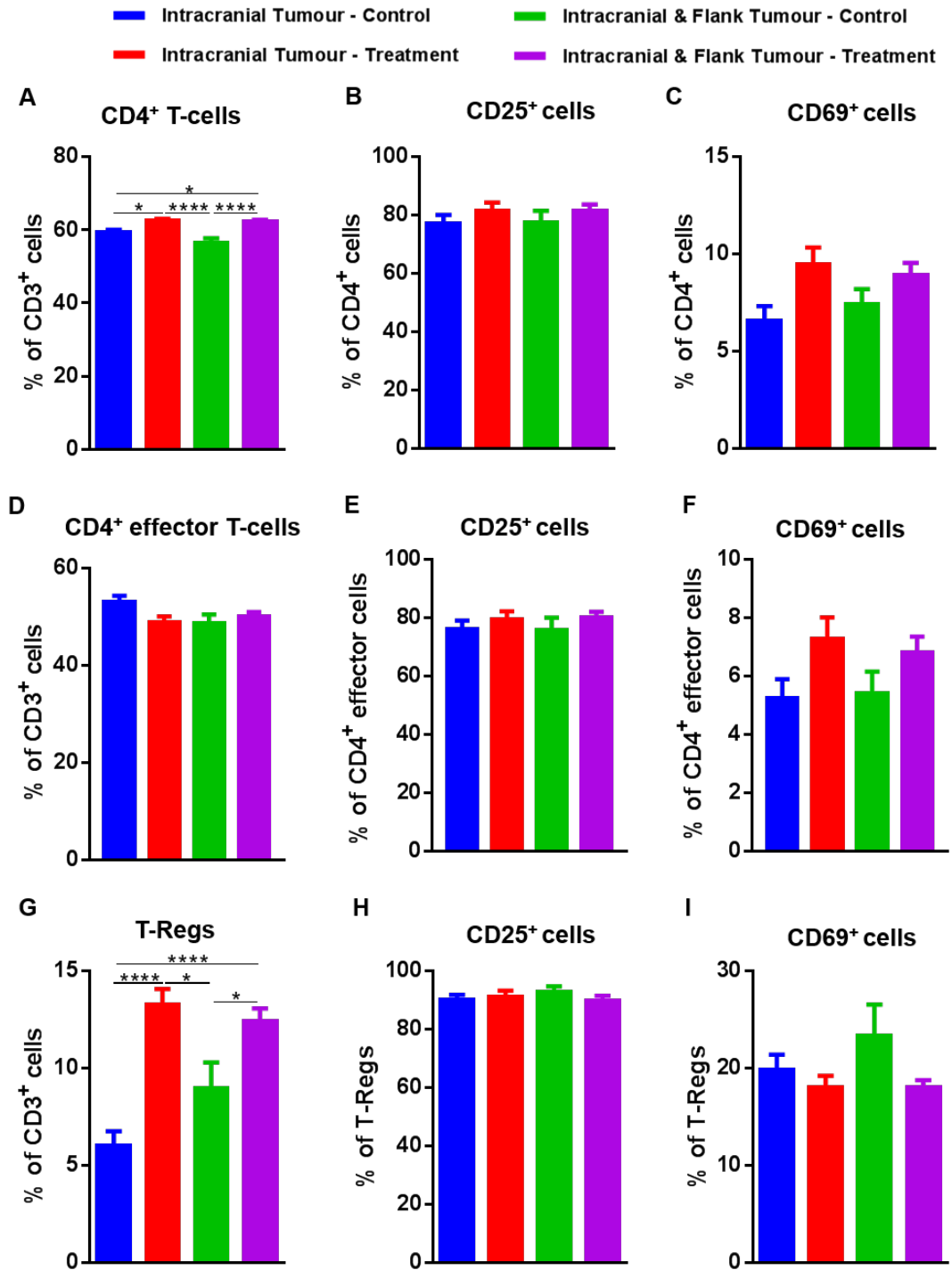


Figure 6.4 Effects of immune checkpoint therapy on CD4⁺ T-cells within the spleen of mice in the presence and absence of a flank tumour

Splenocytes from mice were harvested and processed for flow cytometry analyses of: (A) CD4⁺ T-cells, (B) CD25⁺ CD4⁺ T-cells, (C) CD69⁺ CD4⁺ T-cells, (D) CD4⁺ effector T-cells (E) CD25⁺ CD4⁺ effector T-cells, (F) CD69⁺ CD4⁺ effector T-cells, (G) T-Regs (H) CD25⁺ T-Regs and (I) CD69⁺ T-Regs. (See appendix (pages 212-214) for n numbers, number of independent experiments, statistical tests utilised and P values; error bars represent SEM).

cells in treatment groups compared to the control groups (Figure 6.4C). As with the CD4⁺ effector cells, there were no changes to percentage of these cells (Figure 6.4D) or the percentage of CD25⁺ cells within this population (Figure 6.4E). There was, however, a trend for an increase in CD69⁺ CD4⁺ effector cells in the treatment groups compared to the control groups (Figure 6.4F). The percentage of T-Regs within the CD3⁺ population significantly increased in mice bearing intracranial and flank tumours receiving treatment (Figure 6.4G), as previously seen within intracranial tumours and blood. While there were no changes to the percentage of CD25⁺ T-Regs in response to treatment or the presence of an extracranial tumour (Figure 6.4H), there was a tendency for the control group of mice with intracranial and flank tumours to have a higher percentage of CD69⁺ T-Regs compared to the other groups (Figure 6.4I).

In addition, there was a strong trend towards a lower percentage of NK cells in the spleens of mice with intracranial and flank tumours receiving the treatment, when compared to the three remaining groups (Figure 6.5A). Nonetheless, the percentage of CD107a⁺ and CD27⁺ NK cells remained unaltered between the groups (Figure 6.5B and C).

6.5 Immune checkpoint therapy increases the activation potential of splenocytes

Even though the percentages of particular immune cell populations are informative when it comes to an effective immunotherapy, the ability for these cells to initiate a response to a stimulus is just as - or even more important than - cell numbers. To investigate this, splenocytes were stimulated with a cocktail of phorbol 12-myristate 13-acetate, ionomycin, brefeldin A, monensin and in the presence of a protein-export inhibitor overnight and profiled by flow cytometry for their ability to produce IFN- γ , TNF- α and granzyme B (Figure 6.6).

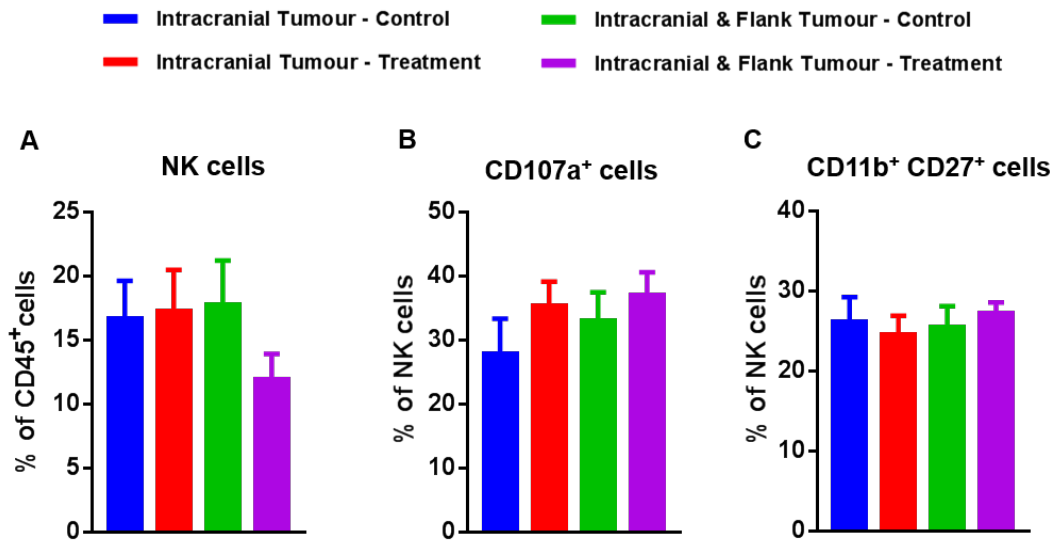


Figure 6.5 Effects of immune checkpoint therapy on NK cells within the spleen of mice in the presence and absence of a flank tumour

Splenocytes from mice were harvested and processed for flow cytometry analyses of: **(A)** NK cells, **(B)** CD107a⁺ NK cells and **(C)** CD11b⁺ CD27⁺ NK cells. (See appendix (page 215) for n numbers, number of independent experiments, statistical tests utilised and P values; error bars represent SEM).

There was a strong trend towards an increase in IFN- γ ⁺ CD8⁺ T-cells in mice with intracranial and flank tumours receiving treatment compared to the other groups (Figure 6.7A). Similar trends were observed in the TNF- α ⁺ CD8⁺ T-cells and this time the increase in the treatment group of mice with intracranial and flank tumours was significantly increased compared to the two groups of mice with intracranial tumours only (Figure 6.7B). With granzyme B⁺ CD8⁺ T-cells, there appeared to be an increase in the percentage of these cells in mice with intracranial and flank tumours when compared to mice with intracranial tumours alone; the difference between the two treatment groups being statistically significant (Figure 6.7C). In contrast, the expression levels of these markers were relatively unchanged, with the exception of a significant increase in granzyme B levels in the control group of mice with intracranial and flank tumours compared to mice with intracranial tumours only receiving the treatment (Figure 6.7D-F).

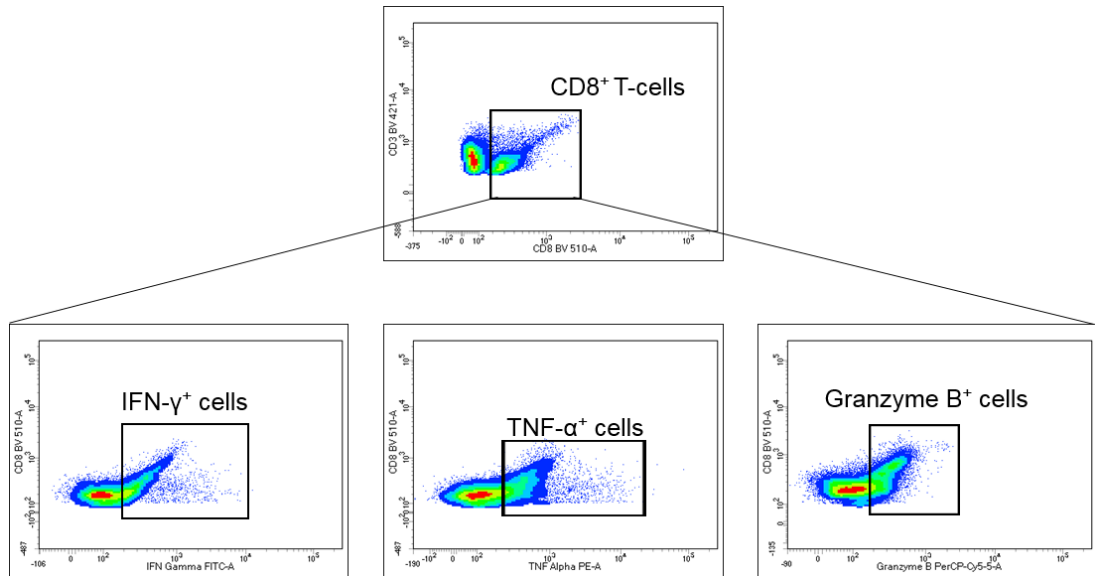


Figure 6.6 Representative flow cytometry plots for *ex vivo*-stimulated splenocytes

CD8⁺ T-cells were gated upon and the IFN- γ ⁺, TNF- α ⁺ and Granzyme B⁺ sub-populations were selected within the CD8⁺ T-cell population.

There was an increase in IFN- γ ⁺ CD4⁺ T-cells in mice with intracranial and flank tumours receiving treatment in comparison to the other groups (Figure 6.8A). The difference, however, was only significant when compared to the control group of mice with intracranial tumours alone. Conversely, there were no changes between the groups in the percentage of TNF- α ⁺ CD4⁺ T-cells (Figure 6.8B). There was a significant increase in the percentage of granzyme B⁺ cells in mice bearing intracranial and flank tumours receiving treatment when compared to the other three groups (Figure 6.8C). There was also a trend towards an increase in the percentage of granzyme B⁺ cells in mice with intracranial tumours alone receiving treatment when compared to the control group of mice with an intracranial tumour only. While the

expression levels of IFN- γ and TNF- α remained unchanged, there was a significant increase in the expression levels of granzyme B in mice with intracranial and flank tumours receiving the treatment compared to the other groups (Figure 6.8D-F).

The NK cells, on the other hand, did not show the same responses. There were no changes to the percentage of IFN- γ^+ or TNF- α^+ NK cells across the groups (Figure 6.9A and B). However, there was an increase in granzyme B⁺ NK in both groups of mice with intracranial and flank tumours compared to mice with intracranial tumours alone receiving treatment (Figure 6.9C). As with the expression level of IFN- γ , there was a tendency for mice in the control group bearing intracranial and flank tumours to have an increase in TNF- α MFI compared to the other groups (Figure 6.9D and E). Additionally, the expression levels of granzyme B significantly increased in the NK cells of mice with intracranial and flank tumours receiving the treatment compared to both groups of mice with intracranial tumours only (Figure 6.9F).

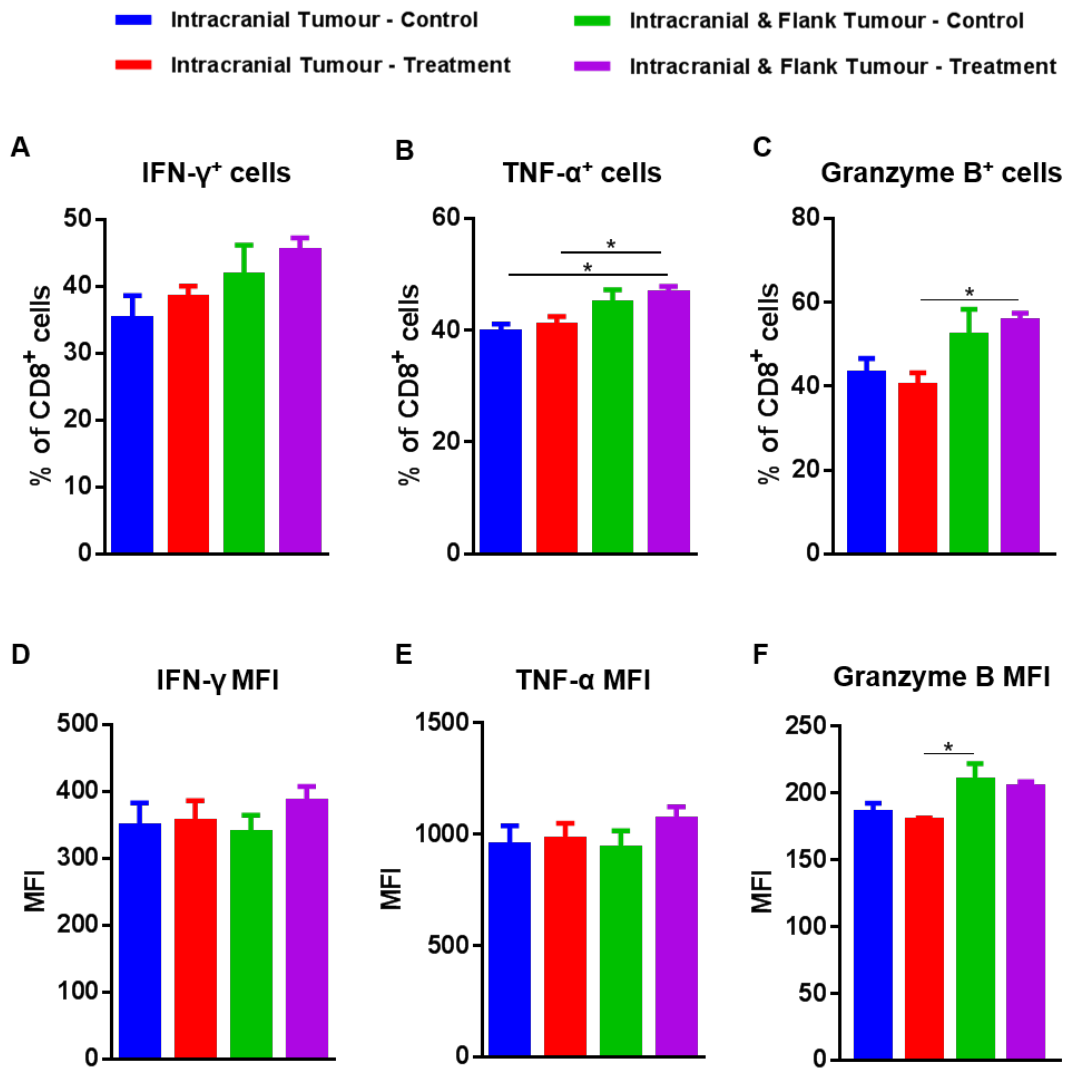


Figure 6.7 Potential of *ex vivo*-stimulated CD8⁺ T-cells to elicit an anti-tumour response

Spleens from mice were harvested, stimulated *ex vivo* with phorbol 12-myristate 13-acetate, ionomycin, brefeldin A, monensin and a protein-export inhibitor overnight and processed for flow cytometry analyses of: **(A)** IFN- γ ⁺ CD8⁺ T-cells, **(B)** TNF- α ⁺ CD8⁺ T-cells, **(C)** Granzyme B⁺ CD8⁺ T-cells and their **(D-F)** MFIs. (See appendix (pages 216-217) for n numbers, number of independent experiments, statistical tests utilised and P values; error bars represent SEM).

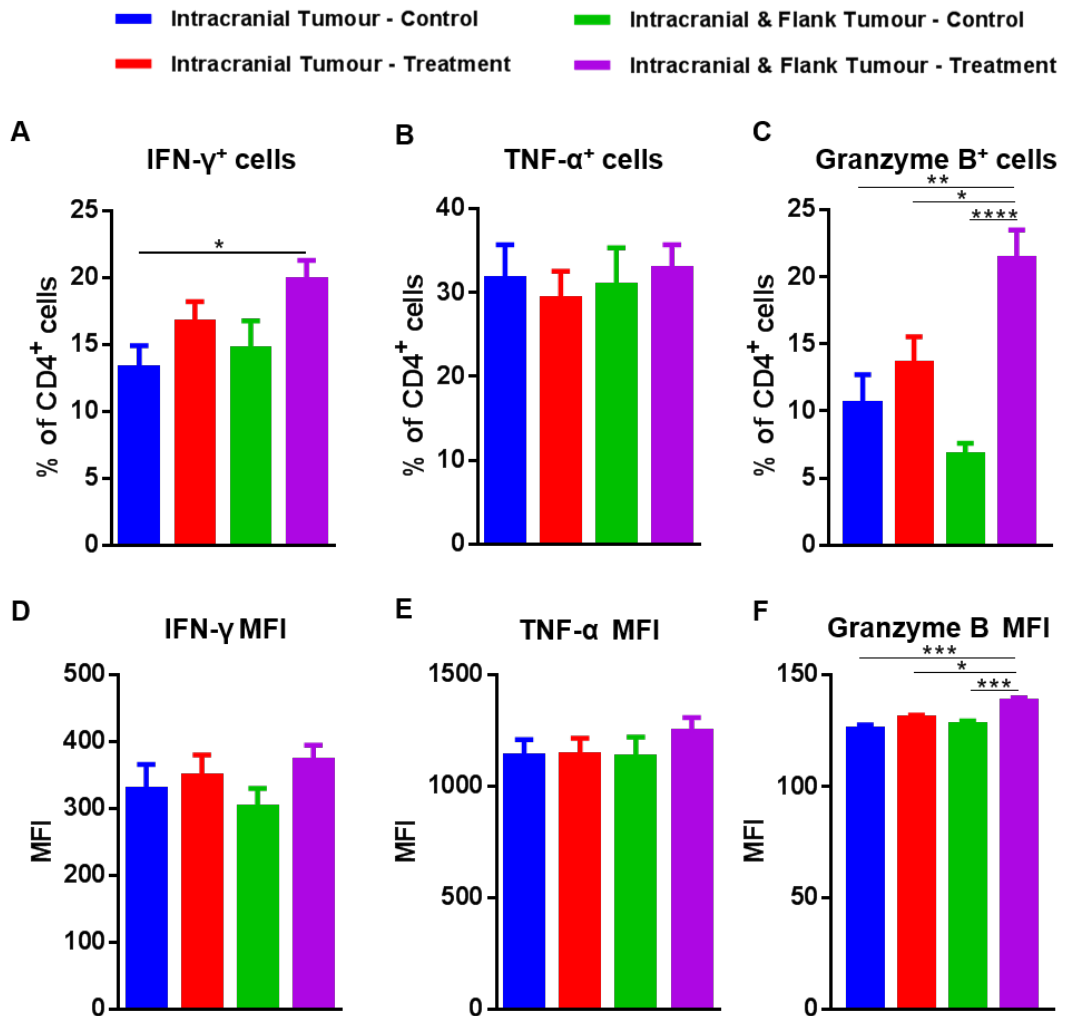


Figure 6.8 Potential of *ex vivo*-stimulated CD4⁺ T-cells to elicit an anti-tumour response

Spleens from mice were harvested, stimulated *ex vivo* with phorbol 12-myristate 13-acetate, ionomycin, brefeldin A, monensin and a protein-export inhibitor overnight and processed for flow cytometry analyses of: **(A)** IFN- γ ⁺ CD4⁺ T-cells, **(B)** TNF- α ⁺ CD4⁺ T-cells **(C)** granzyme B⁺ CD4⁺ T-cells and their **(D-F)** MFIs. (See appendix (pages 218-219) for n numbers, number of independent experiments, statistical tests utilised and P values; error bars represent SEM).

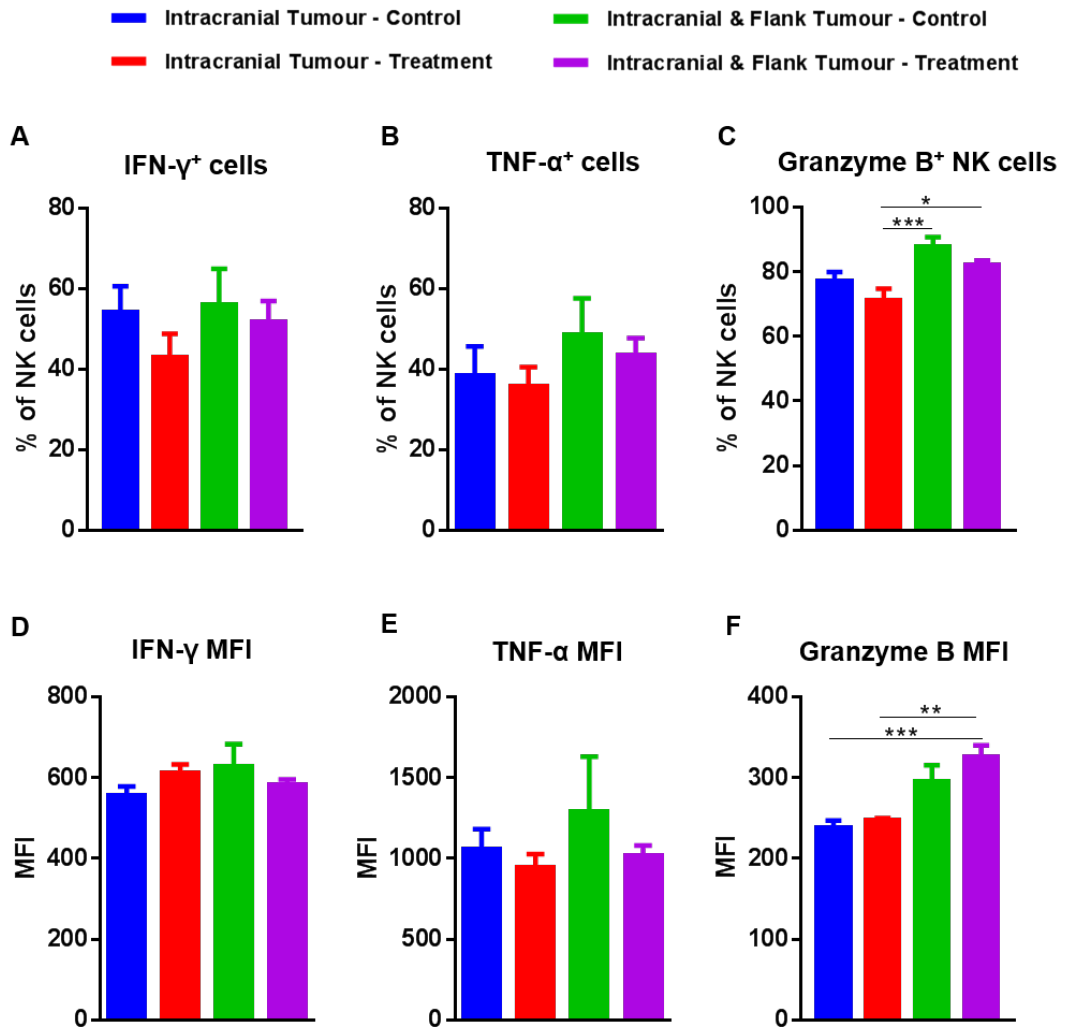


Figure 6.9 Potential of *ex vivo*-stimulated NK cells to elicit an anti-tumour response

Spleens from mice were harvested, stimulated *ex vivo* with phorbol 12-myristate 13-acetate, ionomycin, brefeldin A, monensin and a protein-export inhibitor overnight and processed for flow cytometry analyses of: **(A)** IFN- γ^+ NK cells, **(B)** TNF- α^+ NK cells, **(C)** granzyme B $^+$ NK cells and their **(D-F)** MFIs. (See appendix (pages 220-221) for n numbers, number of independent experiments statistical tests utilised and P values; error bars represent SEM).

6.6 Immune checkpoint therapy increases IFN- γ production by splenocytes

The functional aspects of cells, such as their production of IFN- γ , can also be measured with methods such as ELISA and ELISpot assays. Due to its higher sensitivity, the ELISpot was used to examine the IFN- γ production by splenocytes isolated from mice of each group in both the presence and absence of a number of melanoma-specific stimuli.

Upon analysis of the assay control wells (no stimulus), there were evident distinctions between the mice with intracranial and flank tumours receiving treatment compared to the other groups (Figure 6.10A). Once quantified, there was a significant increase in the average number of spots in this group indicating an increase in IFN- γ production in the absence of *ex vivo* tumour-specific stimulation (Figure 6.10B). Moreover, there was a general trend for mice with intracranial tumours alone receiving treatment to have an increase in IFN- γ production over that observed in the two control groups.

When challenged with a number of melanoma-specific stimuli (gp100 peptide, Trp2 peptide and B16 cell lysate), there were no obvious changes to the IFN- γ production in comparison to non-stimulated controls in any of the groups (Figure 6.10C). The exception to this, however, was stimulation with B16 cell lysate, which proved to have an inhibitory effect and decreased IFN- γ production in all groups.

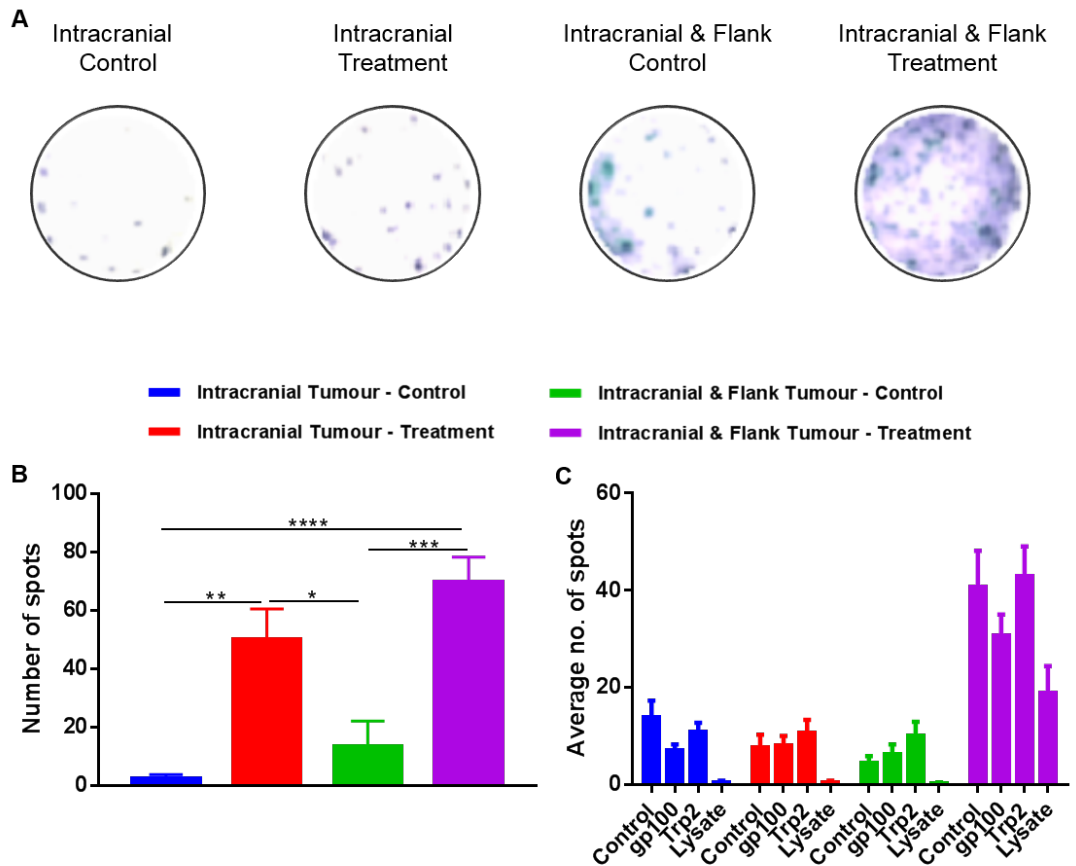


Figure 6.10 Analysis of IFN- γ production by splenocytes in response to melanoma-specific peptides

Spleens from mice were harvested and processed for an ELISpot assay. **(A)** Representative wells of splenocytes cultured overnight without stimulus. **(B)** Quantification of the total number of IFN- γ -producing cells when cultured overnight without stimulus (n= eight, eight, eight, 13, respectively; statistical analysis carried out with one-way ANOVA with a post-hoc test for multiple comparisons). **(C)** Quantification of number of IFN- γ -producing cells when cultured overnight with either no stimulus, gp100 peptide, Trp2 peptide or B16 cell lysate from a separate experiment (n= eight, eight, eight, 13, respectively).

6.7 Tumour-specific CD8⁺ T-cells can be detected in the B16-ova model

Due to the lack of an antigen-specific response observed in the B16 model, we decided to use the B16 cell line which expresses ovalbumin (B16-ova). Due to the expression of the non-mouse-protein, ova, a strong anti-tumour immune response can be generated with the B16-ova cell line³⁶³. It should be noted that due to time restraints, the experiments in the B16-ova model were performed only once without repetition and should be considered preliminary. It was, therefore, used in the MBrM model, as previously outlined in Figure 3.7. As observed in the B16 model, there was significant reduction in flank tumour growth in mice receiving treatment (Figure 6.11A). When the intracranial tumour burden was examined using non-invasive bioluminescence imaging, there was, again, a clear reduction in tumour burden in mice with a flank and intracranial tumour receiving treatment (Figure 6.11B). While this was only significant when the two treatment groups were compared (Figure 6.11C), the trend seen closely followed that seen in the B16 model (Figure 3.11C). The reduction in tumour burden was also confirmed during post-mortem examination (Figure 6.12).

Using an ova TCR-specific pentamer that binds to the ova-specific TCR complex, ova-specific CD8⁺ T-cells can be identified using flow cytometry³⁶⁴ (Figure 6.13A). When CD8⁺ T-cells within the intracranial tumour were examined, there was an increase in ova pentamer⁺ cells within the CD8⁺ T-cell population in mice with an intracranial and flank tumour receiving treatment (Figure 6.13B). While this increase was only significant when this group was compared to control mice with only an intracranial tumour, there was an apparent trend when compared to the other groups. This trend was also observed in the blood (Figure 6.13C) and splenocytes (Figure 6.13D). However, the percentage of ova-pentamer⁺ cells was substantially higher in the intracranial tumours as compared to the blood and spleens.

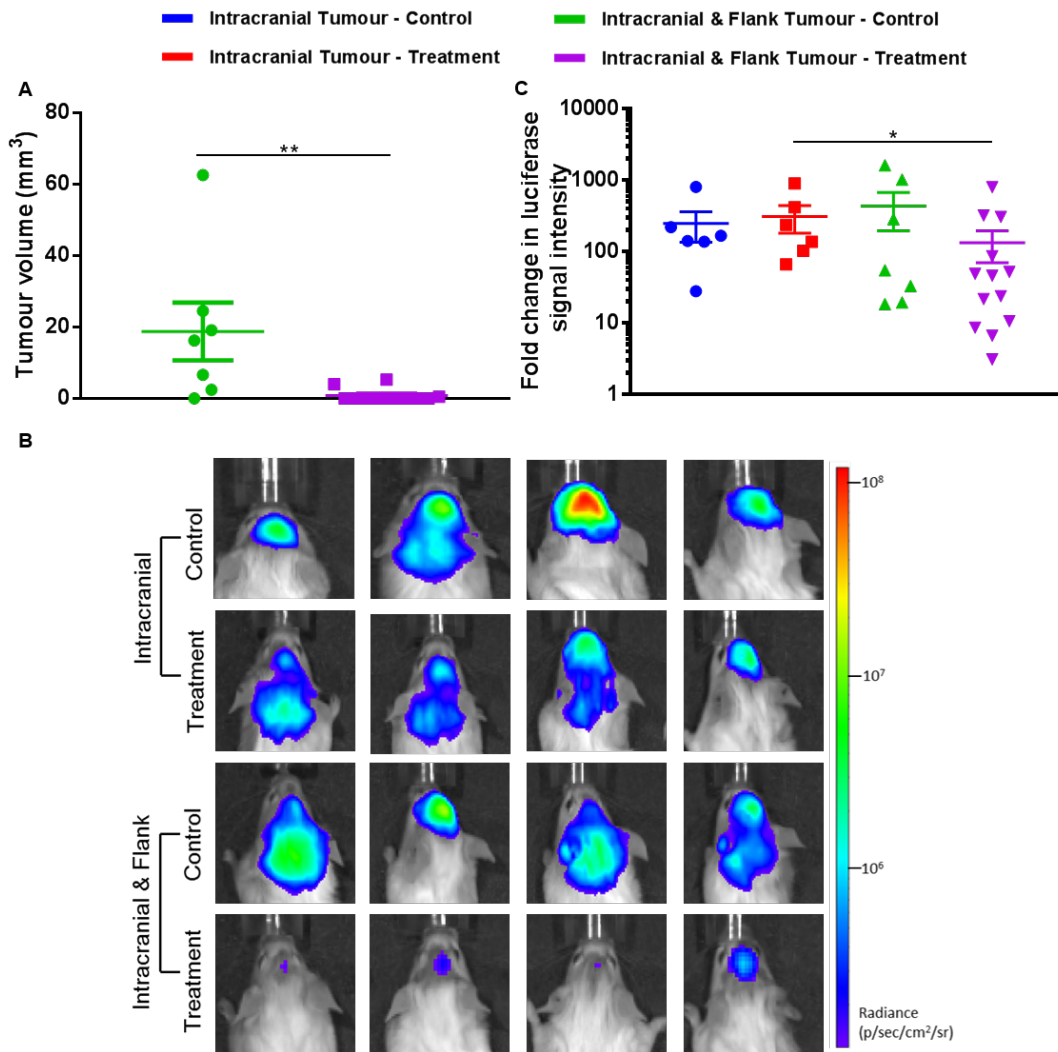


Figure 6.11 The effect of a flank tumour on the intracranial tumour growth of B16-ova cells in mice treated with the combination of anti-PD-1 and anti-CTLA-4

B16-ova/Fluc cells were implanted into albino C57BL6 mice and treatment was administered as outlined previously in Figure 3.7. (A) Flank tumour measurements were taken using calipers the day following the final dose of treatment. Measurements were taken from two dimensions and the tumour volume was subsequently calculated. (B) Representative bioluminescence images of mice taken nine days-post intracranial implantation of cancer cells. (C) The fold change in luciferase signal intensity was calculated between day two and the day after the final dose of treatment was administered. (n = six, six, seven, 13, respectively; error bars represent SEM; statistical significance was determined by pairwise Mann-Whitney tests)

6.8 Tumour-specific CD8⁺ T-cells isolated from spleens have a different phenotype to their non-tumour-specific counterparts

CD8⁺ T-cells were isolated from the spleens of mice with B16-ova tumours and analysed by flow cytometry for the expression of the proliferation marker Ki67 and the apoptosis-inducing protease, granzyme B. Analysis showed there was a significant increase in the percentage of Ki67⁺ cells within the CD8⁺ T-cell population when mice received treatment (Figure 6.14A). This increase was independent of the presence of an extracranial tumour and the same trend was seen when the expression levels of Ki67 were analysed (Figure 6.14B). In the case of granzyme B, there were no changes to the percentage of these cells within the CD8⁺ T-cell population or the expression levels amongst the groups (Figure 6.14C and D).

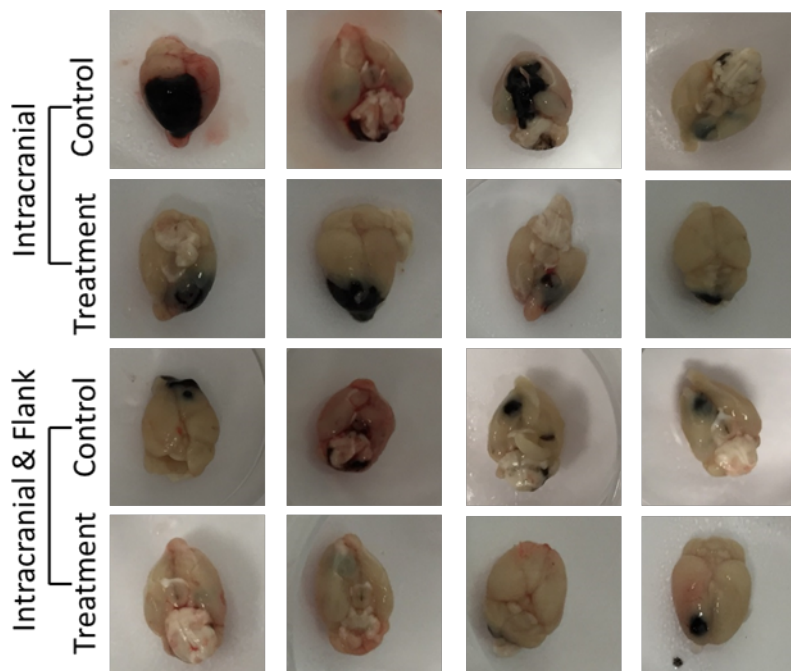


Figure 6.12 Post-mortem images of mice with B16-ova/Fluc tumours treated with anti-PD-1 and anti-CTLA-4 in the presence and absence of a flank tumour

See Figure 6.11 for experimental details. Mice were terminally perfused with PBS the day following the final dose of treatment and brains were removed for post-mortem examination. Tumours are black due to melanin secreted by the B16-ova melanoma cells.

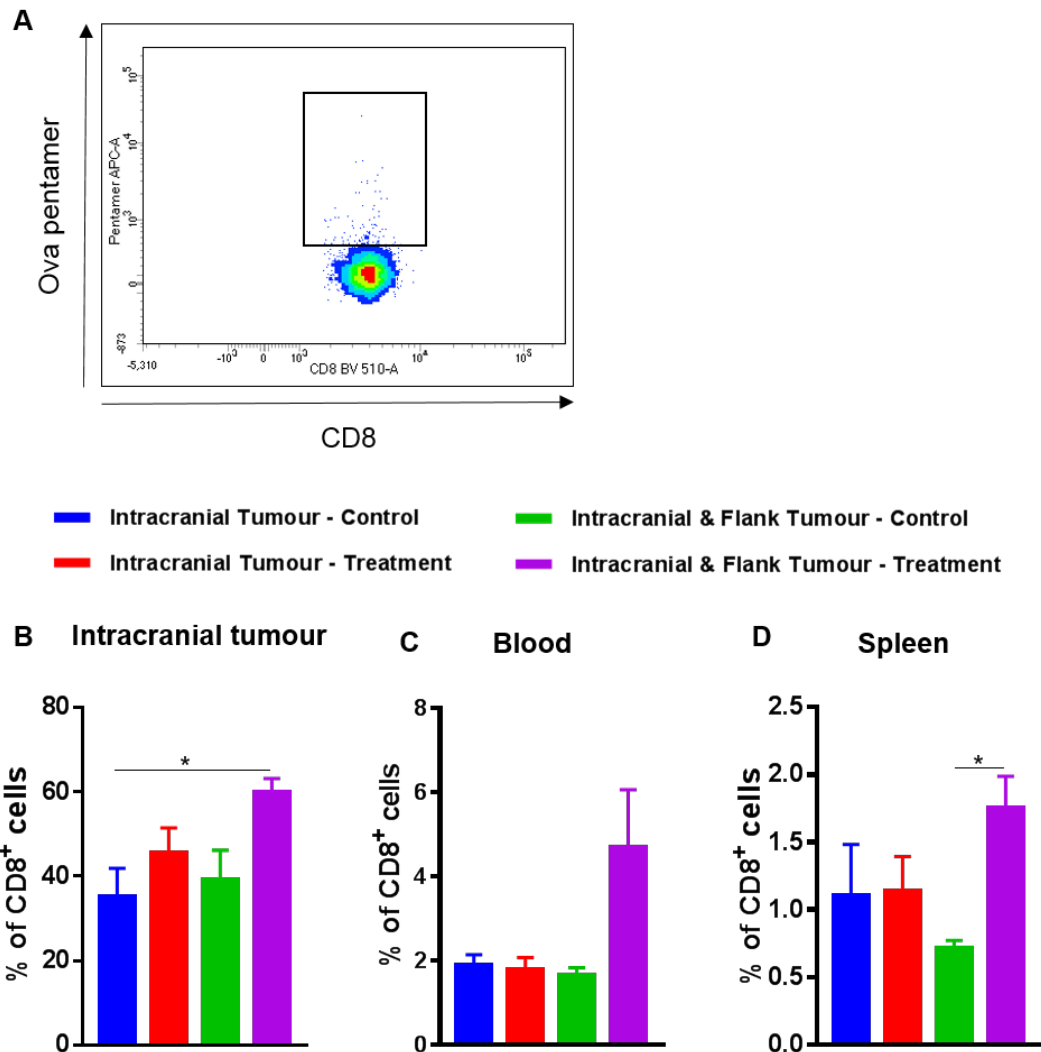


Figure 6.13 The effects of extracranial tumour and immune checkpoint therapy on the B16-ova tumour-specific CD8⁺ T-cell population in the brain, blood and spleen

(A) Tumour-specific CD8⁺ T-cells were gated upon based on pentamer staining for the ova peptide. Analysis was carried out on cells from: (B) the intracranial tumour, (C) the blood and (D) the spleen. (See appendix (page 222) for n numbers, number of independent experiments, statistical tests utilised and P values; error bars represent SEM). See Figure 8.1 on page 242 for example plots of pentamer⁺ staining.

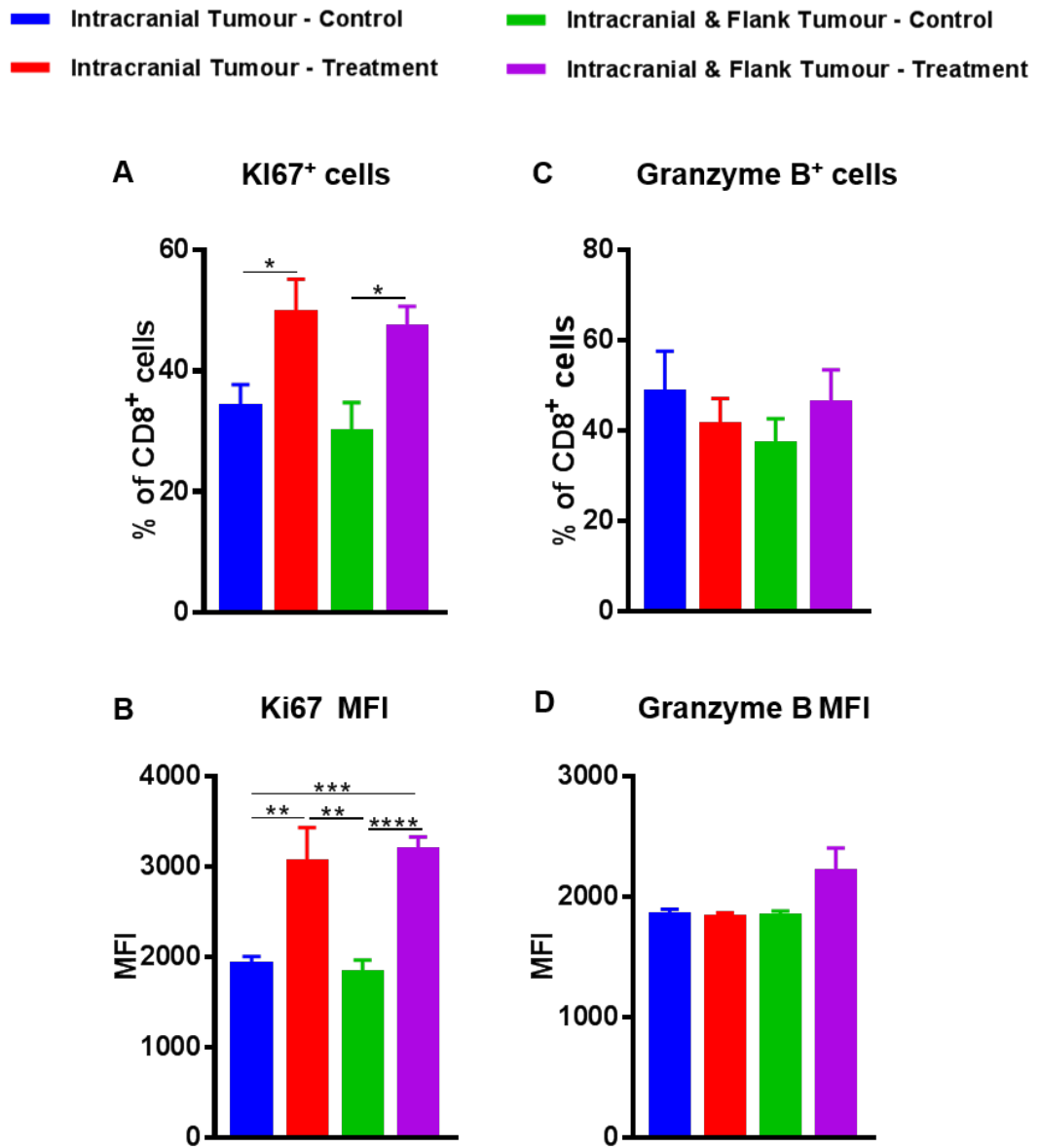


Figure 6.14 The effects of extracranial tumour and immune checkpoint therapy on the phenotype of the CD8⁺ T-cell population in the spleens of mice with B16-ova tumours

Spleens from mice were harvested and processed for flow cytometry analyses of: **(A)** Percentage of Ki67⁺ cells within CD8⁺ T-cells. **(B)** MFI for Ki67 in the CD8⁺ T-cell population. **(C)** Percentage of granzyme B⁺ cells within CD8⁺ T-cells. **(D)** MFI for granzyme B in the CD8⁺ T-cell population. (See appendix (pages 223-224) for n numbers, number of independent experiments, statistical tests utilised and P values; error bars represent SEM).

When these two markers were analysed within the ova-pentamer⁺ CD8⁺ T-cell population, there were no changes in the percentages or expression levels of Ki67 and granzyme B across the groups (Figure 6.15 A, B, C and D). Nevertheless, changes were observed when the ova pentamer⁺ population was compared to the pentamer-negative population in mice bearing an intracranial and flank tumour receiving treatment. The ova-pentamer⁺ population had a significantly higher percentage of Ki67⁺ cells than the pentamer-negative population (Figure 6.16A). Interestingly, the Ki67 expression levels were significantly lower in the ova pentamer⁺ population when compared to the pentamer-negative population (Figure 6.16B). With granzyme B, the ova-pentamer⁺ population had a significantly increased percentage of granzyme B⁺ cells along with its increased expression levels, as compared to the pentamer-negative population (Figure 6.16C and D).

We further examined a number of exhaustion-associated markers, namely EOMES, TIM-3 and PD-1. The percentage of EOMES⁺ cells and its expression level remained unaltered in the CD8⁺ T-cell population when compared amongst the groups, although there was a significant tendency for the expression level to be increased upon therapy (Figure 6.17A and B). There was also an evident trend for an increase in the percentage of TIM-3⁺ cells within the CD8⁺ T-cell population in mice receiving treatment who had an intracranial and flank tumour compared to the other three groups (Figure 6.17C). This trend did not, however, correlate with the expression level of TIM-3, as expression levels remained unchanged amongst the groups (Figure 6.17D). The percentage of PD-1⁺ cells within the CD8⁺ T-cell population increased in mice with a flank and intracranial tumour receiving treatment (Figure 6.17E). This increase was only significant when compared to the two control groups. Like TIM-3, the expression levels of PD-1 remained unaffected by the flank tumour and/or treatment (Figure 6.17F).

As seen previously with the ova-pentamer⁺ CD8⁺ T-cells from the spleen, there were no changes to the exhaustion profile phenotype of the ova-

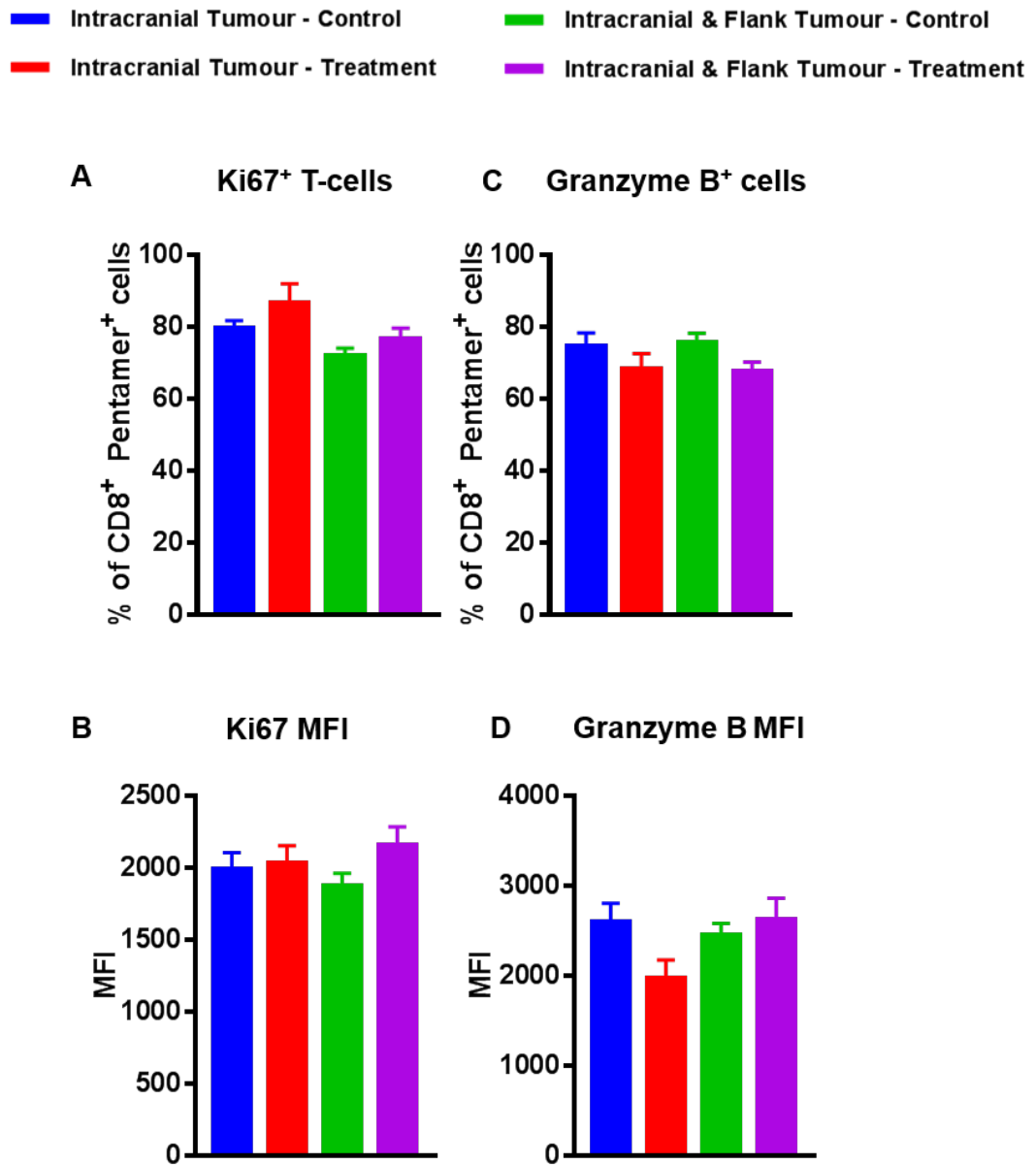


Figure 6.15 The effects of extracranial tumour and immune checkpoint therapy on the phenotype of ova pentamer⁺ CD8⁺ T-cell population in the spleens of mice with B16-ova tumours

Spleens from mice were harvested and processed for flow cytometry analyses of: **(A)** Percentage of Ki67⁺ cells within the pentamer⁺ CD8⁺ T-cells. **(B)** MFI for Ki67 in the pentamer⁺ CD8⁺ T-cell population. **(C)** Percentage of granzyme B⁺ cells within the pentamer⁺ CD8⁺ T-cells. **(D)** MFI for granzyme B in the pentamer⁺ CD8⁺ T-cell population. (See appendix (pages 224-225) for n numbers, number of independent experiments, statistical tests utilised and P values; error bars represent SEM).

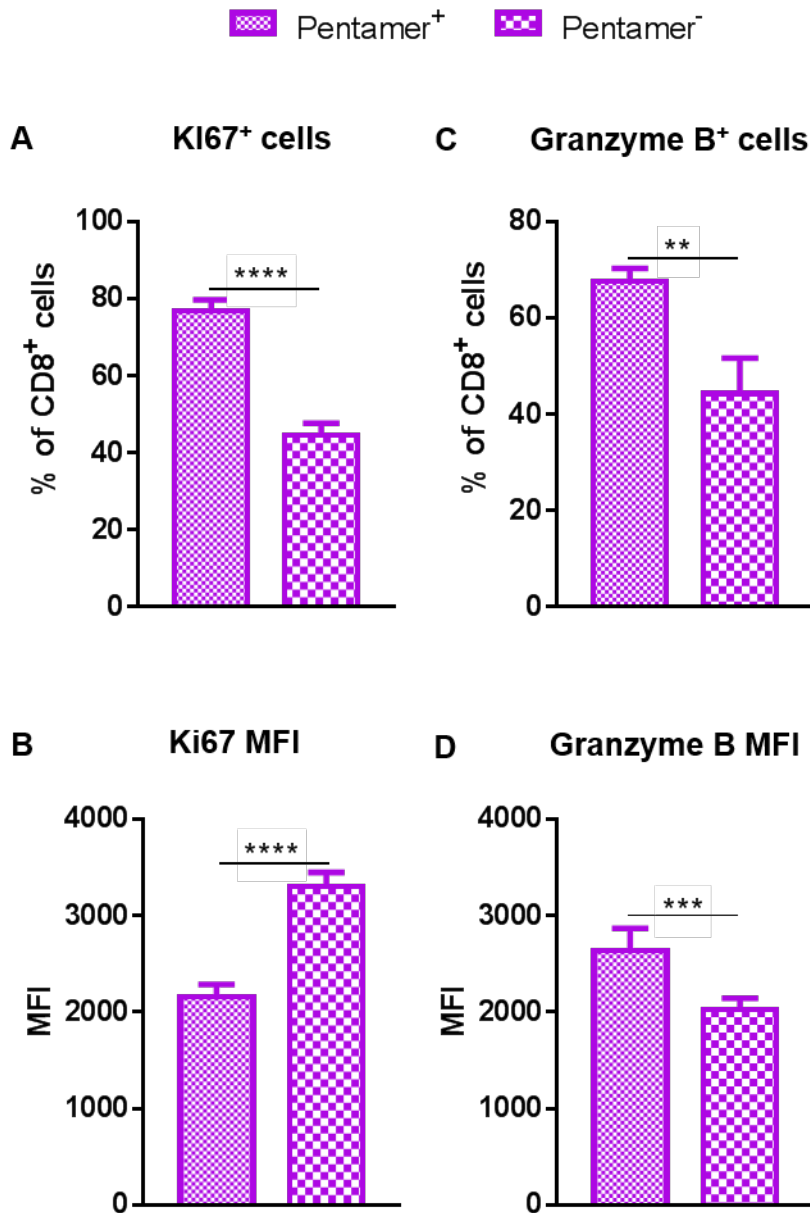


Figure 6.16 Comparison of ova-pentamer⁺ and ova-pentamer⁻ CD8⁺ T-cells for their expression of Ki67 and granzyme B in mice bearing an intracranial and flank tumour receiving treatment

CD8⁺ T-cells were separated based on their ova-pentamer expression. **(A)** Percentage of Ki67⁺ cells within the pentamer⁺ and pentamer⁻ CD8⁺ T-cells is shown. **(B)** MFI for Ki67 in the pentamer⁺ and pentamer⁻ CD8⁺ T-cell population. **(C)** Percentage of granzyme B⁺ cells within the pentamer⁺ and pentamer⁻ CD8⁺ T-cells is shown. **(D)** MFI for granzyme B in the pentamer⁺ and pentamer⁻ CD8⁺ T-cell population. (See appendix (page 225) for n numbers, number of independent experiments, statistical tests utilised and P values; error bars represent SEM).

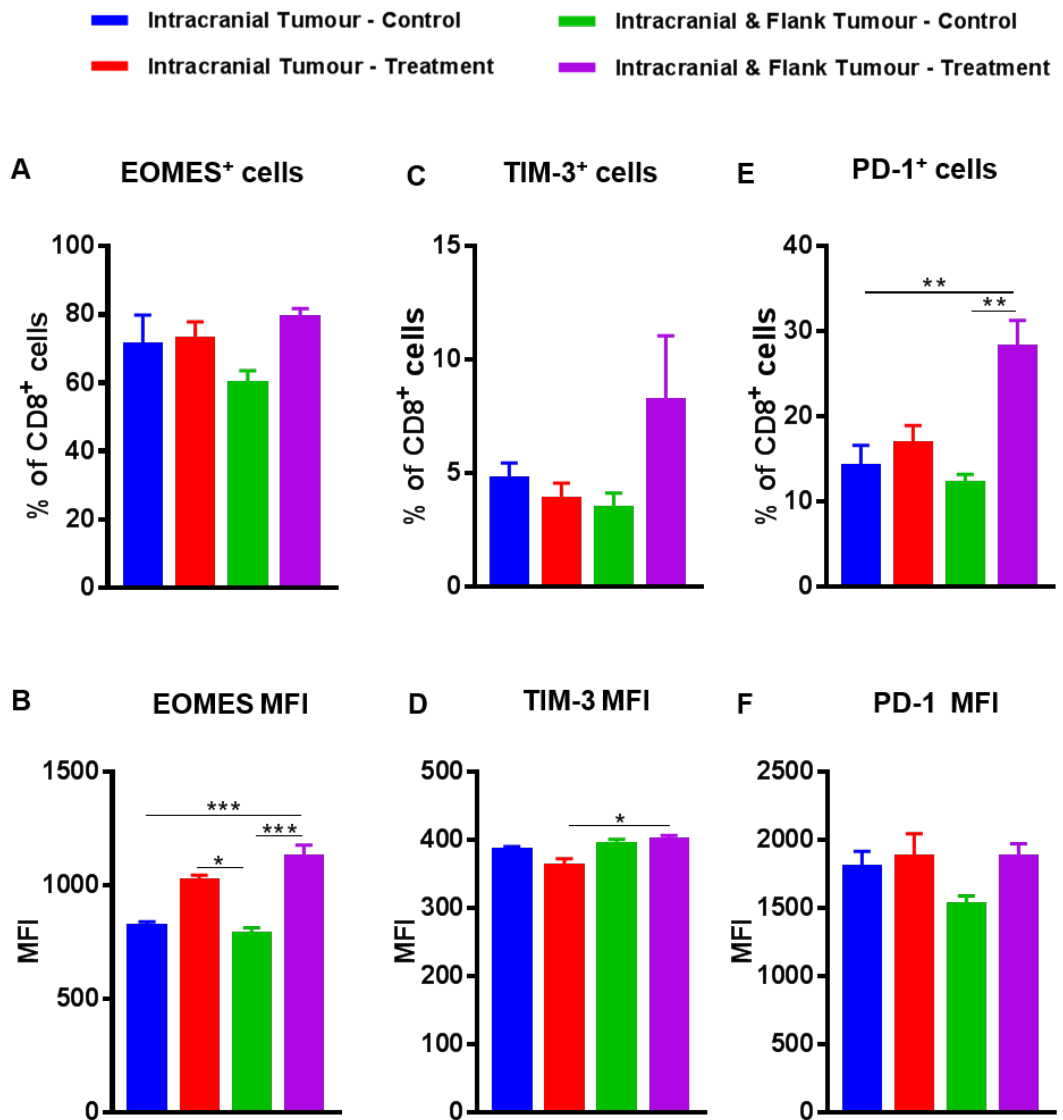


Figure 6.17 The effects of extracranial tumour and immune checkpoint therapy on the inhibitory phenotype of the CD8⁺ T-cell population in the spleens of mice with B16-ova tumours

Spleens from mice were harvested and processed for flow cytometry analyses of: **(A)** Percentage of EOMES⁺ cell within the CD8⁺ T-cells population. **(B)** MFI for EOMES in the CD8⁺ T-cell population. **(C)** Percentage of TIM-3⁺ cells within the CD8⁺ T-cell population. **(D)** MFI for TIM-3 in the CD8⁺ T-cell population. **(E)** Percentage of PD-1⁺ cells within the CD8⁺ T-cell population. **(F)** MFI for PD-1 in the CD8⁺ T-cell population. (See appendix (pages 226-227) for n numbers, number of independent experiments, statistical tests utilised and P values; error bars represent SEM).

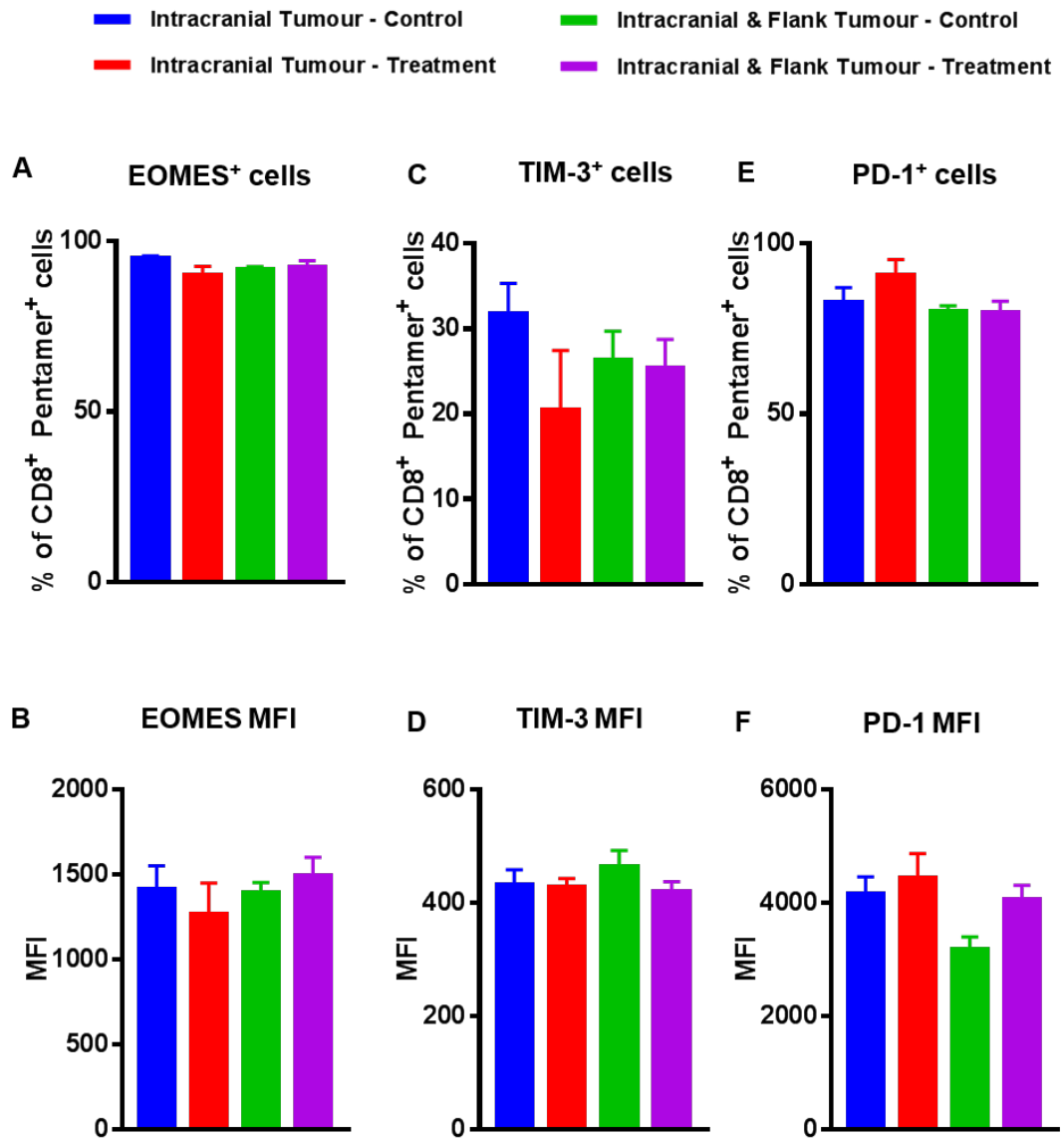


Figure 6.18 The effects of extracranial tumour and immune checkpoint therapy on the inhibitory phenotype of ova pentamer⁺ CD8⁺ T-cell population in the spleens of mice with B16-ova tumours

Spleens from mice were harvested and processed for flow cytometry analysis of **(A)** Percentage of EOMES⁺ cells within the pentamer⁺ CD8⁺ T-cell population. **(B)** MFI for EOMES in the pentamer⁺ CD8⁺ T-cell population. **(C)** Percentage of TIM-3⁺ cells within the pentamer⁺ CD8⁺ T-cell population. **(D)** MFI for TIM-3 in the pentamer⁺ CD8⁺ T-cell population. **(E)** Percentage of PD-1⁺ cells within the pentamer⁺ CD8⁺ T-cell population. **(F)** MFI for PD-1 in the pentamer⁺ CD8⁺ T-cell population. (See appendix (pages 228-229) for n numbers, number of independent experiments, statistical tests utilised and P values; error bars represent SEM).

pentamer⁺ CD8⁺ T-cells amongst the groups (Figure 6.18 A-F). There were, however, alterations, once again between the ova-pentamer⁺ and the pentamer-negative population within the treatment group of mice with an intracranial and flank tumour. The ova-pentamer⁺ population had a significantly higher percentage of cells expressing EOMES, TIM-3 and PD-1 and with, the exception of TIM-3, increased their expression levels when compared to the pentamer-negative population (Figure 6.19A-F).

When the functional potential of these T-cells was investigated through *ex vivo*-stimulation with a cocktail of phorbol 12-myristate 13-acetate, ionomycin, brefeldin A, monensin and in the presence of a protein-export inhibitor, there was an increase in the percentage of CD8⁺ T-cells producing IFN- γ in the treatment groups as compared to the control groups (Figure 6.20A). This increase was significant when mice with an intracranial and flank tumour receiving treatment were compared to the two control groups. Likewise, mice with an intracranial tumour only had a significantly higher percentage of IFN- γ ⁺ CD8⁺ T-cells when compared to the control group of mice bearing intracranial and flank tumours. The expression levels of IFN- γ remained unaffected by the presence of an extracranial tumour and/or treatment (Figure 6.20B). Similar trends were observed in the percentage of TNF- α ⁺ CD8⁺ T-cells and their TNF- α expression levels (Figure 6.20C and D). While the treatment itself, independent of the flank tumour, appeared to result in an increased percentage of TNF- α ⁺ cells, this was only significant when the control and treatment groups of mice bearing intracranial and flank tumours were compared. In contrast to these findings, granzyme B production was seemingly unaffected by the treatment or flank tumour (Figure 6.20E and F).

In the case of CD4⁺ T-cells, the treatment resulted in an increase in the percentage of IFN- γ ⁺ cells which was independent of the presence of a flank tumour (Figure 6.21A). Nevertheless, while this increase was significant

when mice with intracranial tumours only receiving treatment were compared to the two control groups, the increase in mice with intracranial and flank

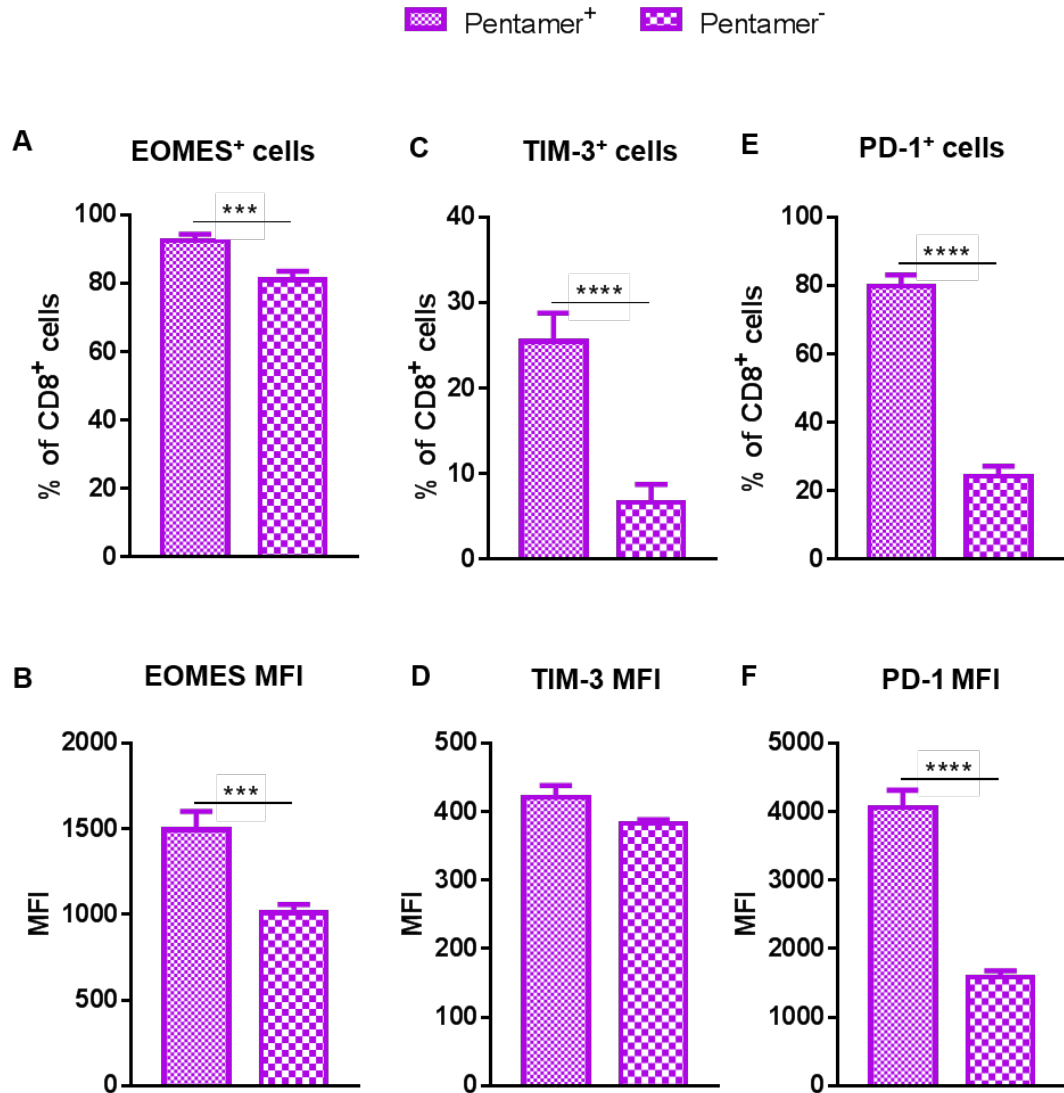


Figure 6.19 Comparison of ova-pentamer⁺ and ova-pentamer⁻ CD8⁺ T-cells for their expression of EOMES, TIM-3 and PD-1 in mice bearing an intracranial and flank tumour receiving treatment

CD8⁺ T-cells were separated based their ova-pentamer expression. **(A)** Percentage of EOMES⁺ cells within the pentamer⁺ and pentamer⁻ CD8⁺ T-cells is shown. **(B)** MFI for EOMES in the pentamer⁺ and pentamer⁻ CD8⁺ T-cell population. **(C)** Percentage of TIM-3⁺ cells within the pentamer⁺ and pentamer⁻ CD8⁺ T-cells is shown. **(D)** MFI for TIM-3 in the pentamer⁺ and pentamer⁻ CD8⁺ T-cell population. **(E)** Percentage of PD-1⁺ cells within the pentamer⁺ and pentamer⁻ CD8⁺ T-cells is shown. **(F)** MFI for PD-1 in the pentamer⁺ and pentamer⁻ CD8⁺ T-cell population. (See appendix (page 230) for n numbers, number of independent experiments statistical tests utilised and P values; error bars represent SEM).

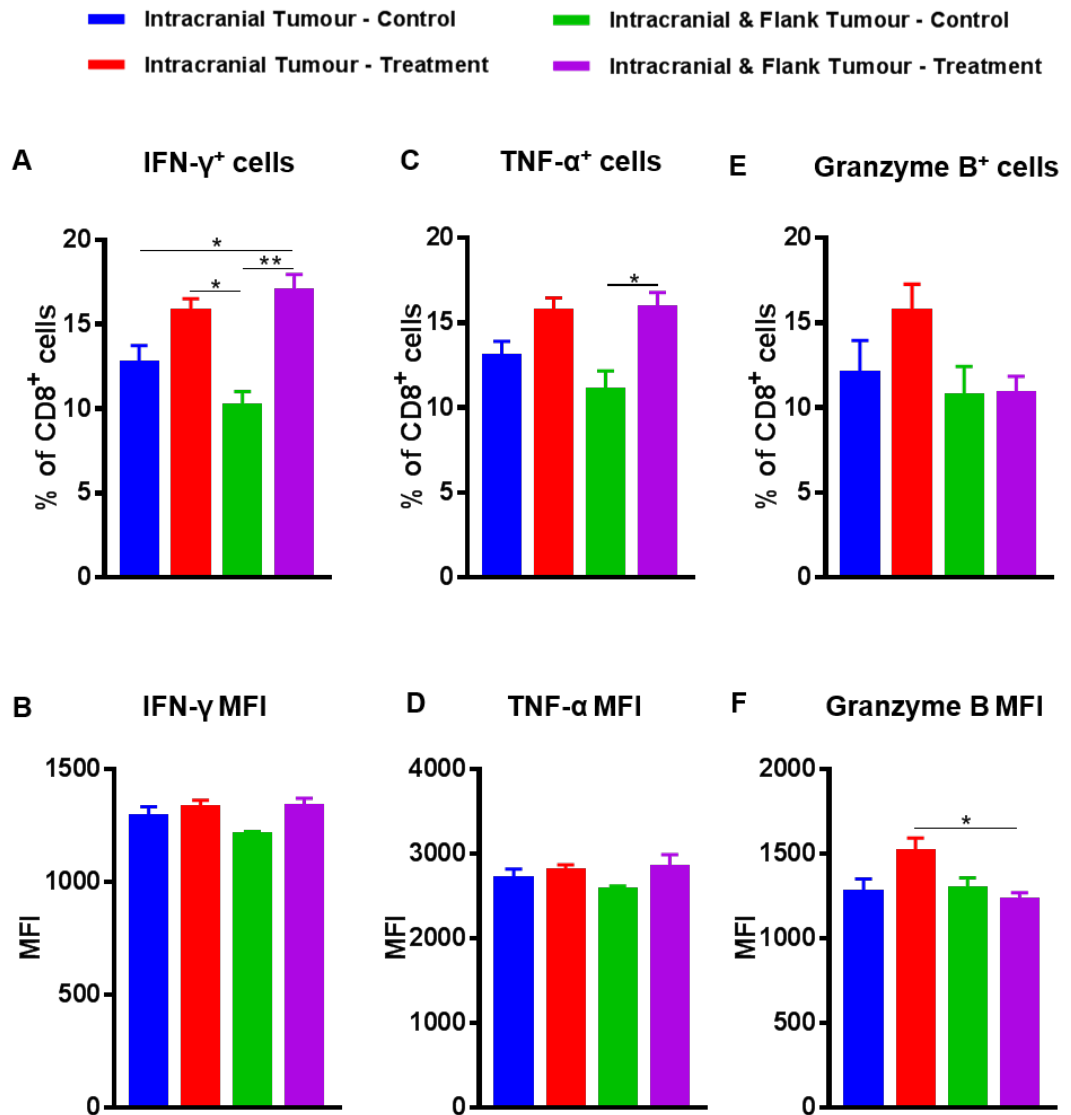


Figure 6.20 Potential of *ex vivo*-stimulated CD8⁺ T-cells to elicit an anti-tumour response from mice with B16-ova tumour

Spleens from mice were harvested, stimulated *ex vivo* with phorbol 12-myristate 13-acetate, ionomycin, brefeldin A, monensin and in the presence of a protein-export inhibitor overnight and processed for flow cytometry analysis. **(A)** Percentage of IFN- γ ⁺ cells within the CD8⁺ T-cell population. **(B)** MFI for IFN- γ in the CD8⁺ T-cell population. **(C)** Percentage of TNF- α ⁺ cells within the CD8⁺ T-cell population. **(D)** MFI for TNF- α in the CD8⁺ T-cell population. **(E)** Percentage of granzyme B⁺ cells within the CD8⁺ T-cell population. **(F)** MFI for granzyme B in the CD8⁺ T-cell population. (See appendix (pages 230-232) for n numbers, number of independent experiments, statistical tests utilised and P values; error bars represent SEM).

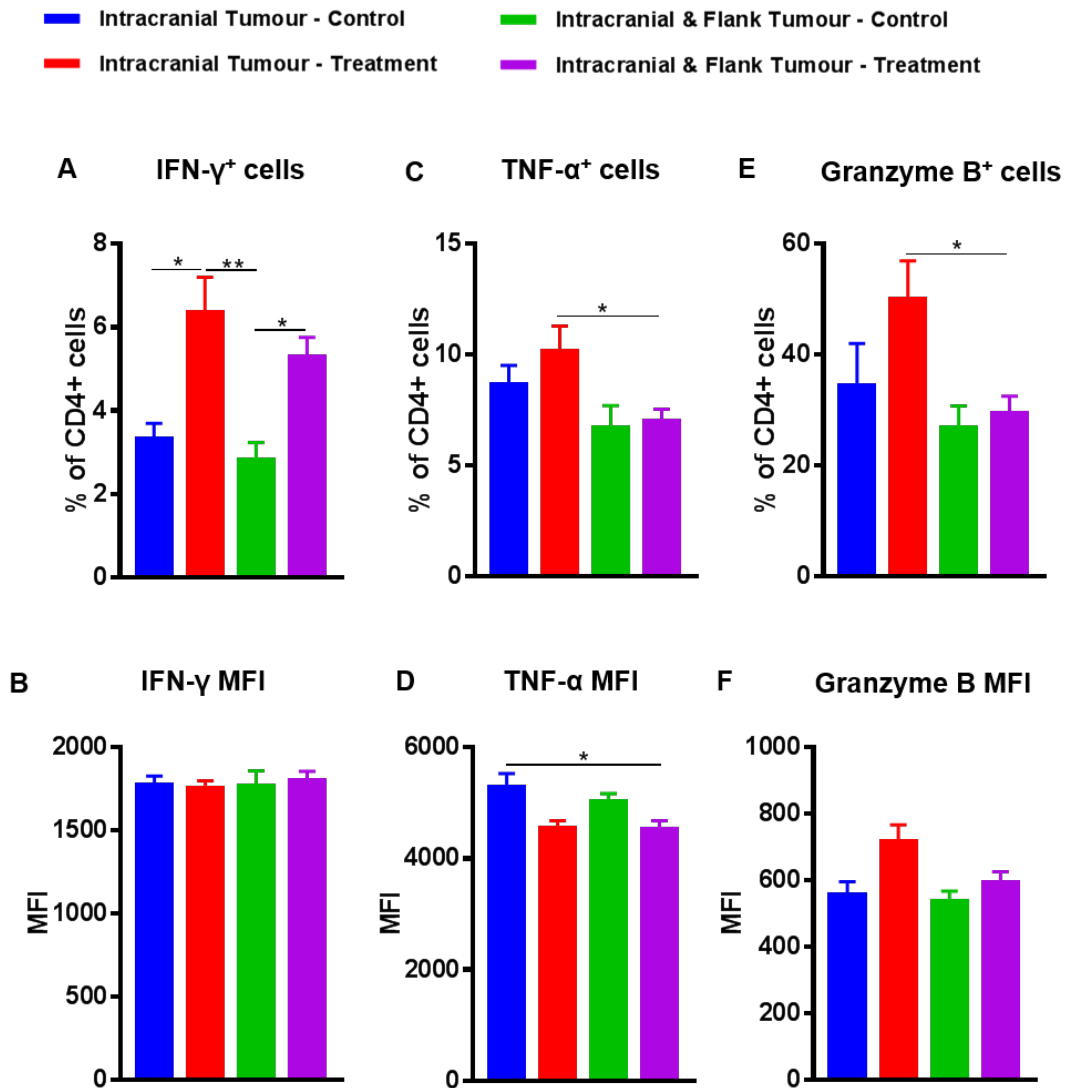


Figure 6.21 Potential of *ex vivo*-stimulated CD4 $^+$ T-cells to elicit an anti-tumour response from mice with B16-ova tumour

Spleens from mice were harvested, stimulated *ex vivo* with phorbol 12-myristate 13-acetate, ionomycin, brefeldin A, monensin and in the presence of a protein-export inhibitor overnight and processed for flow cytometry analysis. **(A)** Percentage of IFN- γ^+ cells within the CD4 $^+$ T-cell population. **(B)** MFI for IFN- γ in the CD4 $^+$ T-cell population. **(C)** Percentage of TNF- α^+ cells within the CD4 $^+$ T-cell population. **(D)** MFI for TNF- α in the CD4 $^+$ T-cell population. **(E)** Percentage of granzyme B $^+$ cells within the CD4 $^+$ T-cell population. **(F)** MFI for granzyme B in the CD4 $^+$ T-cell population. (See appendix (pages 232-234) for n numbers, number of independent

experiments, statistical tests utilised and P values; error bars represent SEM).

tumours receiving treatment was only significant in comparison to the respective control group. As with the CD8⁺ T-cells, there were no changes to the expression levels of IFN- γ in CD4⁺ T-cells (Figure 6.21B). There was a significant increase in the percentage of TNF- α ⁺ cells in mice with an intracranial tumour only receiving treatment as compared to the other three groups (Figure 6.21C). This increase was only significant when compared to the treatment group with an intracranial and flank tumour. Surprisingly, there was a significant decrease in the expression levels of TNF- α in the treatment group of mice bearing an intracranial and flank tumour, when compared to the control group of mice with an intracranial tumour only (Figure 6.21D). With regards to the percentage of cells expressing granzyme B, the trend was the same as that for TNF- α (Figure 6.21E). However, in this case, the expression levels of granzyme B remained the same across the groups (Figure 6.21F).

6.9 Immune checkpoint therapy increases the expression of homing receptors on CD8⁺ T-cells in the circulation

CD8⁺ T-cells express a range of homing markers that are essential for these cells to carry out their cytotoxic function. CCR7 expression is essential for the homing of CD8⁺ T-cells to the lymphoid organs where they can be primed against specific antigens^{365,366}. It has also been suggested that memory CD8⁺ T-cells expressing CCR7 lack an effector function until they home to the lymph nodes, where they will lose their CCR7 expression and gain an effector function³⁶⁵. Moreover, CCR7 has been implicated in the homing of T-cells to the brain³⁶⁷. LFA-1 is a cell surface receptor that is heavily involved in the recruitment of cells to sites of inflammation through binding of ICAM-1³⁶⁸. ICAM-1 is expressed by ECs and binds to the LFA-1 receptor aiding the transmigration of CD8⁺ T-cells from the vasculature into the tissue³⁶⁹. VLA-4 is an integrin dimer that is expressed on T-cells and, like LFA-1, aids the transmigration of T-cells across the endothelium through the

binding of VCAM-1^{146,370}. Likewise, models of multiple sclerosis have demonstrated that this mechanism is essential for T-cells to cross the BBB¹⁴⁶.

The expression of these homing receptors was investigated on CD8⁺ T-cells within the circulation (Figure 6.22). The percentage of CCR7⁺ cells significantly increased in mice receiving treatment, as compared to the control mice (Figure 6.23A). Additionally, the mice bearing intracranial and flank tumours receiving the treatment tended to have more CCR7⁺ cells. The expression levels of CCR7, however, remained unaltered (Figure 6.23B). While the majority of the CD8⁺ T-cell population expressed LFA-1, the level of expression was increased in mice with an intracranial and flank tumour receiving treatment compared to the other groups (Figure 6.23C and D); this increase was significant when compared to the two control groups. The majority of CD8⁺ T-cells expressed VLA-4 in all groups and had similar levels of expression (Figure 6.23E and F).

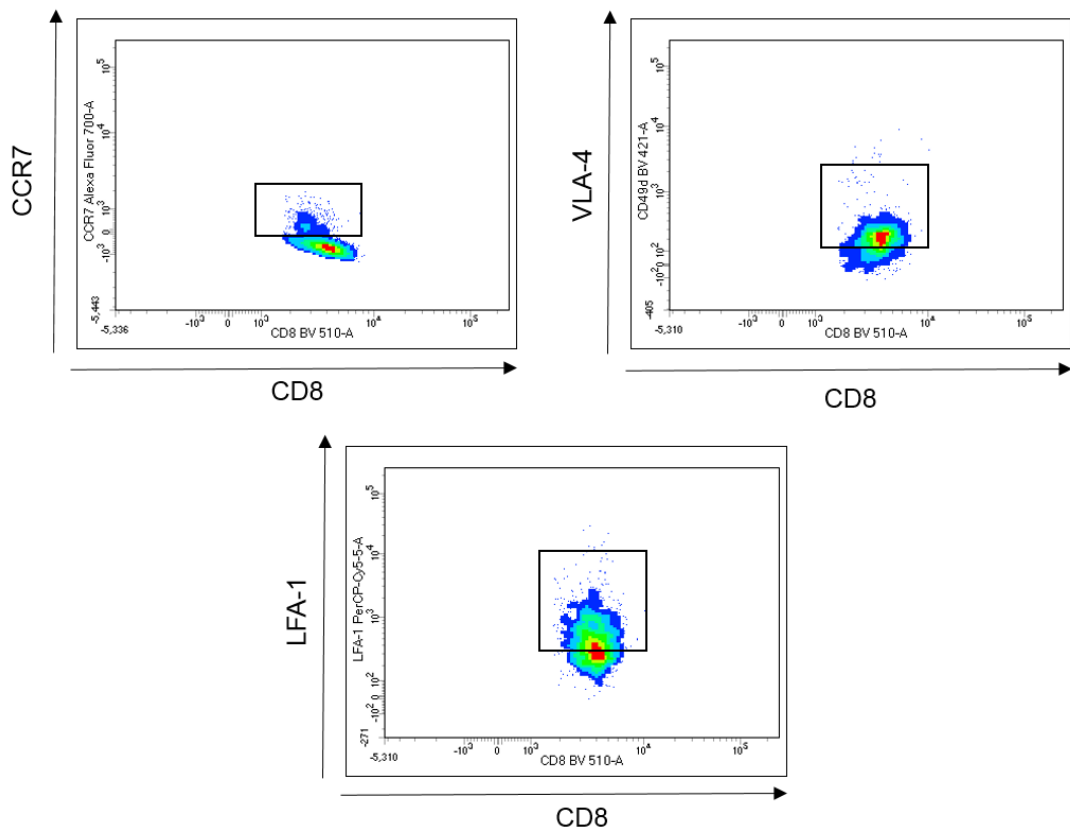


Figure 6.22 Representative flow cytometry plots for homing markers on CD8⁺ T-cells in the blood of mice with B16-ova tumours

Samples of blood were collected for flow cytometry analysis of expression of CCR7, VLA-4 and LFA-1

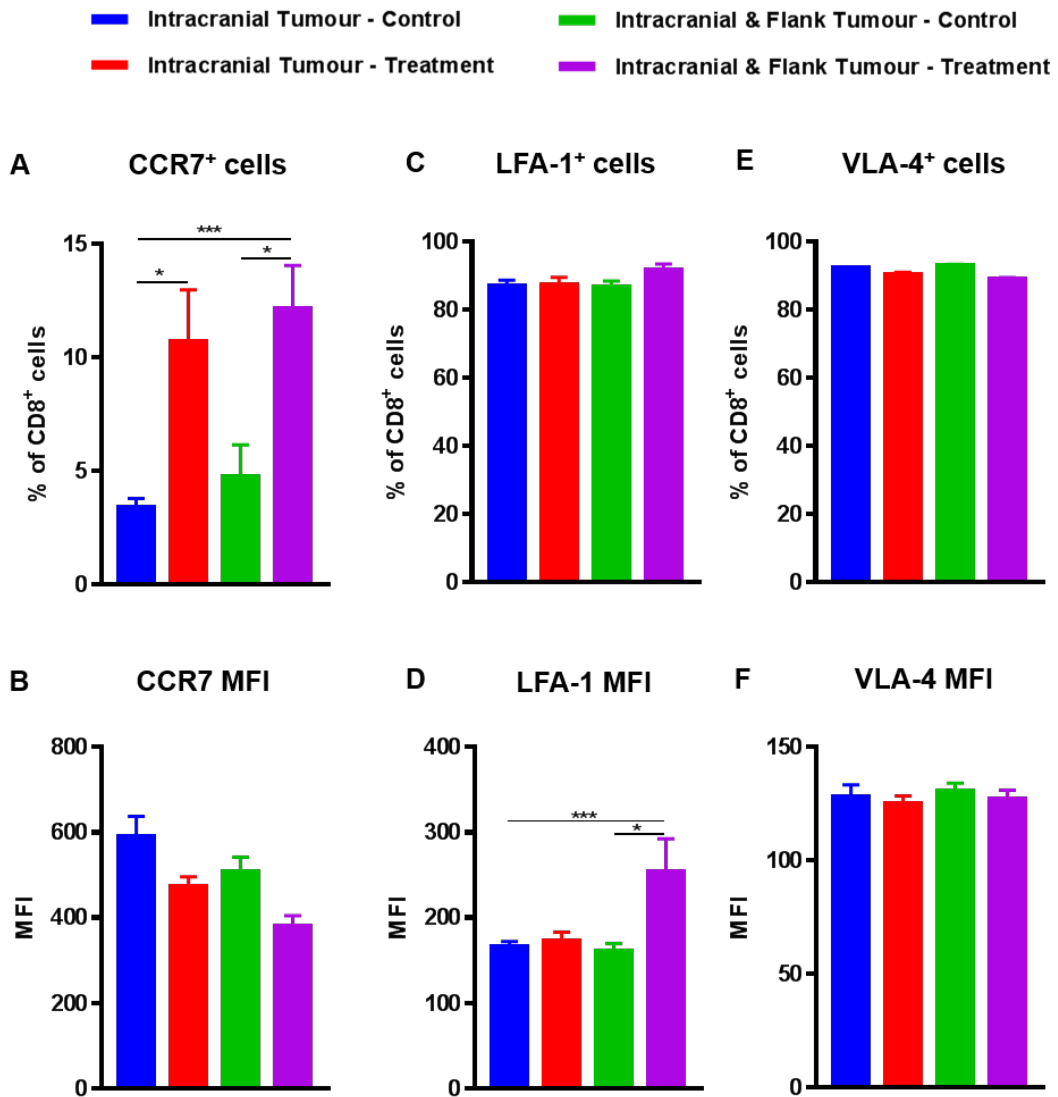


Figure 6.23 The effects of extracranial tumour and immune checkpoint therapy on the homing markers on the CD8⁺ T-cell population in the blood of mice with B16-ova tumours

Blood samples from mice were collected and processed for flow cytometry analyses of: (A) Percentage of CCR7⁺ cells within the CD8⁺ T-cell population. (B) MFI for CCR7 in the CD8⁺ T-cell population. (C) Percentage of LFA-1⁺ cells within the CD8⁺ T-cell population. (D) MFI for LFA-1 in the CD8⁺ T-cell population. (E) Percentage of VLA-4⁺ cells within the CD8⁺ T-cell population. (F) MFI for VLA-1 in the CD8⁺ T-cell population. (See appendix (pages 234-236) for n numbers, number of independent experiments, statistical tests utilised and P values; error bars represent SEM).

When ova-pentamer⁺ CD8⁺ T-cells were examined for these homing receptors, there were no changes between the groups in terms of the percentage of cells expressing these markers or their levels of expression (Figure 6.24A-F). Nonetheless, when the ova-pentamer⁺ population in the mice with intracranial and flank tumours receiving treatment were compared to the negative pentamer population, differences between these populations became apparent. Firstly, the ova-pentamer⁺ population had an increased percentage of CCR7⁺ cells along with an increased level of CCR7 expression compared to the pentamer-negative population (Figure 6.25A and B). This same trend was observed for the expression of LFA-1 (Figure 6.25C and D). While the percentage of cells expressing VLA-4 remained unaltered between the two populations, there was a significant increase in the expression levels of VLA-4 in the ova-pentamer⁺ population (Figure 6.25E and F).

6.10 Immune checkpoint therapy and extracranial tumour synergise to upregulate MHC I and ICAM-1 expression on endothelial cells in intracranial tumours

ECs make up the luminal membrane of the vasculature and express a number of cell-surface molecules that can be used to aid the immune system. This is achieved through the presentation of peptides on MHC molecules to signal to antigen-specific T-cells^{371,372}. Additionally, in response to inflammatory cytokines, ECs upregulate ICAM-1 and VCAM-1 to aid T-cells in migrating to sites of inflammation^{371,372}.

Analysis of intracranial tumours revealed there was a trend for an increase in ECs (CD31^{high} cells)^{372,373} (Figure 6.26) in mice with an extracranial tumour (Figure 6.27A). Likewise, there was a propensity for the ECs to have increased percentage of MHC I⁺ cells in the treatment group of mice with an intracranial and flank tumour as compared to the other groups (Figure 6.27B). This was significant when compared to the control group of mice

with an intracranial and flank tumour. The same tendency was seen when the expression levels of MHC I were examined; however, this failed to

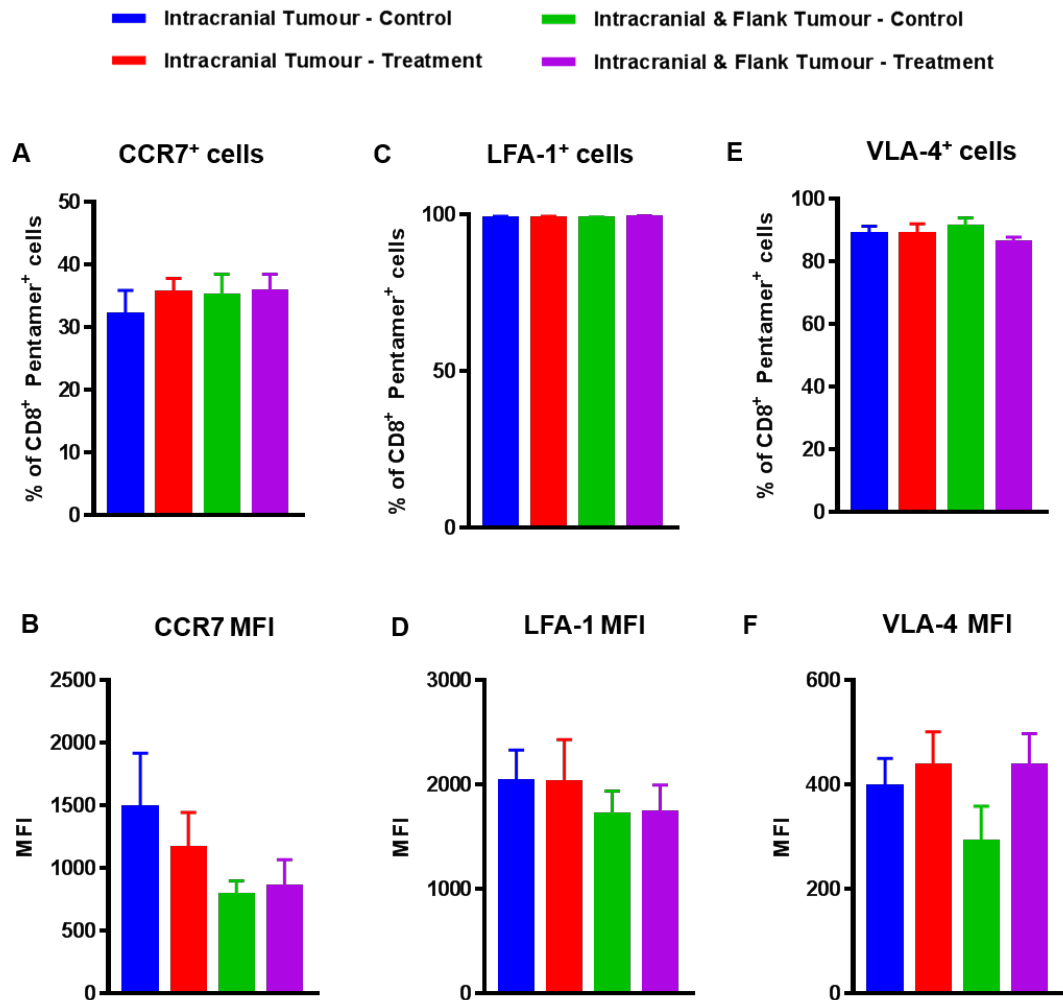


Figure 6.24 The effects of extracranial tumour and immune checkpoint therapy on the homing markers on ova-pentamer⁺ CD8⁺ T-cell population in the blood of mice with B16-ova tumours

Blood samples from mice were collected and processed for flow cytometry analyses of: **(A)** Percentage of CCR7⁺ cells within the pentamer⁺ CD8⁺ T-cell population. **(B)** MFI for CCR7 in the pentamer⁺ CD8⁺ T-cell population. **(C)** Percentage of LFA-1⁺ cells within the pentamer⁺ CD8⁺ T-cell population. **(D)** MFI for LFA-1 in the pentamer⁺ CD8⁺ T-cell population. **(E)** Percentage of VLA-4⁺ cells within the pentamer⁺ CD8⁺ T-cell population. **(F)** MFI for VLA-4 in the pentamer⁺ CD8⁺ T-cell population. (See appendix (pages 236-238) for n numbers, number of independent experiments, statistical tests utilised and P values; error bars represent SEM).

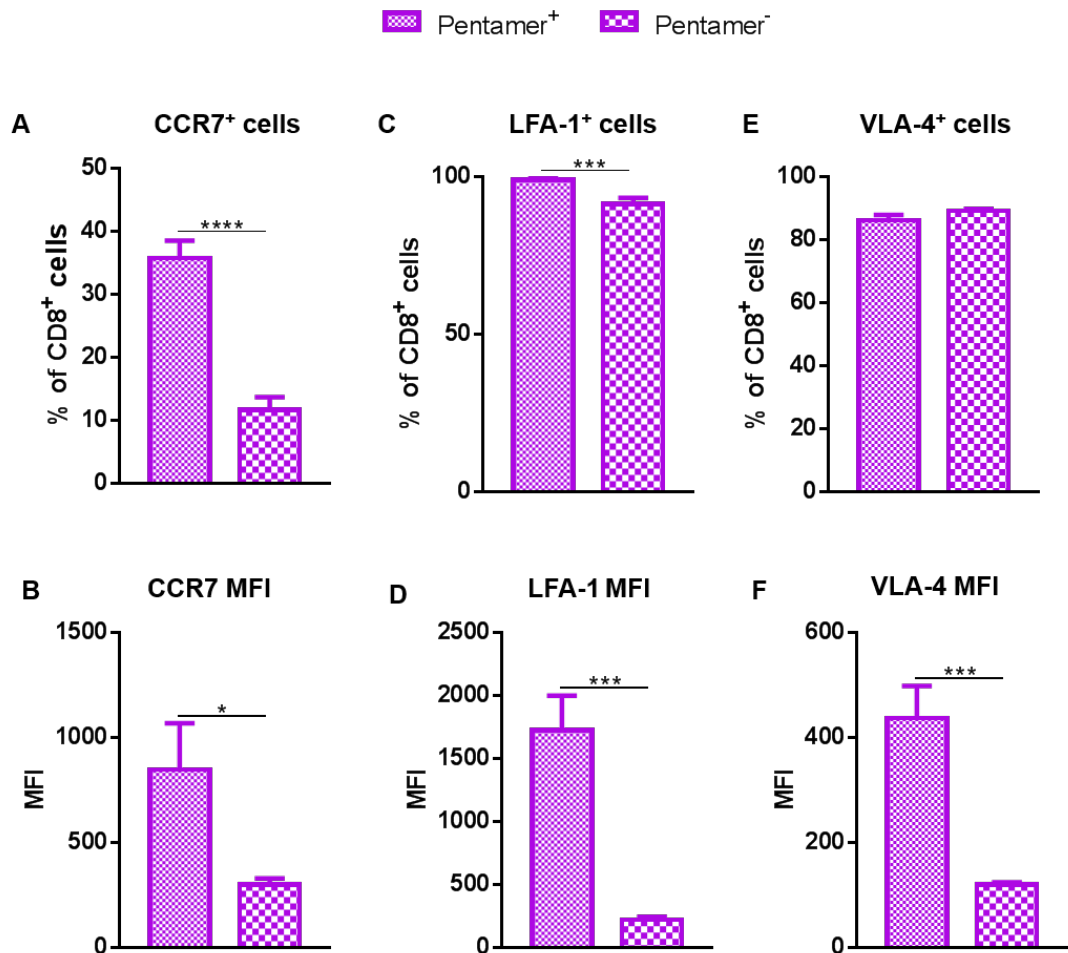


Figure 6.25 Comparison of ova-pentamer⁺ and ova-pentamer⁻ CD8⁺ T-cells for their expression of homing markers in mice bearing an intracranial and flank tumour receiving treatment

CD8⁺ T-cells were separated based their pentamer expression. **(A)** Percentage of CCR7⁺ cells within the pentamer⁺ and pentamer⁻ CD8⁺ T-cell population. **(B)** MFI for CCR7 in the pentamer⁺ and pentamer⁻ CD8⁺ T-cell population. **(C)** Percentage of LFA-1⁺ cells within the pentamer⁺ and pentamer⁻ CD8⁺ T-cell population. **(D)** MFI for LFA-1 in the pentamer⁺ and pentamer⁻ CD8⁺ T-cell population. **(E)** Percentage of VLA-4⁺ cells within the pentamer⁺ and pentamer⁻ CD8⁺ T-cell population. **(F)** MFI for VLA-4 in the pentamer⁺ and pentamer⁻ CD8⁺ T-cell population. (See appendix (page 238) for n numbers, number of independent experiments, statistical tests utilised and P values; error bars represent SEM).

reach a statistical significance (Figure 6.27C). There was a predisposition for the EC population to have an increased percentage of ICAM-1⁺ cells in the mice bearing an intracranial and flank tumour receiving treatment (Figure 6.27D). The expression levels of ICAM-1 also followed the same trend, with a statistically significant difference between the control and treatment group of mice with an intracranial and flank tumour (Figure 6.27E).

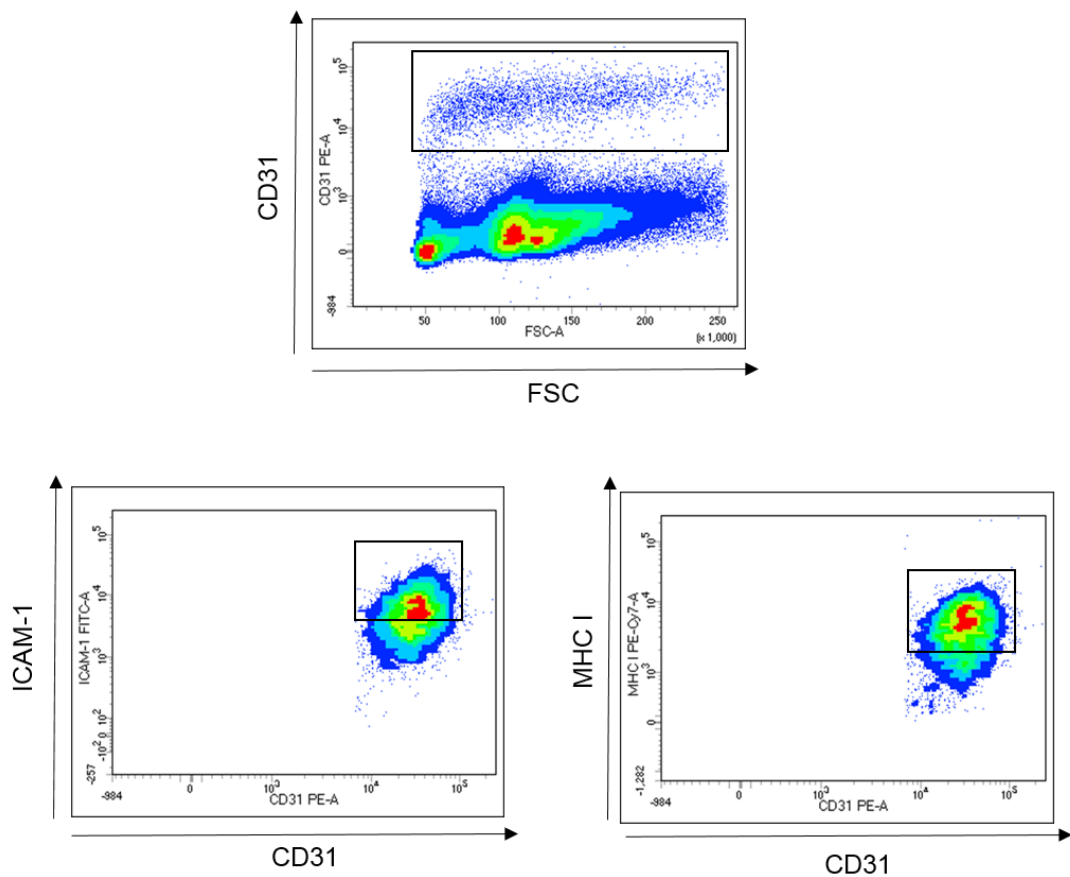


Figure 6.26 Representative plots for ECs and their expression of homing markers

(A) ECs collected from intracranial tumours were analysed by flow cytometry for their expression of: (B) MHC I and (C) ICAM-1.

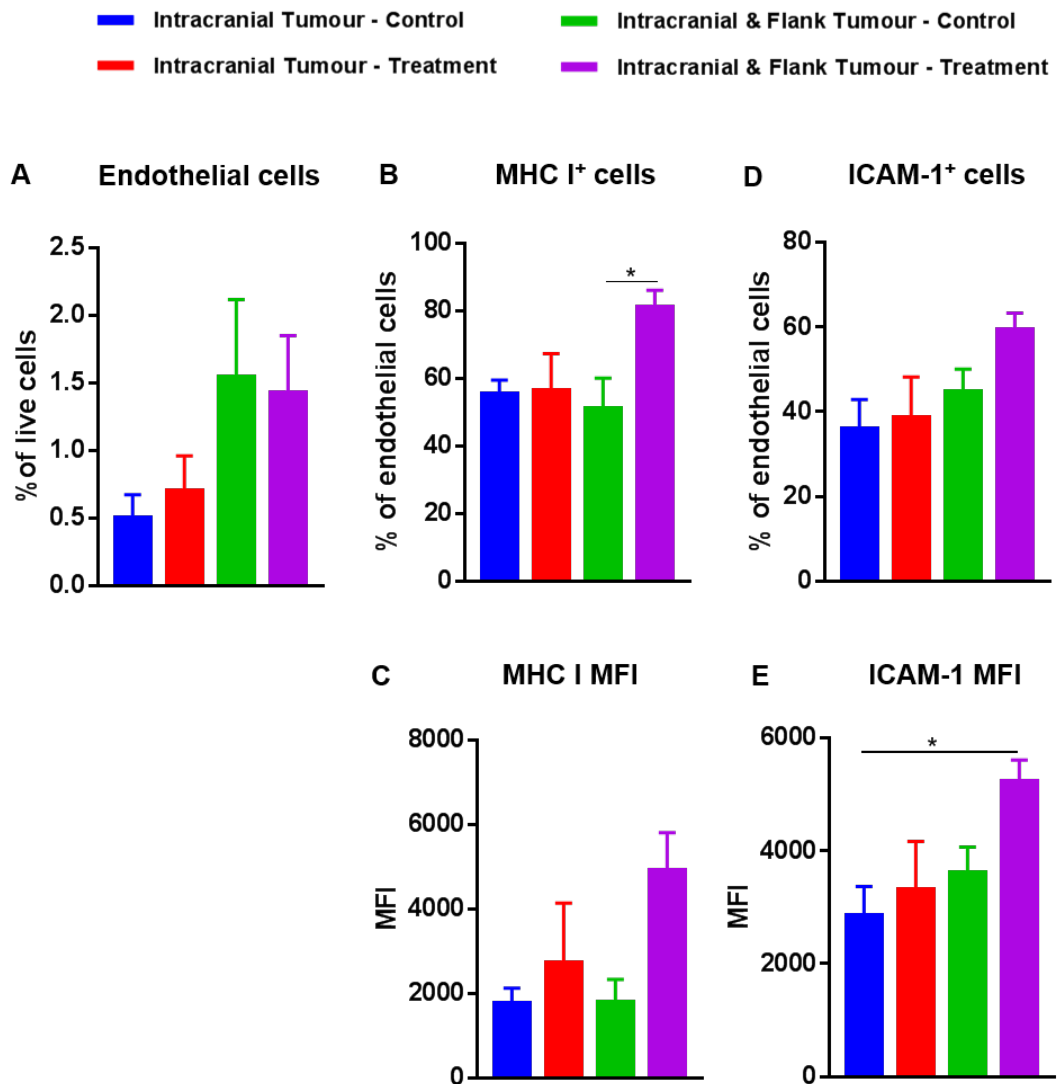


Figure 6.27 The effects of extracranial tumour and immune checkpoint therapy on the homing marker expression on ECs within the intracranial tumours of mice with B16-ova tumours

Intracranial tumours from mice with B16-ova tumours were collected and processed for flow cytometry analyses of: **(A)** CD31^{high} ECs. **(B)** Percentage of MHC I⁺ cells within the EC population. **(C)** MFI for MHC I in CD8⁺ T-cells. **(D)** Percentage of ICAM-1⁺ cells within the EC population. **(E)** MFI for ICAM-1 in CD8⁺ T-cells. (See appendix (pages 238-240) for n numbers, number of independent experiments, statistical tests utilised and P values; error bars represent SEM).

6.11 Discussion

In this chapter we aimed to investigate the effects of immune checkpoint therapy in the periphery. Moreover, we investigated whether the brain tumour vasculature is altered upon therapy. In our B16 MBrM model, there were no changes to the proportion of NK cells, CD8⁺ T-cells or CD4⁺ effector cells in the blood. There was, however, an increase in T-Regs in the circulation in response to treatment, thus suggesting that treatment induces T-Reg proliferation and/or survival. There is conflicting information about the role that CTLA-4 plays in T-Reg biology. It has been claimed that anti-CTLA-4 can deplete and/or inhibit T-Reg proliferation, while others have provided evidence that CTLA-4 blockade induces T-Reg proliferation^{374,375}. Likewise, a study investigating T-Regs in hepatitis C showed PD-L1 blockade resulted in an increase in Ki67⁺ T-Regs, suggesting the PD-1 pathway has an anti-proliferative function in T-Regs³⁷⁶.

Nevertheless, this analysis of the blood did not look at the total number of cells and this may have revealed changes between the different conditions. This would be difficult to achieve in a mouse model, however, as the same volume of blood would be needed from each mouse and this would be technically challenging. Additionally, analysis of cytokine levels in the plasma using a Luminex assay could potentially have revealed interesting changes within the blood. It has been shown in patients receiving anti-PD-1 plus anti-CTLA-4 to have elevated levels of IL-1 α and CCL10, an effect that appears to be synergistic when the inhibitors are administered in combination³⁷⁷.

Analysis of cells within the DCLNs did not reveal any changes in the immune cell populations, apart from an increase in PD-1 expression when treatment was administered. This increase could be a consequence of the treatment increasing CD8⁺ T-cell activation resulting in the upregulation of PD-1^{228,342}. While there were no changes in percentages within the major immune cell populations, a more detailed analysis of their phenotypic markers, such as their activation or inhibitory state, may have resulted in the identification of alterations between the groups. Moreover, it has been previously reported

that while changes in the TILs can be seen in the early stages of immune checkpoint therapy, equivalent changes in the draining lymph nodes are not as apparent³⁵³. This suggests such changes may not be evident in our model due to the short timeline studied. In addition, one population that was neglected from this analysis was DCs. Analysis of this population may have provided valuable information, as an influx in mature DCs would suggest an increase in antigen presentation, which, itself, would contribute to an increase in tumour specific CD8⁺ T-cells. Additionally, the decrease in CD4⁺ effector cells observed in the presence of an extracranial tumour would suggest an inhibitory role of the tumour on this population.

When the main populations of the spleens were investigated, similar trends were seen as those observed in the blood. As such, the only significant difference was an increase in T-Regs in response to the treatment, which is not surprising due to the increase in T-Regs in the circulation. While the examination of activation markers on the cells failed to reveal any changes between the groups, *ex vivo*-stimulation of these cells in mice receiving treatment indicated that these cells do have an anti-tumour phenotype. CD8⁺ T-cells in mice with a flank tumour tended to produce more IFN- γ , TNF- α and granzyme B in the B16 model. This would suggest an enhanced antigen-specific response occurring as a consequence of extracranial tumour being present. This also implies that the intracranial tumour is unable to elicit an antigen-specific response to the same degree as the extracranial tumour, which was again insinuated by the one of the IFN- γ ELISpot results. Nevertheless, this result would need to be replicated and it must be taken into consideration that the ELISpot takes the total splenocyte IFN- γ production into account. Furthermore, the ELISpot revealed that the B16 model is not the most appropriate model when investigating an anti-tumour response. The assay showed the melanoma-specific peptides gp100 and Trp2 were unable to elicit a detectable immune response and that B16 lysate itself was, in fact, inhibitory. The lack of an antigen-specific response is not a total surprise due to the B16 tumours being known as non-immunogenic²⁶⁸, emphasising the need for a more appropriate model.

The B16-ova model allowed for more opportunities to explore the mechanism behind the intracranial therapeutic effect that we saw only in the presence of an extracranial tumour. The lack of efficacy in mice with an intracranial tumour only receiving treatment with the B16-ova model would suggest that even in the presence of a strong antigen such as ova³⁶³, the intracranial tumour is not sufficient to elicit a strong anti-tumour immune response. This was confirmed with the increased presence of tumour-specific CD8⁺ T-cells in mice bearing an intracranial and flank tumour receiving treatment. Further analysis of these cells revealed that these cells have a phenotype associated with an anti-tumour response³⁷⁸. These cells had an increased expression of PD-1 which is associated with functional impairment³⁷⁸; however, PD-1 expression is also a marker of T-cell activation suggesting there was an overall increase in CD8⁺ T-cell activation.

While the ova antigen-specific T-cells found within the spleens of mice with an intracranial and flank tumour receiving treatment appeared to have a more exhausted phenotype due to their increased expression of TIM-3, EOMES and PD-1, this may not be a clear representation of their phenotype. It has been previously demonstrated that CD8⁺ T-cells expressing this exhausted phenotype have the potential to be reinvigorated to an activated phenotype²³¹. This phenotype is based on the expression of granzyme B and Ki67 which, in our studied cells, were also increased compared to the non-ova antigen-specific CD8⁺ T-cells. However, a definitive conclusion on this population of cells cannot be made, due to the rarity of the ova pentamer⁺ CD8⁺ T-cells, insufficient numbers were available for this type of detailed analysis.

Moreover, there were differences between the splenocyte responses in the B16 and B16-ova models. This may be a result of the differences between the cells themselves or it could be due to experimental variability. As discussed previously, further repetitions of the B16-ova experiments would be needed to know the exact reason.

The analysis of ECs within the tumour revealed a possible mechanism that could increase the homing of tumour-specific CD8⁺ T-cells to the intracranial tumour. Notably, these data are preliminary, as the experiment was only performed once and there was no opportunity for repetition due to time restraints. An increase in EC expression of MHC I and ICAM-1, combined with an increase in tumour-specific CD8⁺ T-cells expressing the ICAM-1 receptor, LFA-1, could lead to an increased interaction between these two cell types resulting in the increased homing of tumour-specific CD8⁺ T-cells into the brain. Likewise, an increase in VLA-4 expression on CD8⁺ T-cells could indicate an increase in intracranial infiltration; however, the expression of VCAM-1 on ECs would need to be examined³⁶⁸. Additionally, it has been shown that antigen-specific CD8⁺ T-cells are able to selectively traffic to the brain and cross the BBB. Moreover, this process is dependent on the MHC I presentation of the T-cell-specific antigen by the ECs interacting with TCRs, thus facilitating the extravasation of the antigen-specific CD8⁺ T-cells³⁷⁹. While these data could provide a potential mechanism behind the intracranial therapy with immune checkpoint inhibitors, further experiments would be needed to ensure that these results are not linked to one experiment and can be reproduced.

This chapter demonstrates that neither the flank tumour or treatment alters the percentage of immune cells in the blood, DCLNs and spleen. Nevertheless, the immune cells with the spleen were shown to have an increased percentage of cells expressing IFN- γ , TNF- α and Granzyme B upon *ex vivo* stimulation. We showed the same therapeutic effect was observed when B16-ova cells were used in the MBrM model and that the immune cells from the spleens of these mice increased their percentage of cells expressing IFN- γ , TNF- α and Granzyme B upon *ex vivo* stimulation in response to the treatment independent of flank tumour status. Moreover, in mice with an intracranial and flank tumour receiving the treatment, there was significant increase in the percentage of ova-pentamer⁺ CD8⁺ T-cells in the brain, blood and spleen. These cells also showed an increase in their expression of the T-cell homing receptors VLA-4, CCR7 and LFA-1. Likewise, with the intracranial tumour there was found to be an increase in

ECs and an increase in their expression of MHC I, indicating a possible T-cell homing mechanism behind the therapeutic response.

Chapter 7:

Conclusion

Chapter 7

BrM are one of the most devastating forms of cancer due to their extremely poor prognosis and the lack of effective treatment options. MBrM are becoming an increasing problem, with up to 75% of patients with melanoma-related deaths presenting with MBrM post-mortem^{3,19,26,28}. Historically, these patients were excluded from clinical trials due to their poor prognosis; however, these views are beginning to change as new treatment options, such as immunotherapies, are showing efficacy in the brain^{222,250,253,380}. This has resulted in a number of BrM-specific trials, including trials with immune checkpoint inhibitors^{219,220,222,250}.

The results detailed within this thesis further support the evidence that immune checkpoint therapy can have a therapeutic effect in MBrM. We demonstrated, for the first time, that the combination of anti-PD-1 and anti-CTLA-4 could prolong the survival of mice using a BrM model with B16 melanoma tumours. Moreover, we found that treatment was only effective in mice that had extracranial tumour burden in addition to their intracranial tumours. The addition of the adjuvant therapy, GM-CSF, offered no additional benefit to the anti-PD-1 plus anti-CTLA-4 therapy.

Functional analysis through immune cell-depletion studies revealed that CD8⁺ T-cells and NK cells were the mediators of the therapeutic effect, as their depletion resulted in the loss of the increase in survival gained by the treatment. The depletion of CD4⁺ T-cells had no effect on the survival of mice receiving treatment. While the results of the macrophage depletion studies were inconclusive, their role in the TME and the observed upregulation of MHC II in response to therapy and flank tumour could still warrant further investigation.

Flow cytometry analysis of the intracranial tumours revealed there was an increased influx of CD45⁺ cells in mice bearing intracranial and flank

tumours which received treatment. This increase was mainly caused through increased infiltration of CD3⁺ T-cells, along with an increase in macrophages and microglia. Despite their importance for therapeutic efficacy, there were no changes to the infiltration of NK cells. Likewise, the phenotypes of the infiltrating immune cells remained relatively unaltered in response to treatment and/or flank tumour. Thus, further investigations are required to identify mechanisms underlying the functional contribution of NK cells in the context of immune checkpoint therapy.

Analysis of the effects of treatment in the presence of a flank tumour on the immune cells in the periphery revealed some important changes. There was a trend for an increase in T-Regs in response to treatment, independent of the presence of an extracranial tumour. *Ex vivo*-stimulated splenocytes displayed a tendency towards an increased percentage of IFN- γ ⁺, TNF- α ⁺ and granzyme B⁺ T-cells in mice with intracranial and flank tumours in the B16 model, thus indicating these cells are more capable of eliciting an immune response.

The use of the B16-ova model allowed us to investigate antigen-specific immune responses. In our preliminary study, we observed an increase in ova-antigen-specific CD8⁺ T-cells in the intracranial tumour, spleen and blood of mice with intracranial and flank tumours receiving the treatment. Furthermore, these antigen-specific cells in the spleens had an increased expression of markers associated with activation and anti-tumour responses (Ki67 and granzyme B)²³¹ compared to their non-ova-antigen-specific counterparts. Analysis of the ova-antigen-specific CD8⁺ T-cells revealed an increased expression of T-cell homing markers (CCR7, LFA-1 and VLA-4)^{366,368,370,379} that have been associated with an increase in homing to tumours. This correlated with an increase in the expression of cell-surface markers linked with this process on ECs within intracranial tumours.

As such, the data presented in this thesis would suggest that the extracranial tumour is essential to generate an anti-tumour immune response in the brain. This is most likely a result of insufficient antigen presentation from the intracranial tumour. Additionally, the data would imply the therapeutic effect seen in the presence of a flank tumour and the immune checkpoint therapy is a consequence of enhanced activation and/or upregulation of homing receptors on tumour-specific CD8⁺ T-cells upregulating homing markers. This subsequently allows these to cross the BBB and infiltrate the tumour, where they can provoke an anti-tumour effect.

Furthermore, tumour-infiltrating cells within the intracranial tumour that were not investigated in this study could be addressed through depletion studies and flow cytometry analysis. As previously mentioned, macrophages and microglia should be investigated, alongside immune populations that have yet to be considered in this context: MDSCs, DCs and neutrophils. This work could also be supported with immunofluorescence staining to examine the distribution of immune cells within the TME to learn whether the immune cells are found throughout the tumour or only around the tumour border.

Exploring the functionality and the potential for an anti-tumour response within the tumour-infiltrating cell populations could possibly reveal interesting changes between the groups. This could be achieved by isolating the cells from the intracranial tumour, stimulating them and then looking for the production of IFN- γ , TNF- α and granzyme B. Gene expression analysis of the intracranial tumours would also provide vital information that would not be available through other means. In addition, it could possibly reveal other mechanisms/pathways behind the therapeutic effect that would otherwise not be considered. Likewise, due to the need for smaller amounts of tissue, comparisons between flank and intracranial tumours may be possible.

Additionally, the potential homing mechanism that was indicated in Chapter 6 would need further investigation. The experiment would first need to be

repeated to demonstrate reproducibility. The expression of molecules involved in T-cell homing could also be investigated through immunofluorescence co-staining for the respective T-cell entry receptor and the EC ligands. The expression of these homing markers could be investigated in a clinical setting on immune cells in the blood of patients before and after they receive immune checkpoint therapy.

The work presented here was carried out in a melanoma model, therefore, it would be interesting to test this therapy in other BrM tumours to determine if this effect is model specific. Additionally, the necessity for extracranial disease could be tested in a more immunogenic model to investigate whether therapeutic activity in the brain can be achieved in the absence of extracranial disease.

While our therapy prolonged the survival of some of the mice, there was still a number of mice in which the treatment was ineffective. Further research into adjuvant therapies would need to focus on therapies that make the tumour more immunogenic to enhance the immune checkpoint therapy. Nevertheless, the adjuvant therapy would need to be carefully selected so as to not increase toxicity already associated with immune checkpoint therapy²⁴⁶.

In conclusion, the data presented within this thesis provides evidence that immune checkpoint therapy can effectively treat MBrM. Therefore, these patients should not be excluded from this type of treatment based on their disease status, as they could still benefit from this therapy.

Appendix

8.1 List of suppliers

AgnTho's	AgnTho's AB, Agavägen 52, 181 55 Lidingö, Sweden
AID Diagnostika	Ebinger Strasse 4, D-72479 Strassberg, Germany
ATCC	LGC Standards, Queens Road, Teddington, Middlesex TW11 0LY, UK
Bayer	Bayer AG, 51368 Leverkusen, Germany
BD Biosciences	Edmund Halley Road, Oxford Science Park, OX4 4DQ Oxford, UK
Bio Rad	Bio-Rad House, Maxted Road, Hemel Hempstead, Hertfordshire HP2 7DX
Bio X Cell	10 Technology Drive, Suite 2B, West Lebanon, NH 03784-1671, USA
Biolegend	9727 Pacific Heights Blvd., San Siego, CA 92121, USA
Boehringer Ingelheim	Ellesfield Avenue, Bracknell, Berkshire, RG12 8YS, UK
Cedarlane	4410 Paletta Court, Burlington, Ontario, L7L 5R2, Canada
Charles River	Chesterford Research Park, Saffron Walden CB10 1XL, UK
Corning	Fogostraat 12, 1060 LJ Amsterdam, The Netherlands
Dechra	Snaygill Industrial Estate, Keighley Rd, Skipton BD23 2RW
eBiosciences	3rd Floor, 1 Ashley Road, Altrincham, Cheshire, WA14 2DT, UK
Fannin	Fannin House, South County Business Park, Leopardstown, Dublin, Ireland

Fine Science Tools	Fine Science Tools GmbH, Vangerowstraße 14, D-69115 Heidelberg, Germany
Gibco	Stafford House, 1 Boundary Park, Hemel Hempstead, HP2 7GE,
Graph Pad Software	7825 Fay Avenue, Suite 230, La Jolla, CA 92037 USA
Greiner Bio-one	Brunel Way, Stroudwater Business Park, Stonehouse, UK
Hamilton	Via Crusch 8, CH-7402 Bonaduz, GR, Switzerland
Harvard Apparatus	East Wing, Building 1020, Cambourne Business Park, Cambourne, Cambridge, CB23 6DW, UK
Hyclone	GE Healthcare Life Sciences, Amersham Place, Little Chalfont, Buckinghamshire, HP7 9NA, UK
Mabtech	Mabtech AB, Box 1233, SE-131 28, Nacka Strand, Sweden
Mahr	Mahr GmbH, Carl-Mahr-Str. 1, 37073 Göttingen, Germany
Merial	Merial Animal Research, Ash Rd, Woking GU24 0NQ, UK
Millipore	Suite 21, Building 6, Croxley Green Business Park, Watford, Hertfordshire, WD18 8YH, UK
Miltenyi	Almac House, Church Lane, Bisley, Surrey GU24 9DR, UK
Mölnlycke Health Care	Mölnlycke Health Care Ltd, The Arenson Centre, Arenson Way, Dunstable, Bedfordshire, LU5 5UL, UK
Omano	1222 McDowell Avenue, Roanoke, VA 24012, USA

PeproTech	PeproTech House, 29 Margravine Road, London W6 8LL, UK
Perkin Elmer	940 Winter Street, Waltham, Minneapolis, MN 55413, USA
Proimmune	Magdalen Centre, 1 Robert Robinson Ave, Oxford OX4 4GA, UK
Prometheus	9410 Carroll Park Drive, San Diego, CA 92121, USA
Regis	8210 Austin Ave, Morton Grove, IL 60053, USA
Roboz	Surgical Instrument Co., Inc., P.O. Box 10710, Gaithersburg, USA
Roche	Roche Diagnostics Limited, Charles Avenue, Burgess Hill, West Sussex, RH15 9RY, UK
Sanyo	Panasonic House, Willoughby Road, Bracknell, RG12 8FP, UK
Sigma-Aldrich	The Old Brickyard, New Rd, Gillingham SP8 4XT, UK
Terumo	3 Unity Grove, Knowsley, Prescot L34 9GT, UK
Thermo Fisher Scientific	Factory One/Ion Path/Road Three, Winsford CW7 3GA
Santa Cruz Animal Health	10410 Finnell Street, Dallas, Texas 75220, USA
Weber Scientific	2732 Kuser Road Hamilton, NJ 08691, USA
Zoetis	5th Floor, 6 St Andrew Street, London, EC4A 3AE UK

8.2 Statistical analyses tables

Figure 5.2A ANOVA with post hoc test No. of independent experiments = 3		Intracranial tumour		Intracranial & flank tumour	
		Control n = 13	Treatment n = 16	Control n = 19	Treatment n = 24
Intracranial tumour	Control		0.4876	> 0.9999	< 0.0001
	Treatment	0.4876		0.3959	0.0006
Intracranial & flank tumour	Control	> 0.9999	0.3959		< 0.0001
	Treatment	< 0.0001	0.0006	< 0.0001	

Figure 5.2B ANOVA with post hoc test No. of independent experiments = 3		Intracranial tumour		Intracranial & flank tumour	
		Control n = 14	Treatment n = 16	Control n = 17	Treatment n = 22
Intracranial tumour	Control		0.9596	0.8623	< 0.0001
	Treatment	0.9596		0.5461	0.0003
Intracranial & flank tumour	Control	0.8623	0.5461		< 0.0001
	Treatment	< 0.0001	0.0003	< 0.0001	

Figure 5.2C ANOVA with post hoc test No. of independent experiments = 3		Intracranial tumour		Intracranial & flank tumour	
		Control n = 14	Treatment n = 16	Control n = 17	Treatment n = 22
Intracranial tumour	Control		0.9359	0.9660	< 0.0001
	Treatment	0.9359		0.9992	< 0.0001
Intracranial & flank tumour	Control	0.9660	0.9992		< 0.0001
	Treatment	< 0.0001	< 0.0001	< 0.0001	

Figure 5.5A ANOVA with post hoc test No. of independent experiments = 3		Intracranial tumour		Intracranial & flank tumour	
		Control n = 14	Treatment n = 16	Control n = 17	Treatment n = 22
Intracranial tumour	Control		0.9942	0.9119	< 0.0001
	Treatment	0.9942		0.7669	< 0.0001
Intracranial & flank tumour	Control	0.9119	0.7669		< 0.0001
	Treatment	< 0.0001	< 0.0001	< 0.0001	

Figure 5.5B ANOVA with post hoc test No. of independent experiments = 3		Intracranial tumour		Intracranial & flank tumour	
		Control n = 14	Treatment n = 16	Control n = 17	Treatment n = 22
Intracranial tumour	Control		0.9423	0.7967	0.0130
	Treatment	0.9423		0.9834	0.0416
Intracranial & flank tumour	Control	0.7967	0.9834		0.0939
	Treatment	0.0130	0.0416	0.0939	

Figure 5.5C ANOVA with post hoc test No. of independent experiments = 3		Intracranial tumour		Intracranial & flank tumour	
		Control n = 14	Treatment n = 16	Control n = 17	Treatment n = 22
Intracranial tumour	Control		0.4879	0.3874	0.5524
	Treatment	0.4879		0.9985	0.9966
Intracranial & flank tumour	Control	0.3874	0.9985		0.9797
	Treatment	0.5524	0.9966	0.9797	

Figure 5.5D ANOVA with post hoc test No. of independent experiments = 3		Intracranial tumour		Intracranial & flank tumour	
		Control n = 14	Treatment n = 16	Control n = 17	Treatment n = 22
Intracranial tumour	Control		0.9756	0.8256	0.8783
	Treatment	0.9756		0.9554	0.9832
Intracranial & flank tumour	Control	0.8256	0.9554		0.9978
	Treatment	0.8783	0.9832	0.9978	

Figure 5.5E ANOVA with post hoc test No. of independent experiments = 3		Intracranial tumour		Intracranial & flank tumour	
		Control n = 14	Treatment n = 16	Control n = 17	Treatment n = 22
Intracranial tumour	Control		0.9993	0.9834	0.9999
	Treatment	0.9993		0.9536	0.9962
Intracranial & flank tumour	Control	0.9834	0.9536		0.9864
	Treatment	0.9999	0.9962	0.9864	

Figure 5.5F ANOVA with post hoc test No. of independent experiments = 3		Intracranial tumour		Intracranial & flank tumour	
		Control n = 14	Treatment n = 16	Control n = 17	Treatment n = 22
Intracranial tumour	Control		0.8742	0.9975	0.9969
	Treatment	0.8742		0.9217	0.9077
Intracranial & flank tumour	Control	0.9975	0.9217		> 0.9999
	Treatment	0.9969	0.9077	> 0.9999	

Figure 5.6A ANOVA with post hoc test No. of independent experiments = 2		Intracranial tumour		Intracranial & flank tumour	
		Control n = 7	Treatment n = 11	Control n = 11	Treatment n = 11
Intracranial tumour	Control		0.9967	0.9805	0.3249
	Treatment	0.9967		0.9972	0.3274
Intracranial & flank tumour	Control	0.9805	0.9972		0.4346
	Treatment	0.3249	0.3274	0.4346	

Figure 5.6B ANOVA with post hoc test No. of independent experiments = 2		Intracranial tumour		Intracranial & flank tumour	
		Control n = 7	Treatment n = 11	Control n = 11	Treatment n = 11
Intracranial tumour	Control		0.8114	0.9848	0.7966
	Treatment	0.8114		0.9293	> 0.9999
Intracranial & flank tumour	Control	0.9848	0.9293		0.9186
	Treatment	0.7966	> 0.9999	0.9186	

Figure 5.6C ANOVA with post hoc test No. of independent experiments = 2		Intracranial tumour		Intracranial & flank tumour	
		Control n = 7	Treatment n = 11	Control n = 11	Treatment n = 11
Intracranial tumour	Control		0.9885	0.9996	0.9995
	Treatment	0.9885		0.9947	0.9952
Intracranial & flank tumour	Control	0.9996	0.9947		> 0.9999
	Treatment	0.9995	0.9952	> 0.9999	

Figure 5.6D ANOVA with post hoc test No. of independent experiments = 2		Intracranial tumour		Intracranial & flank tumour	
		Control n = 7	Treatment n = 11	Control n = 11	Treatment n = 11
Intracranial tumour	Control		> 0.9999	0.9988	0.9458
	Treatment	> 0.9999		0.9996	0.9433
Intracranial & flank tumour	Control	0.9988	0.9996		0.9679
	Treatment	0.9458	0.9433	0.9679	

Figure 5.6E ANOVA with post hoc test No. of independent experiments = 2		Intracranial tumour		Intracranial & flank tumour	
		Control n = 7	Treatment n = 11	Control n = 11	Treatment n = 11
Intracranial tumour	Control		0.9967	0.9936	0.9960
	Treatment	0.9967		> 0.9999	> 0.9999
Intracranial & flank tumour	Control	0.9936	> 0.9999		> 0.9999
	Treatment	0.9960	> 0.9999	> 0.9999	

Figure 5.6F ANOVA with post hoc test No. of independent experiments = 2		Intracranial tumour		Intracranial & flank tumour	
		Control n = 7	Treatment n = 11	Control n = 11	Treatment n = 11
Intracranial tumour	Control		0.5313	0.3662	0.0756
	Treatment	0.5313		0.9881	0.5686
Intracranial & flank tumour	Control	0.3662	0.9881		0.7635
	Treatment	0.0756	0.5686	0.7635	

Figure 5.7A ANOVA with post hoc test No. of independent experiments = 2		Intracranial tumour		Intracranial & flank tumour	
		Control n = 7	Treatment n = 11	Control n = 11	Treatment n = 11
Intracranial tumour	Control		> 0.9999	0.9355	> 0.9999
	Treatment	> 0.9999		0.8854	> 0.9999
Intracranial & flank tumour	Control	0.9355	0.8854		0.9074
	Treatment	> 0.9999	> 0.9999	0.9074	

Figure 5.7B ANOVA with post hoc test No. of independent experiments = 2		Intracranial tumour		Intracranial & flank tumour	
		Control n = 7	Treatment n = 11	Control n = 11	Treatment n = 11
Intracranial tumour	Control		0.8979	0.9526	0.6186
	Treatment	0.8979		0.9973	0.9333
Intracranial & flank tumour	Control	0.9526	0.9973		0.8592
	Treatment	0.6186	0.9333	0.8592	

Figure 5.7C ANOVA with post hoc test No. of independent experiments = 2		Intracranial tumour		Intracranial & flank tumour	
		Control n = 8	Treatment n = 13	Control n = 12	Treatment n = 16
Intracranial tumour	Control		0.5032	0.0190	0.7537
	Treatment	0.5032		0.2390	0.9493
Intracranial & flank tumour	Control	0.0190	0.2390		0.0692
	Treatment	0.7537	0.9493	0.0692	

Figure 5.7D ANOVA with post hoc test No. of independent experiments = 2		Intracranial tumour		Intracranial & flank tumour	
		Control n = 8	Treatment n = 13	Control n = 12	Treatment n = 16
Intracranial tumour	Control		0.9843	0.3729	0.7799
	Treatment	0.9843		0.4710	0.9082
Intracranial & flank tumour	Control	0.3729	0.4710		0.8182
	Treatment	0.7799	0.9082	0.8182	

Figure 5.8A ANOVA with post hoc test No. of independent experiments = 2		Intracranial tumour		Intracranial & flank tumour	
		Control n = 9	Treatment n = 7	Control n = 11	Treatment n = 11
Intracranial tumour	Control		0.0063	> 0.9999	< 0.0001
	Treatment	0.0063		0.0058	0.7052
Intracranial & flank tumour	Control	> 0.9999	0.0058		< 0.0001
	Treatment	< 0.0001	0.7052	< 0.0001	

Figure 5.8B ANOVA with post hoc test No. of independent experiments = 2		Intracranial tumour		Intracranial & flank tumour	
		Control n = 9	Treatment n = 7	Control n = 11	Treatment n = 11
Intracranial tumour	Control		0.0521	0.9938	0.7262
	Treatment	0.0521		0.0900	0.2687
Intracranial & flank tumour	Control	0.9938	0.0900		0.8692
	Treatment	0.7262	0.2687	0.8692	

Figure 5.8C ANOVA with post hoc test No. of independent experiments = 2		Intracranial tumour		Intracranial & flank tumour	
		Control n = 9	Treatment n = 7	Control n = 11	Treatment n = 11
Intracranial tumour	Control		0.0138	0.9965	0.0015
	Treatment	0.0138		0.0162	0.9773
Intracranial & flank tumour	Control	0.9965	0.0162		0.0015
	Treatment	0.0015	0.9773	0.0015	

Figure 5.8D ANOVA with post hoc test No. of independent experiments = 2		Intracranial tumour		Intracranial & flank tumour	
		Control n = 9	Treatment n = 7	Control n = 11	Treatment n = 11
Intracranial tumour	Control		0.4147	0.9839	0.9969
	Treatment	0.4147		0.5744	0.4874
Intracranial & flank tumour	Control	0.9839	0.5744		0.9985
	Treatment	0.9969	0.4874	0.9985	

Figure 5.8E ANOVA with post hoc test No. of independent experiments = 2		Intracranial tumour		Intracranial & flank tumour	
		Control n = 9	Treatment n = 7	Control n = 11	Treatment n = 11
Intracranial tumour	Control		0.0136	0.9994	< 0.0001
	Treatment	0.0136		0.0072	0.4187
Intracranial & flank tumour	Control	0.9994	0.0072		< 0.0001
	Treatment	< 0.0001	0.4187	< 0.0001	

Figure 5.8F ANOVA with post hoc test No. of independent experiments = 2		Intracranial tumour		Intracranial & flank tumour	
		Control n = 9	Treatment n = 7	Control n = 11	Treatment n = 11
Intracranial tumour	Control		0.0099	0.8180	0.1042
	Treatment	0.0099		0.0510	0.5635
Intracranial & flank tumour	Control	0.8180	0.0510		0.4101
	Treatment	0.1042	0.5635	0.4101	

Figure 5.9A ANOVA with post hoc test No. of independent experiments = 2		Intracranial tumour		Intracranial & flank tumour	
		Control n = 9	Treatment n = 7	Control n = 11	Treatment n = 11
Intracranial tumour	Control		0.9809	0.5972	0.9927
	Treatment	0.9809		0.3932	0.9079
Intracranial & flank tumour	Control	0.5972	0.3932		0.7109
	Treatment	0.9927	0.9079	0.7109	

Figure 5.9B ANOVA with post hoc test No. of independent experiments = 2		Intracranial tumour		Intracranial & flank tumour	
		Control n = 9	Treatment n = 7	Control n = 11	Treatment n = 11
Intracranial tumour	Control		0.9992	0.9883	0.9886
	Treatment	0.9992		0.9979	> 0.9999
Intracranial & flank tumour	Control	0.9883	0.9979		0.9977
	Treatment	0.9886	> 0.9999	0.9977	

Figure 5.9C ANOVA with post hoc test No. of independent experiments = 2		Intracranial tumour		Intracranial & flank tumour	
		Control n = 9	Treatment n = 7	Control n = 11	Treatment n = 11
Intracranial tumour	Control		0.9961	0.9202	0.8333
	Treatment	0.9961		0.8443	0.7418
Intracranial & flank tumour	Control	0.9202	0.8443		0.9961
	Treatment	0.8333	0.7418	0.9961	

Figure 5.9D ANOVA with post hoc test No. of independent experiments = 2		Intracranial tumour		Intracranial & flank tumour	
		Control n = 9	Treatment n = 7	Control n = 11	Treatment n = 11
Intracranial tumour	Control		0.9702	0.9147	0.9762
	Treatment	0.9702		0.9990	0.9998
Intracranial & flank tumour	Control	0.9147	0.9990		0.9942
	Treatment	0.9762	0.9998	0.9942	

Figure 5.9E ANOVA with post hoc test No. of independent experiments = 2		Intracranial tumour		Intracranial & flank tumour	
		Control n = 9	Treatment n = 7	Control n = 11	Treatment n = 11
Intracranial tumour	Control		0.9683	0.9664	0.7943
	Treatment	0.9683		> 0.9999	0.9808
Intracranial & flank tumour	Control	0.9664	> 0.9999		0.9628
	Treatment	0.7943	0.9808	0.9628	

Figure 5.9F ANOVA with post hoc test No. of independent experiments = 2		Intracranial tumour		Intracranial & flank tumour	
		Control n = 9	Treatment n = 7	Control n = 11	Treatment n = 11
Intracranial tumour	Control		0.9596	0.9999	0.9875
	Treatment	0.9596		0.9413	0.9968
Intracranial & flank tumour	Control	0.9999	0.9413		0.9769
	Treatment	0.9875	0.9968	0.9769	

Figure 5.10A ANOVA with post hoc test No. of independent experiments = 2		Intracranial tumour		Intracranial & flank tumour	
		Control n = 9	Treatment n = 7	Control n = 11	Treatment n = 11
Intracranial tumour	Control		0.4773	0.9991	0.8391
	Treatment	0.4773		0.4038	0.8799
Intracranial & flank tumour	Control	0.9991	0.4038		0.7645
	Treatment	0.8391	0.8799	0.7645	

Figure 5.10B ANOVA with post hoc test No. of independent experiments = 2		Intracranial tumour		Intracranial & flank tumour	
		Control n = 9	Treatment n = 7	Control n = 11	Treatment n = 11
Intracranial tumour	Control		0.9992	0.9515	0.9766
	Treatment	0.9992		0.9846	0.9543
Intracranial & flank tumour	Control	0.9515	0.9846		0.7572
	Treatment	0.9766	0.9543	0.7572	

Figure 5.11A ANOVA with post hoc test No. of independent experiments = 3		Intracranial tumour		Intracranial & flank tumour	
		Control n = 13	Treatment n = 16	Control n = 19	Treatment n = 24
Intracranial tumour	Control		0.9965	0.9991	0.9199
	Treatment	0.9965		0.9822	0.9748
Intracranial & flank tumour	Control	0.9991	0.9822		0.8203
	Treatment	0.9199	0.9748	0.8203	

Figure 5.11B ANOVA with post hoc test No. of independent experiments = 3		Intracranial tumour		Intracranial & flank tumour	
		Control n = 13	Treatment n = 16	Control n = 19	Treatment n = 24
Intracranial tumour	Control		0.6632	0.9974	0.0493
	Treatment	0.6632		0.4687	0.4766
Intracranial & flank tumour	Control	0.9974	0.4687		0.0114
	Treatment	0.0493	0.4766	0.0114	

Figure 5.11C ANOVA with post hoc test No. of independent experiments = 3		Intracranial tumour		Intracranial & flank tumour	
		Control n = 13	Treatment n = 16	Control n = 19	Treatment n = 24
Intracranial tumour	Control		0.9981	0.9932	0.4732
	Treatment	0.9981		0.9998	0.3221
Intracranial & flank tumour	Control	0.9932	0.9998		0.2213
	Treatment	0.4732	0.3221	0.2213	

Figure 5.11D ANOVA with post hoc test No. of independent experiments = 3		Intracranial tumour		Intracranial & flank tumour	
		Control n = 13	Treatment n = 16	Control n = 19	Treatment n = 24
Intracranial tumour	Control		0.9994	0.9183	0.9876
	Treatment	0.9994		0.8547	0.9629
Intracranial & flank tumour	Control	0.9183	0.8547		0.9808
	Treatment	0.9876	0.9629	0.9808	

Figure 5.11E ANOVA with post hoc test No. of independent experiments = 3		Intracranial tumour		Intracranial & flank tumour	
		Control n = 13	Treatment n = 16	Control n = 19	Treatment n = 24
Intracranial tumour	Control		0.5903	0.9981	0.4783
	Treatment	0.5903		0.6278	0.0215
Intracranial & flank tumour	Control	0.9981	0.6278		0.2724
	Treatment	0.4783	0.0215	0.2724	

Figure 5.11F ANOVA with post hoc test No. of independent experiments = 3		Intracranial tumour		Intracranial & flank tumour	
		Control n = 13	Treatment n = 16	Control n = 19	Treatment n = 24
Intracranial tumour	Control		0.8996	0.9721	0.5263
	Treatment	0.8996		0.9900	0.9222
Intracranial & flank tumour	Control	0.9721	0.9900		0.7391
	Treatment	0.5263	0.9222	0.7391	

Figure 5.13A ANOVA with post hoc test No. of independent experiments = 3		Intracranial tumour		Intracranial & flank tumour	
		Control n = 13	Treatment n = 16	Control n = 19	Treatment n = 24
Intracranial tumour	Control		0.8177	0.8331	0.0058
	Treatment	0.8177		0.9999	0.0500
Intracranial & flank tumour	Control	0.8331	0.9999		0.0294
	Treatment	0.0058	0.0500	0.0294	

Figure 5.13B ANOVA with post hoc test No. of independent experiments = 3		Intracranial tumour		Intracranial & flank tumour	
		Control n = 13	Treatment n = 16	Control n = 19	Treatment n = 24
Intracranial tumour	Control		0.9982	0.9929	0.7603
	Treatment	0.9982		0.9996	0.6004
Intracranial & flank tumour	Control	0.9929	0.9996		0.4912
	Treatment	0.7603	0.6004	0.4912	

Figure 5.13C ANOVA with post hoc test No. of independent experiments = 3		Intracranial tumour		Intracranial & flank tumour	
		Control n = 13	Treatment n = 16	Control n = 19	Treatment n = 24
Intracranial tumour	Control		0.4072	0.1627	< 0.0001
	Treatment	0.4072		0.9560	0.0010
Intracranial & flank tumour	Control	0.1627	0.9560		0.0032
	Treatment	< 0.0001	0.0010	0.0032	

Figure 5.13D ANOVA with post hoc test No. of independent experiments = 3		Intracranial tumour		Intracranial & flank tumour	
		Control n = 13	Treatment n = 16	Control n = 19	Treatment n = 24
Intracranial tumour	Control		0.5635	0.7740	0.1424
	Treatment	0.5635		0.9738	0.8517
Intracranial & flank tumour	Control	0.7740	0.9738		0.5552
	Treatment	0.1424	0.8517	0.5552	

Figure 5.13E ANOVA with post hoc test No. of independent experiments = 3		Intracranial tumour		Intracranial & flank tumour	
		Control n = 13	Treatment n = 16	Control n = 19	Treatment n = 24
Intracranial tumour	Control		0.5624	0.8028	0.0533
	Treatment	0.5624		0.9602	0.5153
Intracranial & flank tumour	Control	0.8028	0.9602		0.2097
	Treatment	0.0533	0.5153	0.2097	

Figure 5.15A ANOVA with post hoc test No. of independent experiments = 3		Intracranial tumour		Intracranial & flank tumour	
		Control n = 13	Treatment n = 16	Control n = 19	Treatment n = 24
Intracranial tumour	Control		0.3259	0.9997	0.0029
	Treatment	0.3259		0.2898	0.2367
Intracranial & flank tumour	Control	0.9997	0.2898		0.0010
	Treatment	0.0029	0.2367	0.0010	

Figure 5.15B ANOVA with post hoc test No. of independent experiments = 3		Intracranial tumour		Intracranial & flank tumour	
		Control n = 13	Treatment n = 16	Control n = 19	Treatment n = 24
Intracranial tumour	Control		0.4911	0.8931	0.2282
	Treatment	0.4911		0.8491	0.9766
Intracranial & flank tumour	Control	0.8931	0.2282		0.5504
	Treatment	0.8491	0.9766	0.5504	

Figure 5.15C ANOVA with post hoc test No. of independent experiments = 3		Intracranial tumour		Intracranial & flank tumour	
		Control n = 13	Treatment n = 16	Control n = 19	Treatment n = 24
Intracranial tumour	Control		0.0319	0.8412	0.0088
	Treatment	0.0319		0.1291	0.9949
Intracranial & flank tumour	Control	0.8412	0.1291		0.0419
	Treatment	0.0088	0.9949	0.0419	

Figure 5.15D ANOVA with post hoc test No. of independent experiments = 3		Intracranial tumour		Intracranial & flank tumour	
		Control n = 13	Treatment n = 16	Control n = 19	Treatment n = 24
Intracranial tumour	Control		0.8061	0.5552	0.8262
	Treatment	0.8061		0.9766	0.9993
Intracranial & flank tumour	Control	0.5552	0.9766		0.9373
	Treatment	0.8262	0.9993	0.9373	

Figure 5.15E ANOVA with post hoc test No. of independent experiments = 3		Intracranial tumour		Intracranial & flank tumour	
		Control n = 13	Treatment n = 16	Control n = 19	Treatment n = 24
Intracranial tumour	Control		0.9877	0.8861	0.9975
	Treatment	0.9877		0.6713	0.9368
Intracranial & flank tumour	Control	0.8861	0.6713		0.9194
	Treatment	0.9975	0.9368	0.9194	

Figure 6.1A ANOVA with post hoc test No. of independent experiments = 3		Intracranial tumour		Intracranial & flank tumour	
		Control n = 23	Treatment n = 24	Control n = 24	Treatment n = 38
Intracranial tumour	Control		0.8772	0.9996	0.3816
	Treatment	0.8772		0.9152	0.8605
Intracranial & flank tumour	Control	0.9996	0.9152		0.4373
	Treatment	0.3816	0.8605	0.4373	

Figure 6.1B ANOVA with post hoc test No. of independent experiments = 3		Intracranial tumour		Intracranial & flank tumour	
		Control n = 23	Treatment n = 24	Control n = 24	Treatment n = 38
Intracranial tumour	Control		0.8874	0.8507	0.9996
	Treatment	0.8874		0.4129	0.7953
Intracranial & flank tumour	Control	0.8507	0.4129		0.8562
	Treatment	0.9996	0.7953	0.8562	

Figure 6.1C ANOVA with post hoc test No. of independent experiments = 3		Intracranial tumour		Intracranial & flank tumour	
		Control n = 23	Treatment n = 24	Control n = 24	Treatment n = 38
Intracranial tumour	Control		0.3961	0.6021	0.2214
	Treatment	0.3961		0.2673	0.9975
Intracranial & flank tumour	Control	0.6021	0.2673		0.0662
	Treatment	0.2214	0.9975	0.0662	

Figure 6.1D ANOVA with post hoc test No. of independent experiments = 3		Intracranial tumour		Intracranial & flank tumour	
		Control n = 23	Treatment n = 24	Control n = 24	Treatment n = 38
Intracranial tumour	Control		0.9414	0.4187	0.8815
	Treatment	0.9414		0.1507	0.5124
Intracranial & flank tumour	Control	0.4187	0.1507		0.7648
	Treatment	0.8815	0.5124	0.7648	

Figure 6.1E ANOVA with post hoc test No. of independent experiments = 3		Intracranial tumour		Intracranial & flank tumour	
		Control n = 23	Treatment n = 24	Control n = 24	Treatment n = 38
Intracranial tumour	Control		0.0065	0.0633	< 0.0001
	Treatment	0.0065		0.8438	0.1631
Intracranial & flank tumour	Control	0.0633	0.8438		0.0175
	Treatment	< 0.0001	0.1631	0.0175	

Figure 6.1F ANOVA with post hoc test No. of independent experiments = 3		Intracranial tumour		Intracranial & flank tumour	
		Control n = 15	Treatment n = 15	Control n = 15	Treatment n = 25
Intracranial tumour	Control		0.6958	0.2158	0.1883
	Treatment	0.6958		0.8244	0.8443
Intracranial & flank tumour	Control	0.2158	0.8244		0.9992
	Treatment	0.1883	0.8443	0.9992	

Figure 6.1G ANOVA with post hoc test No. of independent experiments = 3		Intracranial tumour		Intracranial & flank tumour	
		Control n = 15	Treatment n = 15	Control n = 15	Treatment n = 25
Intracranial tumour	Control		0.0291	0.6700	0.0002
	Treatment	0.0291		0.3288	0.6155
Intracranial & flank tumour	Control	0.6700	0.3288		0.0136
	Treatment	0.0002	0.6155	0.0136	

Figure 6.2A ANOVA with post hoc test No. of independent experiments = 1		Intracranial tumour		Intracranial & flank tumour	
		Control n = 4	Treatment n = 4	Control n = 4	Treatment n = 12
Intracranial tumour	Control		0.7077	0.7661	0.6177
	Treatment	0.7077		0.9996	0.9997
Intracranial & flank tumour	Control	0.7661	0.9996		> 0.9999
	Treatment	0.6177	0.9997	> 0.9999	

Figure 6.2B ANOVA with post hoc test No. of independent experiments = 1		Intracranial tumour		Intracranial & flank tumour	
		Control n = 4	Treatment n = 4	Control n = 4	Treatment n = 12
Intracranial tumour	Control		0.4465	0.5231	0.0627
	Treatment	0.4465		0.9991	0.8398
Intracranial & flank tumour	Control	0.5231	0.9991		0.7556
	Treatment	0.0627	0.8398	0.7556	

Figure 6.2C ANOVA with post hoc test No. of independent experiments = 1		Intracranial tumour		Intracranial & flank tumour	
		Control n = 4	Treatment n = 4	Control n = 4	Treatment n = 12
Intracranial tumour	Control		0.9637	0.8507	0.5474
	Treatment	0.9637		0.9871	0.8707
Intracranial & flank tumour	Control	0.8507	0.9871		0.9841
	Treatment	0.5474	0.8707	0.9841	

Figure 6.2D ANOVA with post hoc test No. of independent experiments = 1		Intracranial tumour		Intracranial & flank tumour	
		Control n = 4	Treatment n = 4	Control n = 4	Treatment n = 12
Intracranial tumour	Control		0.0875	0.4570	0.2775
	Treatment	0.0875		0.0035	0.6182
Intracranial & flank tumour	Control	0.4570	0.0035		0.0073
	Treatment	0.2775	0.6182	0.0073	

Figure 6.2E ANOVA with post hoc test No. of independent experiments = 1		Intracranial tumour		Intracranial & flank tumour	
		Control n = 4	Treatment n = 4	Control n = 4	Treatment n = 12
Intracranial tumour	Control		0.8854	0.0877	0.7380
	Treatment	0.8854		0.3069	0.9991
Intracranial & flank tumour	Control	0.0877	0.3069		0.2006
	Treatment	0.7380	0.9991	0.2006	

Figure 6.2F ANOVA with post hoc test No. of independent experiments = 1		Intracranial tumour		Intracranial & flank tumour	
		Control n = 4	Treatment n = 4	Control n = 4	Treatment n = 12
Intracranial tumour	Control		0.1300	0.0037	0.0927
	Treatment	0.1300		0.3555	0.9863
Intracranial & flank tumour	Control	0.0037	0.3555		0.1083
	Treatment	0.0927	0.9863	0.1083	

Figure 6.2G ANOVA with post hoc test No. of independent experiments = 1		Intracranial tumour		Intracranial & flank tumour	
		Control n = 4	Treatment n = 4	Control n = 4	Treatment n = 12
Intracranial tumour	Control		0.8156	0.9997	0.9014
	Treatment	0.8156		0.7673	0.9809
Intracranial & flank tumour	Control	0.9997	0.7673		0.8551
	Treatment	0.9014	0.9809	0.8551	

Figure 6.3A ANOVA with post hoc test No. of independent experiments = 2		Intracranial tumour		Intracranial & flank tumour	
		Control n = 15	Treatment n = 16	Control n = 13	Treatment n = 26
Intracranial tumour	Control		0.0140	0.9939	0.3367
	Treatment	0.0140		0.0051	0.3152
Intracranial & flank tumour	Control	0.9939	0.0051		0.1888
	Treatment	0.3367	0.3152	0.1888	

Figure 6.3B ANOVA with post hoc test No. of independent experiments = 2		Intracranial tumour		Intracranial & flank tumour	
		Control n = 15	Treatment n = 16	Control n = 13	Treatment n = 26
Intracranial tumour	Control		0.3501	0.9992	0.1144
	Treatment	0.3501		0.4266	0.4977
Intracranial & flank tumour	Control	0.9992	0.4266		0.1751
	Treatment	0.1144	0.4977	0.1751	

Figure 6.3C ANOVA with post hoc test No. of independent experiments = 2		Intracranial tumour		Intracranial & flank tumour	
		Control n = 15	Treatment n = 16	Control n = 13	Treatment n = 26
Intracranial tumour	Control		0.2552	0.2208	0.3787
	Treatment	0.2552		0.0015	0.9501
Intracranial & flank tumour	Control	0.2208	0.0015		0.0010
	Treatment	0.3787	0.9501	0.0010	

Figure 6.3D ANOVA with post hoc test No. of independent experiments = 2		Intracranial tumour		Intracranial & flank tumour	
		Control n = 15	Treatment n = 16	Control n = 13	Treatment n = 26
Intracranial tumour	Control		0.3524	0.8662	> 0.9999
	Treatment	0.3524		0.8242	0.2446
Intracranial & flank tumour	Control	0.8662	0.8242		0.8281
	Treatment	> 0.9999	0.2446	0.8281	

Figure 6.3E ANOVA with post hoc test No. of independent experiments = 2		Intracranial tumour		Intracranial & flank tumour	
		Control n = 15	Treatment n = 16	Control n = 13	Treatment n = 26
Intracranial tumour	Control		0.8823	0.3875	0.9941
	Treatment	0.8823		0.7979	0.6825
Intracranial & flank tumour	Control	0.3875	0.7979		0.1719
	Treatment	0.9941	0.6825	0.1719	

Figure 6.3F ANOVA with post hoc test No. of independent experiments = 2		Intracranial tumour		Intracranial & flank tumour	
		Control n = 15	Treatment n = 16	Control n = 13	Treatment n = 26
Intracranial tumour	Control		0.5113	0.6536	> 0.9999
	Treatment	0.5113		0.9976	0.4154
Intracranial & flank tumour	Control	0.6536	0.9976		0.5823
	Treatment	> 0.9999	0.4154	0.5823	

Figure 6.4A ANOVA with post hoc test No. of independent experiments = 2		Intracranial tumour		Intracranial & flank tumour	
		Control n = 15	Treatment n = 16	Control n = 13	Treatment n = 26
Intracranial tumour	Control		0.0448	0.0738	0.0332
	Treatment	0.0448		< 0.0001	0.9983
Intracranial & flank tumour	Control	0.0738	< 0.0001		< 0.0001
	Treatment	0.0332	0.9983	< 0.0001	

Figure 6.4B ANOVA with post hoc test No. of independent experiments = 2		Intracranial tumour		Intracranial & flank tumour	
		Control n = 15	Treatment n = 16	Control n = 13	Treatment n = 26
Intracranial tumour	Control		0.7370	> 0.9999	0.6649
	Treatment	0.7370		0.7678	> 0.9999
Intracranial & flank tumour	Control	> 0.9999	0.7678		0.7013
	Treatment	0.6649	> 0.9999	0.7013	

Figure 6.4C ANOVA with post hoc test No. of independent experiments = 2		Intracranial tumour		Intracranial & flank tumour	
		Control n = 15	Treatment n = 16	Control n = 13	Treatment n = 26
Intracranial tumour	Control		0.0632	0.8975	0.1206
	Treatment	0.0632		0.2743	0.9398
Intracranial & flank tumour	Control	0.8975	0.2743		0.4706
	Treatment	0.1206	0.9398	0.4706	

Figure 6.4D ANOVA with post hoc test No. of independent experiments = 2		Intracranial tumour		Intracranial & flank tumour	
		Control n = 15	Treatment n = 16	Control n = 13	Treatment n = 26
Intracranial tumour	Control		0.1420	0.1179	0.2824
	Treatment	0.1420		0.9984	0.9245
Intracranial & flank tumour	Control	0.1179	0.9984		0.8644
	Treatment	0.2824	0.9245	0.8644	

Figure 6.4E ANOVA with post hoc test No. of independent experiments = 2		Intracranial tumour		Intracranial & flank tumour	
		Control n = 15	Treatment n = 16	Control n = 13	Treatment n = 26
Intracranial tumour	Control		0.8857	> 0.9999	0.7729
	Treatment	0.8857		0.8709	0.9985
Intracranial & flank tumour	Control	> 0.9999	0.8709		0.7510
	Treatment	0.7729	0.9985	0.7510	

Figure 6.4F ANOVA with post hoc test No. of independent experiments = 2		Intracranial tumour		Intracranial & flank tumour	
		Control n = 15	Treatment n = 16	Control n = 13	Treatment n = 26
Intracranial tumour	Control		0.2037	0.9991	0.3449
	Treatment	0.2037		0.2617	0.9489
Intracranial & flank tumour	Control	0.9991	0.2617		0.4316
	Treatment	0.3449	0.9489	0.4316	

Figure 6.4G ANOVA with post hoc test No. of independent experiments = 2		Intracranial tumour		Intracranial & flank tumour	
		Control n = 15	Treatment n = 16	Control n = 13	Treatment n = 26
Intracranial tumour	Control		< 0.0001	0.1622	< 0.0001
	Treatment	< 0.0001		0.0181	0.9149
Intracranial & flank tumour	Control	0.1622	0.0181		0.0279
	Treatment	< 0.0001	0.9149	0.0279	

Figure 6.4H ANOVA with post hoc test No. of independent experiments = 2		Intracranial tumour		Intracranial & flank tumour	
		Control n = 15	Treatment n = 16	Control n = 13	Treatment n = 26
Intracranial tumour	Control		0.9781	0.7784	0.9997
	Treatment	0.9781		0.9377	0.9438
Intracranial & flank tumour	Control	0.7784	0.9377		0.6439
	Treatment	0.9997	0.9438	0.6439	

Figure 6.4I ANOVA with post hoc test No. of independent experiments = 2		Intracranial tumour		Intracranial & flank tumour	
		Control n = 15	Treatment n = 16	Control n = 13	Treatment n = 26
Intracranial tumour	Control		0.8848	0.5436	0.8496
	Treatment	0.8848		0.1607	> 0.9999
Intracranial & flank tumour	Control	0.5436	0.1607		0.1009
	Treatment	0.8496	> 0.9999	0.1009	

Figure 6.5A ANOVA with post hoc test No. of independent experiments = 2		Intracranial tumour		Intracranial & flank tumour	
		Control n = 15	Treatment n = 16	Control n = 13	Treatment n = 26
Intracranial tumour	Control		0.9991	0.9942	0.6150
	Treatment	0.9991		0.9993	0.4868
Intracranial & flank tumour	Control	0.9942	0.9993		0.4059
	Treatment	0.6150	0.4868	0.4059	

Figure 6.5B ANOVA with post hoc test No. of independent experiments = 2		Intracranial tumour		Intracranial & flank tumour	
		Control n = 15	Treatment n = 16	Control n = 13	Treatment n = 26
Intracranial tumour	Control		0.6701	0.8645	0.4209
	Treatment	0.6701		0.9850	0.9898
Intracranial & flank tumour	Control	0.8645	0.9850		0.9014
	Treatment	0.4209	0.9898	0.9014	

Figure 6.5C ANOVA with post hoc test No. of independent experiments = 2		Intracranial tumour		Intracranial & flank tumour	
		Control n = 15	Treatment n = 16	Control n = 13	Treatment n = 26
Intracranial tumour	Control		0.9654	0.9975	0.9854
	Treatment	0.9654		0.9922	0.8052
Intracranial & flank tumour	Control	0.9975	0.9922		0.9401
	Treatment	0.9854	0.8052	0.9401	

Figure 6.7A ANOVA with post hoc test No. of independent experiments = 3		Intracranial tumour		Intracranial & flank tumour	
		Control n = 18	Treatment n = 21	Control n = 21	Treatment n = 36
Intracranial tumour	Control		0.8992	0.4852	0.0667
	Treatment	0.8992		0.8702	0.2726
Intracranial & flank tumour	Control	0.4852	0.8702		0.7742
	Treatment	0.0667	0.2726	0.7742	

Figure 6.7B ANOVA with post hoc test No. of independent experiments = 3		Intracranial tumour		Intracranial & flank tumour	
		Control n = 18	Treatment n = 21	Control n = 21	Treatment n = 36
Intracranial tumour	Control		0.9618	0.1806	0.0179
	Treatment	0.9618		0.3634	0.0495
Intracranial & flank tumour	Control	0.1806	0.3634		0.8680
	Treatment	0.0179	0.0495	0.8680	

Figure 6.7C ANOVA with post hoc test No. of independent experiments = 1		Intracranial tumour		Intracranial & flank tumour	
		Control n = 6	Treatment n = 7	Control n = 7	Treatment n = 12
Intracranial tumour	Control		0.9524	0.3936	0.0941
	Treatment	0.9524		0.1441	0.0182
Intracranial & flank tumour	Control	0.3936	0.1441		0.9031
	Treatment	0.0941	0.0182	0.9031	

Figure 6.7D ANOVA with post hoc test No. of independent experiments = 3		Intracranial tumour		Intracranial & flank tumour	
		Control n = 18	Treatment n = 21	Control n = 21	Treatment n = 36
Intracranial tumour	Control		0.9988	0.9959	0.8059
	Treatment	0.9988		0.9793	0.8619
Intracranial & flank tumour	Control	0.9959	0.9793		0.6217
	Treatment	0.8059	0.8619	0.6217	

Figure 6.7E ANOVA with post hoc test No. of independent experiments = 3		Intracranial tumour		Intracranial & flank tumour	
		Control n = 18	Treatment n = 21	Control n = 21	Treatment n = 36
Intracranial tumour	Control		0.9960	0.9991	0.6779
	Treatment	0.9960		0.9819	0.7883
Intracranial & flank tumour	Control	0.9991	0.9819		0.5424
	Treatment	0.6779	0.7883	0.5424	

Figure 6.7F ANOVA with post hoc test No. of independent experiments = 1		Intracranial tumour		Intracranial & flank tumour	
		Control n = 6	Treatment n = 7	Control n = 7	Treatment n = 12
Intracranial tumour	Control		0.9509	0.1392	0.2222
	Treatment	0.9509		0.0361	0.0540
Intracranial & flank tumour	Control	0.1392	0.0361		0.9491
	Treatment	0.2222	0.0540	0.9491	

Figure 6.8A ANOVA with post hoc test No. of independent experiments = 3		Intracranial tumour		Intracranial & flank tumour	
		Control n = 18	Treatment n = 21	Control n = 21	Treatment n = 36
Intracranial tumour	Control		0.5579	0.9480	0.0319
	Treatment	0.5579		0.8571	0.4844
Intracranial & flank tumour	Control	0.9480	0.8571		0.1066
	Treatment	0.0319	0.4844	0.1066	

Figure 6.8B ANOVA with post hoc test No. of independent experiments = 3		Intracranial tumour		Intracranial & flank tumour	
		Control n = 18	Treatment n = 21	Control n = 21	Treatment n = 36
Intracranial tumour	Control		0.9757	0.9990	0.9954
	Treatment	0.9757		0.9920	0.8797
Intracranial & flank tumour	Control	0.9990	0.9920		0.9759
	Treatment	0.9954	0.8797	0.9759	

Figure 6.8C ANOVA with post hoc test No. of independent experiments = 1		Intracranial tumour		Intracranial & flank tumour	
		Control n = 6	Treatment n = 7	Control n = 7	Treatment n = 12
Intracranial tumour	Control		0.7853	0.6387	0.0038
	Treatment	0.7853		0.1444	0.0349
Intracranial & flank tumour	Control	0.6387	0.1444		< 0.0001
	Treatment	0.0038	0.0349	< 0.0001	

Figure 6.8D ANOVA with post hoc test No. of independent experiments = 3		Intracranial tumour		Intracranial & flank tumour	
		Control n = 18	Treatment n = 21	Control n = 21	Treatment n = 36
Intracranial tumour	Control		0.9746	0.9371	0.7153
	Treatment	0.9746		0.7188	0.9215
Intracranial & flank tumour	Control	0.9371	0.7188		0.2806
	Treatment	0.7153	0.9215	0.2806	

Figure 6.8E ANOVA with post hoc test No. of independent experiments = 3		Intracranial tumour		Intracranial & flank tumour	
		Control n = 18	Treatment n = 21	Control n = 21	Treatment n = 36
Intracranial tumour	Control		> 0.9999	> 0.9999	0.7167
	Treatment	> 0.9999		0.9997	0.7138
Intracranial & flank tumour	Control	> 0.9999	0.9997		0.6604
	Treatment	0.7167	0.7138	0.6604	

Figure 6.8F ANOVA with post hoc test No. of independent experiments = 1		Intracranial tumour		Intracranial & flank tumour	
		Control n = 6	Treatment n = 7	Control n = 7	Treatment n = 12
Intracranial tumour	Control		0.3484	0.8996	0.0002
	Treatment	0.3484		0.7288	0.0148
Intracranial & flank tumour	Control	0.8996	0.7288		0.0007
	Treatment	0.0002	0.0148	0.0007	

Figure 6.9A ANOVA with post hoc test No. of independent experiments = 2		Intracranial tumour		Intracranial & flank tumour	
		Control n = 13	Treatment n = 15	Control n = 14	Treatment n = 15
Intracranial tumour	Control		0.6738	0.9975	0.9942
	Treatment	0.6738		0.5360	0.7251
Intracranial & flank tumour	Control	0.9975	0.5360		0.9630
	Treatment	0.9942	0.7251	0.9630	

Figure 6.9B ANOVA with post hoc test No. of independent experiments = 2		Intracranial tumour		Intracranial & flank tumour	
		Control n = 13	Treatment n = 15	Control n = 14	Treatment n = 15
Intracranial tumour	Control		0.9921	0.7110	0.9359
	Treatment	0.9921		0.5080	0.7826
Intracranial & flank tumour	Control	0.7110	0.5080		0.9220
	Treatment	0.9359	0.7826	0.9220	

Figure 6.9C ANOVA with post hoc test No. of independent experiments = 1		Intracranial tumour		Intracranial & flank tumour	
		Control n = 6	Treatment n = 7	Control n = 7	Treatment n = 12
Intracranial tumour	Control		0.4746	0.0546	0.4757
	Treatment	0.4746		0.0010	0.0154
Intracranial & flank tumour	Control	0.0546	0.0010		0.3872
	Treatment	0.4757	0.0154	0.3872	

Figure 6.9D ANOVA with post hoc test No. of independent experiments = 2		Intracranial tumour		Intracranial & flank tumour	
		Control n = 13	Treatment n = 15	Control n = 14	Treatment n = 15
Intracranial tumour	Control		0.5749	0.3933	0.9106
	Treatment	0.5749		0.9868	0.8453
Intracranial & flank tumour	Control	0.3933	0.9868		0.6430
	Treatment	0.9106	0.9868	0.6430	

Figure 6.9E ANOVA with post hoc test No. of independent experiments = 2		Intracranial tumour		Intracranial & flank tumour	
		Control n = 13	Treatment n = 15	Control n = 14	Treatment n = 15
Intracranial tumour	Control		0.9667	0.7839	0.9984
	Treatment	0.9667		0.4742	0.9825
Intracranial & flank tumour	Control	0.7839	0.4742		0.5918
	Treatment	0.9984	0.9825	0.5918	

Figure 6.9F ANOVA with post hoc test No. of independent experiments = 1		Intracranial tumour		Intracranial & flank tumour	
		Control n = 6	Treatment n = 7	Control n = 7	Treatment n = 12
Intracranial tumour	Control		0.9784	0.0741	0.0008
	Treatment	0.9784		0.1376	0.0015
Intracranial & flank tumour	Control	0.0741	0.1376		0.3799
	Treatment	0.0008	0.0015	0.3799	

Figure 6.13B ANOVA with post hoc test No. of independent experiments = 1		Intracranial tumour		Intracranial & flank tumour	
		Control n = 3	Treatment n = 4	Control n = 4	Treatment n = 6
Intracranial tumour	Control		0.6328	0.9632	0.0342
	Treatment	0.6328		0.8450	0.2313
Intracranial & flank tumour	Control	0.9632	0.8450		0.0520
	Treatment	0.0342	0.2313	0.0520	

Figure 6.13C ANOVA with post hoc test No. of independent experiments = 1		Intracranial tumour		Intracranial & flank tumour	
		Control n = 8	Treatment n = 8	Control n = 8	Treatment n = 12
Intracranial tumour	Control		0.9998	0.9983	0.1590
	Treatment	0.9998		0.9998	0.1323
Intracranial & flank tumour	Control	0.9983	0.9998		0.1114
	Treatment	0.1590	0.1323	0.1114	

Figure 6.13D ANOVA with post hoc test No. of independent experiments = 1		Intracranial tumour		Intracranial & flank tumour	
		Control n = 6	Treatment n = 5	Control n = 6	Treatment n = 12
Intracranial tumour	Control		0.9997	0.7990	0.3041
	Treatment	0.9997		0.7732	0.4115
Intracranial & flank tumour	Control	0.7990	0.7732		0.0415
	Treatment	0.3041	0.4115	0.0415	

Figure 6.14A ANOVA with post hoc test No. of independent experiments = 1		Intracranial tumour		Intracranial & flank tumour	
		Control n = 6	Treatment n = 5	Control n = 6	Treatment n = 12
Intracranial tumour	Control		0.1451	0.9211	0.1298
	Treatment	0.1451		0.0428	0.9802
Intracranial & flank tumour	Control	0.9211	0.0428		0.0283
	Treatment	0.1298	0.9802	0.0283	

Figure 6.14B ANOVA with post hoc test No. of independent experiments = 1		Intracranial tumour		Intracranial & flank tumour	
		Control n = 6	Treatment n = 5	Control n = 6	Treatment n = 12
Intracranial tumour	Control		0.0056	0.9880	0.0002
	Treatment	0.0056		0.0026	0.9659
Intracranial & flank tumour	Control	0.9880	0.0026		< 0.0001
	Treatment	0.0002	0.9659	< 0.0001	

Figure 6.14C ANOVA with post hoc test No. of independent experiments = 1		Intracranial tumour		Intracranial & flank tumour	
		Control n = 6	Treatment n = 5	Control n = 6	Treatment n = 12
Intracranial tumour	Control		0.9462	0.7845	0.9963
	Treatment	0.9462		0.9853	0.9744
Intracranial & flank tumour	Control	0.7845	0.9853		0.8212
	Treatment	0.9963	0.9744	0.8212	

Figure 6.14D ANOVA with post hoc test No. of independent experiments = 1		Intracranial tumour		Intracranial & flank tumour	
		Control n = 6	Treatment n = 5	Control n = 6	Treatment n = 12
Intracranial tumour	Control		0.9997	> 0.9999	0.4266
	Treatment	0.9997		> 0.9999	0.4170
Intracranial & flank tumour	Control	> 0.9999	> 0.9999		0.3900
	Treatment	0.4266	0.4170	0.3900	

Figure 6.15A ANOVA with post hoc test No. of independent experiments = 1		Intracranial tumour		Intracranial & flank tumour	
		Control n = 6	Treatment n = 5	Control n = 6	Treatment n = 12
Intracranial tumour	Control		0.5781	0.4323	0.9044
	Treatment	0.5781		0.0610	0.2055
Intracranial & flank tumour	Control	0.4323	0.0610		0.6951
	Treatment	0.9044	0.2055	0.6951	

Figure 6.15B ANOVA with post hoc test No. of independent experiments = 1		Intracranial tumour		Intracranial & flank tumour	
		Control n = 6	Treatment n = 5	Control n = 6	Treatment n = 12
Intracranial tumour	Control		0.9981	0.9323	0.7896
	Treatment	0.9981		0.8942	0.9271
Intracranial & flank tumour	Control	0.9323	0.8942		0.3882
	Treatment	0.7896	0.9271	0.3882	

Figure 6.15C ANOVA with post hoc test No. of independent experiments = 1		Intracranial tumour		Intracranial & flank tumour	
		Control n = 6	Treatment n = 5	Control n = 6	Treatment n = 12
Intracranial tumour	Control		0.6849	0.9971	0.3952
	Treatment	0.6849		0.5771	0.9989
Intracranial & flank tumour	Control	0.9971	0.5771		0.2829
	Treatment	0.3952	0.9989	0.2829	

Figure 6.15D ANOVA with post hoc test No. of independent experiments = 1		Intracranial tumour		Intracranial & flank tumour	
		Control n = 6	Treatment n = 5	Control n = 6	Treatment n = 12
Intracranial tumour	Control		0.4288	0.9742	0.9997
	Treatment	0.4288		0.6535	0.2954
Intracranial & flank tumour	Control	0.9742	0.6535		0.9372
	Treatment	0.9997	0.2954	0.9372	

Figure 6.16 Paired t-test No. of independent experiments = 1	P value n = 12
Ki67 ⁺ cells	< 0.0001
Ki67 MFI	< 0.0001
Granzyme B ⁺ cells	0.0018
Granzyme B MFI	0.0007

Figure 6.17A ANOVA with post hoc test No. of independent experiments = 1		Intracranial tumour		Intracranial & flank tumour	
		Control n = 6	Treatment n = 5	Control n = 6	Treatment n = 12
Intracranial tumour	Control		0.9975	0.4496	0.6181
	Treatment	0.9975		0.3838	0.7870
Intracranial & flank tumour	Control	0.4496	0.3838		0.0315
	Treatment	0.6181	0.7870	0.0315	

Figure 6.17B ANOVA with post hoc test No. of independent experiments = 1		Intracranial tumour		Intracranial & flank tumour	
		Control n = 6	Treatment n = 5	Control n = 6	Treatment n = 12
Intracranial tumour	Control		0.0918	0.9635	0.0006
	Treatment	0.0918		0.0351	0.4588
Intracranial & flank tumour	Control	0.9635	0.0351		0.0002
	Treatment	0.0006	0.4588	0.0002	

Figure 6.17C ANOVA with post hoc test No. of independent experiments = 1		Intracranial tumour		Intracranial & flank tumour	
		Control n = 6	Treatment n = 5	Control n = 6	Treatment n = 12
Intracranial tumour	Control		0.9960	0.9857	0.7228
	Treatment	0.9960		0.9996	0.6096
Intracranial & flank tumour	Control	0.9857	0.9996		0.4836
	Treatment	0.7228	0.6096	0.4836	

Figure 6.17D ANOVA with post hoc test No. of independent experiments = 1		Intracranial tumour		Intracranial & flank tumour	
		Control n = 6	Treatment n = 5	Control n = 6	Treatment n = 12
Intracranial tumour	Control		0.3149	0.9054	0.4275
	Treatment	0.3149		0.1020	0.0100
Intracranial & flank tumour	Control	0.9054	0.1020		0.8698
	Treatment	0.4275	0.0100	0.8698	

Figure 6.17E ANOVA with post hoc test No. of independent experiments = 1		Intracranial tumour		Intracranial & flank tumour	
		Control n = 6	Treatment n = 5	Control n = 6	Treatment n = 12
Intracranial tumour	Control		0.9404	0.9739	0.0077
	Treatment	0.9404		0.7660	0.0560
Intracranial & flank tumour	Control	0.9739	0.7660		0.0023
	Treatment	0.0077	0.0560	0.0023	

Figure 6.17F ANOVA with post hoc test No. of independent experiments = 1		Intracranial tumour		Intracranial & flank tumour	
		Control n = 6	Treatment n = 5	Control n = 6	Treatment n = 12
Intracranial tumour	Control		0.9715	0.4483	0.9563
	Treatment	0.9715		0.2643	> 0.9999
Intracranial & flank tumour	Control	0.4483	0.2643		0.1377
	Treatment	0.9563	> 0.9999	0.1377	

Figure 6.18A ANOVA with post hoc test No. of independent experiments = 1		Intracranial tumour		Intracranial & flank tumour	
		Control n = 6	Treatment n = 5	Control n = 6	Treatment n = 12
Intracranial tumour	Control		0.3987	0.6493	0.7158
	Treatment	0.3987		0.9460	0.8214
Intracranial & flank tumour	Control	0.6493	0.9460		0.9910
	Treatment	0.7158	0.8214	0.9910	

Figure 6.18B ANOVA with post hoc test No. of independent experiments = 1		Intracranial tumour		Intracranial & flank tumour	
		Control n = 6	Treatment n = 5	Control n = 6	Treatment n = 12
Intracranial tumour	Control		0.8998	0.9995	0.9639
	Treatment	0.8998		0.9335	0.6430
Intracranial & flank tumour	Control	0.9995	0.9335		0.9305
	Treatment	0.9639	0.6430	0.9305	

Figure 6.18C ANOVA with post hoc test No. of independent experiments = 1		Intracranial tumour		Intracranial & flank tumour	
		Control n = 6	Treatment n = 5	Control n = 6	Treatment n = 12
Intracranial tumour	Control		0.3819	0.8208	0.6520
	Treatment	0.3819		0.8289	0.8491
Intracranial & flank tumour	Control	0.8208	0.8289		0.9984
	Treatment	0.6520	0.8491	0.9984	

Figure 6.18D ANOVA with post hoc test No. of independent experiments = 1		Intracranial tumour		Intracranial & flank tumour	
		Control n = 6	Treatment n = 5	Control n = 6	Treatment n = 12
Intracranial tumour	Control		0.9996	0.7897	0.9825
	Treatment	0.9996		0.7886	0.9968
Intracranial & flank tumour	Control	0.7897	0.7886		0.4871
	Treatment	0.9825	0.9968	0.4871	

Figure 6.18E ANOVA with post hoc test No. of independent experiments = 1		Intracranial tumour		Intracranial & flank tumour	
		Control n = 6	Treatment n = 5	Control n = 6	Treatment n = 12
Intracranial tumour	Control		0.5690	0.9739	0.9439
	Treatment	0.5690		0.3540	0.2384
Intracranial & flank tumour	Control	0.9739	0.3540		0.9999
	Treatment	0.9439	0.2384	0.9999	

Figure 6.18F ANOVA with post hoc test No. of independent experiments = 1		Intracranial tumour		Intracranial & flank tumour	
		Control n = 6	Treatment n = 5	Control n = 6	Treatment n = 12
Intracranial tumour	Control		0.9491	0.1587	0.9931
	Treatment	0.9491		0.0883	0.8387
Intracranial & flank tumour	Control	0.1587	0.0883		0.1398
	Treatment	0.9931	0.8387	0.1398	

Figure 6.19 Paired t-test No. of independent experiments = 1	P value n = 12
EOMES ⁺ cells	0.0006
EOMES MFI	0.0006
TIM-3 ⁺ cells	< 0.0001
TIM-3 MFI	0.0516
PD-1 ⁺ cells	< 0.0001
PD-1 MFI	< 0.0001

Figure 6.20A ANOVA with post hoc test No. of independent experiments = 1		Intracranial tumour		Intracranial & flank tumour	
		Control n = 6	Treatment n = 5	Control n = 4	Treatment n = 13
Intracranial tumour	Control		0.3146	0.5368	0.0260
	Treatment	0.3146		0.0369	0.8365
Intracranial & flank tumour	Control	0.5368	0.0369		0.0018
	Treatment	0.0260	0.8365	0.0018	

Figure 6.20B ANOVA with post hoc test No. of independent experiments = 1		Intracranial tumour		Intracranial & flank tumour	
		Control n = 6	Treatment n = 5	Control n = 4	Treatment n = 13
Intracranial tumour	Control		0.9343	0.6418	0.8573
	Treatment	0.9343		0.3595	0.9999
Intracranial & flank tumour	Control	0.6418	0.3595		0.2081
	Treatment	0.8573	0.9999	0.2081	

Figure 6.20C ANOVA with post hoc test No. of independent experiments = 1		Intracranial tumour		Intracranial & flank tumour	
		Control n = 6	Treatment n = 5	Control n = 4	Treatment n = 13
Intracranial tumour	Control		0.3994	0.6763	0.1872
	Treatment	0.3994		0.0810	0.9994
Intracranial & flank tumour	Control	0.6763	0.0810		0.0251
	Treatment	0.1872	0.9994	0.0251	

Figure 6.20D ANOVA with post hoc test No. of independent experiments = 1		Intracranial tumour		Intracranial & flank tumour	
		Control n = 6	Treatment n = 5	Control n = 4	Treatment n = 13
Intracranial tumour	Control		0.9834	0.9563	0.9280
	Treatment	0.9834		0.8465	0.9985
Intracranial & flank tumour	Control	0.9563	0.8465		0.6927
	Treatment	0.9280	0.9985	0.6927	

Figure 6.20E ANOVA with post hoc test No. of independent experiments = 1		Intracranial tumour		Intracranial & flank tumour	
		Control n = 6	Treatment n = 5	Control n = 4	Treatment n = 13
Intracranial tumour	Control		0.4084	0.9500	0.9286
	Treatment	0.4084		0.2388	0.1066
Intracranial & flank tumour	Control	0.9500	0.2388		0.9998
	Treatment	0.9286	0.1066	0.9998	

Figure 6.20F ANOVA with post hoc test No. of independent experiments = 1		Intracranial tumour		Intracranial & flank tumour	
		Control n = 6	Treatment n = 5	Control n = 4	Treatment n = 13
Intracranial tumour	Control		0.1016	0.9960	0.9467
	Treatment	0.1016		0.2292	0.0153
Intracranial & flank tumour	Control	0.9960	0.2292		0.8875
	Treatment	0.9467	0.0153	0.8875	

Figure 6.21A ANOVA with post hoc test No. of independent experiments = 1		Intracranial tumour		Intracranial & flank tumour	
		Control n = 6	Treatment n = 5	Control n = 4	Treatment n = 13
Intracranial tumour	Control		0.0120	0.9453	0.0567
	Treatment	0.0120		0.0047	0.5325
Intracranial & flank tumour	Control	0.9453	0.0047		0.0201
	Treatment	0.0567	0.5325	0.0201	

Figure 6.21B ANOVA with post hoc test No. of independent experiments = 1		Intracranial tumour		Intracranial & flank tumour	
		Control n = 6	Treatment n = 5	Control n = 4	Treatment n = 13
Intracranial tumour	Control		0.9982	> 0.9999	0.9876
	Treatment	0.9982		0.9995	0.9575
Intracranial & flank tumour	Control	> 0.9999	0.9995		0.9816
	Treatment	0.9876	0.9575	0.9816	

Figure 6.21C ANOVA with post hoc test No. of independent experiments = 1		Intracranial tumour		Intracranial & flank tumour	
		Control n = 6	Treatment n = 5	Control n = 4	Treatment n = 13
Intracranial tumour	Control		0.6494	0.5101	0.4047
	Treatment	0.6494		0.1025	0.0422
Intracranial & flank tumour	Control	0.5101	0.1025		0.9965
	Treatment	0.4047	0.0422	0.9965	

Figure 6.21D ANOVA with post hoc test No. of independent experiments = 1		Intracranial tumour		Intracranial & flank tumour	
		Control n = 6	Treatment n = 5	Control n = 4	Treatment n = 13
Intracranial tumour	Control		0.1144	0.8654	0.0333
	Treatment	0.1144		0.5271	> 0.9999
Intracranial & flank tumour	Control	0.8654	0.5271		0.3728
	Treatment	0.0333	> 0.9999	0.3728	

Figure 6.21E ANOVA with post hoc test No. of independent experiments = 1		Intracranial tumour		Intracranial & flank tumour	
		Control n = 6	Treatment n = 5	Control n = 4	Treatment n = 13
Intracranial tumour	Control		0.2626	0.8320	0.8841
	Treatment	0.2626		0.0828	0.0388
Intracranial & flank tumour	Control	0.8320	0.0828		0.9868
	Treatment	0.8841	0.0388	0.9868	

Figure 6.21F ANOVA with post hoc test No. of independent experiments = 1		Intracranial tumour		Intracranial & flank tumour	
		Control n = 6	Treatment n = 5	Control n = 4	Treatment n = 13
Intracranial tumour	Control		0.1181	0.9904	0.9141
	Treatment	0.1181		0.1047	0.1813
Intracranial & flank tumour	Control	0.9904	0.1047		0.8037
	Treatment	0.9141	0.1813	0.8037	

Figure 6.23A ANOVA with post hoc test No. of independent experiments = 1		Intracranial tumour		Intracranial & flank tumour	
		Control n = 8	Treatment n = 8	Control n = 8	Treatment n = 12
Intracranial tumour	Control		0.0449	0.9559	0.0052
	Treatment	0.0449		0.1326	0.9288
Intracranial & flank tumour	Control	0.9559	0.1326		0.0215
	Treatment	0.0052	0.9288	0.0215	

Figure 6.23B ANOVA with post hoc test No. of independent experiments = 1		Intracranial tumour		Intracranial & flank tumour	
		Control n = 8	Treatment n = 8	Control n = 8	Treatment n = 12
Intracranial tumour	Control		0.0921	0.3406	0.0002
	Treatment	0.0921		0.8852	0.1836
Intracranial & flank tumour	Control	0.3406	0.8852		0.0345
	Treatment	0.0002	0.1836	0.0345	

Figure 6.23C ANOVA with post hoc test No. of independent experiments = 1		Intracranial tumour		Intracranial & flank tumour	
		Control n = 8	Treatment n = 8	Control n = 8	Treatment n = 12
Intracranial tumour	Control		> 0.9999	0.9990	0.3661
	Treatment	> 0.9999		0.9973	0.3986
Intracranial & flank tumour	Control	0.9990	0.9973		0.2903
	Treatment	0.3661	0.3986	0.2903	

Figure 6.23D ANOVA with post hoc test No. of independent experiments = 1		Intracranial tumour		Intracranial & flank tumour	
		Control n = 8	Treatment n = 8	Control n = 8	Treatment n = 12
Intracranial tumour	Control		0.9983	0.9994	0.0974
	Treatment	0.9983		0.9920	0.1403
Intracranial & flank tumour	Control	0.9994	0.9920		0.0748
	Treatment	0.0974	0.1403	0.0748	

Figure 6.23E ANOVA with post hoc test No. of independent experiments = 1		Intracranial tumour		Intracranial & flank tumour	
		Control n = 8	Treatment n = 8	Control n = 8	Treatment n = 12
Intracranial tumour	Control		0.0648	0.7352	< 0.0001
	Treatment	0.0648		0.0053	0.0984
Intracranial & flank tumour	Control	0.7352	0.0053		< 0.0001
	Treatment	< 0.0001	0.0984	< 0.0001	

Figure 6.23F ANOVA with post hoc test No. of independent experiments = 1		Intracranial tumour		Intracranial & flank tumour	
		Control n = 8	Treatment n = 8	Control n = 8	Treatment n = 12
Intracranial tumour	Control		0.9662	0.9832	0.9988
	Treatment	0.9662		0.8404	0.9835
Intracranial & flank tumour	Control	0.9832	0.8404		0.9469
	Treatment	0.9988	0.9835	0.9469	

Figure 6.24A ANOVA with post hoc test No. of independent experiments = 1		Intracranial tumour		Intracranial & flank tumour	
		Control n = 8	Treatment n = 8	Control n = 8	Treatment n = 12
Intracranial tumour	Control		0.8734	0.9194	0.8265
	Treatment	0.8734		0.9994	> 0.9999
Intracranial & flank tumour	Control	0.9194	0.9994		0.9985
	Treatment	0.8265	> 0.9999	0.9985	

Figure 6.24B ANOVA with post hoc test No. of independent experiments = 1		Intracranial tumour		Intracranial & flank tumour	
		Control n = 8	Treatment n = 8	Control n = 8	Treatment n = 12
Intracranial tumour	Control		0.8632	0.3566	0.3602
	Treatment	0.8632		0.8107	0.8504
Intracranial & flank tumour	Control	0.3566	0.8107		0.9983
	Treatment	0.3602	0.8504	0.9983	

Figure 6.24C ANOVA with post hoc test No. of independent experiments = 1		Intracranial tumour		Intracranial & flank tumour	
		Control n = 8	Treatment n = 8	Control n = 8	Treatment n = 12
Intracranial tumour	Control		> 0.9999	0.9992	0.9985
	Treatment	> 0.9999		0.9996	0.9977
Intracranial & flank tumour	Control	0.9992	0.9996		0.9902
	Treatment	0.9985	0.9977	0.9902	

Figure 6.24D ANOVA with post hoc test No. of independent experiments = 1		Intracranial tumour		Intracranial & flank tumour	
		Control n = 8	Treatment n = 8	Control n = 8	Treatment n = 12
Intracranial tumour	Control		> 0.9999	0.8927	0.8841
	Treatment	> 0.9999		0.8997	0.8920
Intracranial & flank tumour	Control	0.8927	0.8997		> 0.9999
	Treatment	0.8841	0.8920	> 0.9999	

Figure 6.24E ANOVA with post hoc test No. of independent experiments = 1		Intracranial tumour		Intracranial & flank tumour	
		Control n = 8	Treatment n = 8	Control n = 8	Treatment n = 12
Intracranial tumour	Control		0.9999	0.9087	0.9049
	Treatment	0.9999		0.9327	0.8735
Intracranial & flank tumour	Control	0.9087	0.9327		0.5037
	Treatment	0.9049	0.8735	0.5037	

Figure 6.24F ANOVA with post hoc test No. of independent experiments = 1		Intracranial tumour		Intracranial & flank tumour	
		Control n = 8	Treatment n = 8	Control n = 8	Treatment n = 12
Intracranial tumour	Control		0.9761	0.6905	0.9652
	Treatment	0.9761		0.4410	> 0.9999
Intracranial & flank tumour	Control	0.6905	0.4410		0.3517
	Treatment	0.9652	> 0.9999	0.3517	

Figure 6.19 Paired t-test No. of independent experiments = 1	P value n = 12
CCR7 ⁺ cells	< 0.0001
CCR7 MFI	0.0337
LFA-1 ⁺ cells	0.0002
LFA-1 MFI	0.0002
VLA-4 ⁺ cells	0.0868
VLA-4 MFI	0.0003

Figure 6.27A ANOVA with post hoc test No. of independent experiments = 1		Intracranial tumour		Intracranial & flank tumour	
		Control n = 3	Treatment n = 4	Control n = 5	Treatment n = 8
Intracranial tumour	Control		0.9944	0.5447	0.5772
	Treatment	0.9944		0.6418	0.6801
Intracranial & flank tumour	Control	0.5447	0.6418		0.9974
	Treatment	0.5772	0.6801	0.9974	

Figure 6.27B ANOVA with post hoc test No. of independent experiments = 1		Intracranial tumour		Intracranial & flank tumour	
		Control n = 3	Treatment n = 4	Control n = 5	Treatment n = 8
Intracranial tumour	Control		0.9999	0.9831	0.1657
	Treatment	0.9999		0.9635	0.1296
Intracranial & flank tumour	Control	0.9831	0.9635		0.0329
	Treatment	0.1657	0.1296	0.0329	

Figure 6.27C ANOVA with post hoc test No. of independent experiments = 1		Intracranial tumour		Intracranial & flank tumour	
		Control n = 3	Treatment n = 4	Control n = 5	Treatment n = 8
Intracranial tumour	Control		0.9344	> 0.9999	0.1744
	Treatment	0.9344		0.9132	0.3732
Intracranial & flank tumour	Control	> 0.9999	0.9132		0.0886
	Treatment	0.1744	0.3732	0.0886	

Figure 6.27D ANOVA with post hoc test No. of independent experiments = 1		Intracranial tumour		Intracranial & flank tumour	
		Control n = 3	Treatment n = 4	Control n = 5	Treatment n = 8
Intracranial tumour	Control		0.9936	0.8042	0.0831
	Treatment	0.9936		0.9012	0.0913
Intracranial & flank tumour	Control	0.8042	0.9012		0.2583
	Treatment	0.0831	0.0913	0.2583	

Figure 6.27E ANOVA with post hoc test No. of independent experiments = 1		Intracranial tumour		Intracranial & flank tumour	
		Control n = 3	Treatment n = 4	Control n = 5	Treatment n = 8
Intracranial tumour	Control		0.9587	0.8252	0.0456
	Treatment	0.9587		0.9820	0.0821
Intracranial & flank tumour	Control	0.8252	0.9820		0.1271
	Treatment	0.0456	0.0821	0.1271	

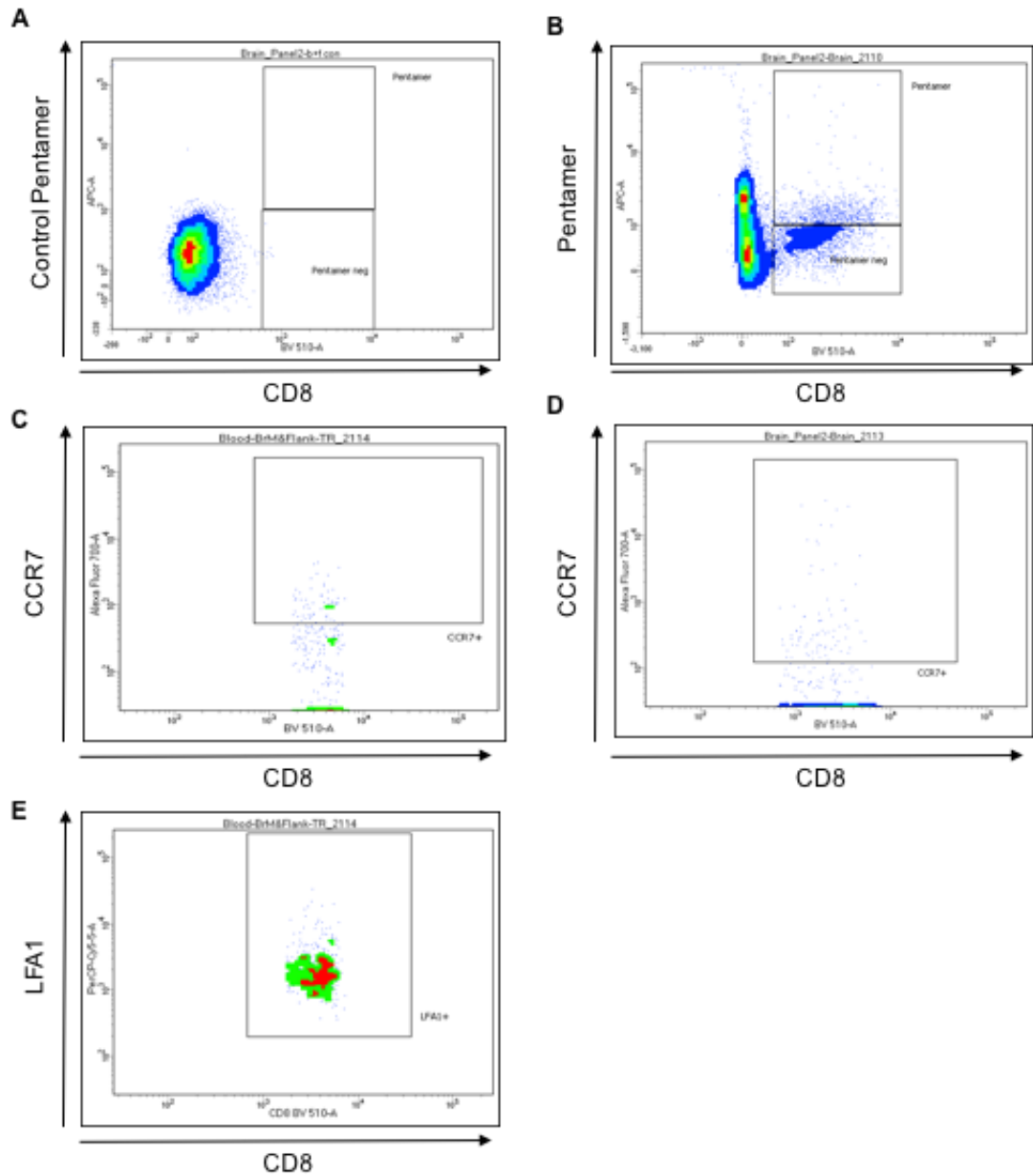


Figure 8.1 Example plots of OVA pentamer⁺ cells

Example plots showing (A) the CD8 isotype staining along with the control pentamer staining and (B) the staining of the staining of CD8⁺ and OVA pentamer⁺ cells within the intracranial tumour. (C) Example plots of CCR7⁺ CD8⁺ cells within the CD8⁺ pentamer⁺ cell population in the blood and (D) intracranial tumour. (E) Example plot of LFA1⁺ CD8⁺ cells within the CD8⁺ pentamer⁺ cell population in the intracranial tumour.

References

1. Fabi A, Felici A, Metro G, et al. Brain metastases from solid tumors: disease outcome according to type of treatment and therapeutic resources of the treating center. *J Exp Clin Cancer Res*. 2011;30:10.
2. Barnholtz-Sloan JS, Sloan AE, Davis FG, Vignneau FD, Lai P, Sawaya RE. Incidence proportions of brain metastases in patients diagnosed (1973 to 2001) in the Metropolitan Detroit Cancer Surveillance System. *J Clin Oncol*. 2004;22(14):2865-2872.
3. Nayak L, Lee EQ, Wen PY. Epidemiology of brain metastases. *Curr Oncol Rep*. 2012;14(1):48-54.
4. Walker AE, Robins M, Weinfeld FD. Epidemiology of brain tumors: the national survey of intracranial neoplasms. *Neurology*. 1985;35(0028-3878 (Print)):219-226.
5. Huntington RW, Cummings KL, Moe TI, O'Connell H V., Wybel R. Discovery of fatal primary intracranial neoplasms at medicolegal autopsies. *Cancer*. 1965;18(1):117-127.
6. Suki D. The Epidemiology of Brain Metastasis. In: wiley; 2008:20-34.
7. Campos S, Davey P, Hird a, et al. Brain metastasis from an unknown primary, or primary brain tumour? A diagnostic dilemma. *Curr Oncol*. 2009;16(1):62-66.
8. Lin NU, Winer EP. Brain metastases: The HER2 paradigm. *Clin Cancer Res*. 2007;13(6):1648-1655.
9. Bendell JC, Domchek SM, Burstein HJ, et al. Central nervous system metastases in women who receive trastuzumab-based therapy for metastatic breast carcinoma. *Cancer*. 2003;97(12):2972-2977.
10. Clayton AJ, Danson S, Jolly S, et al. Incidence of cerebral metastases in patients treated with trastuzumab for metastatic breast cancer. *Br J Cancer*. 2004;91(4):639-643.
11. Rippaus N, Taggart D, Williams J, Andreou T, Wronski K, Loriger M. Metastatic site-specific polarization intracranial breast cancer metastases of macrophages in. *Oncotarget*. 2016.
12. Nussbaum ES, Djalilian HR, Cho KH, Hall WA. Brain metastases: Histology, multiplicity, surgery, and survival. *Cancer*. 1996;78(8):1781-1788.
13. Stark AM, Tscheslog H, Buhl R, Held-Feindt J, Mehdorn HM. Surgical treatment for brain metastases: Prognostic factors and survival in 177 patients. *Neurosurg Rev*. 2005;28(2):115-119.
14. Davies MA, Liu P, McIntyre S, et al. Prognostic factors for survival in melanoma patients with brain metastases. *Cancer*. 2011;117(8):1687-1696.
15. Vuong DA, Rades D, Vo SQ, Busse R. Extracranial metastatic patterns on occurrence of brain metastases. *J Neurooncol*. 2011;105(1):83-90.
16. Delattre JY, Krol G, Thaler HT, Posner JB. Distribution of brain metastases. *Arch Neurol*. 1988;45(7):741-744.

17. Mavrakis AN, Halpern EF, Barker FG, Gonzalez RG, Henson JW. Diagnostic evaluation of patients with a brain mass as the presenting manifestation of cancer. *Neurology*. 2005;65(6):908-911.
18. Rudà R, Borgognone M, Benech F, Vasario E, Soffietti R. Brain metastases from unknown primary tumour: a prospective study. *J Neurol*. 2001;248(5):394-398. <http://www.ncbi.nlm.nih.gov/pubmed/11437161>.
19. Damsky W, Theodosakis N, Bosenberg M. Melanoma metastasis: new concepts and evolving paradigms. *Oncogene*. 2013;33:2413-2422.
20. Clark WH, Elder DE, Guerry D, Epstein MN, Greene MH, Van Horn M. A study of tumor progression: The precursor lesions of superficial spreading and nodular melanoma. *Hum Pathol*. 1984;15(12):1147-1165.
21. Arrangoiz R, Dorantes J, Cordera F, Juarez MM, Paquentin EM, León EL De. Melanoma Review : Epidemiology , Risk Factors , Diagnosis and Staging To cite this article : 2016;4(1):1-15.
22. M BC. Final Version of the American Joint Committee on Cancer Staging System for cutaneous Melanoma. *J Clin Oncol*. 2001;Vol. 19 No(16):3635-3648.
23. Trotter SC, Sroa N, Winkelmann RR, Olencki T, Bechtel M. A global review of melanoma follow-up guidelines. *J Clin Aesthet Dermatol*. 2013;6(9):18-26.
24. Balch CM, Urist MM, Karakousis CP, et al. Efficacy of 2-cm surgical margins for intermediate-thickness melanomas (1 to 4 mm). Results of a multi-institutional randomized surgical trial. *Ann Surg*. 1993;218(3):262-7-9.
25. Smalley KSM, Fedorenko I V., Kenchappa RS, Sahebjam S, Forsyth PA. Managing leptomeningeal melanoma metastases in the era of immune and targeted therapy. *Int J Cancer*. 2016;139(6):1195-1201.
26. Goldinger SM, Panje C, Nathan P. Treatment of melanoma brain metastases. *Curr Opin Oncol*. 2016;28:159-165.
27. Fife KM, Colman MH, Stevens GN, et al. Determinants of outcome in melanoma patients with cerebral metastases. *J Clin Oncol*. 2004;22(7):1293-1300.
28. Agarwala SS, Kirkwood JM, Gore M, et al. Temozolomide for the treatment of brain metastases associated with metastatic melanoma: a phase II study. *J Clin Oncol*. 2004;22(11):2101-2107.
29. Lyle M, Long G V. The role of systemic therapies in the management of melanoma brain metastases. *Curr Opin Oncol*. 2014;26(2):222-229.
30. Staudt M, Lasithiotakis K, Leiter U, et al. Determinants of survival in patients with brain metastases from cutaneous melanoma. *Br J Cancer*. 2010;102(8):1213-1218.
31. Sampson JH, Carter JH, Friedman a H, Seigler HF. Demographics, prognosis, and therapy in 702 patients with brain metastases from malignant melanoma. *J Neurosurg*. 1998;88(1):11-20.
32. Sul J, Posner JB. Brain Metastases: Epidemiology and Pathophysiology. In: Raizer JJ, Abrey LE, eds. *Brain Metastases*. Boston, MA: Springer US; 2007:1-21.
33. Daryanani D, Plukker JT, de Jong M a, et al. Increased incidence of brain metastases in cutaneous head and neck melanoma. *Melanoma Res*.

2005;15(2):119-124.

34. Raizer JJ, Hwu W-J, Panageas KS, et al. Brain and leptomeningeal metastases from cutaneous melanoma: survival outcomes based on clinical features. *Neuro Oncol.* 2008;10:199-207.
35. Wroński M, Arbit E. Surgical treatment of brain metastases from melanoma: a retrospective study of 91 patients. *J Neurosurg.* 2000;93(1):9-18.
36. Liew DN, Kano H, Kondziolka D, et al. Outcome predictors of Gamma Knife surgery for melanoma brain metastases. Clinical article. *J Neurosurg.* 2011;114(3):769-779.
37. Kenchappa RS, Tran N, Rao NG, et al. Novel treatments for melanoma brain metastases. *Cancer Control.* 2013;20(4):298-306.
38. Miller D, Zappala V, El Hindy N, et al. Intracerebral metastases of malignant melanoma and their recurrences--a clinical analysis. *Clin Neurol Neurosurg.* 2013;115(9):1721-1728.
39. Frakes JM, Figura ND, Ahmed KA, et al. Potential role for LINAC-based stereotactic radiosurgery for the treatment of 5 or more radioresistant melanoma brain metastases. *J Neurosurg.* 2015:1-7.
40. Avril MF, Aamdal S, Grob JJ, et al. Fotemustine compared with dacarbazine in patients with disseminated malignant melanoma: A phase III study. *J Clin Oncol.* 2004;22(6):1118-1125.
41. Hanahan D, Weinberg R a, Francisco S. The Hallmarks of Cancer. *Cell.* 2000;100:57-70.
42. Hanahan D, Weinberg RA. Hallmarks of cancer: The next generation. *Cell.* 2011;144(5):646-674.
43. Cao Y, DePinho R a, Ernst M, Vousden K. Cancer research: past, present and future. *Nat Rev Cancer.* 2011;11(10):749-754.
44. Parish CR. Cancer immunotherapy: The past, the present and the future. *Immunol Cell Biol.* 2003;81(2):106-113.
45. Hadrup S, Donia M, Straten P thor. Effector CD4 and CD8 T Cells and Their Role in the Tumor Microenvironment. *Cancer Microenviron.* 2013;6(2):123-133.
46. Michor F, Polyak K. The origins and implications of intratumor heterogeneity. *Cancer Prev Res.* 2010;3(11):1361-1364.
47. Marusyk A, Polyak K. Tumor heterogeneity: causes and consequences. *Biochim Biophys Acta.* 2010;1805(1):105-117.
48. Muenst S, Laubli H, Soysal SD, Zippelius A, Tzankov A, Hoeller S. The immune system and cancer evasion strategies: Therapeutic concepts. *Journal of Internal Medicine.* 2016.
49. Dudley AC. Tumor endothelial cells. *Cold Spring Harb Perspect Med.* 2012;2(3):1-18.
50. Xing F, Saidou J, Watabe K. Cancer associated fibroblasts (CAFs) in tumor microenvironment. *Front Biosci (Landmark Ed.* 2010;15(2):166-179.
51. Shiga K, Hara M, Nagasaki T, Sato T, Takahashi H, Takeyama H. Cancer-associated fibroblasts: Their characteristics and their roles in tumor growth.

Cancers (Basel). 2015;7(4):2443-2458.

52. Kamoun WS, Chae S-S, Lacorre D a, et al. Simultaneous measurement of RBC velocity, flux, hematocrit and shear rate in vascular networks. *Nat Methods*. 2010;7(8):655-660.
53. Tammela T, Alitalo K. Lymphangiogenesis: Molecular Mechanisms and Future Promise. *Cell*. 2010;140(4):460-476.
54. Vivier E, Ugolini S, Blaise D, Chabannon C, Brossay L. Targeting natural killer cells and natural killer T cells in cancer. *NatRevImmunol*. 2012;12(1474-1741 (Electronic)):239-252.
55. Bruno A, Ferlazzo G, Albini A, Noonan DM. A think tank of TINK/TANKs: Tumor-infiltrating/tumor-associated natural killer cells in tumor progression and angiogenesis. *J Natl Cancer Inst*. 2014;106(8).
56. Imai K, Matsuyama S, Miyake S, Suga K, Nakachi K. Natural cytotoxic activity of peripheral-blood lymphocytes and cancer incidence: an 11-year follow-up study of a general population. *Lancet*. 2000;356(9244):1795-1799.
57. Larsen SK, Gao Y, Basse PH. NK cells in the tumor microenvironment. *Crit Rev Oncog*. 2014;19(1-2):91-105.
58. Burke S, Lakshmikanth T, Colucci F, Carbone E. New views on natural killer cell-based immunotherapy for melanoma treatment. *Trends Immunol*. 2010;31(9):339-345.
59. Matta J, Baratin M, Chiche L, et al. Induction of B7-H6, a ligand for the natural killer cell-activating receptor NKp30, in inflammatory conditions. *Blood*. 2013;122(3):394-404.
60. Flajnik MF, Tlapakova T, Criscitiello MF, Krylov V, Ohta Y. Evolution of the B7 family: Co-evolution of B7H6 and NKp30, identification of a new B7 family member, B7H7, and of B7's historical relationship with the MHC. *Immunogenetics*. 2012;64(8):571-590.
61. Anfossi N, Andre P, Guia S, et al. Human NK Cell Education by Inhibitory Receptors for MHC Class I. *Immunity*. 2006;25(2):331-342.
62. Kim S, Poursine-Laurent J, Truscott SM, et al. Licensing of natural killer cells by host major histocompatibility complex class I molecules. *Nature*. 2005;436(7051):709-713.
63. Vivier E, Raulet DH, Moretta A, et al. Innate or adaptive immunity? The example of natural killer cells. *Science*. 2011;331(6013):44-49.
64. Fruci D, Benevolo M, Cifaldi L, et al. Major histocompatibility complex class I and tumour immuno-evasion: How to fool T cells and natural killer cells at one time. *Curr Oncol*. 2012;19(1):39-41.
65. Balsamo M, Vermi W, Parodi M, et al. Melanoma cells become resistant to NK-cell-mediated killing when exposed to NK-cell numbers compatible with NK-cell infiltration in the tumor. *Eur J Immunol*. 2012;42(7):1833-1842.
66. Gross E, Sunwoo JB, Bui JD. Cancer immunosurveillance and immunoediting by natural killer cells. *Cancer J*. 2013;19(6):483-489.
67. Viel S, Marcais A, Guimaraes FS-F, et al. TGF- inhibits the activation and functions of NK cells by repressing the mTOR pathway. *Sci Signal*. 2016;9(415):ra19-ra19.

68. Gallois A, Silva I, Osman I, Bhardwaj N. Reversal of natural killer cell exhaustion by TIM-3 blockade. *Oncoimmunology*. 2014;3(12):e946365.
69. Yui MA, Rothenberg E V. Developmental gene networks : a triathlon on the course to T cell identity. *Nat Publ Gr*. 2014;14(8):529-545.
70. Reiser J, Banerjee A. Effector , Memory and Dysfunctional CD8 + T Cell Fates in the Antitumor Immune Response. 2016;2016.
71. Gajewski TF, Schreiber H, Fu Y-X. Innate and adaptive immune cells in the tumor microenvironment. *Nat Immunol*. 2013;14(10):1014-1022.
72. Savage PA, Leventhal DS, Malchow S. Shaping the repertoire of tumor-infiltrating effector and regulatory T cells. *Immunol Rev*. 2014;259(1):245-258.
73. Fridman WH, Remark R, Goc J, et al. The immune microenvironment: A major player in human cancers. *Int Arch Allergy Immunol*. 2014;164(1):13-26.
74. Norton SE, Ward-Hartstonge K a, Taylor ES, Kemp R a. Immune cell interplay in colorectal cancer prognosis. *World J Gastrointest Oncol*. 2015;7(10):221-232.
75. Bachmayr-Heyda A, Aust S, Heinze G, et al. Prognostic impact of tumor infiltrating CD8+ T cells in association with cell proliferation in ovarian cancer patients - a study of the OVCAD consortium. *BMC Cancer*. 2013;13(1):422.
76. Liu S, Lachapelle J, Leung S, Gao D, Foulkes WD, Nielsen TO. CD8+ lymphocyte infiltration is an independent favorable prognostic indicator in basal-like breast cancer. *Breast Cancer Res*. 2012;14(2):R48.
77. Miyashita M, Sasano H, Tamaki K, et al. Prognostic significance of tumor-infiltrating CD8+ and FOXP3+ lymphocytes in residual tumors and alterations in these parameters after neoadjuvant chemotherapy in triple-negative breast cancer: a retrospective multicenter study. *Breast Cancer Res*. 2015;17(1):124.
78. Shang B, Liu YYYYY, Jiang S, Liu YYYYY. Prognostic value of tumor-infiltrating FoxP3+ regulatory T cells in cancers: a systematic review and meta-analysis. *Sci Rep*. 2015;5(October):15179.
79. Fridman WH, Pagès F, Sautès-Fridman C, Galon J. The immune contexture in human tumours: impact on clinical outcome. *Nat Rev Cancer*. 2012;12(4):298-306.
80. Palucka K, Banchereau J. Cancer immunotherapy via dendritic cells. *Nat Rev Cancer*. 2012;12(4):265-277.
81. Rosenberg SA, Restifo NP. Adoptive cell transfer as personalized immunotherapy for human cancer. *Science (80-)*. 2015;348(6230):62-68.
82. Brown SD, Warren RL, Gibb EA, et al. Neo-antigens predicted by tumor genome meta-analysis correlate with increased patient survival. *Genome Res*. 2014;24(5):743-750.
83. Vesely MD, Kershaw MH, Schreiber RD, Smyth MJ. Natural innate and adaptive immunity to cancer. *Annu Rev Immunol*. 2011;29:235-271.
84. Lefrançois L. Dual personality of memory T cells. *Trends Immunol*. 2002;23(5):226-228.
85. Klebanoff CA, Gattinoni L, Restifo NP. CD8+ T-cell memory in tumor

- immunology and immunotherapy. *Immunol Rev.* 2006;211:214-224.
86. Jochems C, Schlom J. Tumor-infiltrating immune cells and prognosis: the potential link between conventional cancer therapy and immunity. *Exp Biol Med (Maywood).* 2011;236(5):567-579.
 87. Mittendorf E a, Philips A V, Meric-Bernstam F, et al. PD-L1 expression in triple-negative breast cancer. *Cancer Immunol Res.* 2014;2(4):361-370.
 88. Hamanishi J, Mandai M, Matsumura N, Abiko K, Baba T, Konishi I. PD-1/PD-L1 blockade in cancer treatment: perspectives and issues. *Int J Clin Oncol.* 2016;21(3):1-12.
 89. McDermott DF, Atkins MB. PD-1 as a potential target in cancer therapy. *Cancer Med.* 2013;2(5):662-673.
 90. Filippi CM, Juedes AE, Oldham JE, et al. Transforming growth factor-alpha suppresses the activation of cd8 + t-cells when naive but promotes their survival and function once antigen experienced: a two-faced impact on autoimmunity. *Diabetes.* 2008;57(10):2684-2692.
 91. Sakaguchi S, Wing K, Onishi Y, Prieto-Martin P, Yamaguchi T. Regulatory T cells: How do they suppress immune responses? *Int Immunol.* 2009;21(10):1105-1111.
 92. Filaci G, Fenoglio D, Fravega M, et al. CD8+ CD28- T regulatory lymphocytes inhibiting T cell proliferative and cytotoxic functions infiltrate human cancers. *J Immunol.* 2007;179(7):4323-4334.
 93. Peggs KS, Quezada SA, Chambers CA, Korman AJ, Allison JP. Blockade of CTLA-4 on both effector and regulatory T cell compartments contributes to the antitumor activity of anti-CTLA-4 antibodies. *J Exp Med.* 2009;206(8):1717-1725.
 94. Baran Y, Nalbant A. T cells in tumor microenvironment. *Tumour Biol.* 2016;37(1):39-45.
 95. Romagnani S. T-cell subsets (Th1 versus Th2). *Ann Allergy Asthma Immunol.* 2000;85(1):9-18, 21.
 96. Bailey SR, Nelson MH, Himes RA, Li Z, Mehrotra S, Paulos CM. Th17 cells in cancer: The ultimate identity crisis. *Front Immunol.* 2014;5(JUN).
 97. Gagliani N, Vesely MCA, Iseppon A, et al. Th17 cells transdifferentiate into regulatory T cells during resolution of inflammation. *Nature.* 2015;523(7559):221-225.
 98. Greenplate AR, Johnson DB, Ferrell Jr. PB, Irish JM. Systems immune monitoring in cancer therapy. *Eur J Cancer.* 2016;61:77-84.
 99. Liu C, Workman CJ, Vignali DAA. Targeting regulatory T cells in tumors. *FEBS Journal.* 2016.
 100. Serrels A, Lund T, Serrels B, et al. Nuclear FAK Controls Chemokine Transcription, Tregs, and Evasion of Anti-tumor Immunity. *Cell.* 2015;163(1):160-173.
 101. Sojka DK, Huang YH, Fowell DJ. Mechanisms of regulatory T-cell suppression - A diverse arsenal for a moving target. *Immunology.* 2008;124(1):13-22.
 102. Schmidt A, Oberle N, Krammer PH. Molecular mechanisms of treg-mediated

- T cell suppression. *Front Immunol.* 2012;3:51.
103. Nishikawa H, Sakaguchi S. Regulatory T cells in cancer immunotherapy. *Curr Opin Immunol.* 2014;27(1):1-7.
 104. Gondek DC, Lu L-F, Quezada SA, Sakaguchi S, Noelle RJ. Cutting Edge: Contact-Mediated Suppression by CD4+CD25+ Regulatory Cells Involves a Granzyme B-Dependent, Perforin-Independent Mechanism. *J Immunol.* 2005;174(4):1783-1786.
 105. Cao X, Cai SF, Fehniger TA, et al. Granzyme B and Perforin Are Important for Regulatory T Cell-Mediated Suppression of Tumor Clearance. *Immunity.* 2007;27(4):635-646.
 106. Balkwill FR, Capasso M, Hagemann T. The tumor microenvironment at a glance. *J Cell Sci.* 2012;125(23):5591-5596.
 107. Milne K, Kobel M, Kalloger SE, et al. Systematic analysis of immune infiltrates in high-grade serous ovarian cancer reveals CD20, FoxP3 and TIA-1 as positive prognostic factors. *PLoS One.* 2009;4(7).
 108. Coronella JA, Telleman P, Kingsbury GA, Truong TD, Hays S, Junghans RP. Evidence for an antigen-driven humoral immune response in medullary ductal breast cancer. *Cancer Res.* 2001;61(21):7889-7899.
 109. Mauri C, Bosma A. Immune regulatory function of B cells. *Annu Rev Immunol.* 2012;30:221-241.
 110. Siewe B, Wallace J, Rygielski S, et al. Regulatory B cells inhibit cytotoxic T lymphocyte (CTL) activity and elimination of infected CD4 T cells after in vitro reactivation of HIV latent reservoirs. *PLoS One.* 2014;9(4).
 111. Das A, Ellis G, Pallant C, et al. IL-10-producing regulatory B cells in the pathogenesis of chronic hepatitis B virus infection. *J Immunol.* 2012;189(8):3925-3935.
 112. Schioppa T, Moore R, Thompson RG, et al. B regulatory cells and the tumor-promoting actions of TNF- α during squamous carcinogenesis. *Proc Natl Acad Sci U S A.* 2011;108(26):10662-10667.
 113. Olkhanud PB, Damdinsuren B, Bodogai M, et al. Tumor-evoked regulatory B cells promote breast cancer metastasis by converting resting CD4+ T cells to T-regulatory cells. *Cancer Res.* 2011;71(10):3505-3515.
 114. Adams S, O'Neill DW, Bhardwaj N. Recent advances in dendritic cell biology. *J Clin Immunol.* 2005;25(2):87-98.
 115. Ferlazzo G, Tsang ML, Moretta L, Melioli G, Steinman RM, Münz C. Human dendritic cells activate resting natural killer (NK) cells and are recognized via the NKp30 receptor by activated NK cells. *J Exp Med.* 2002;195(3):343-351.
 116. Roothans D, Smits E, Lion E, Tel J, Anguille S. CD56 marks human dendritic cell subsets with cytotoxic potential. *Oncoimmunology.* 2013;2(2):e23037.
 117. Trombetta ES, Mellman I. Cell biology of antigen processing in vitro and in vivo. *Annu Rev Immunol.* 2005;23:975-1028.
 118. Itano A a, Jenkins MK. Antigen presentation to naive CD4 T cells in the lymph node. *Nat Immunol.* 2003;4(8):733-739.
 119. Chomarat P, Banchereau J, Davoust J, Palucka a K. IL-6 switches the differentiation of monocytes from dendritic cells to macrophages. *Nat*

Immunol. 2000;1(6):510-514.

120. Hiltbold EM, Vlad AM, Ciborowski P, Watkins SC, Finn OJ. The Mechanism of Unresponsiveness to Circulating Tumor Antigen MUC1 Is a Block in Intracellular Sorting and Processing by Dendritic Cells. *J Immunol.* 2000;165(7):3730-3741.
121. Fiorentino DF, Zlotnik A, Vieira P, et al. IL-10 acts on the antigen-presenting cell to inhibit cytokine production by Th1 cells. *J Immunol.* 1991;146(10):3444-3451.
122. Vinogradov S, Warren G, Wei X. Macrophages associated with tumors as potential targets and therapeutic intermediates. *Nanomedicine.* 2014;9:695-707.
123. Chanmee T, Ontong P, Konno K, Itano N. Tumor-associated macrophages as major players in the tumor microenvironment. *Cancers (Basel).* 2014;6(3):1670-1690.
124. Galdiero MR, Bonavita E, Barajon I, Garlanda C, Mantovani A, Jaillon S. Tumor associated macrophages and neutrophils in cancer. *Immunobiology.* 2013;218(11):1402-1410.
125. Martinez FO, Gordon S. The M1 and M2 paradigm of macrophage activation: time for reassessment. *F1000Prime Rep.* 2014;6:13.
126. Curiel TJ, Wei S, Dong H, et al. Blockade of B7-H1 improves myeloid dendritic cell-mediated antitumor immunity. *Nat Med.* 2003;9(5):562-567.
127. Wang B, Li Q, Qin L, Zhao S, Wang J, Chen X. Transition of tumor-associated macrophages from MHC class IIhi to MHC class IIlo mediates tumor progression in mice. *BMC Immunol.* 2011;12(1):43.
128. Quatromoni JG, Eruslanov E. Tumor-associated macrophages: function, phenotype, and link to prognosis in human lung cancer. *Am J Transl Res.* 2012;4(4):376-389.
129. Zhang Q, Liu L, Gong C, et al. Prognostic significance of tumor-associated macrophages in solid tumor: a meta-analysis of the literature. *PLoS One.* 2012;7(12):e50946.
130. Marvel D, Gabrilovich DI. Myeloid-derived suppressor cells in the tumor microenvironment: expect the unexpected. *J Clin Invest.* 2015;125(9):1-9.
131. Umansky V, Sevko A. Tumor microenvironment and myeloid-derived suppressor cells. *Cancer Microenviron.* 2013;6(2):169-177.
132. Weide B, Martens A, Zelba H, et al. Myeloid-derived suppressor cells predict survival of advanced melanoma patients: comparison with regulatory T cells and NY-ESO-1- or Melan-A-specific T cells. *Clin Cancer Res.* 2013:1601-1609.
133. Fridlender ZG, Albelda SM. Tumor-associated neutrophils: Friend or foe? *Carcinogenesis.* 2012;33(5):949-955.
134. Mantovani A. Macrophages, Neutrophils, and Cancer: A Double Edged Sword. *New J Sci.* 2014;2014(1):1-14.
135. Ransohoff RM, Engelhardt B. The anatomical and cellular basis of immune surveillance in the central nervous system. *Nat Rev Immunol.* 2012;12(9):623-635.

136. Van Gool SW. Brain Tumor Immunotherapy: What have We Learned so Far? *Front Oncol.* 2015;5(June):98.
137. Loriger M. Tumor microenvironment in the brain. *Cancers (Basel).* 2012;4(1):218-243.
138. Weller RO, Engelhardt B, Phillips MJ. Lymphocyte targeting of the central nervous system: a review of afferent and efferent CNS-immune pathways. *Brain Pathol.* 1996;6(3):275-288.
139. Walter B a, Valera V a, Takahashi S, Matsuno K, Ushiki T. Evidence of antibody production in the rat cervical lymph nodes after antigen administration into the cerebrospinal fluid. *Arch Histol Cytol.* 2006;69(1):37-47.
140. Louveau A, Smirnov I, Keyes TJ, et al. Structural and functional features of central nervous system lymphatic vessels. *Nature.* 2015;523(7560):337-341.
141. Charles NA, Holland EC, Gilbertson R, Glass R, Kettenmann H. The brain tumor microenvironment. *Glia.* 2011;59(8):1169-1180.
142. Ridley A, Cavanagh JB. Lymphocytic infiltration in gliomas: Evidence of possible host resistance. *Brain.* 1971;94(1):117 LP-124.
143. Dunn G, Dunn I, Curry W. Focus on TILs: Prognostic significance of tumor infiltrating lymphocytes in human glioma. *Cancer Immun.* 2007;7(December):12.
144. D'Agostino PM, Gottfried-Blackmore A, Anandasabapathy N, Bulloch K. Brain dendritic cells: Biology and pathology. *Acta Neuropathol.* 2012;124(5):599-614.
145. Berghoff AS, Preusser M. The inflammatory microenvironment in brain metastases : potential treatment target ? *Chinese Clin Oncol.* 2015;4(2):1-9.
146. Larochelle C, Alvarez JI, Prat A. How do immune cells overcome the blood-brain barrier in multiple sclerosis? *FEBS Lett.* 2011;585(23):3770-3780.
147. Ballabh P, Braun A, Nedergaard M. The blood-brain barrier: An overview: Structure, regulation, and clinical implications. *Neurobiol Dis.* 2004;16(1):1-13.
148. Hamilton A, Sibson NR. Role of the systemic immune system in brain metastasis. *Mol Cell Neurosci.* 2013;53:42-51.
149. Zhang RD, Price JE, Fujimaki T, Bucana CD, Fidler IJ. Differential permeability of the blood-brain barrier in experimental brain metastases produced by human neoplasms implanted into nude mice. *Am J Pathol.* 1992;141(5):1115-1124.
150. Loriger M, Krueger JS, O'Neal M, Staflin K, Felding-Habermann B. Activation of tumor cell integrin $\alpha v \beta 3$ controls angiogenesis and metastatic growth in the brain. *Proc Natl Acad Sci U S A.* 2009;106(26):10666-10671.
151. Reid DM, Perry VH, Andersson PB, Gordon S. Mitosis and apoptosis of microglia in vivo induced by an anti-CR3 antibody which crosses the blood-brain barrier. *Neuroscience.* 1993;56(3):529-533.
152. Armulik A, Genové G, Mäe M, et al. Pericytes regulate the blood-brain barrier. *Nature.* 2010;468(7323):557-561.
153. Lockman PR, Mittapalli RK, Taskar KS, et al. Heterogeneous blood-tumor

- barrier permeability determines drug efficacy in experimental brain metastases of breast cancer. *Clin Cancer Res.* 2010;16(23):5664-5678.
154. Chai Q, He WQ, Zhou M, Lu H, Fu ZF. Enhancement of blood-brain barrier permeability and reduction of tight junction protein expression are modulated by chemokines/cytokines induced by rabies virus infection. *J Virol.* 2014;88(9):4698-4710.
 155. Tsuge M, Yasui K, Ichiyawa T, et al. Increase of tumor necrosis factor-alpha in the blood induces early activation of matrix metalloproteinase-9 in the brain. *Microbiol Immunol.* 2010;54(7):417-424.
 156. Streit WJ, Conde JR, Fendrick SE, Flanary BE, Mariani CL. Role of microglia in the central nervous system's immune response. *Neurol Res.* 2005;27(7):685-691.
 157. Ginhoux F, Greter M, Leboeuf M, et al. Fate mapping analysis reveals that adult microglia derive from primitive macrophages. *Science.* 2010;330(6005):841-845.
 158. London A, Cohen M, Schwartz M. Microglia and monocyte-derived macrophages: functionally distinct populations that act in concert in CNS plasticity and repair. *Front Cell Neurosci.* 2013;7(April):34.
 159. Bennetta ML, Bennetta C, Liddelowa SA, et al. New tools for studying microglia in the mouse and human CNS. *PNAS.* 2016:1525528113-.
 160. Davis EJ, Foster TD, Thomas WE. Cellular forms and functions of brain microglia. *Brain Res Bull.* 1994;34(1):73-78.
 161. Yang I, Han SJ, Kaur G, Crane C, Parsa AT. The role of microglia in central nervous system immunity and glioma immunology. *J Clin Neurosci.* 2010;17(1):6-10.
 162. Prinz M, Tay TL, Wolf Y, Jung S. Microglia: Unique and common features with other tissue macrophages. *Acta Neuropathol.* 2014;128(3):319-331.
 163. Lorger M, Felding-Habermann B. Capturing changes in the brain microenvironment during initial steps of breast cancer brain metastasis. *Am J Pathol.* 2010;176(6):2958-2971.
 164. Badie B, Schartner J, Klaver J, Vorpahl J. In vitro modulation of microglia motility by glioma cells is mediated by hepatocyte growth factor/scatter factor. *Neurosurgery.* 1999;44(5):1077-1083.
 165. Okada M, Saio M, Kito Y, et al. Tumor-associated macrophage/microglia infiltration in human gliomas is correlated with MCP-3, but not MCP-1. *Int J Oncol.* 2009;34(6):1621-1627.
 166. Leung SY, Wong MP, Chung LP, Chan AS, Yuen ST. Monocyte chemoattractant protein-1 expression and macrophage infiltration in gliomas. *Acta Neuropathol.* 1997;93(5):518-527.
 167. Nishie a, Ono M, Shono T, et al. Macrophage infiltration and heme oxygenase-1 expression correlate with angiogenesis in human gliomas. *Clin Cancer Res.* 1999;5(May):1107-1113.
 168. Haiyan Zhai, Frank L. Heppner SET. Microglia/Macrophages Promote Glioma Progression. *Glia.* 2011;4(164):472-485.
 169. Graeber MB, Scheithauer BW, Kreutzberg GW. Microglia in brain tumors. *Glia.* 2002;40(2):252-259.

170. Badie B, Schartner J, Prabakaran S, Paul J, Vorpahl J. Expression of Fas ligand by microglia: Possible role in glioma immune evasion. *J Neuroimmunol.* 2001;120(1-2):19-24.
171. Lodge PA, Sriram S. Regulation of microglial activation by TGF-beta, IL-10, and CSF-1. *J Leukoc Biol.* 1996;60(4):502-508.
172. Schartner JM, Hagar AR, Van Handel M, Zhang L, Nadkarni N, Badie B. Impaired capacity for upregulation of MHC class II in tumor-associated microglia. *Glia.* 2005;51(4):279-285.
173. Pico de Coaña Y, Choudhury A, Kiessling R. Checkpoint blockade for cancer therapy: Revitalizing a suppressed immune system. *Trends Mol Med.* 2015;21(8):482-491.
174. Rosenberg S a, Yang JC, Restifo NP. Cancer immunotherapy: moving beyond current vaccines. *Nat Med.* 2004;10(9):909-915.
175. Schwartzenuber DJ, Lawson DH, Richards JM, et al. gp100 peptide vaccine and interleukin-2 in patients with advanced melanoma. *N Engl J Med.* 2011;364(22):2119-2127.
176. Farkona S, Diamandis EP, Blasutig IM. Cancer immunotherapy: the beginning of the end of cancer? *BMC Med.* 2016;14(1):73.
177. Kantoff PW, Higano CS, Shore ND, et al. Sipuleucel-T immunotherapy for castration-resistant prostate cancer. *N Engl J Med.* 2010;363(5):411-422.
178. Kaufman HL, Kohlhapp FJ, Zloza A. Oncolytic viruses: a new class of immunotherapy drugs. *Nat Rev Drug Discov.* 2015;14(9):642-662.
179. Kaufman H, Ruby C, Hughes T, Slingsluff C. Current status of granulocyte-macrophage colony-stimulating factor in the immunotherapy of melanoma. *J Immunother cancer.* 2014;2(1):11.
180. Andtbacka RHI, Kaufman HL, Collichio F, et al. Talimogene laherparepvec improves durable response rate in patients with advanced melanoma. *J Clin Oncol.* 2015;33(25):2780-2788.
181. Freeman a, Zakay-Rones Z, Gomoril J, et al. Phase I/II Trial of Intravenous NDV-HUJ Oncolytic Virus in Recurrent Glioblastoma Multiforme. *Mol Ther.* 2006;13(1):221-228.
182. Adair RA, Scott KJ, Fraser S, et al. Cytotoxic and immune-mediated killing of human colorectal cancer by reovirus-loaded blood and liver mononuclear cells. *Int J Cancer.* 2013;132(10):2327-2338.
183. Hinrichs CS, Rosenberg SA. Exploiting the curative potential of adoptive T-cell therapy for cancer. *Immunol Rev.* 2014;257(1):56-71.
184. Newick K, Moon E, Albelda SM. Chimeric antigen receptor T-cell therapy for solid tumors. *Mol Ther — Oncolytics.* 2016;3(October 2015):16006.
185. Maude SL, Frey N, Shaw PA, et al. Chimeric Antigen Receptor T Cells for Sustained Remissions in Leukemia. *N Engl J Med.* 2014;371(16):1507-1517.
186. Chandramohan V, Mitchell D a, Johnson L a, Sampson JH, Bigner DD. Antibody, T-cell and dendritic cell immunotherapy for malignant brain tumors. *Future Oncol.* 2013;9(7):977-990.
187. Morgan R a, Yang JC, Kitano M, Dudley ME, Laurencot CM, Rosenberg S a. Case report of a serious adverse event following the administration of T cells

- transduced with a chimeric antigen receptor recognizing ERBB2. *Mol Ther.* 2010;18(4):843-851.
188. van den Berg JH, Gomez-Eerland R, van de Wiel B, et al. Case report of a fatal Serious Adverse Event upon administration of T cells transduced with a MART-1 specific T cell receptor. *Mol Ther.* 2015;23(9):1-10.
 189. Gutin PH, Iwamoto FM, Beal K, et al. Safety and Efficacy of Bevacizumab With Hypofractionated Stereotactic Irradiation for Recurrent Malignant Gliomas. *Int J Radiat Oncol Biol Phys.* 2009;75(1):156-163.
 190. Diaz-Miqueli A, Martinez GS. Nimotuzumab as a radiosensitizing agent in the treatment of high grade glioma: Challenges and opportunities. *Onco Targets Ther.* 2013;6:931-942.
 191. Brown CE, Starr R, Aguilar B, et al. Stem-like tumor-initiating cells isolated from IL13R alpha 2 expressing gliomas are targeted and killed by IL13-zetakine-redirected T cells. *Clin Cancer Res.* 2012;18(8):2199-2209.
 192. Brown CE, Badie B, Barish ME, et al. Bioactivity and Safety of IL13R α 2-Redirected Chimeric Antigen Receptor CD8+ T Cells in Patients with Recurrent Glioblastoma. *Clin Cancer Res.* 2015;21(18):4062-4072.
 193. Pardoll DM. The blockade of immune checkpoints in cancer immunotherapy. *Nat Rev Cancer.* 2012;12(4):252-264.
 194. Nguyen LT, Ohashi PS. Clinical blockade of PD1 and LAG3 — potential mechanisms of action. *Nat Rev Immunol.* 2014;15(1):45-56.
 195. Sakuishi K, Apetoh L, Sullivan JM, Blazar BR, Kuchroo VK, Anderson AC. Targeting Tim-3 and PD-1 pathways to reverse T cell exhaustion and restore anti-tumor immunity. *J Exp Med.* 2010;207(10):2187-2194.
 196. Grosso JF, Jure-Kunkel MN. CTLA-4 blockade in tumor models: an overview of preclinical and translational research. *Cancer Immun.* 2013;13:5.
 197. Schwartz RH. Costimulation of T lymphocytes: the role of CD28, CTLA-4, and B7/BB1 in interleukin-2 production and immunotherapy. *Cell.* 1992;71(7):1065-1068.
 198. Rudd CE, Taylor A, Schneider H. CD28 and CTLA-4 coreceptor expression and signal transduction. *Immunol Rev.* 2009;229(1):12-26.
 199. Parry R V, Chemnitz JM, Frauwirth K a, et al. CTLA-4 and PD-1 Receptors Inhibit T-Cell Activation by Distinct Mechanisms CTLA-4 and PD-1 Receptors Inhibit T-Cell Activation by Distinct Mechanisms †. *Mol Cell Biol.* 2005;25(21):9543-9553.
 200. Qureshi OS, Zheng Y, Nakamura K, et al. Trans-endocytosis of CD80 and CD86: a molecular basis for the cell-extrinsic function of CTLA-4. *Science (80-).* 2011;332:600-603.
 201. Khattry R, Auger J a, Griffin MD, Sharpe a H, Bluestone J a. Lymphoproliferative disorder in CTLA-4 knockout mice is characterized by CD28-regulated activation of Th2 responses. *J Immunol.* 1999;162(10):5784-5791.
 202. Leach DR, Krummel MF, Allison JP. Enhancement of Antitumor Immunity by. 1988;7(23):1734-1736.
 203. Leach DR, Krummel MF, Allison JP. Enhancement of antitumor immunity by CTLA-4 blockade. *Science.* 1996;271(5256):1734-1736.

204. van Elsas A, Hurwitz AA, Allison JP. Combination immunotherapy of B16 melanoma using anti-cytotoxic T lymphocyte-associated antigen 4 (CTLA-4) and granulocyte/macrophage colony-stimulating factor (GM-CSF)-producing vaccines induces rejection of subcutaneous and metastatic tumors accompanied . *J Exp Med*. 1999;190(3):355-366.
205. Hodi FS, Mihm MC, Soiffer RJ, et al. Biologic activity of cytotoxic T lymphocyte-associated antigen 4 antibody blockade in previously vaccinated metastatic melanoma and ovarian carcinoma patients. *Proc Natl Acad Sci*. 2003;100(8):4712-4717.
206. Grauer OM, Nierkens S, Bennink E, et al. CD4+FoxP3+ regulatory T cells gradually accumulate in gliomas during tumor growth and efficiently suppress antitumor immune responses in vivo. *Int J Cancer*. 2007;121(1):95-105.
207. Fecci PE, Ochi H, Mitchell DA, et al. Systemic CTLA-4 blockade ameliorates glioma-induced changes to the CD4 + T cell compartment without affecting regulatory T-cell function. *Clin Cancer Res*. 2007;13(7):2158-2167.
208. Mangsbo SM, Sandin LC, Anger K, Korman AJ, Loskog A, Tötterman TH. Enhanced tumor eradication by combining CTLA-4 or PD-1 blockade with CpG therapy. *J Immunother*. 2010;33(3):225-235.
209. Curran MA, Montalvo W, Yagita H, Allison JP. PD-1 and CTLA-4 combination blockade expands infiltrating T cells and reduces regulatory T and myeloid cells within B16 melanoma tumors. *Proc Natl Acad Sci U S A*. 2010;107(9):4275-4280.
210. Sorensen MR, Holst PJ, Steffensen MA, Christensen JP, Thomsen AR. Adenoviral vaccination combined with CD40 stimulation and CTLA-4 blockage can lead to complete tumor regression in a murine melanoma model. *Vaccine*. 2010;28(41):6757-6764.
211. Pilonis KA, Kawashima N, Yang AM, Babb JS, Formenti SC, Demaria S. Invariant natural killer T cells regulate breast cancer response to radiation and CTLA-4 blockade. *Clin Cancer Res*. 2009;15(2):597-606.
212. Demaria S, Kawashima N, Yang AM, et al. Immune-Mediated Inhibition of Metastases after Treatment with Local Radiation and CTLA-4 Blockade in a Mouse Model of Breast Cancer Immune-Mediated Inhibition of Metastases after Treatment with Local Radiation and CTLA-4 Blockade in a Mouse Model of Breas. 2005:728-734.
213. Phan GQ, Yang JC, Sherry RM, et al. Cancer regression and autoimmunity induced by cytotoxic T lymphocyte-associated antigen 4 blockade in patients with metastatic melanoma. *Proc Natl Acad Sci U S A*. 2003;100(14):8372-8377.
214. Ribas A. Clinical development of the antiCTLA-4 antibody tremelimumab. *Semin Oncol*. 2010;37(5):450-454.
215. Hodi FS, O'Day SJ, McDermott DF, et al. Improved survival with ipilimumab in patients with metastatic melanoma. *N Engl J Med*. 2010;363(8):711-723.
216. NICE proposes ipilimumab as a first treatment for advanced skin cancer.
217. Institute NC. Clinical Trials Search Results. <http://www.cancer.gov/about-cancer/treatment/clinical-trials/search/results?protocolsearchid=6138091>.
218. Knisely JPS, Yu JB, Flanigan J, Sznol M, Kluger HM, Chiang VLS.

Radiosurgery for melanoma brain metastases in the ipilimumab era and the possibility of longer survival. *J Neurosurg.* 2012;117(2):227-233.

219. Tazi K, Hathaway A, Chiuzan C, Shirai K. Survival of melanoma patients with brain metastases treated with ipilimumab and stereotactic radiosurgery. *Cancer Med.* 2015;4(1):1-6.
220. Konstantinou MP, Dutriaux C, Gaudy-Marqueste C, et al. Ipilimumab in melanoma patients with brain metastasis: A retrospective multicentre evaluation of thirty-eight patients. *Acta Derm Venereol.* 2014;94(1):45-49.
221. Scharz NEC, Farges C, Madelaine I, et al. *Complete Regression of a Previously Untreated Melanoma Brain Metastasis with Ipilimumab.* *Melanoma research* 20, 247-250 (2010).
222. Margolin K, Ernstoff MS, Hamid O, et al. Ipilimumab in patients with melanoma and brain metastases: An open-label, phase 2 trial. *Lancet Oncol.* 2012;13(5):459-465.
223. Margolin K. Ipilimumab in a Phase II trial of melanoma patients with brain metastases. *Oncoimmunology.* 2012;1(7):1197-1199.
224. Keir ME, Butte MJ, Freeman GJ, Sharpe AH. PD-1 and its ligands in tolerance and immunity. *Annu Rev Immunol.* 2008;26:677-704.
225. Jin HT, Ahmed R, Okazaki T. Role of PD-1 in regulating T-cell immunity. *Curr Top Microbiol Immunol.* 2011;350:17-37.
226. Liu L, Zheng Q, Lee J, Ma Z, Zhu Q, Wang Z. PD-1/PD-L1 expression on CD⁴⁺ T cells and myeloid DCs correlates with the immune pathogenesis of atrial fibrillation. *J Cell Mol Med.* 2015;19(6):1223-1233.
227. Butte MJ, Keir ME, Phamduy TB, Sharpe AH, Freeman GJ. Programmed Death-1 Ligand 1 Interacts Specifically with the B7-1 Costimulatory Molecule to Inhibit T Cell Responses. *Immunity.* 2007;27(1):111-122.
228. Hong JJ, Amancha PK, Rogers K, Ansari AA, Villinger F. Re-Evaluation of PD-1 Expression by T Cells as a Marker for Immune Exhaustion during SIV Infection. *PLoS One.* 2013;8(3).
229. Callahan MK, Postow M a, Wolchok JD. CTLA-4 and PD-1 Pathway Blockade: Combinations in the Clinic. *Front Oncol.* 2014;4(January):385.
230. Francisco LM, Salinas VH, Brown KE, et al. PD-L1 regulates the development, maintenance, and function of induced regulatory T cells. *J Exp Med.* 2009;206(13):3015-3029.
231. Victor CT-S, Rech AJ, Maity A, et al. Radiation and dual checkpoint blockade activate non-redundant immune mechanisms in cancer. *Nature.* 2015;520(7547):373-377.
232. Brown J a, Dorfman DM, Ma F-R, et al. Blockade of Programmed Death-1 Ligands on Dendritic Cells Enhances T Cell Activation and Cytokine Production. *J Immunol.* 2003;170(3):1257-1266.
233. Konishi J, Yamazaki K, Azuma M, Kinoshita I, Dosaka-Akita H, Nishimura M. B7-H1 expression on non-small cell lung cancer cells and its relationship with tumor-infiltrating lymphocytes and their PD-1 expression. *Clin Cancer Res.* 2004;10(15):5094-5100.
234. Dong H, Strome SE, Salomao DR, et al. Tumor-associated B7-H1 promotes T-cell apoptosis: a potential mechanism of immune evasion. *Nat Med.*

2002;8(8):793-800.

235. Nishimura H, Minato N, Nakano T, Honjo T. Immunological studies on PD-1 deficient mice: implication of PD-1 as a negative regulator for B cell responses. *Int Immunol*. 1998;10(10):1563-1572.
236. Brahmer JR, Drake CG, Wollner I, et al. Phase I study of single-agent anti-programmed death-1 (MDX-1106) in refractory solid tumors: Safety, clinical activity, pharmacodynamics, and immunologic correlates. *J Clin Oncol*. 2010;28(19):3167-3175.
237. Sznol M, Powderly JD, Smith DC, et al. Safety and antitumor activity of biweekly MDX-1106 (Anti-PD-1, BMS-936558/ONO-4538) in patients with advanced refractory malignancies. *J Clin Oncol*. 2010;28(15 SUPPL. 1):no pagination.
238. McDermott D., Drake C., Szno M, et al. A phase I study to evaluate safety and antitumor activity of biweekly BMS-936558 (Anti-PD-1, MDX-1106/ONO-4538) in patients with RCC and other advanced refractory malignancies. *J Clin Oncol*. 2011;29(7 SUPPL. 1).
239. Kim JE, Patel MA, Mangraviti A, et al. The Combination of anti-TIM-3 and anti-PD-1 Checkpoint Inhibitors With Focused Radiation Resulted in a Synergistic Antitumor Immune Response in a Preclinical Glioma Model. *Neurosurgery*. 2015;62 Suppl 1(1):212.
240. Reardon DA, Gokhale PC, Klein SR, et al. Glioblastoma Eradication Following Immune Checkpoint Blockade in an Orthotopic, Immunocompetent Model. *Cancer Immunol Res*. 2015;4(February):1-12.
241. Guo Z, Wang H, Meng F, Li J, Zhang S. Combined Trabectedin and anti-PD1 antibody produces a synergistic antitumor effect in a murine model of ovarian cancer. *J Transl Med*. 2015;13(1):247.
242. Chen S, Lee L-F, Fisher TS, et al. Combination of 4-1BB Agonist and PD-1 Antagonist Promotes Antitumor Effector/Memory CD8 T Cells in a Poorly Immunogenic Tumor Model. *Cancer Immunol Res*. 2014;3(2):149-160.
243. Rajani K, Parrish C, Kottke T, et al. Combination Therapy With Reovirus and Anti-PD-1 Blockade Controls Tumor Growth Through Innate and Adaptive Immune Responses. *Mol Ther*. 2015;24(1):1-9.
244. Sharabi AB, Nirschl CJ, Kochel CM, et al. Stereotactic Radiation Therapy Augments Antigen-Specific PD-1-Mediated Antitumor Immune Responses via Cross-Presentation of Tumor Antigen. *Cancer Immunol Res*. 2015;3(4):345-355.
245. Kim K, Skora AD, Li Z, et al. Eradication of metastatic mouse cancers resistant to immune checkpoint blockade by suppression of myeloid-derived cells. *Proc Natl Acad Sci U S A*. 2014;111(32):11774-11779.
246. Weber J. Review: anti-CTLA-4 antibody ipilimumab: case studies of clinical response and immune-related adverse events. *Oncologist*. 2007;12(7):864-872.
247. Hao MZ, Zhou WY, Du XL, et al. Novel anti-melanoma treatment: Focus on immunotherapy. *Chin J Cancer*. 2014;33(9):458-465.
248. Ribas A, Puzanov I, Dummer R, et al. Pembrolizumab versus investigator-choice chemotherapy for ipilimumab-refractory melanoma (KEYNOTE-002): A randomised, controlled, phase 2 trial. *Lancet Oncol*. 2015;16(8):908-918.

249. Robert C, Schachter J, Long G V, et al. Pembrolizumab versus Ipilimumab in Advanced Melanoma. *N Engl J Med*. 2015;372(26):2521-2532.
250. Goldberg SB, Gettinger SN, Mahajan A, et al. Pembrolizumab for patients with melanoma or non-small-cell lung cancer and untreated brain metastases: early analysis of a non-randomised, open-label, phase 2 trial. *Lancet Oncol*. 2016;17(7):976-983.
251. Wolchok JD, Kluger H, Callahan MK, et al. Nivolumab plus ipilimumab in advanced melanoma. *N Engl J Med*. 2013;369(2):122-133.
252. McDermott DF, Kluger H, Sznol M, et al. Long-term survival of ipilimumab-naive patients (pts) with advanced melanoma (MEL) treated with nivolumab (anti-PD-1, BMS-936558, ONO-4538) in a phase I trial. *Ann Onc*. 2014;25(suppl_4):iv375-a-376.
253. Larkin J, Chiarion-Sileni V, Gonzalez R, et al. Combined Nivolumab and Ipilimumab or Monotherapy in Untreated Melanoma. *N Engl J Med*. 2015;373(1):23-34.
254. FDA. Nivolumab in combination with ipilimumab.
255. NICE. Nivolumab in combination with ipilimumab for treating advanced melanoma.
256. Daud AI, Mirza N, Lenox B, et al. Phenotypic and functional analysis of dendritic cells and clinical outcome in patients with high-risk melanoma treated with adjuvant granulocyte macrophage colony-stimulating factor. *J Clin Oncol*. 2008;26(19):3235-3241.
257. Kemp V, Hoeben RC, van den wollenberg DJM. Exploring reovirus plasticity for improving its use as oncolytic virus. *Viruses*. 2015;8(1).
258. Ilett E, Kottke T, Donnelly O, et al. Cytokine conditioning enhances systemic delivery and therapy of an oncolytic virus. *Mol Ther*. 2014;22(10):1851-1863.
259. Quezada SA, Peggs KS, Curran MA, Allison JP. CTLA4 blockade and GM-CSF combination immunotherapy alters the intratumor balance of effector and regulatory T cells. *J Clin Invest*. 2006;116(7):1935-1945.
260. GM-CSF/Ipilimumab Combination Extends Melanoma Survival. *Cancer Discov*. June 2013.
261. Li B, Vanroey M, Wang C, Chen THT, Korman A, Jooss K. Anti-programmed death-1 synergizes with granulocyte macrophage colony-stimulating factor-secreting tumor cell immunotherapy providing therapeutic benefit to mice with established tumors. *Clin Cancer Res*. 2009;15(5):1623-1634.
262. Nivolumab and Ipilimumab With or Without Sargramostim in Treating Patients With Stage III-IV Melanoma That Cannot Be Removed by Surgery.
263. Workman P, Aboagye EO, Balkwill F, et al. Guidelines for the welfare and use of animals in cancer research. *Br J Cancer*. 2010;102(11):1555-1577.
264. Jensen MM, Jørgensen JT, Binderup T, Kjaer A. Tumor volume in subcutaneous mouse xenografts measured by microCT is more accurate and reproducible than determined by 18F-FDG-microPET or external caliper. *BMC Med Imaging*. 2008;8(1):16.
265. Overwijk WW, Restifo NP. B16 as a mouse model for human melanoma. *Curr Protoc Immunol*. 2001;Chapter 20:Unit 20.1.

266. Peter I, Nawrath M, Kamarashev J, Odermatt B, Mezzacasa A, Hemmi S. Immunotherapy for murine K1735 melanoma: combinatorial use of recombinant adenovirus expressing CD40L and other immunomodulators. *Cancer Gene Ther.* 2002;9(7):597-605.
267. Lejeune FJ. Harding-Passey Melanoma in the BALB / C Mouse as a Model for Studying the Interactions Between Host Macrophages and Tumor Cells '. *Yale J Biol Med.* 1973;383(46):368-383.
<http://www.ncbi.nlm.nih.gov/pmc/articles/PMC2592040/>.
268. Turk MJ, Guevara-Patiño JA, Rizzuto GA, Engelhorn ME, Sakaguchi S, Houghton AN. Concomitant tumor immunity to a poorly immunogenic melanoma is prevented by regulatory T cells. *J Exp Med.* 2004;200(6):771-782.
269. Kato M, Takahashi M, Akhand a a, et al. Transgenic mouse model for skin malignant melanoma. *Oncogene.* 1998;17(14):1885-1888.
270. Walker GJ, Soyer HP, Terzian T, Box NF. Modelling melanoma in mice. *Pigment Cell Melanoma Res.* 2011;24(6):1158-1176.
271. Schwartz H, Blacher E, Amer M, et al. Incipient melanoma brain metastases instigate astrogliosis and neuroinflammation. *Cancer Res.* 2016.
272. Cranmer LD, Trevor KT, Bandlamuri S, Hersh EM. Rodent models of brain metastasis in melanoma. *Melanoma Res.* 2005;15(5):325-356.
273. Arguello F, Baggs RB, Frantz CN. A murine model of experimental metastasis to bone and bone marrow. *Cancer Res.* 1988;48:6876-6881.
274. Leslie LK, Cohen JT, Newburger JW, et al. Measuring Brain Tumor Growth: A Combined BLI / MRI Strategy. *Mol Imaging.* 2013;125(21):2621-2629.
275. Zinn KR, Chaudhuri TR, Szafran a. a., et al. Noninvasive Bioluminescence Imaging in Small Animals. *ILAR J.* 2008;49(1):103-115.
276. Curtis A, Calabro K, Galarneau JR, Bigio IJ, Krucker T. Temporal variations of skin pigmentation in C57Bl/6 mice affect optical bioluminescence quantitation. *Mol Imaging Biol.* 2011;13(6):1114-1123.
277. Szentirmai O, Baker CH, Lin N, et al. Noninvasive bioluminescence imaging of luciferase expressing intracranial U87 xenografts: Correlation with magnetic resonance imaging determined tumor volume and longitudinal use in assessing tumor growth and antiangiogenic treatment effect. *Neurosurgery.* 2006;58(2):365-372.
278. Rehemtulla a, Stegman LD, Cardozo SJ, et al. Rapid and quantitative assessment of cancer treatment response using in vivo bioluminescence imaging. *Neoplasia.* 2000;2(6):491-495.
279. Curran MA, Kim M, Montalvo W, Al-Shamkhani A, Allison JP. Combination CTLA-4 blockade and 4-1BB activation enhances tumor rejection by increasing T-cell infiltration, proliferation, and cytokine production. *PLoS One.* 2011;6(4).
280. Müller P, Kreuzaler M, Khan T, et al. Trastuzumab emtansine (T-DM1) renders HER2+ breast cancer highly susceptible to CTLA-4/PD-1 blockade. *Sci Transl Med.* 2015;7(315):315ra188-315ra188.
281. Dovedi SJ, Adlard AL, Lipowska-Bhalla G, et al. Acquired resistance to fractionated radiotherapy can be overcome by concurrent PD-L1 blockade.

Cancer Res. 2014;74(19):5458-5468.

282. Shi Y, Liu CH, Roberts AI, et al. Granulocyte-macrophage colony-stimulating factor (GM-CSF) and T-cell responses: what we do and don't know. *Cell Res.* 2006;16(2):126-133.
283. Chen TW, Razak AR, Bedard PL, Siu LL, Hansen AR. A systematic review of immune-related adverse event reporting in clinical trials of immune checkpoint inhibitors. *Ann Oncol.* 2015;(April):mdv182-.
284. Chen R, Peng P-C, Wen B, et al. Anti-Programmed Cell Death (PD)-1 Immunotherapy for Malignant Tumor: A Systematic Review and Meta-Analysis. *Transl Oncol.* 2016;9(1):32-40.
285. Weinstock M, McDermott D. Targeting PD-1/PD-L1 in the treatment of metastatic renal cell carcinoma. *Ther Adv Urol.* 2015;7(6):365-377.
286. Patnaik A, Kang SP, Rasco D, et al. Phase I Study of Pembrolizumab (MK-3475; Anti-PD-1 Monoclonal Antibody) in Patients with Advanced Solid Tumors. *Clin Cancer Res.* 2015;21(19):4286-4293.
287. Callahan MK, Wolchok JD, Allison JP. AntiCTLA-4 antibody therapy: Immune monitoring during clinical development of a novel immunotherapy. *Semin Oncol.* 2010;37(5):473-484.
288. Dai M, Yip YY, Hellstrom I, Hellstrom KE. Curing mice with large tumors by locally delivering combinations of immunomodulatory antibodies. *Clin Cancer Res.* 2015;21(5):1127-1138.
289. Patel SP, Kurzrock R. PD-L1 Expression as a Predictive Biomarker in Cancer Immunotherapy. *Mol Cancer Ther.* 2015;14(4):847-856.
290. Meng X, Huang Z, Teng F, Xing L, Yu J. Predictive biomarkers in PD-1/PD-L1 checkpoint blockade immunotherapy. *Cancer Treat Rev.* 2015;41(10):868-876.
291. Remon J, Chaput N, Planchard D. Predictive biomarkers for programmed death-1/programmed death ligand immune checkpoint inhibitors in nonsmall cell lung cancer. *Curr Opin Oncol.* 2016;28:122-129.
292. Hugo W, Zaretsky JM, Sun L, et al. Genomic and Transcriptomic Features of Response to Anti-PD-1 Therapy in Metastatic Melanoma. *Cell.* 2016;165(1):35-44.
293. Carson MJ, Doose JM, Melchior B, Schmid CD, Ploix CC. CNS immune privilege: Hiding in plain sight. *Immunol Rev.* 2006;213(1):48-65.
294. Aspelund a., Antila S, Proulx ST, et al. A dural lymphatic vascular system that drains brain interstitial fluid and macromolecules. *J Exp Med.* 2015;212(7):991-999.
295. Deng L, Liang H, Burnette B, et al. Irradiation and anti – PD-L1 treatment synergistically promote antitumor immunity in mice. 2014;124(2):687-695.
296. Ribas A, Shin DS, Zaretsky J, et al. PD-1 Blockade Expands Intratumoral Memory T Cells. *Cancer Immunol Res.* 2016;4(3):194-203.
297. Kuang Y, Zhang L, Weng X, Liu X, Zhu H. Combination immunotherapy with 4-1BBL and CTLA-4 blockade for the treatment of prostate cancer. *Clin Dev Immunol.* 2012;2012.
298. Jadus MR, Irwin MC, Irwin MR, et al. Macrophages can recognize and kill

tumor cells bearing the membrane isoform of macrophage colony-stimulating factor. *Blood*. 1996;87(12):5232-5241.
<http://www.ncbi.nlm.nih.gov/pubmed/8652838>.

299. Adams DO, Nathan CF. Molecular mechanisms in tumor-cell killing by activated macrophages. *Immunol Today*. 1983;4(6):166-170.
300. Mantovani a., Allavena P. The interaction of anticancer therapies with tumor-associated macrophages. *J Exp Med*. 2015;212(4):435-445.
301. Tidball JG, Wehling-Henricks M. Macrophages promote muscle membrane repair and muscle fibre growth and regeneration during modified muscle loading in mice in vivo. *J Physiol*. 2007;578(Pt 1):327-336.
302. Bacci M, Capobianco A, Monno A, et al. Macrophages are alternatively activated in patients with endometriosis and required for growth and vascularization of lesions in a mouse model of disease. *Am J Pathol*. 2009;175(2):547-556.
303. Zamarin D, Holmgaard RB, Subudhi SK, et al. Localized oncolytic virotherapy overcomes systemic tumor resistance to immune checkpoint blockade immunotherapy. *Sci Transl Med*. 2014;6(226):226ra32.
304. Shortman K, Heath WR. The CD8+ dendritic cell subset. *Immunol Rev*. 2010;234:18-31.
305. Gibbings D, Befus a D. CD4 and CD8: an inside-out coreceptor model for innate immune cells. *J Leukoc Biol*. 2009;86(2):251-259.
306. Churlaud G, Pitoiset F, Jebbawi F, et al. Human and Mouse CD8+CD25+FOXP3+ Regulatory T Cells at Steady State and during Interleukin-2 Therapy. *Front Immunol*. 2015;6(April):2-11.
307. Byrom B, Barbet AF, Obwolo M, Mahan SM. CD8+ T cell knockout mice are less susceptible to *Cowdria ruminantium* infection than athymic, CD4+ T cell knockout, and normal C57BL/6 mice. *Vet Parasitol*. 2000;93(2):159-172.
308. Merad M, Sathe P, Helft J, Miller J, Mortha A. The dendritic cell lineage: ontogeny and function of dendritic cells and their subsets in the steady state and the inflamed setting. *Annu Rev Immunol*. 2013;31:563-604.
309. Mittal D, Young A, Stannard K, et al. Antimetastatic effects of blocking PD-1 and the adenosine A2A receptor. *Cancer Res*. 2014;74(14):3652-3658.
310. Swaika A, Hammond WA, Joseph RW. Current state of anti-PD-L1 and anti-PD-1 agents in cancer therapy. *Mol Immunol*. 2015;67(2):4-17.
311. Hideto N, Kaori M, Yohei K, Yoshiyuki M, Hajime K. NK Cell-Depleting Anti-Asialo GM1 Ab Exhibits a Lethal Off-Target Effect on Basophils In Vivo. *J Immunol*. 2011;186:5766-5771.
312. Satoskar AR, Stamm LM, Zhang X, et al. NK cell-deficient mice develop a Th1-like response but fail to mount an efficient antigen-specific IgG2a antibody response. *J Immunol*. 1999;163(10):5298-5302.
<http://www.jimmunol.org/content/163/10/5298.full>.
313. Harshan K V., Gangadharam PRJ. In vivo depletion of natural killer cell activity leads to enhanced multiplication of *Mycobacterium avium* complex in mice. *Infect Immun*. 1991;59(8):2818-2821.
314. Davila E, Kennedy R, Cells E. Generation of antitumor immunity by cytotoxic T lymphocyte epitope peptide vaccination, CpG-oligodeoxynucleotide

- adjuvant, and CTLA-4 blockade. *Cancer Res.* 2003;63(12):3281-3288.
315. Gubin MM, Zhang X, Schuster H, et al. Checkpoint blockade cancer immunotherapy targets tumour-specific mutant antigens. *Nature.* 2014;515(7528):577-581.
316. Vremec D, Pooley J, Hochrein H, Wu L, Shortman K. CD4 and CD8 Expression by Dendritic Cell Subtypes in Mouse Thymus and Spleen. *J Immunol.* 2000;164(6):2978-2986.
317. Esashi E, Ito H, Ishihara K, Hirano T, Koyasu S, Miyajima A. Development of CD4+ macrophages from intrathymic T cell progenitors is induced by thymic epithelial cells. *J Immunol.* 2004;173(7):4360-4367.
318. Zhu J, Yamane H, Paul W. Differentiation of effector CD4 T cell populations. *Annu Rev Immunol.* 2010;28(1):445-489.
319. Simpson TR, Li F, Montalvo-Ortiz W, et al. Fc-dependent depletion of tumor-infiltrating regulatory T cells co-defines the efficacy of anti-CTLA-4 therapy against melanoma. *J Exp Med.* 2013;210(9):1695-1710.
320. Setiady YY, Coccia JA, Park PU. In vivo depletion of CD4+FOXP3+ Treg cells by the PC61 anti-CD25 monoclonal antibody is mediated by Fc gamma RIII+ phagocytes. *Eur J Immunol.* 2010;40(3):780-786.
321. Couper KN, Lanthier PA, Perona-Wright G, et al. Anti-CD25 antibody-mediated depletion of effector T cell populations enhances susceptibility of mice to acute but not chronic *Toxoplasma gondii* infection. *J Immunol.* 2009;182(7):3985-3994.
322. Kim HL. Antibody-based depletion of Foxp3+ T cells potentiates antitumor immune memory stimulated by mTOR inhibition. *Oncoimmunology.* 2014;3(June):e29081.
323. Lahl K, Loddenkemper C, Drouin C, et al. Selective depletion of Foxp3+ regulatory T cells induces a scurfy-like disease. *J Exp Med.* 2007;204(1):57-63.
324. Duffield JS, Forbes SJ, Constandinou CM, et al. Selective depletion of macrophages reveals distinct, opposing roles during liver injury and repair. *J Clin Invest.* 2005;115(1):56-65.
325. Ueno M, Fujita Y, Tanaka T, et al. Layer V cortical neurons require microglial support for survival during postnatal development. *Nat Neurosci.* 2013;16(5):543-551.
326. Weisser SB, van Rooijen N, Sly LM. Depletion and Reconstitution of Macrophages in Mice. *J Vis Exp.* 2012;(66):5-11.
327. Fritz JM, Tennis MA, Orlicky DJ, et al. Depletion of tumor-associated macrophages slows the growth of chemically induced mouse lung adenocarcinomas. *Front Immunol.* 2014;5(NOV):1-11.
328. Jordan MB, Van Rooijen N, Izui S, Kappler J, Marrack P. Liposomal clodronate as a novel agent for treating autoimmune hemolytic anemia in a mouse model. *Blood.* 2003;101(2):594-601.
329. Ma Y, Li Y, Jiang L, et al. Macrophage depletion reduced brain injury following middle cerebral artery occlusion in mice. *J Neuroinflammation.* 2016;13(1):38.
330. Ferenbach D a, Sheldrake T a, Dhaliwal K, et al. Macrophage/monocyte

depletion by clodronate, but not diphtheria toxin, improves renal ischemia/reperfusion injury in mice. *Kidney Int.* 2012;82(8):928-933.

331. Vermeer a W, Norde W. The thermal stability of immunoglobulin: unfolding and aggregation of a multi-domain protein. *Biophys J.* 2000;78(1):394-404.
332. Lin H-H, Faunce DE, Stacey M, et al. The macrophage F4/80 receptor is required for the induction of antigen-specific efferent regulatory T cells in peripheral tolerance. *J Exp Med.* 2005;201(10):1615-1625.
333. Goren I, Allmann N, Yogev N, et al. A Transgenic Mouse Model of Inducible Macrophage Depletion. *Am J Pathol.* 2009;175(1):132-147.
334. Watters JJ, Schartner JM, Badie B. Microglia function in brain tumors. *J Neurosci Res.* 2005;81(3):447-455.
335. Nakano A, Harada T, Morikawa S, Kato Y. Expression of leukocyte common antigen (CD45) on various human leukemia/lymphoma cell lines. *Acta Pathol Jpn.* 1990;40(2):107-115.
336. Mannering SI, Zhong J, Cheers C. T-cell activation, proliferation and apoptosis in primary *Listeria monocytogenes* infection. *Immunology.* 2002;106(1):87-95.
337. Borrego F, Robertson MJ, Ritz J, Pena J, Solana R. CD69 is a stimulatory receptor for natural killer cell and its cytotoxic effect is blocked by CD94 inhibitory receptor. *Immunology.* 1999;97(1):159-165.
338. Scholzen T, Gerdes J. The Ki-67 protein: From the known and the unknown. *J Cell Physiol.* 2000;182(3):311-322.
339. Zhou Q, Munger ME, Veenstra RG, et al. Coexpression of Tim-3 and PD-1 identifies a CD8+ T-cell exhaustion phenotype in mice with disseminated acute myelogenous leukemia. *Blood.* 2011;117(17):4501-4510.
340. Anderson AC. Tim-3: An Emerging Target in the Cancer Immunotherapy Landscape. *Cancer Immunol Res.* 2014;2(5):393-398.
341. Dolan DE, Gupta S. PD-1 pathway inhibitors: Changing the landscape of cancer immunotherapy. *Cancer Control.* 2014;21(3):231-237.
342. Hokey DA, Johnson FB, Smith J, et al. Activation drives PD-1 expression during vaccine-specific proliferation and following lentiviral infection in macaques. *Eur J Immunol.* 2008;38(5):1435-1445.
343. del Rio ML, Penuelas-Rivas G, Dominguez-Perles R, Ramirez P, Parrilla P, Rodriguez-Barbosa JI. Antibody-mediated signalling through PD-1 costimulates T cells and enhances CD28-dependent proliferation. *Eur J Immunol.* 2005;35(12):3545-3560.
344. Gray SM, Kaech SM, Staron MM. The interface between transcriptional and epigenetic control of effector and memory CD8+ T-cell differentiation. *Immunol Rev.* 2014;261(1):157-168.
345. Intlekofer AM, Takemoto N, Wherry EJ, et al. Effector and memory CD8+ T cell fate coupled by T-bet and eomesodermin. *Nat Immunol.* 2005;6(12):1236-1244.
346. Zhu Y, Ju S, Chen E, et al. T-bet and Eomesodermin Are Required for T Cell-Mediated Antitumor Immune Responses. *J Immunol.* 2010;185(6):3174-3183.

347. Alter G, Malenfant JM, Altfeld M. CD107a as a functional marker for the identification of natural killer cell activity. *J Immunol Methods*. 2004;294(1-2):15-22.
348. Hayakawa Y, Smyth MJ. CD27 dissects mature NK cells into two subsets with distinct responsiveness and migratory capacity. *J Immunol*. 2006;176(3):1517-1524.
349. Perry VH, Teeling J. Microglia and macrophages of the central nervous system: The contribution of microglia priming and systemic inflammation to chronic neurodegeneration. *Semin Immunopathol*. 2013;35(5):601-612.
350. Kodumudi KN, Siegel J, Weber AM, Scott E, Sarnaik AA, Pilon-Thomas S. Immune Checkpoint Blockade to Improve Tumor Infiltrating Lymphocytes for Adoptive Cell Therapy. *PLoS One*. 2016;11(4):e0153053.
351. Strik HM, Stoll M, Meyermann R. Immune Cell Infiltration of Intrinsic and Metastatic Intracranial Tumours. *Anticancer Res*. 2004;24(1):37-42.
352. Wherry EJ, Kurachi M. Molecular and cellular insights into T cell exhaustion. *Nat Rev Immunol*. 2015;15(8):486-499.
353. Spranger S, Koblish HK, Horton B, Scherle PA, Newton R, Gajewski TF. Mechanism of tumor rejection with doublets of CTLA-4, PD-1/PD-L1, or IDO blockade involves restored IL-2 production and proliferation of CD8(+) T cells directly within the tumor microenvironment. *J Immunother cancer*. 2014;2:3.
354. Selby MJ, Engelhardt JJ, Quigley M, et al. Anti-CTLA-4 antibodies of IgG2a isotype enhance antitumor activity through reduction of intratumoral regulatory T cells. *Cancer Immunol Res*. 2013;1(1):32-42.
355. Park YJ, Song B, Kim YS, et al. Tumor microenvironmental conversion of natural killer cells into myeloid-derived suppressor cells. *Cancer Res*. 2013;73(18):5669-5681.
356. McNab FW, Berry MPR, Graham CM, et al. Programmed death ligand 1 is over-expressed by neutrophils in the blood of patients with active tuberculosis. *Eur J Immunol*. 2011;41(7):1941-1947.
357. Lim TS, Chew V, Sieow JL, et al. PD-1 expression on dendritic cells suppresses CD8 + T cell function and anti-tumor immunity. *Oncoimmunology*. 2015:00-00.
358. Kakavand H, Vilain RE, Wilmott JS, et al. Tumor PD-L1 expression, immune cell correlates and PD-1+ lymphocytes in sentinel lymph node melanoma metastases. *Mod Pathol*. 2015;28(12):1535-1544.
359. Ngiow SF, Von Scheidt B, Akiba H, Yagita H, Teng MWL, Smyth MJ. Anti-TIM3 antibody promotes T cell IFN-gamma-mediated antitumor immunity and suppresses established tumors. *Cancer Res*. 2011;71(10):3540-3551.
360. Sakuishi K, Ngiow SF, Sullivan JM, et al. TIM3 + FOXP3 + regulatory T cells are tissue-specific promoters of T-cell dysfunction in cancer. *Oncoimmunology*. 2013;2(4):e23849.
361. Dissing-Olesen L, Hong S, Stevens B. New Brain Lymphatic Vessels Drain Old Concepts. *EBioMedicine*. 2015;2(8):776-777.
362. Tiron A, Vasilescu C. Role of the spleen in immunity. Immunologic consequences of splenectomy. *Chirurgia*. <http://www.ncbi.nlm.nih.gov/pubmed/18717273>. Published 2008.

363. Kedl RM, Jordan M, Potter T, Kappler J, Marrack P, Dow S. CD40 stimulation accelerates deletion of tumor-specific CD8⁺ T cells in the absence of tumor-antigen vaccination. *Proc Natl Acad Sci U S A*. 2001;98(19):10811-10816.
364. Kline J, Zhang L, Battaglia L, Cohen KS, Gajewski TF. Cellular and molecular requirements for rejection of B16 melanoma in the setting of regulatory T cell depletion and homeostatic proliferation. *J Immunol*. 2012;188(6):2630-2642.
365. Sallusto F, Lenig D, Förster R. Pillars Article : Two Subsets of Memory T Lymphocytes with Distinct Homing Potentials and Effector Functions . *Nature* . 2014:34-38.
366. Förster R, Davalos-Miszlitz AC, Rot A. CCR7 and its ligands: balancing immunity and tolerance. *Nat Rev Immunol*. 2008;8(5):362-371.
367. Buonamici S, Trimarchi T, Ruocco MG, et al. CCR7 signalling as an essential regulator of CNS infiltration in T-cell leukaemia. *Nature*. 2009;459(7249):1000-1004.
368. Smith A, Stanley P, Jones K, Svensson L, McDowall A, Hogg N. The role of the integrin LFA-1 in T-lymphocyte migration. *Immunol Rev*. 2007;218(1):135-146.
369. Frank PG, Lisanti MP. ICAM-1: role in inflammation and in the regulation of vascular permeability. *Am J Physiol - Hear Circ Physiol*. 2008;295(3):H926-H927.
370. Pacheco KA, Tarkowski M, Klemm J, Rosenwasser LJ. CD49d expression and function on allergen-stimulated T cells from blood and airway. *Am J Respir Cell Mol Biol*. 1998;18(2):286-293.
371. Lidington EA, Moyes DL, McCormack AM, Rose ML. A comparison of primary endothelial cells and endothelial cell lines for studies of immune interactions. *Transpl Immunol*. 1999;7(4):239-246.
372. Penfold PL, Wen L, Madigan MC, King NJC, Provis JM. Modulation of permeability and adhesion molecule expression by human choroidal endothelial cells. *Investig Ophthalmol Vis Sci*. 2002;43(9):3125-3130.
373. Payton M, Jun T, Wayne W, et al. Antagonism of Ang-Tie2 and Dll4-Notch signaling has opposing effects on tumor endothelial cell proliferation, evidenced by a new flow cytometry method. *Lab Invest*. 2014;0(August):1-13.
374. Kavanagh B, O'Brien S, Lee D, et al. CTLA4 blockade expands FoxP3⁺ regulatory and activated effector CD4⁺ T cells in a dose-dependent fashion. *Blood*. 2008;112(4):1175-1183.
375. Walker LSK. Treg and CTLA-4: Two intertwining pathways to immune tolerance. *J Autoimmun*. 2013;45:49-57.
376. Franceschini D, Paroli M, Francavilla V, et al. PD-L1 negatively regulates CD4⁺CD25⁺Foxp3⁺ Tregs by limiting STAT-5 phosphorylation in patients chronically infected with HCV. *J Clin Invest*. 2009;119(3):551-564.
377. Das R, Verma R, Sznol M, et al. Combination therapy with anti-CTLA-4 and anti-PD-1 leads to distinct immunologic changes in vivo. *J Immunol*. 2015;194(3):950-959.

378. Ahmadzadeh M, Johnson LA, Heemskerk B, et al. Tumor antigen-specific CD8 T cells infiltrating the tumor express high levels of PD-1 and are functionally impaired. *Blood*. 2009;114(8):1537-1544.
379. Galea I, Bernardes-Silva M, Forse P a, van Rooijen N, Liblau RS, Perry VH. An antigen-specific pathway for CD8 T cells across the blood-brain barrier. *J Exp Med*. 2007;204(9):2023-2030.
380. Carden CP, Agarwal R, Saran F, Judson IR. Eligibility of patients with brain metastases for phase I trials: time for a rethink? *Lancet Oncol*. 2008;9(10):1012-1017.